Spring 5-31-2019

Electrochemically reactive membranes for efficient biomass recovery, pollutant degradation and commercialization

Likun Hua
New Jersey Institute of Technology

Recommended Citation

ABSTRACT

ELECTROCHEMICALLY REACTIVE MEMBRANES FOR EFFICIENT BIOMASS RECOVERY, POLLUTANT DEGRADATION AND COMMERCIALIZATION

by
Likun Hua

Micropollution in natural waters such as rivers and groundwater aquifers is a widespread problem that prevents these potentially potable sources from being used as drinking water. In the United States, approximately two-thirds of the over 1,200 most serious hazardous waste sites in the nation are contaminated with trichloroethylene (TCE), a potentially carcinogenic compound. Other emerging and environmentally persistent organic micropollutants include polyromantic hydrocarbons (PAHs), organophosphate flame retardants, endocrine disrupting compounds (EDCs), pesticides, herbicides, pharmaceuticals and personal care products (PPCPs). Membrane filtration is one of the most efficient separation processes widely used for water treatment and pollutant removal. However, traditional membrane separations suffer from membrane fouling due to either the formation of a cake layer of biomass or more commonly due to organic matter adsorption onto the membrane surface. Moreover, some trace level organic micropollutants are not effectively removed particularly in microfiltration processes, where pore sizes are not small enough to capture small molecular weight organics. This study demonstrated an innovative and multifunctional reactive electrochemical membrane (REM) that acts as both a filter and a reactive anode. REM filtration has significant mitigation of membrane surface and efficient degradation of water contaminant fouling through electrochemical oxidation powered by anodic polarization

under a DC current. This research demonstrate: (1) the use of the Ti_4O_7 REM to separate and oxidize potentially pathogenic microorganisms (e.g., algal cells and bacteria) in aqueous suspension with evidence of cell damage and removal; (2) Evaluation of the performance of REMs for the removal of antibiotic compound (sulfamethoxazole) and 1,4-dioxane; (3) fouling mitigation and development of antifouling strategies via DC current applications and anode/cathode switch; (4) Radical formation mechanisms under DC currents in the REM filtration system. Overall, this project aims to demonstrate next generation reactive membrane filtration systems with high pollutant rejection or removal efficiencies toward water contaminants on electrochemical oxidation reactions on REM surfaces.

ELECTROCHEMICALLY REACTIVE MEMBRANES FOR EFFICIENT BIOMASS RECOVERY, POLLUTANT DEGRADATION AND COMMERCIALIZATION

by
Likun Hua

A Dissertation
Submitted to the Faculty of
New Jersey Institute of Technology
in Partial Fulfilment of the Requirements for the Degree of
Doctor of Philosophy in Environmental Engineering

John A. Reif, Jr. Department of Civil and Environmental Engineering

May 2019

APPROVAL PAGE

ELECTROCHEMICALLY REACTIVE MEMBRANES FOR EFFICIENT BIOMASS RECOVERY, POLLUTANT DEGRADATION AND COMMERCIALIZATION

Likun Hua

Dr. Wen Zhang, Dissertation Advisor	Date
Associate Professor of Civil and Environmental Engineering, NJIT	

Dr. Taha F. Marhaba, Committee Member	Date
Professor and Chair of Civil and Environmental Engineering, NJIT	

Dr. Kamalesh K. Sirkar, Committee Member	Date
Distinguished Professor of Chemical Biological and Pharmaceutical Engineering, NJIT	

Dr. Sagnik Basuray, Committee Member	Date
Assistant Professor of Chemical Biological and Pharmaceutical Engineering, NJIT	

Dr. Charles Liu, Committee Member	Date
Principal Engineer of Pall Corporation	

BIOGRAPHICAL SKETCH

Author: Likun Hua

Degree: Doctor of Philosophy

Date: August 13th 1990

Undergraduate and Graduate Education:

- Doctor of Philosophy in Environmental Engineering,
  New Jersey Institute of Technology, Newark, NJ, 2019

- Master of Science in Environmental Engineering,
  New Jersey Institute of Technology, Newark, NJ, 2014

- Bachelor of Science in Environmental Engineering,
  Tianjin University, Tianjin, P. R. China, 2012

Major: Environmental Engineering

Presentations and Publications:

Hua, L.; Guo, L.; Thakkar, M.; Wei, D.; Agbakpe, M.; Kuang, L.; Magpile, M.;
Chaplin, B. P.; Tao, Y; Shuai, D; Zhang, X; Mitra, S; Zhang, W., Effects of
anodic oxidation of a substoichiometric titanium dioxide reactive electrochemical
membrane on algal cell destabilization and lipid extraction. *Bioresource
technology* 203 (2016): 112-117

Zheng, Q.; Durkin, D. P.; Elenewski, J. E.; Sun, Y.-X.; Banek, N. A.; Hua, L.;
Chen, H.; Wagner, M. J.; Zhang, W.; Shuai, D., Visible-light-responsive graphitic
carbon nitride (g-c$_3$n$_4$): rational design and photocatalytic applications
for water treatment. *Environmental Science & Technology.* 2016.
DOI: 10.1021/acs.est.6b02579

Fu, W.; Hua, L.; Zhang, W., Experimental and modeling assessment of the roles of
hydrophobicity and zeta potential in chemically modified poly (ether sulfone)
membrane fouling kinetics. *Industrial & Engineering Chemistry Research* 2017,
56 (30), 8580-8589

Khaled Abdella Ahmed, A.; Sun, C.; Hua, L.; Zhang, Z.; Zhang, Y.; Marhaba, T.; Zhang, W., Colloidal Properties of Air, Oxygen, and Nitrogen Nanobubbles in Water: Effects of Ionic Strength, Natural Organic Matters, and Surfactants. *Environmental Engineering Science* 2017. DOI: 10.1089/ees.2017.0377

Fu, W.; Hua, L.; Zhang, W., Experimental and Modeling Assessment of the Roles of Hydrophobicity and Zeta Potential in Chemically Modified Poly (ether sulfone) Membrane Fouling Kinetics. *Industrial & Engineering Chemistry Research* 2017, *56* (30), 8580-8589

Ahmed, A. K. A.; Shi, X.; Hua, L.; Manzueta, L.; Qing, W.; Marhaba, T.; Zhang, W., Influences of Air, Oxygen, Nitrogen, and Carbon Dioxide Nanobubbles on Seed Germination and Plant Growth. *Journal of agricultural and food chemistry* 2018, *66* (20), 5117-5124

Liu, X.; Liu, T.; Yue, X.; Komatsu, M.; Zhang, Y.; Hua, L.; Zhang, W.; Bondar, M.; Belfield, K., Tumor Vasculature Imaging using Polymer Nanoparticles in the Near-Infrared Window. *Scientific Reports.* 2018. (Accepted)

Likun Hua, Reactive Electrochemical Membranes (REM) for Emerging Contaminant Removal, *American Water Works Association NJ 83rd Annual Conference*, Atlantic City, March 22, 2018

Likun Hua, Algal Harvesting and Destabilization by Ti_4O_7 Reactive Electrochemical Membrane, A*merican Chemical Society 251st National Meeting*, San Diego, March 17, 2016

Likun Hua, Algal Destabilization and Harvesting by a Ti_4O_7 Reactive Electrochemical Membrane Filtration, *Symposium presentation to Department of Chemistry and Environmental Science*, NJIT October 21, 2015

Likun Hua, Algal Destabilization and Harvesting by a Ti_4O_7 Reactive Electrochemical Membrane Filtration, *NJ Tech Summer Intern and Research Project*, New Jersey Technology Council, August 11, 2015

Likun Hua, Multifunctional Reactive Electrochemical Membranes (REM) for Emerging Contaminant Removal, *American Water Works Association NJ 83rd Annual Conference*, Atlantic City, March 21, 2018

Likun Hua, Evaluation of Ti_4O_7 Ceramic Membrane Filtration and Fouling Mitigation under DC Currents, *Membrane Science Engineering and Technology Center Industrial Advisory Board poster session*, NJIT, October 22, 2017

Likun Hua, Evaluation of Ti_4O_7 Ceramic Membrane Filtration and Fouling
Mitigation under DC Currents, *2017-18 Association of Environmental Engineering and Science Professors Distinguished Lecture poster session*, NJIT, September 20, 2017

Likun Hua, Wen Zhang. Algal Harvesting and Destabilization by Ti_4O_7 Reactive
Electrochemical Membrane. *2016 Dana Knox Student Research Showcase*, NJIT, April 20, 2016

Likun Hua, Algal Biomass Destabilization by Titania Reactive Membrane Filtration
for Lipid Extraction, *New Jersey Entrepreneur Network annual poster session,* Princeton University, March 01, 2016

Likun Hua, Algal Destabilization by Titania Reactive Membrane Filtration and
Effects on Lipid, *Otto York Center Workshop*, NJIT, October 13, 2015

To my parents, relatives, friends and everyone accompanied me through this journey.
Thank you for making my life confident and colorful.
感谢我的父母、亲属、朋友以及所有陪伴我一路走过来的人们
你们令我的人生自信而绚丽多彩

ACKNOWLEDGEMENTS

First and foremost, I would like to express my sincere thanks to my dissertation advisor and the research project PI, Dr. Wen Zhang. He imparted upon me with his knowledge and insightful vision that brought me to an exciting and highly creative research field, where I gained and benefited from interdisciplinary training. He has continuously provided me guidance, insightful suggestions, and support throughout the course of my PhD research. Moreover, Dr. Zhang has always been supportive of the ideas I created, most of which have proven to be of great importance for the success of my research.

Special thanks go to my Committee members, Prof. Taha F. Marhaba, Prof. Kamalesh K. Sirkar, Dr. Sagnik Basuray, and Dr. Charles Liu. I want to especially thank them for finding time in their busy schedules to review this dissertation and provide suggestions, constructive and critical comments. I particularly want to thank Dr. Basuray for his guidance on electrochemistry. His insight and suggestions have pushed me toward a better and deeper understanding of electrooxidation processes. Dr. Liu provided me with helpful advice on water treatment and membrane commercializing. Prof. Marhaba and Prof. Sirkar both emphasized to me the importance of a clear and well-organized presentation in scientific research communications, which is truly beneficial to me. I want to thank them all for their considerate advice, important feedback and input.

It was my great honor to work with Paul Schorr from 2016 to 2017 during National NSF I-Corps program. As my industrial mentor, Paul deeply influenced me with his efficient, diligent, and dedicated character. He emphasized the importance of being a successful entrepreneur leader and how to achieve this goal. More importantly,

he gave me rigorous but valuable training on planning business models and stressed to me the importance of the "take-home lesson" of interviewing different potential customers, which is one of my greatest treasures received from working with him.

It was also a great honor to work with Orren Schneider from 2018 to 2019 during the second National NSF I-Corps program. Orren also served as our industrial mentor.

Many thanks go to Ms. Judith Sheft, the Associate Vice President of New Jersey Innovation Institute at NJIT for providing me with much advice and chances to join entrepreneur activities. I also want to thank Dr. Michael A Ehrlich from the NJIT Martin Tuchman School of Management for the instructions and assistance at the early stages of my I-Corps journey.

I want to thank Ms. Yuhong Jiang, the president of Brisea Group, Inc. for the support from her and her company during my application experience to SBIR and STTR programs held by NSF, EPA and other federal agencies which have small business innovation programs.

I also want to acknowledge Dr. Mengyan Li for sharing lab equipment with me and assisting my research from time to time, and his student Mr. Fei Li for their help on GC operation for 1,4-dioxane measurements.

Thanks to Prof. Boris Khusid and his student Mr. Lei Qian for sharing ideas of AC electrochemistry oxidation and cooperating with the experimental setup.

Thanks to Dr. Xueyan Zhang for advice and training on Raman, AFM, and SEM measurement and operation; Dr. Jeong Seop Shim for advice and training on XRD measurement and operation; Dr. Larisa G. Krishtopa for advice on HPLC operation; Dr. Liu from Wirtz Tech on the Raman test of algal and REM surface.

TABLE OF CONTENTS

Chapter	Page

Blank Page

LIST OF TABLES

LIST OF FIGURES

Figure   **Page**

CHAPTER 1

INTRODUCTION

1.1 Background and Challenges

Utilization of biomass-based raw materials (e.g., bacteria, algae, and cellulose) for the production of high value chemicals such as proteins, pharmaceuticals, and biofuels is gaining an increasing interest. Due to the complex nature of biomass, a common major challenge in its refining is the low efficient separation processes. For instance, oleaginous microalgae usually grow in low cell density in aqueous media (e.g., 0.1-1 g L^{-1}), and thus, dewatering of algae slurries contributes 20–30% of the total biorefinery cost for biofuel. Compared to many other separation methods, such as gravitational sedimentation, centrifugation, coagulation, chemical precipitation, filtration, and flotation, membrane separation processes such as ultrafiltration (UF) and nanofiltration (NF) have gained much attention in the biomass separation industry due to their high selectivity, relatively low energy costs and reduced chemical usage.[1-2] UF membranes can selectively remove not only large molecules such as proteins, viruses, and microorganisms through size sieving mechanisms but can also substantially reduce emulsion to improve the successive solvent extraction efficiency. MF membrane filtration was proved to separate algal biomass up to 150 g L^{-1} (dry weight) and ~99% volume reduction with relatively low energy consumption (Table 1.1).[3-9] However, traditional membrane separations suffer from membrane fouling due to either the formation of a cake layer of algal cells, or more commonly due to extracellular organic matter (EOM) adsorption onto the membrane surface.[10-11] Algal cells and EOMs are a complex mixture of polysaccharides, proteins,

1

nucleic acids, and other small biomolecules,[12-13] which could clog the micropores of membrane filter and reduce permeate flux. Once membrane fouls, frequent backwash or even replacement of membrane materials are needed, which substantially increase the operational cost and energy footprint of bioenergy produced.

Table 1.1 Comparison of Installation Cost, Energy Consumption and Dry Solid Concentration for Different Algal Separation Processes

Process	Installation cost	Energy Consumption ($kWh \cdot m^{-3}$)	Dry algal concentration
Chemical Flocculation	Low to median	0.3 or less	3-8 %
Centrifugation	High	8	10-22 %
Gravity sedimentation	Low	0.1	0.1-1.5 %
Membrane filtration	Median to High	1-3	2-27 %
Electrocoagulation	High	0.3-2	3-5 %
Flocculation-flotation	High	10-20	7 %

Algal biomass is the third generation feedstock for biodiesel or biofuel production. However, expensive algal harvesting, biomass pretreatment, and lipid extraction represent the major hurdles for producing cheap biofuels at industrial scales. Typical structures of algal cell walls contain uronic acids, glucosamine, and polysaccharides that provide cells with formidable defense against environmental conditions [14]. Extraction of biolipid that is usually located in globules or bound to cell membranes often involves the use of organic solvents such as n-hexane, chloroform and methanol because of their high selectivity and solubility towards lipids [15-16]. An efficient extraction requires that the solvent penetrates completely into the biomass and physically contacts the lipid (e.g., triglycerides-esters) located in the photosynthetically active membranes. Therefore, cell disruption is a necessary pretreatment step prior to lipid extraction.

Cell disruption and lipid extraction processes can be energy-intensive, time-consuming and costly. Current cell disruption methods include mechanical and non-mechanical techniques. Mechanical techniques destroy the cell wall using non-specific solid and liquid shear forces or energy transfer through heating and waves [17], which include compression, high-pressure homogenization (HPH) [18], ultrasonic bath [19], autoclave [15], bead mill, microwave and magnetic stirring [20-21]; while non-mechanical techniques include chemical lysing using enzymes or chemical agents and osmotic shock [22-23]. Selective interactions between chemical agents (enzymes, antibiotics, chelating agents, chaotropes, detergents, hypochlorite, acids and alkali) and the cell wall or membrane are designed to facilitate biolipid leaching [17]. Life-cycle assessment (LCA) of biofuel production from microalgae feedstock determined that cultivation, harvesting and lipid extraction accounted for up to 90% of the total process energy [24]. Further decreasing solvent consumption, preventing pollution, and enhancing lipid production (efficiency) are the major challenges in this field.

1.2 Relevance and Impact of the Research

Rapid and highly efficient biomass harvesting is not only critical for biomass engineering and biofuel production but also important water or wastewater treatment industries to produce cleaned water. Highly efficient algal biomass removal from water will lower the operational cost and increase the economic viability of produced products (biomass, biofuel or bioenergy, and cleaned water). However, traditional membrane separations suffer from membrane fouling due to either the formation of a cake layer onto the membrane surface that may consist of biomass debris, cells and organic matters. Thus,

developing innovative membrane filtration processes that can efficiently separate algae with strong antifouling characteristics is a pressing task.

My research aims to develop multifunctional reactive electrochemical membranes (REMs) that facilitated filtration technologies for efficient algal recovery with multiple potential synergies. Algae was used as a model biomass substituting microbial pathogen or biofuel feedstock materials to evaluate the bioseparation performances because, algae are considered the third generation of biodiesel fuel feedstock, but dewatering of algae slurries is a major bottleneck towards the implementation of large-scale industrial processing. The anticipated impacts from my work includes (1) significantly decreasing fouling during biomass separation through electrochemical oxidation and repelling algogenic organic matters (AOMs), (2) destabilizing cell walls to facilitate lipid extraction from algal cells while concentrating algae, (3) promoting water and nutrient reuse for continual algal growth, and (4) reduce cost and energy consumption for algal biofuel production. The REM technology was addressed many of the limitations associated with traditional membrane bioseparation processes and increase sustainability to our society by reducing the stress from water, resource, and renewable energy production.

1.3 Innovation

The REM we developed are based on Ti_4O_7 , a porous substoichiometric TiO_2 anodic material in various forms (i.e., monolithic porous ceramics). Ti_4O_7 is selected because of its high performance in generating hydroxyl radical (OH•) from water oxidation, stability under anodic and cathodic polarization, and low cost.[25-27] The monolithic porous Ti_4O_7

membrane shows a high water flux in filtration (5000-6000 L m^{-2} h^{-1} bar^{-1} or LMH bar^{-1}). These properties make Ti$_4$O$_7$ membranes an ideal material for sustainable algal recovery and biomass processing for lipid extraction. By applying a positive DC potential or current to the REM surface, the produced OH$\bullet$ oxidized EOMs to maintain a clean membrane surface and degrade inhibitors to promote water and nutrient reuse as shown in Figure 1.1. The positive charge imposed on the membrane also acted to electrostatically repel positively charged EOMs near the surface to prevent EOM adsorption and fouling. In addition, the oxidative surface of REM may also lead to partial chemical oxidation and breakdown of the cell walls during backwash, which may facilitate the downstream biomass processing such as lipid extraction, which has been verified in previous study. There have been no studies or commercialized applications of REMs for algal harvesting or removal. Specifically for this research, performance and mechanisms of algal destabilization that both remain elusive were addressed for the first time.
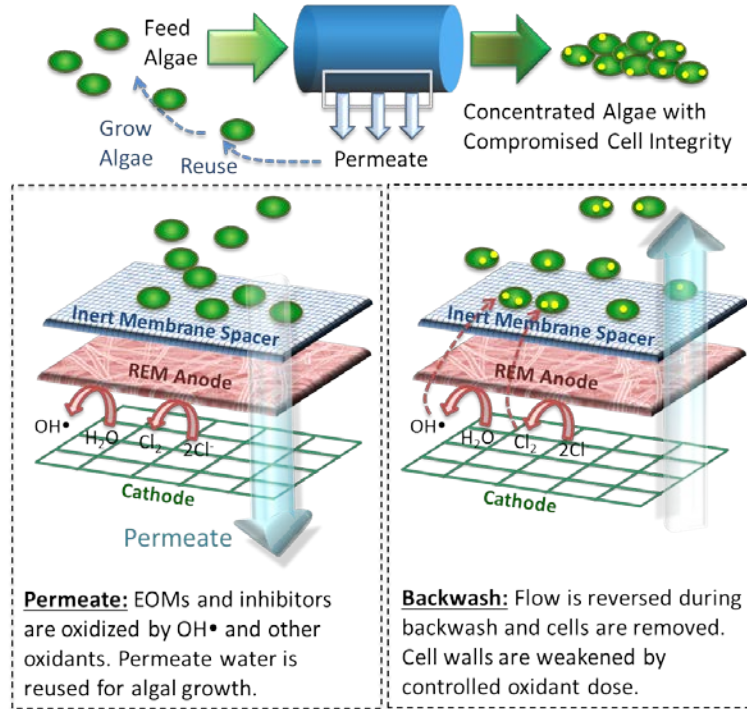
Figure 1.1 Schematic of the REM for algal separation basic flow diagram (a); and illustrations of the REM during filtration (b) and backwash.

1.4 Social Impacts.

This research primarily employed oleaginous microalgae as a model organism to evaluate separation efficiency and other anticipated benefits using REM. Algae hold great promise to be a sustainable biodiesel fuel feedstock, but dewatering of algae slurries is a major bottleneck towards the implementation of large-scale industrial processing. For example, dewatering process contributes 20–30% of the total biomass production cost.[3] Membrane filtration is superior to other separation techniques because of its enhanced efficiency, improved reliability, and reduced reactor dimensions, cost, and energy footprint.[3-4, 6, 28-30] However, physical membrane separation suffers from membrane fouling due to algal cell

deposition as well as EOM adsorption, and frequent membrane backwashing and cleaning is required to maintain a desired separation performance, which elevates the operational cost. Moreover, algal culture media contain a large amount of water (> 90% water compared with algal dry weight), unutilized nutrients, as well as algae produced inhibitors (e.g., H_2S, NH_3). Permeate after simple physical filtration is usually not suitable for continual algal growth because of the presence of inhibitors. Treatment for selective removal of inhibitors is required to reuse water and nutrient, which could significantly enhance the sustainability of algae-based biofuel production.

This work was transformative because it creates one integrated system to tackle several pressing challenges at energy-water nexus of bioseparation and water treatment. The results not only provided fundamental guidelines as to the rational design of REMs with controlled and efficient performance, flexible structure, and durability of operation, but also lead to an avenue for the applications of new generations of reactive transformative membranes in many industrial applications in addition to algal separation. For example, REMs can be used in food processing (e.g., wine or milk purification), drinking water treatment, bacterial separation, cellulose separation and oxidation, and biomolecule purification in pharmaceutical industries. This work greatly extends the application scopes of reactive membrane technologies and lay foundation toward versatile, efficient, flexible, durable, and sustainable membrane systems. Such an accomplishment would be transformative and radically change the fields of Energy, Environmental and Chemical Engineering, and has broad impacts on algal biofuel industries.

Algae-based bioreactor techniques are being revived for wastewater treatment and nutrient removal while the harvested algal biomass may be used for broad applications such as biodiesel and fertilizer production. [31-35]

Phototrophic growth studies provide critical information about the kinetics of phototrophic growth and their linkage to nutrient uptake, which are essential for the design and operation of algal ponds or photobioreactors.

Algal growth kinetics are often studied in batch experiments by determining the changes in biomass concentration (optical density or OD) [36-37], cell numbers[38], and chlorophyll *a* content[39]. However, these experiments often require a long period (>10 days) of cultivation to differentiate the changes and the results can be easily affected by biomass debris formation.[40] Furthermore, the changes in water pH, nutrient availability, biomass concentration, and self-shading of light by algae affect algal growth during the cultivation period, which may lead to an underestimation or overestimation of growth kinetics.[31]

Other techniques have been explored to determine algal growth kinetics by quantifying the photosynthetic products, such as oxygen or ^{14}C assimilation products from the Calvin cycle.[41-42] Oxygen evolution measurements with O_2 electrodes allow for oxygen production measurements in the light.[43] An extension of this method is the microamperometric oxygen evolution measurements by determining photosynthetic oxygen evolution using microelectrodes.[44-45] However, the insertion of microelectrodes could physically injure cells and trigger undesired intracellular.[44] Direct chlorophyll fluorescence measurement provides a sensitive analysis of photosynthetic activity based on the short-term change in chlorophyll fluorescence after light exposure.[46-48] However,

interference from light absorbing compounds, such as dissolved organic matter may cause a significant underestimation of photosynthetic activity.[48] On the other hand, ^{14}C-assimilation rate measurements reflect the activity of photosynthesis by quantifying the amount of dissolved inorganic carbon converted into cell biomass during photosynthesis. However, the ^{14}C techniques require the use of special equipment such as liquid scintillation counter and could result in significant variation in carbon fixed per unit chlorophyll due to nutrient limitation.[49] The variation of photosynthetic activities revealed by the above methods were not only caused by the use of different test endpoints, but were also affected by many important factors such as initial phototrophic cell density, light intensity and exposure time.[42] Therefore, it is necessary to develop a rapid, simple and reliable method to determine the photosynthetic activity of phototrophs upon light irradiation.[31]

Respirometry based on oxygen production has been proposed as a non-destructive and non-invasive approach to rapidly determine phototrophic activity.[43] Extant respirometry, which is reflective of conditions immediately before the assay, allows estimation of activated sludge growth kinetics and sludge decay rate coefficients by recording the dissolved oxygen (DO) profiles.[50-51] A high-throughput respirometric assay results in information-rich data, which can translate into high precision of estimated parameters.[52] The application of extant respirometry can be easily extended to phototrophic systems where the phototrophic activity and decay rate constant can be determined through the measurements of specific oxygen production rate (SOPR) in the light and specific oxygen uptake rate (SOUR) in the dark, respectively. Like SOUR measurement in extant respirometry, SOPR measurement is analytically facile because

the continuous acquisition of oxygen production by the phototrophs can be fully automated to avoid sampling errors and bias. In fact, respirometric methods have been explored and evaluated in photosynthetic studies for biokinetic parameter estimation. For example, photosynthetic rates obtained from respirometry suggest that the growth of diatoms is inhibited at higher light intensities. The respirometric method has been proposed for algal growth inhibition.[53] Unfortunately, previous methods to determine photosynthetic activity by measuring O_2 evolution are often ambiguous on what exact test devices are needed (e.g., the type and size of the bottles and whether or not the respirometric bottles should be filled completely without headspace) or test conditions such as carbon dioxide concentration in the mixed liquor, water pH and temperature, nitrogen source, light intensity, wavelength and light–dark period. The objective of this research was to develop a standard procedure to rapidly determine algal and cyanobacterial activities through SOPR measurement by taking into account these important factors affecting photosynthesis. The proposed SOPR measurement would, therefore, allow for determination of algal/cyanobacterial growth kinetics within minutes under different environmental and stress conditions (e.g., pH, nitrogen sources, chemical and metal exposure).[31, 54]

1.5 Algal Cell Pretreatment for Lipid Extraction

A variety of disruption methods is currently available for cell disruption. In general, these techniques are divided into two main groups based on the working mechanism of microalgal cellular disintegration, which is (i) mechanical and (ii) non-mechanical methods as shown in **Fig. 1.2**.[55]
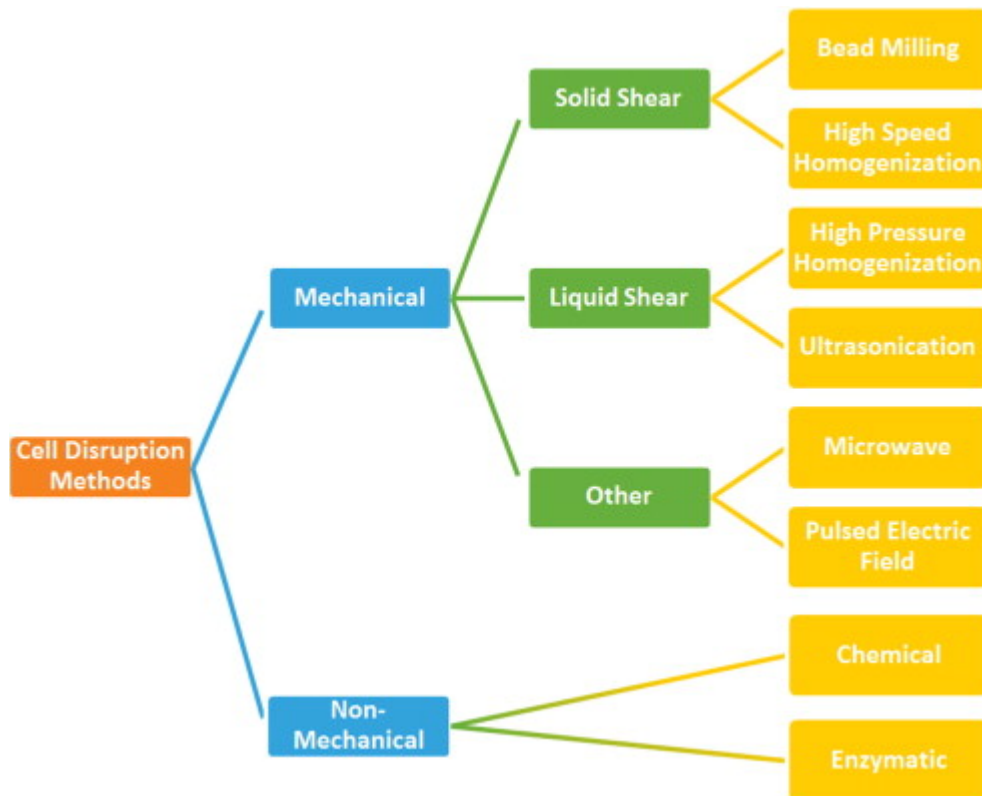
Figure 1.2 Classification of the cell disruption methods.[55]

1.5.1 Algal Cell pretreatment: methods and challenges

The ultrasound power is a very important parameter in sonochemistry. Normally, higher ultrasound power causes more violent cavitation and accelerates reactions.[56] But higher power costs more energy and is not always desirable. Table 1.2 reports the algae removal rate constants (k) under different ultrasound power levels.[57] The increase of ultrasound power from 32 W to 80 W (80 kHz) increased the k value from 0.007 min^{-1} to 0.023 min^{-1}. To achieve 90% cell removal efficiency, 328 min was needed at 32 W and 100 min was required at 80 W; the corresponding total energy consumption was 0.175 kW h at 32 W and 0.134 kW h at 80 W. Therefore, higher power was more energy efficient than lower power for algae cell removal. However, high power (80 W) increased microcystins concentrations in water, which was not observed under the ultrasonic power

of 32 W. Therefore, low ultrasound power was recommended for use in drinking water supply.[57]

Table 1.2. Impact of ultrasonic power on ultrasonic algae removal, 80 kHz

Power (W)	32	48	64	80
k (min^{-1})	0.007	0.013	0.018	0.023

Ultrasound frequency is another important parameter that defines the sound field and significantly influences the reaction kinetics. There was little difference in the algae removal rate constants among the low frequency range (20–150 kHz), but there was significant increase in the algae removal rate constant by increasing the frequency from 150 kHz to 410 kHz. The k value was 0.114 min^{-1} at 1320 kHz and 0.0224 min^{-1} at 20 kHz. This could be explained by the closeness of the size of algae gas vacuoles and the resonance size of cavitation bubbles. Ultrasound can collapse gas vacuoles that control algae movement during cavitation.[58-60] When the size of the gas vacuoles and the resonance size of cavitation bubbles are of the same order of magnitude, the gas vacuoles are more likely to resonate, undergo acoustic cavitation, and thus collapse. The resonance size of free bubbles at given ultrasound frequency can be estimated by:[57]

$$f = \frac{1}{2\pi a} \sqrt{\frac{3\gamma}{\rho}\left(p_0 + \frac{2\sigma}{a}\right) - \frac{2\sigma}{a\rho}},$$

where f is the ultrasound frequency, γ is the ratio of heat capacities of the gas at constant pressure and volume, a is the radius of the bubble, p_0 is the ambient pressure, σ is the surface tension, and ρ is the density of the surrounding medium. γ is 1.39 for air, ignoring the surface tension and assuming a density of 1.0 g·cm^{-3}, the resonance size of free air bubble in water is 0.166 mm at 20 kHz and 2.47 μm at 1320 kHz. Usually the gas vesicles of *microcystis aeruginosa* are up to 1 μm in length, so

algae gas vesicles are more likely to resonate with the sound wave and collapse at higher frequencies than at lower frequencies. Thus, the algae cells can be removed quicker at higher frequencies. To reach 90 % cell removal efficiency, 20 min was sufficient at 1320 kHz while 102 min was needed at 20 kHz.

The effectiveness of ultrasonic irradiation on algae removal by coagulation was studied. Laboratory results suggest that ultrasonic treatment at 40 kHz and 60 W for 15 s can improve algae coagulation removal by 12.4 % as compared with direct coagulation. A photometric dispersion analyzer was employed to monitor the algae coagulation in this study. It is also indicated that variation in ultrasonic frequency does not have a notable effect on algae removal while increasing ultrasonic power to more than 60 W produces a negative result. The optimal irradiation duration is determined as 15 s. In conclusion, ultrasonic irradiation-coagulation proves effective for algae removal. However, practical application still takes time due to certain limitations of the technique.[61]

1.5.2 Lipid extraction: methods and challenges

Chemical solvent extraction is the most common method because of high selectivity and solubility toward lipids including inter-lipid content, and the low cost of solvents and equipment that would allow scaling up this technology. However, petroleum solvents such as conventional n-hexane, chloroform and methanol, are highly energy-consumption and environmentally damaging. An efficient extraction requires that the solvent penetrates completely into the biomass and has a connection corresponding to the polarity of the target compound, thus physical contact between the material and the lipid solvent is related to the successful extraction. Because the major form of the lipids in algae is triglycerides-esters, located in the photosynthetically active membranes, cell

disruption usually is required prior to lipid extraction step in order to retrieve these intracellular-membrane lipids more efficiently. The cell disruption methods aim to increase the lipid release from the microalgae using mechanical and non-mechanical techniques. In spite of advances in developed methods, due to the thick and rigid cell wall of microalgae that blocks the release of intra-lipids, the cell disruption and lipid extraction from microalgae often turn to be energy-intensive, time-consuming and costly.

The disrupted algal cells have ruptured cell walls/membranes that facilitate the contact of solvent and biolipid and thus enhance the biolipid extraction.

Currently, several studies are focused in solvent extraction and supercritical solvent extraction, for dry and wet paste microalgae biomass. Other extraction processes such as supercritical CO_2, expelling, microwave-ultrasonic assisted extraction have also been reported. A recent life-cycle assessment (LCA) of biofuel production from microalgae feedstocks mentioned that drying and n-hexane extraction accounted for up to 90% of the total process energy. Thus, the current challenges are how to decrease the solvent consumption, to increase pollution prevention and the extraction yield, to enhance the quality of final products (to preserve lipids' unsaturated bonds), and to shorten the extraction time.

Mechanical techniques include compression, high-pressure homogenization, ultrasonic bath, autoclave, bead mill, microwave and magnetic stirring, pulsed electric field (PEF) charging, while non-mechanical techniques include chemical lysing and osmotic shock. The common structure of algal cell wall contains uronic acids and glucosamine in addition to other polysaccharides such as glucose, rhamnose, galactose,

xylose, arabinose, mannose and glycoprotein matrix, providing the cells with formidable defense against its environment. Therefore, in spite of advances in developed methods, the cell disruption and lipid extraction from microalgae often turn to be energy-intensive, time-consuming and costly. Clearly, it is highly desirable to develop a faster and environmentally safer microalgal lipid extraction technique, which is the thrust of this patent application.

As a way to massively pretreat algal cells and break down cell walls prior to biolipid extraction has potential to: decrease the organic (toxic) solvent consumption, increase pollution prevention and the extraction yield, enhance the quality of final products (to preserve lipids' unsaturated bonds), and shorten the extraction time.

Viral infection results in algal cell lysis and account for acceptable cell disruption in algae prior to lipid extraction compared to other harsh cell rupturing processes that consume more energy or time.

Thus, compared to the harsh cell treatment using mechanical or non-mechanical processes, it is highly desirable to develop a faster and environmentally safer cell disruption process to facilitate microalgal lipid extraction. The overall aims are to decrease the solvent consumption, to increase pollution prevention and the extraction yield, to enhance the quality of final products (to preserve lipids' unsaturated bonds), and to shorten the extraction time. This patent describes a biological method using virus-host interaction mechanisms to effectively rupture algal cells without the intensive use of chemicals. The treated algal cells are ready for lipid extraction at a reduced demand of organic solvent and thus increase the economic viability and environment benefit.

Another possible process is gasification of the algae, where the biomass is heated up to high temperature of about 1000 degrees Celsius. The partial oxidation of the biomass produces a mixture of combustible gases known as syngas. Then syngas can be used directly to produce energy or can be used as a fuel to power diesel or gasoline engines. This is an environmentally friendly method of converting biomass into energy, because it is not heavily-energy depended and only uses super-heated water as a solvent. The water breaks and completely dissolves the organic compounds in the algae and heats the components to form the syngas.

One of the promising new technologies used for extractions has been pyrolysis and catalytic cracking; a process where the algal biomass is heated in the absence of oxygen. This produces liquid fuel, which is very similar to traditional petroleum diesel. The fuel produced is sufficient to use in engines and does not release large amounts of sulfur oxides and does not corrode copper. However, this method is not viable at the moment due to elevated levels of carbon residues which result from the burning of this fuel. More research needs to be done to bring this technology within current acceptable environmental levels.

The extraction technology that is gaining the most traction in its environmental and economic feasibility is hydrothermal liquefaction (HTL); a process where the algal biomass is converted into liquid fuel. Basically, the process involves heated water (250-350°C) interacting with biomass in the presence of a catalyst2. The biomass breaks into small, reactive and unstable molecules and then recombines to form a range of molecular products. Recent studies have shown that, depending on the species, liquefaction of microalgae can produce between 30%-65% dry weight of oil. The

bioreactors necessary to perform this process are the major cost in extracting oil, but this method has been found to be energy positive and more effective than conventional extraction. HTL experimental studies have shown that the process produces higher bio-oil yields and produces a better quality of bio-oil for upgrading to fuel2. Presently, there are several methods of extraction that are still being tested for production and cost-effectiveness; and more research needs to be done to create a universally acceptable system that meets environmental guidelines. Currently, the hydrothermal liquefaction method appears to be leading the way in overall oil yield and quality as well as return on monetary investment in the process.

1.6 Emerging contaminates

Poly- and perfluoroalkyl substances (PFASs) are a group of anthropogenic chemicals which have been produced for over 60 years., Their uses include military applications, and consumer products, such as nonstick coatings, food packaging such as ScotchGard[TM] and Teflon[TM], water-proof clothing, fire extinguishing equipment, electronics, and aqueous film-forming foams (AFFFs).[62] For example, AFFF formulations that have been used to suppress fires contain significant quantities of PFOS and related perfluoroalkyl sulfonates such as PFHxS. As a result, hundreds of sites are found with associated PFAS contamination due to the DoD's legacy use of AFFF.

PFASs are also commonly referred to as perfluorinated chemicals or PFCs. The most notable PFASs are perfluorooctanoic acid (PFOA) and perfluorooctane sulfonate (PFOS) due to their toxicity and recalcitrance to many natural and enhanced degradation mechanisms such as hydrolysis, photolysis, microbial degradation, and metabolism by

organisms. The PFAS structure consists of a totally fluorinated carbon chain of varying length and a charged functional group, such as carboxylic or sulfonic acid.[63] Thus, they are also soluble in water and can enter source waters through industrial releases, discharges from wastewater treatment plants, storm water runoff, release of firefighting foams, and land application of contaminated biosolids. As a result, PFASs are increasingly found in environmental media worldwide, including finished drinking water, surface water, groundwater, air, sludge, soils, sediments, outdoor and indoor dust, biota, and the polar ice caps.[63-65]

PFASs are suspected of endocrine disrupting, and have been shown to bioaccumulate and cause acute/chronic toxicity in certain organisms. Exposure to PFASs can occur through use of products or consumption of food or water containing PFASs. Long-term contact with such material may increase the risk of kidney cancer, thyroid disease, high plasma lipids, liver and body weight reduction, alveolar wall thickening, mitochondrial damage, gene induction, increases in larval mortality, and increased susceptibility to disease.[66] According to the San Antonio Statement and the Madrid Statement,[67-68] PFASs are a concern because they have been shown to have adverse effects on animal health in studies. Data from some human studies suggest that PFASs also affect human health. The EPA's health advisory levels (HALs) indicates that drinking water, with individual or combined concentrations of PFOA and PFOS, (below 70 parts per trillion), is not expected to result in adverse health effects over a lifetime of exposure.[69] However a recent report documented that up to 6 million U.S. residents might be exposed to drinking water that exceeds these HALs.[70-71]

Recent studies have shown that conventional water or wastewater treatment processes are ineffective at removing perfluorochemicals.[72] The Water Research Foundation (WRF) has released findings of a study addressing effective methods for removing poly- and perfluoroalkyl substances (PFASs) on waters collected from 13 water and wastewater treatment plants in the United States. The research report (WRF project #4322) indicated that aeration, chlorine dioxide, dissolved air flotation, coagulation, flocculation, sedimentation, granular filtration, and microfiltration are all ineffective for removing PFASs including PFOA and PFOS. Activated carbon and anion exchange can remove most of PFASs but are less effective at removing shorter chain PFOA and PFOS. The most effective treatment technologies are nanofiltration and reverse osmosis, which have costly investment, operation and maintenance (due to fouling). More importantly, these removal methods do not completely result in chemical degradation and destruction, but rather a separation and concentration of PFASs, which require further disposal of the concentrated slurry (perhaps via landfill or incineration). However, landfilling or incineration is both costly and poses additional transportation requirements. Thus, more sophisticated and novel treatment technologies are in need to effectively address real-world complexities of PFOA and PFOS mixtures and contaminants present in environmental matrices.

CHAPTER 2

ALGAL DESTABILIZATION BY Ti$_4$O$_7$ REACTIVE MEMBRANE FILTRATION AND EFFECTS ON LIPID EXTRACTION

2.1 Introduction

Algae are one of typical water contaminants that affect water quality and drinking water security. Meanwhile, algal biomass can be the third generation feedstock for biodiesel or biofuel production. Thus, efficient algal separation or removal from water is not only critical for safe drinking water supply but also important for biofuel production. Due to the small size (typically 2–20 µm in diameter) and low density (e.g., 0.5–5 g-dry weight·L^{-1}) of algal cells in growth media, most conventional algal separation methods such as gravitational sedimentation, centrifugation, microstraining, chemical coagulation, precipitation, filtration and flotation are often cost prohibitive, energy- or time-consuming.[73-75] Rapid and high efficient algal harvesting or removal is clearly critical for water treatment industries as well as for biomass engineering and biofuel production. Specifically, high efficient algal biomass removal from water could lower the operational cost and increase the economic viability of produced products (biomass and cleaned water).

Membrane filtration is one of the potentially efficient processes for algal separations because of its simple operation and energy savings. However, traditional membrane separations suffer from membrane fouling due to either the formation of a cake layer of algal cells, or more commonly due to organic matter adsorption onto the

membrane surface.[76-77] Thus, developing innovative membrane filtration processes that can efficiently separate algae with strong antifouling characteristics is a pressing task.

Reactive electrochemical membranes (REMs) based on electrochemical advanced oxidation processes (EAOPs) are a cutting-edge class of membranes that holding great promise in revolutionizing water and wastewater treatment and bioseparation.[78-79] REMs are porous and act as three-dimensional electrodes that are operated in flow-through mode.[78, 80] Radicals such as hydroxyl radicals (OH•) could be formed via water oxidation at an anode surface when the electric potential is supplied.[81-82] Thus, the antifouling potential of REM is promising, as organic foulants could undergo electrochemical adsorption and rapid oxidation by OH•.[83] Recent work has shown that the use of porous substoichiometric TiO_2 (e.g., Ti_4O_7) anodes in flow-through filtration mode creates a REM, which combines microfiltration with electrochemical oxidation.[78, 83] The micrometer-sized pores of the REM produced a high electroactive surface area and advection-enhanced mass transfer rates approximately 10-fold higher than those obtained in traditional flow-by mode. By converting TiO_2 to Ti_4O_7 (usually at temperatures above 900 °C under a H_2 atmosphere),[84] electrical conductivity can be increased from 10^{-9} $\Omega^{-1} \cdot cm^{-1}$ (TiO_2) to 166 $\Omega^{-1} \cdot cm^{-1}$ (Ti_4O_7).[85] The REM also utilized Ti_4O_7 electrodes supported on monolithic porous ceramics or electrospun carbon nanofibers (CNFs). This type of membrane shows a high water flux in filtration and superior properties in both flexibility and mechanical strength. REM presents a new viable technology that holds potential for efficient sustainable algal separation. Past research with REMs has focused only on dissolved compound oxidation, but their ability to provide efficient algal separations is unexplored. Therefore, there is a pressing need to apply REM to algal

separation and to evaluate its technical feasibility and cost effectiveness, compared to traditional membranes or other algal harvesting methods. Additional synergistic benefits are also worth investigating, including algal pretreatment via anodic oxidation, antifouling characteristics, and removal of algal growth inhibitors from water media that could be reused.

Expensive cell concentration and lipid extraction procedures represent one of the bottlenecks of large-scale algal biotechnological processes. One of the key challenges faced by algae biofuel industry is lack of energy-efficient and cost effective methods for disrupting algae cells for the separation and extraction of bioproducts.

Typical structures of algal cell walls contain uronic acids, glucosamine, and polysaccharides that provide cells with formidable defense against the environment.[14, 86] Extraction of biolipid that is usually located in globules or bound to cell membranes often involves the use of chemical solvents such as n-hexane, chloroform and methanol because of high selectivity and solubility toward lipids.[15,16] An efficient extraction requires that the solvent penetrates completely into the biomass and physically contacts the lipid (e.g., triglycerides-esters) located in the photosynthetically active membranes. Therefore, cell disruption is a pretreatment step prior to lipid extraction. Current cell disruption methods include mechanical and non-mechanical techniques. Mechanical techniques destroy the cell wall using non-specific solid and liquid shear forces or energy transfer through heating and waves,[17] which include compression,[87] high-pressure homogenization (HPH),[88] ultrasonic bath,[89] autoclave,[15] bead mill,[90] microwave and magnetic stirring,[20,21] pulsed electric field (PEF) charging,[91] while non-mechanical techniques include chemical lysing using enzymes or chemical agents and osmotic shock.

Non-mechanical methods are viewed as less harmful than mechanical processes as the cells are not shredded but perforated. Selective interactions between chemical agents (enzymes, antibiotics, chelating agents, chaotropes, detergents, solvents, hypochlorites, acids and alkali) and the cell wall or membrane are designed to allows biolipid to leach.[17] Cell disruption and lipid extraction processes can be energy-intensive, time-consuming and costly. A recent life-cycle assessment (LCA) of biofuel production from microalgae feedstock mentioned that cultivation, drying and n-hexane extraction accounted for up to 90% of the total process energy.[92] How to decrease the solvent consumption, to prevent pollution, and to enhance the quality of final products (to preserve lipids' unsaturated bonds) and lipid production (efficiency) are the major challenges in this field.

Our overall research aim is to explore substoichiometric TiO_2 REMs for efficient algal recovery and pretreatment with potential antifouling capability while maintaining high flux and excellent stability under anodic and cathodic polarization.[25, 93-94] The specific hypothesis to be tested in this study is that with a positive electrical potential applied to the REM surface during membrane backwash, the negatively charged algae may have intensive surface contact with REM due to electrostatic interactions. As shown in Figure 2.1, the produced OH• and other oxidative species oxidized the surface algal cells, which could promote cell disruption, reduce surface fouling, and potentially degrade algal growth inhibitors to permit water and nutrient reuse. The disrupted or ruptured cell walls/membranes may facilitate the contact of solvent and biolipid and thus enhance the biolipid extraction, which was investigated.
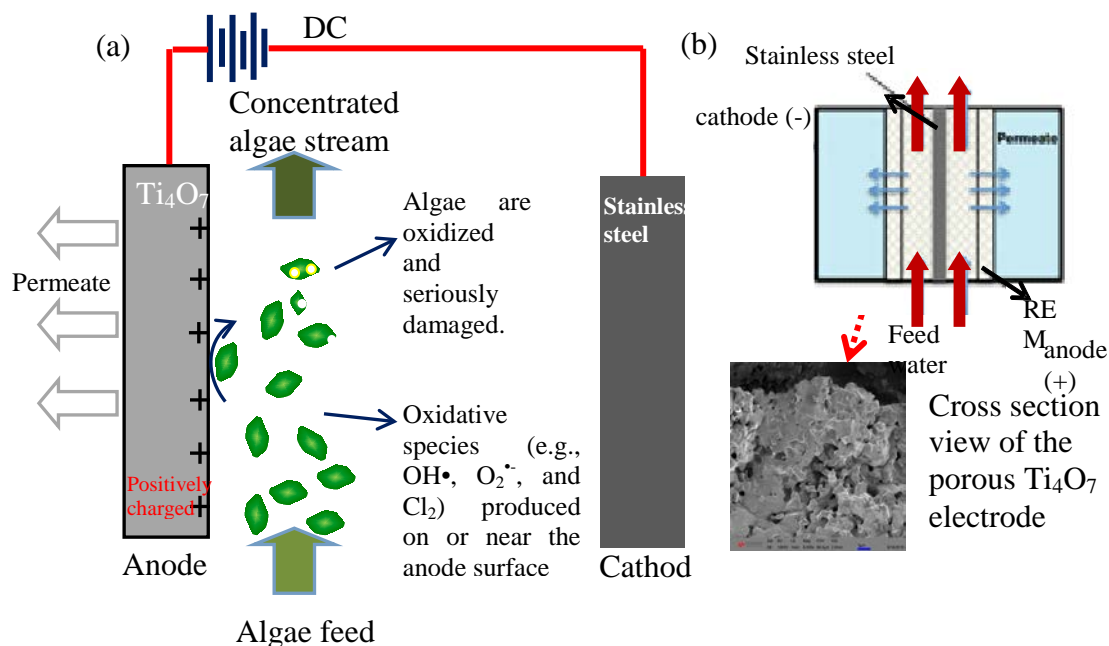
Figure 2.1 (a) Schematics of algal concentration and destabilization during the REM filtration process. (b) the configuration of the feed water and permeate flux through the REM (adapted from ref.[78]).

2.2 Method and Materials

2.2.1 Synthesis of Ti$_4$O$_7$ REM electrodes

The REM used in this study was a 10-cm long Ebonex one-channel tubular electrode, with the outer and inner diameters of 10 mm and 6 mm respectively (Vector Corrosion Technologies, Inc.). Ebonex is a Magneli phase suboxide of TiO$_2$, which consists primarily of Ti$_5$O$_9$ and Ti$_4$O$_7$.[85] In order to increase conductivity of the electrode and obtain a higher Ti$_4$O$_7$ content, the as received electrodes were subjected to another reduction process. The tubular electrode was first soaked in a 0.625-M sodium hydroxide solution for 24 hours to remove possible organic contaminants, and then rinsed with DI water. The clean electrode was placed into a tube furnace (MTI OTF-1200X). The

furnace was purged with N_2 gas (Praxair 99.99%) for 30 min, and then purged with H_2 gas (Praxair 99.99%) to remove oxygen. The furnace was heated to 200^oC for 1 hour, to desorb water, and then was reduced under H_2 flow at 1050 ^oC for 10 hours with a heating and cooling rate of $5^oC \cdot min^{-1}$.

As we reported earlier,[78, 83] the Ti_4O_7 electrode has a median pore diameter of 1.7 μm with pore diameters of <10 nm accounting for >90% of the surface area. The Ti_4O_7 electrode had porosity of $30.7 \pm 2.8\%$ and a specific surface area of 2.8 ± 0.7 $m^2 \cdot g^{-1}$, and a roughness factor of 619. FE-scanning electron microscope (SEM) and Energy-dispersive X-ray spectroscopy (EDS) were performed on a JSM-6010PLUS/LA (JEOL USA, Inc.). X-ray Diffraction (XRD) was recorded for the crystallography using a Philips PW3040 X-Ray Diffractometer. The BET surface area was measured with the Micromeritics® AutoChem II 2920 equipped with a thermal conductivity detector (TCD). Raman tests were executed for surface composition analysis by using a WITEC ALPHA300 Confocal Raman microscope.

.
2.2.2 Algal cultivation and preparation

Oleaginous algal cells (*Scenedesmus dimorphus* or *S. dimorphus*) were cultivated in the modified Bold's Basal Medium (MBBM) with details reported in our previous works.[73-75] Briefly, *S. dimorphus* was cultivated in a 2-L Erlenmeyer flasks at the room temperature (25 ± 1 °C) with CO_2 at a rate of 8.5×10^{-4} $L\text{-}CO_2 \cdot min^{-1} \cdot (L\text{-medium})^{-1}$.[95-96] The light-dark cycle (12 h/12 h) was maintained at a photon flux of approximately 4200 $mWatt \cdot m^{-2}$ measured by a spectroradiometer (Spectral Evolution, SR-1100). The algal concentration ($g \cdot L^{-1}$) was characterized by the dry cell weight (DCW). The steady-state algal

concentration after 14-day incubation was around 1.4 $g \cdot L^{-1}$, which was then subject to algal harvesting experiments and other tests.

2.2.3 Cell treatment by DC-charged REM and the cellular impact characterization

To study the cell damage by the exposure to electrochemical reactions at the REM, an electrochemical batch reactor was used (Figure 2.2). The reactor was filled with the algal suspension (the green liquid in Figure 2.2a), where the REM was immerged as the anode (the dark gray rod in the center), which was surrounded by a stainless steel circular mesh as the cathode with a spacing of 2.5 cm. The REM was operated at a constant current (100–500 mA) using a DC power supply (Proteck P6035, Tempe, AZ) corresponding to cell voltages between 10–20 V and for different times (30–120 min) to achieve different algal disruption. The effective exposed surface area of the REM was 25.4 cm^2. The conductivity of algal medium was 1040±5 $\mu m \cdot cm^{-1}$, whereas the conductivity of algal medium with algal cells ranged from 1580±20 to 2520±10 $\mu m \cdot cm^{-1}$ for newly inoculated algal culture and the culture after 14 days of incubation, respectively.

2.2.4 Cellular impact characterization

The impacts of REM exposure on the algal cell integrity were assessed by (1) morphologic changes, (2) surface composition changes, (3) photosynthetic activity, and (4) dissolved organic matter (DOM) in algal suspension.

2.2.4.1 Morphology and surface composition. Cell morphology (size and shape) was examined by a fluorescent microscope (3012 Series, Miller Microscopes, Feasterville, PA) and a Keysignt 8500B scanning electron microscope (SEM). Surface morphology,

roughness, and rigidity were also examined by Atomic Force Microscope (AFM) on a NT-MDT AFM (NTEGRA Prima, Tempe, AZ) using a rectangular silicon nitride (Si_4N_3) cantilever (MLCT model; Bruker AFM Probes). Algal surface compositions were assessed by Fourier Transform Infrared (FTIR) Spectrometer. FTIR was performed on a Nicolet ThermoElectron FTIR spectrometer.

2.2.4.2 Algal photosynthetic activity. Algal photosynthetic activity was monitored by *in vivo* fluorescence using a Turner Designs' Trilogy Fluorometer with an optical block for *in vivo* chlorophyll a measurement (excitation 485 nm; emission 685 nm with bandwidth of 50 nm).[97] Briefly, 25 μl of algal suspension was taken and stabilized in the dark for 10 min. Then, 2 ml of media was added to the algal suspension, which was then subject to the fluorescence measurement immediately. Moreover, the specific oxygen production rate (SOPR) was monitored as a non-destructive and non-invasive approach to determine phototrophic activity of algae.[31]

2.2.4.3 The specific oxygen production rate (SOPR). SOPR serves as a non-destructive and non-invasive approach to rapidly determine phototrophic activity of algae.[31] Due to photosynthesis under light illumination, the dissolved oxygen (DO) profiles over time were recorded and compared for treated and untreated algal cells. Prior to the SOPR tests, the algal suspension (0.7~1 g·L^{-1} and 500 ml) was purged with N_2 gas to reduce the initial DO to approximately 1–3 mg/L or less. Sodium biocarbonate ($NaHCO_3$) was added to the suspension at a final concentration of 4 mM to supply sufficient CO_2 for photosynthesis. The suspension pH was adjusted to 7.0 by 1 M HCl or 1 M NaOH. The suspension in the bottles was stirred

at 100 rpm to ensure complete mixing. With the bottles covered with aluminum foil, the test culture was kept in the dark for a short period before it was exposed to a fluorescent light at an intensity of 50 ± 5 $\mu mol \cdot m^{-2} \cdot s^{-1}$. As shown in Figure 2.2b, the DO
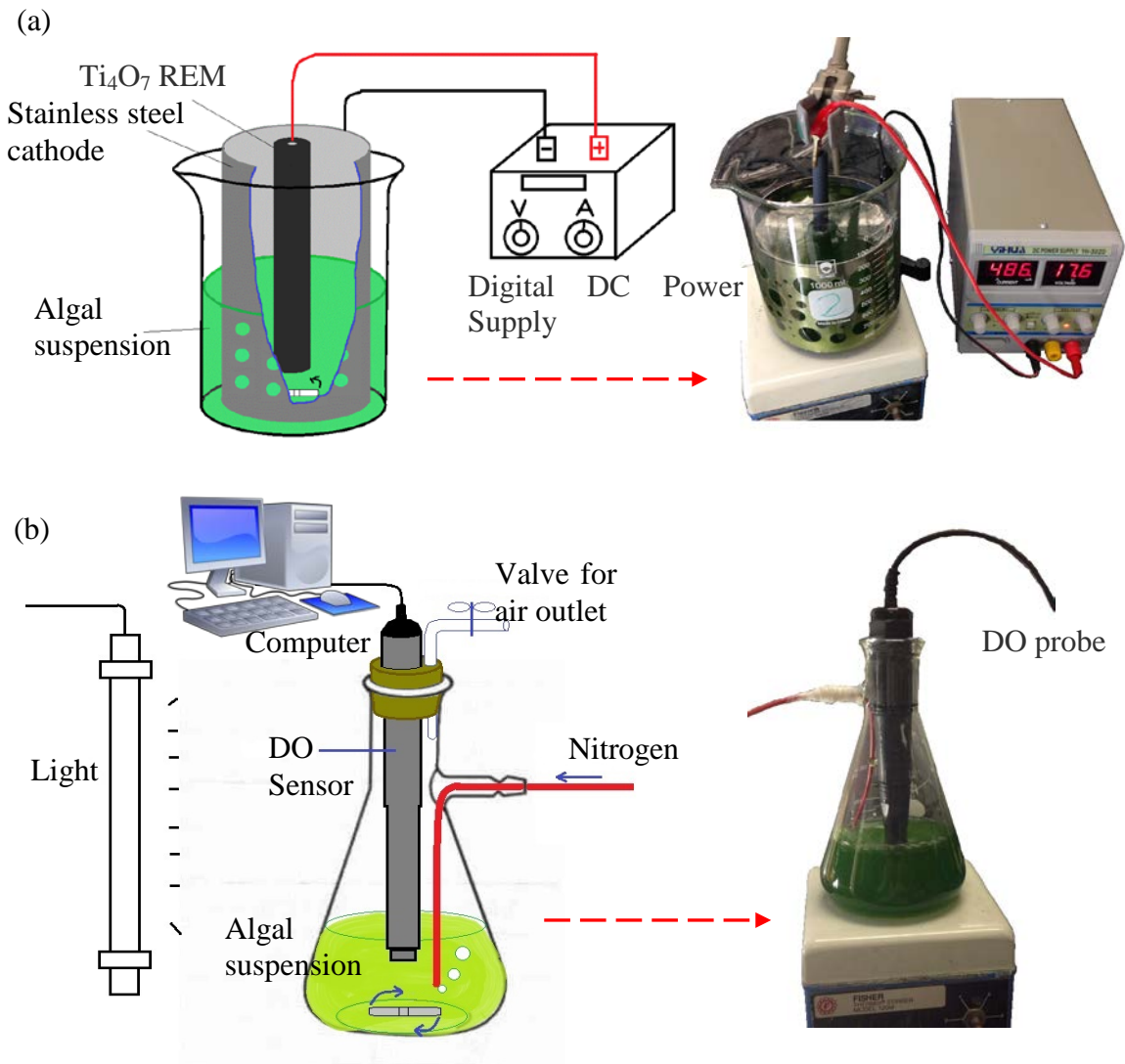
concentration in the bottle due to photosynthesis was measured by a DO probe (PASPORT Optical Dissolved Oxygen Sensor, PASCO scientific, California, USA) at the room temperature of 23 ± 1 °C and continuously monitored at 1 Hz by the Pasco Capstone software on a computer.

Figure 2.2 Bench setup for (a) REM treatment and (b) the measurement of photosynthetic activity of untreated or treated algae.

2.2.4.4 DOM analysis using UV-vis and EEM spectra. DOM in algal suspension could originate from the released extracellular polymeric substances (EPS) from algae. Particularly for the damaged or lysed algae, the cytoplasm could be released leading to changes of the DOM types and concentrations. DOM was characterized by a Thermo scientific Evolution 201PC UV-vis spectrophotometer and a Hitachi FL4500 fluorescent spectrophotometer. The algal suspension was first centrifuged at $10,000 \times g$ for 15 min to remove suspended particles or large debris. The supernatant was then tested in a quartz cuvette by the UV-vis and florescence spectrophotometer. The UV-vis and fluorescent spectra as well as the 3D excitation/emission matrix (EEM) spectra were all obtained. The slit for excitation and emission was 10 nm, and the voltage of the photomultiplier tube was set to 400 V at a sample scan rate of 12,000 nm·min^{-1}. Deionized (DI) water blanks were run to monitor the instrument stability. The data were analyzed by Excel 2007 (Microsoft Company) and Origin 9.1 (Origin Lab Company).

2.2.4.5 Molecular weight (MW) distribution of DOM. The MW distribution of DOM was analyzed by both DLS and high performance liquid chromatography (HPLC). DLS was performed on a Zetasizer nano ZS instrument (Malvern Instruments, UK), while HPLC used an HPSEC (LC-20AT, Shimadzu, Japan) system with the combination of a TSK gel G3000PWXL column (0.78 cm × 30 cm) and a TSK gel G2500PWXL column (0.78 cm × 30 cm) in series. The HPSEC was coupled to a photodiode array detector (SPD-M20A, Shimadzu, Japan) and an on-line TOC detector (TOC, Sievers 900 Turbo TOC, GE, USA). The mobile phase was a phosphate buffer (2.4 mmol·L^{-1}

NaH$_2$PO$_4$ and 1.6 mmol·L^{-1} Na$_2$HPO$_4$) and 25 mmol·L^{-1} Na$_2$SO$_4$. The flow rate was 0.5 mL·min^{-1}. Sodium polystyrene sulphonate standards (34700, 10600, 6800, 4300 and 1670 Da, PSS Polymer Standards Service GmbH, Germany) were used to calibrated the MW distribution. The supernatant of the algal suspension was subject to 0.45-μm polyethersulfone membrane filtration prior to the injection into HPLC.

2.2.4.6 Fluorescent staining.   Propidium iodide(PI) binds to DNA and emit 617-nm fluorescent at excitation wavelengths of 460-490 nm.[98] Generally, PI is impermeable to cell membrane and thus cannot stain viable cells. PI was used to stain treated and untreated algal cells to indicate cell damage from REM exposure. Damaged algae allowed PI to penetrate into cytoplasm and bind to DNA. Briefly, PI was first pre-diluted using DI 10 μL of pre-diluted PI solution was added into 1 ml of algae suspension (1.4 g/L) and incubated for 15 minutes in the dark. The stained suspension was then spread on glass slides and observed under fluorescent microscope (EVOS™ FL Cell Imaging System, Thermo Fisher Scientific).

2.2.5 Lipid extraction

2.2.5.1 Heterogeneous extraction

The untreated and treated algal biomass was vacuum dried at room temperature prior to the solvent extraction, where non-polar organic solvents disrupt the hydrophobic interactions between non-polar/neutral lipids of the algae cells.[99-100] By breaking down the cell, the lipids can be extracted leaving behind the residual biomass called the lipid-extracted algae (LEA), which can be as much as 85% of the dry weight of the algae. To extract lipid, aliquots (*ca.* 0.5 g) of dried algal biomass were extracted with 40 ml of 2:1

dichloromethane: methanol with 400-W microwave irradiation for 45 min, and then centrifuged at 1,000×g for 15 min. The supernatant was transferred into a preweighed test tube while the pellet was successively re-extracted with a 1:1 and then a 1:2 dichloromethane: methanol solution. The supernatant from each step was transferred to the same test tube. DI water (50 ml) was added to the test tube and incubated at 4°C overnight. The lower organic layer was collected and evaporated using a Thermo Savant AES1010 Automatic Environmental Speedvac system (Thermo Fisher Scientific, Waltham, MA). Dry weights of the samples were determined. Lipid content was calculated by dividing the dry weight of the extracted lipid by the dry weight of the samples used for lipid extraction (g-lipid·g-algae^{-1}).

2.2.5.1 Homogeneous extraction

Algal cell suspensions of 500 mL at 1.4 g/L of biomass were treated under 500 mA (with different time duration), and then each suspension had 150 mL n-hexane added and was stirred for 2 h with a magnetic stirrer to extract lipid. After the extraction, the mixture was centrifuged to separate the water phase and organic solvent phase. Then, the hexane phase and the emulsified phase had water added and was further stirred to break emulsion and wash out the hygrophilous substances. The hexane phase was collected again through separating funnel and the lipid was obtained from the hexane phase by evaporating n-hexane. The extracted lipid was weighed after being dried in an oven at 80 °C for 2 h.[101]

2.2.6 Fatty acid composition analysis

A fatty acid composition analysis was performed using a gas chromatograph (Shimadzu GC-2010, Japan). Fifty milligram samples were placed into capped test tubes, saponified with 1 ml of a saturated KOH–CH$_3$OH solution at 75 °C for 10 min, and then submitted

to methanolysis with 5% HCl in methanol at 75 $^{\circ}$C for another 10 min. Thereafter, the phase containing the fatty acids was separated by adding 2 ml of distilled water and then recovered. The components were identified by comparing their retention times and fragmentation patterns with those for standards.[102] Six fatty acids (C16:1, C17:0, C18:0, C18:1, C18:2, and C18:3) were used as the standard materials.

2.2.7 Statistical Analysis

Algal treatment experiments were carried out in duplicate for each condition. Filtration and lipid extraction were performed in duplicate or higher. The presented results are mean values ± standard deviation from three independent experiments. The differences between experimental groups and control groups were tested for significance using one-way analysis of variance (ANOVA) at a 5% significance level ($p= 0.05$).

2.3 Results and discussion

2.3.1 Characterization of REM

The morphology of the REM surface was characterized using SEM previously (Figure 2.1b),[78] which showed a pore size range of approximately 1–6 μm, a porosity of 30.7 ± 2.8% and a specific surface area of 2.78 ± 0.7 m^2·g^{-1}. The XRD data in Figure 2.3 shows that the lab-synthesized Ti_4O_7 exhibited similar crystallinity as compared to the standard Ti_4O_7.
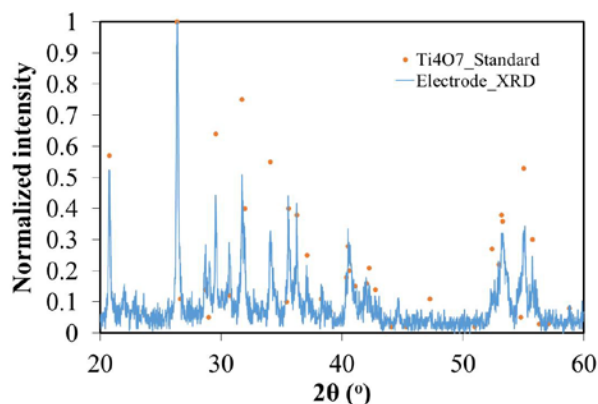
Figure 2.3 XRD spectra for standard Ti_4O_7 and our lab-synthesized Ti_4O_7.

2.3.1 Fluorescent properties of REM and algae

The Fluorescent properties of the REM and dried algae surface were investigated using Confocal Raman microscope. Figure 2.4 shows different titanium oxide species existed on the REM surface. Three peaks with strong intensities at 148.17, 436.7, and 619.25 cm^{-1} can be observed in the Raman spectra of the REM debris, which are close to that of reported titanium oxide anatase.[103] Figure 2.5 shows Raman spectra of the on the dried and treated algae surface. The peak at wavelength 575.37nm is believed to be the NOM of algae cells.
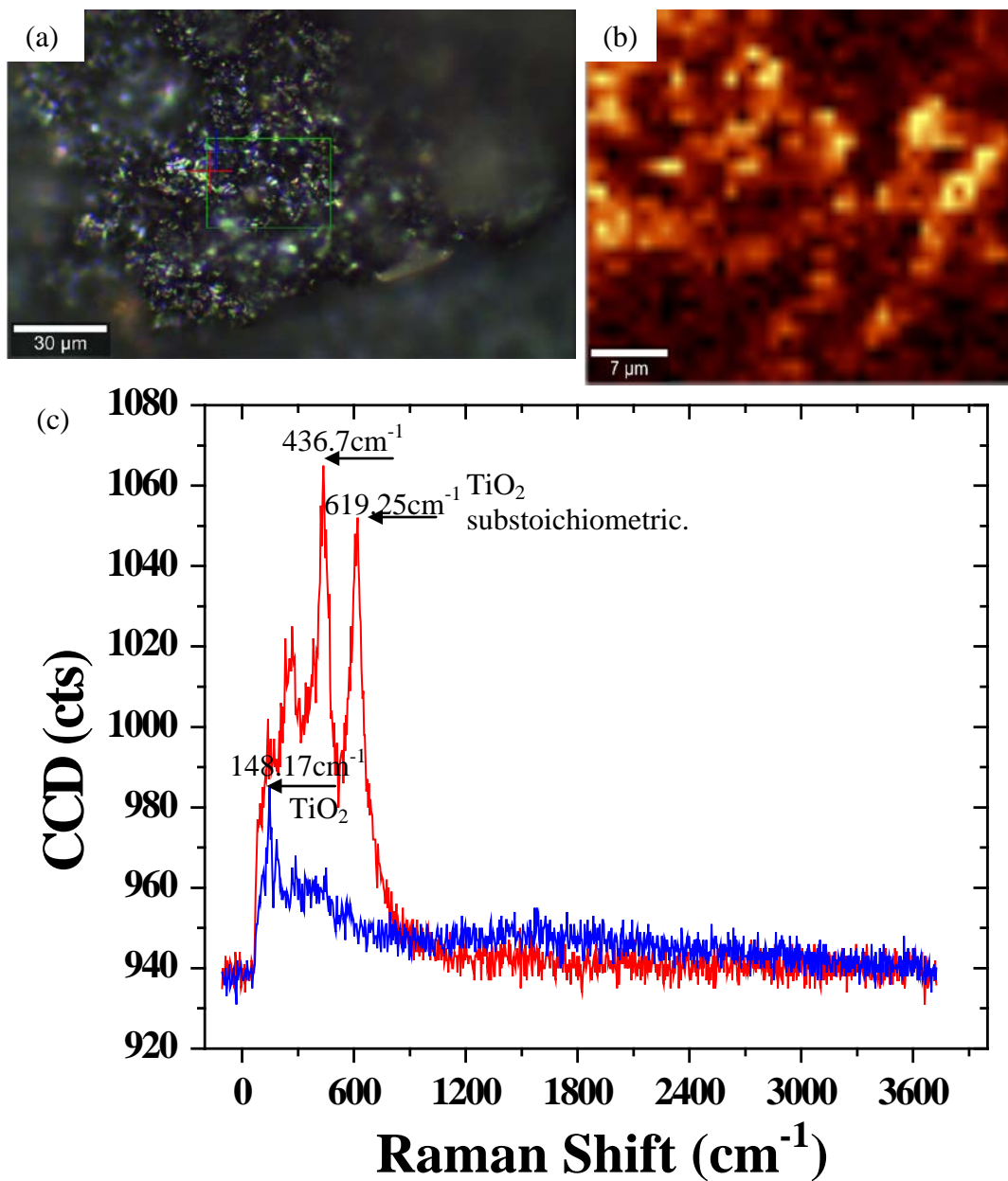
Figure 2.4 Raman scope (WITEC ALPHA300) image and spectrum of Ebonex REM. (a) the image took under scope; (b) Raman image of the red square in (a); (c) comparison of Raman spectrum at red and blue cross in (a), Raman peaks at black arrow represent different titanium oxide species (e.g., TiO_2, Ti_4O_7 and Ti_5O_9).

(a)

10 µm

(b)

3 µm

(c)
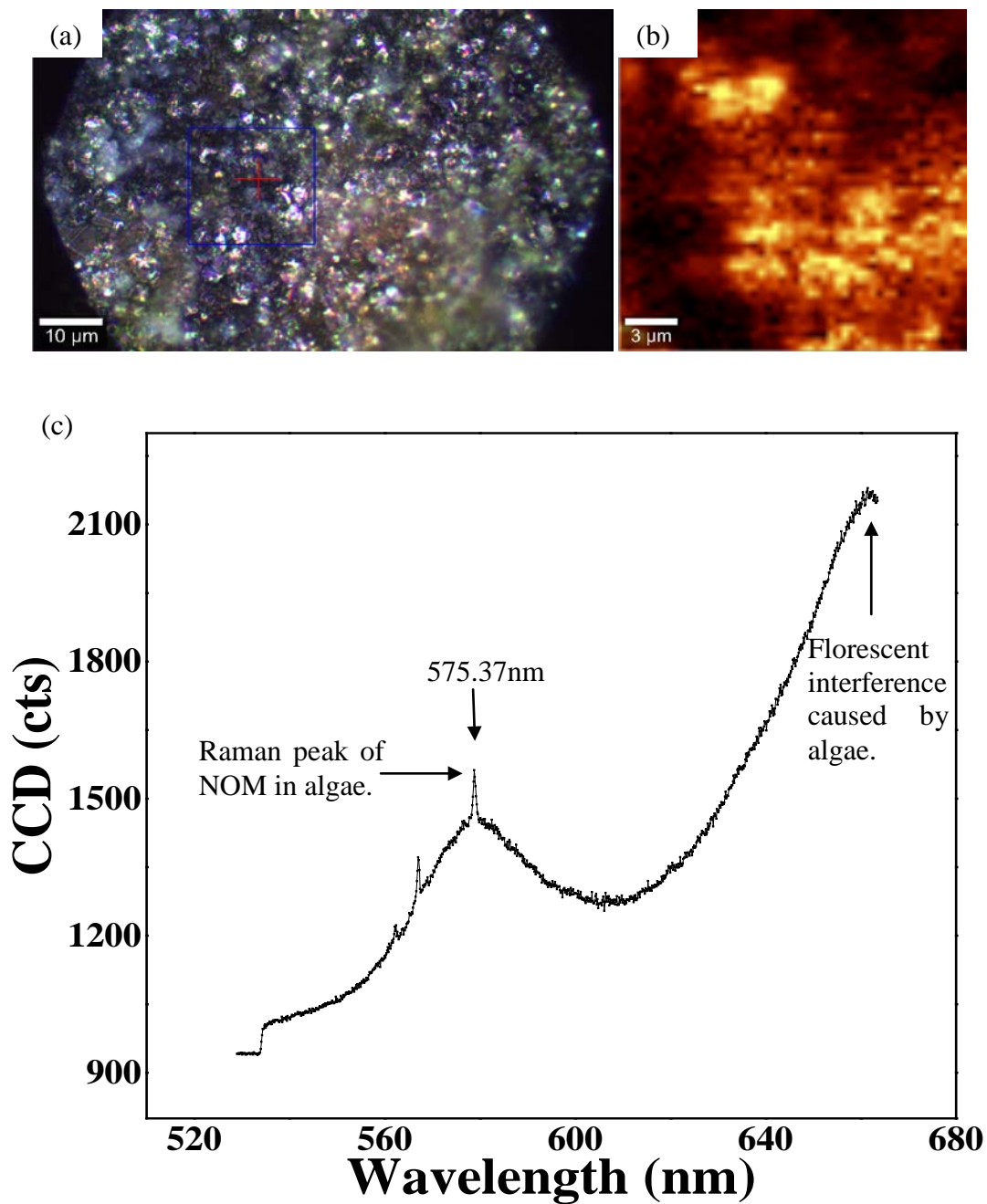
Figure 2.5 Raman scope image and spectrum of dried algae. (a) the image took under scope; (b) Raman image of the blue square in (a); (c) Raman spectrum at red cross in (a).

2.3.2 Algal morphological changes before and after exposure to DC-charged REM

Figure 2.6 compares the algal biomass with and without REM treatment. From the photos, the black color of algal biomass appears to fade slightly. As shown in Figure 2.6c and 2.6d, although no major changes to the morphology or deformation in algal cells, there could be a major damage to the cellular structures with the REM treatment. As pointed by the red arrows, the treated algae had evident white-colored dots, which might be the pits (cavitation) on the damaged algal cell wall. This formation of white dots was repeatedly observed on numerous treated algal cells, which are not there (or at least not significant) on untreated algae. The SEM images in Figure 2.6e and 2.6f show that untreated algae had normal shapes and edges, whereas treated algae samples appear to have rough surfaces and some scattered debris surrounding algal cells that were likely damaged. To further verify the surface disruption, surface mapping by AFM was performed with the results compared in Figure 2.7. Figure 2.7a shows the same morphology as the SEM image in Figure 2.6e. By comparing Figure 2.7b and 2.7c, treated algae cells are likely to have some release of intracellular substances as marked by the red arrow.

A similar observation was obtained on algae after ozonation, which led to the appearance of submicron particles due to lysis.[104] Also, the reduction of algal size probably resulted from the disintegration of EOM from algal surface.[76] cavity formation is common in algal cell treatment.[17, 89, 91] Figure 2.8 compares algal suspension before and after REM treatment at different times, which shows that algal suspension had a transition from dark green to lighter over time of REM treatment. This may indicate the surface oxidation of algae by charged REM. Figure2.9 shows the fluorescent microscopy images of PI-stained algal cells after exposure to REM at different power intensities.

Figure 2.9a, 2.9c and 2.9e show the microscope images of PI-stained algal suspension without laser excitation. Figure 2.9b, 2.9d and 2.9f are microscope images under GRN fluorescence. The density of visible cells (dark dots in the optical microscope images) were almost same after REM treatment. Under florescent microscope, damaged cells became green dots, which increased from nearly invisible to a high density with the increasing REM treatment intensity.
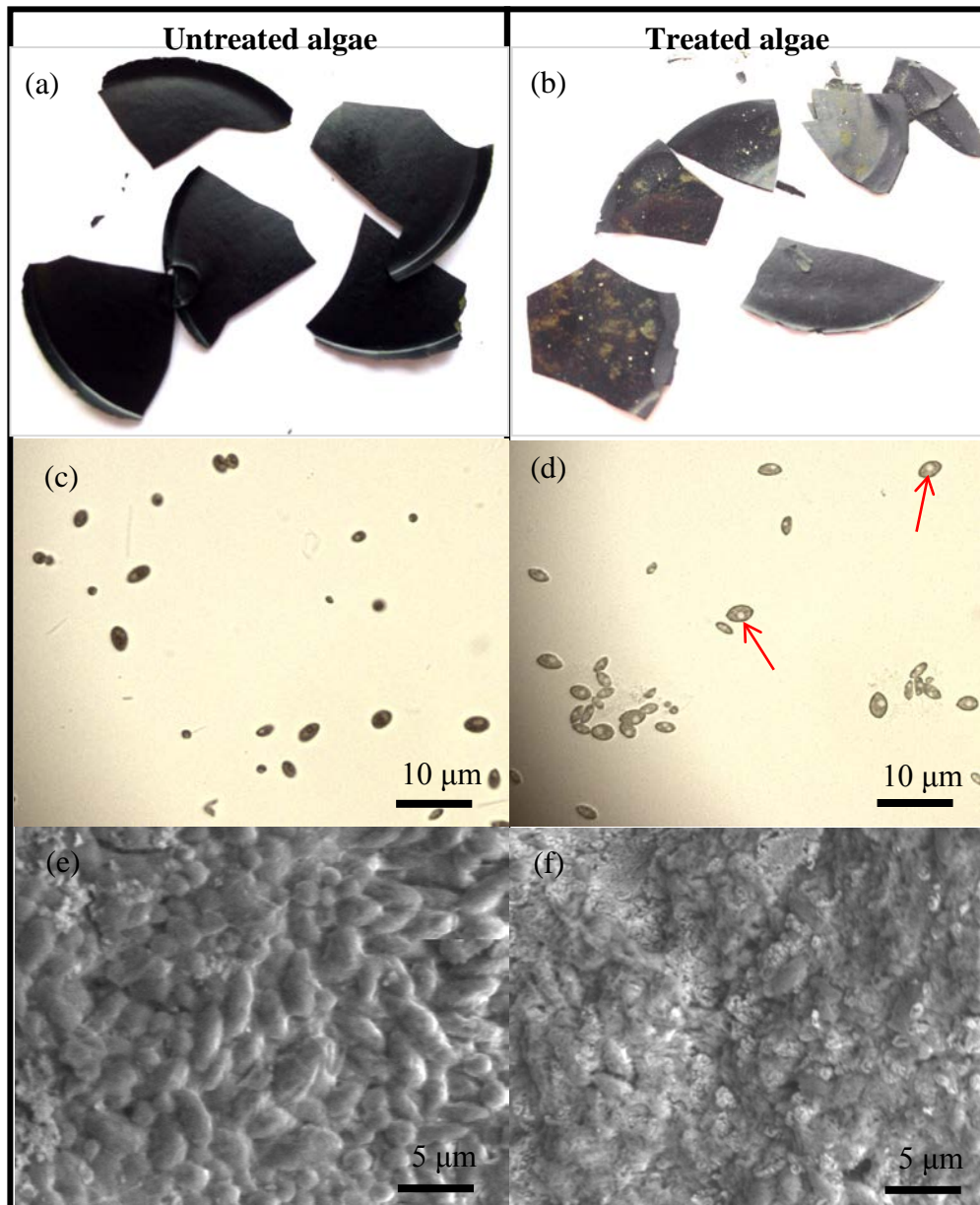
Figure 2.6 Comparison of morphology of untreated dried algae and treated dried algae with and without treatment by REM under 200 mA and 20 V for 60 min with photos of dried algal fragments in (a) and (b), optical microscopic images in (c) and (d), and SEM images in (e) and (f).
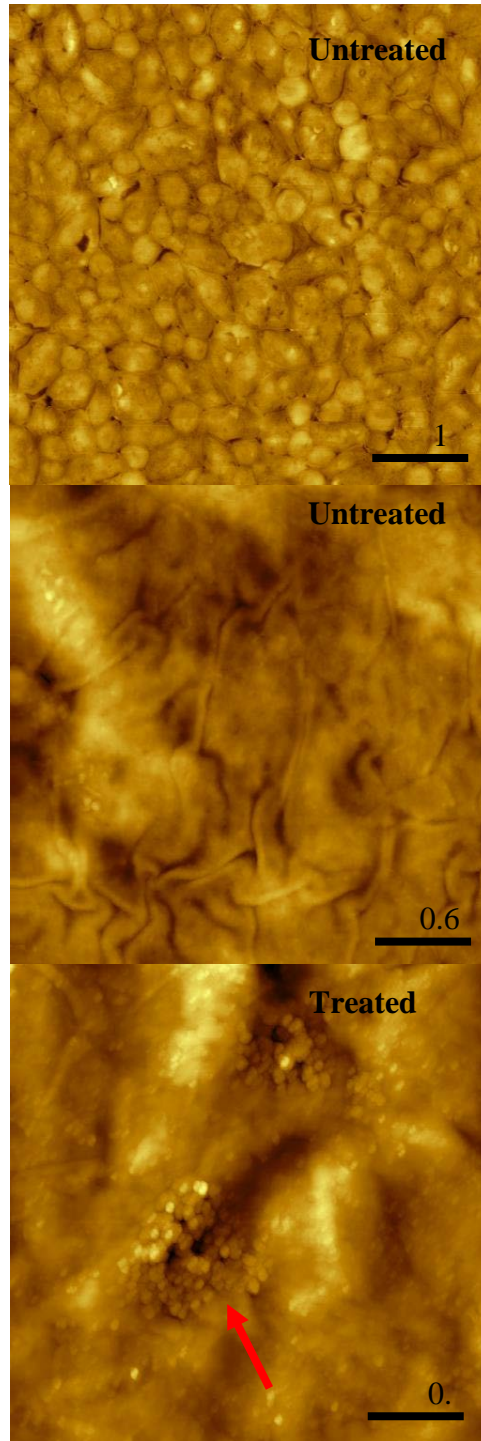
Figure 2.7 Morphological images of untreated and treated algae acquired by AFM.
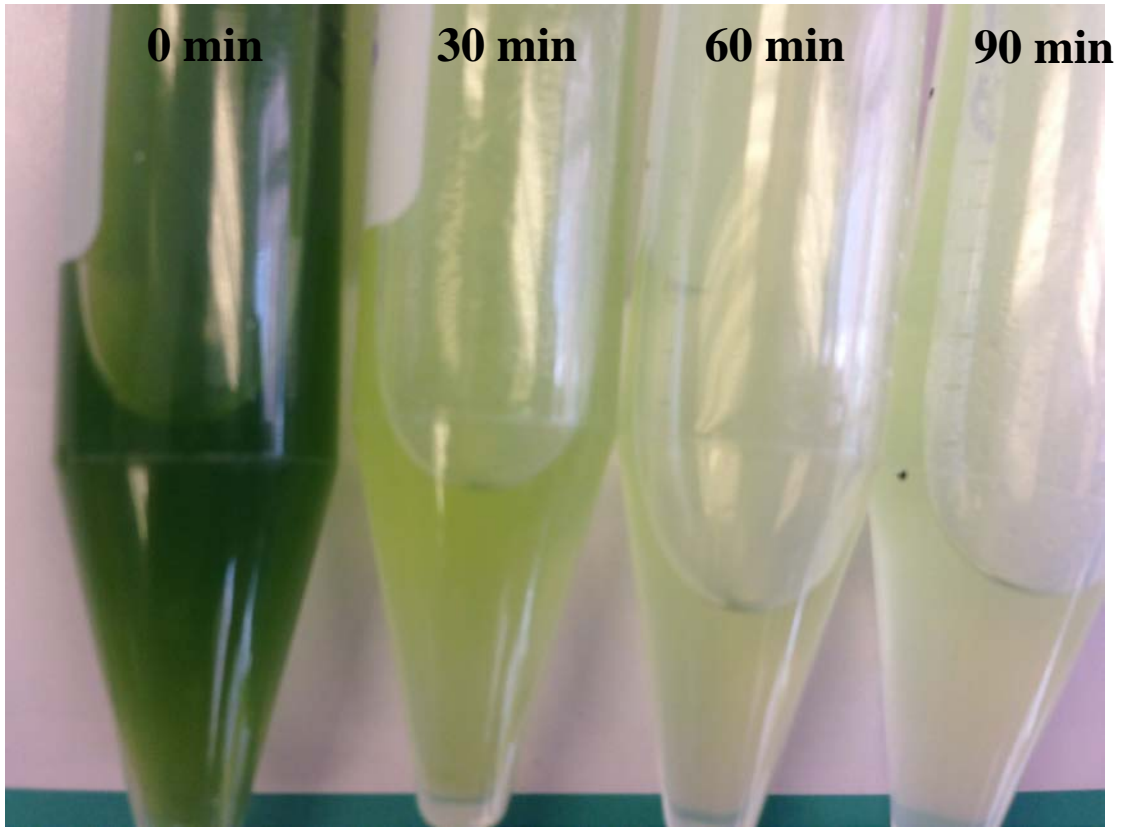
Figure 2.8 Photos of algal suspension after REM treatment.

Optical microscope image   Fluorescent microscope image
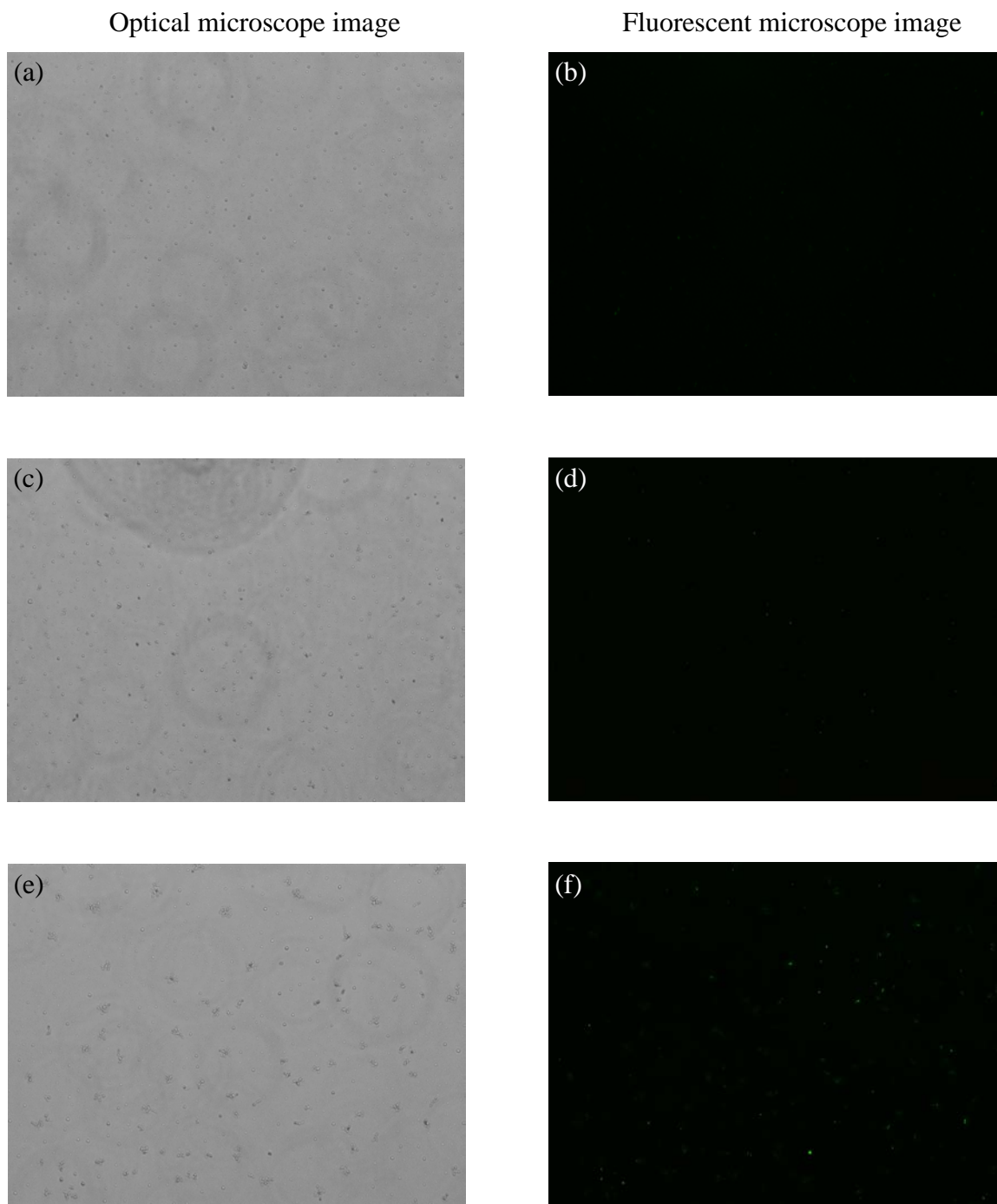
Figure 2.9 Microscopy fluorescent images of intact algae (a and b) and damaged algae (c, d, e and f) with PI staining after exposure to REM under 0h·A, 0.375h·A and 0.75h·A REM treatment intensities.

2.3.3 Algal surface composition changes

Surface disruption may also lead to the disintegration of extracellular organic matter (EOM) from the algal surface.[76] FTIR was utilized to examine the effect of REM treatment on algal surface properties (e.g., characteristic functional groups). Typical components on algal surfaces are polysaccharides, protein, lipid and phosphates. As indicated in Figure 2.10, the characteristic peaks at 3550–3200, 2925, 1260–1000 cm^{-1} are associated with polysaccharide or polysaccharide-like substances, such as N–H stretching occurred at 3300 cm^{-1}, aliphatic ($-CH_2$) peak at 2930 cm^{-1}, carboxylic (C–O) at 1250 cm^{-1} as well as at 1000 cm^{-1}.[104-105] The absorption peaks at 1650 cm^{-1} and 1550 cm^{-1} are related to the peptide carbonyls (C = O, amide I band) and the N–H (amide II) bonding, respectively.[106-107] FTIR spectra indicated that protein and polysaccharide-like substances were major constituents on the surface of *S. dimorphus*. As shown in Figure 2.10, all major functional groups remained with the intensity slightly decreased with the REM treatment, implying EOM (e.g., polysaccharides) were likely released from algal surface due to the oxidative attack of radicals on the cell wall of algae and subsequently algal lysis. Furthermore, similar changes in cell surface characteristics and in cell viability upon additions of oxidant was observed in previous works.[104, 108]
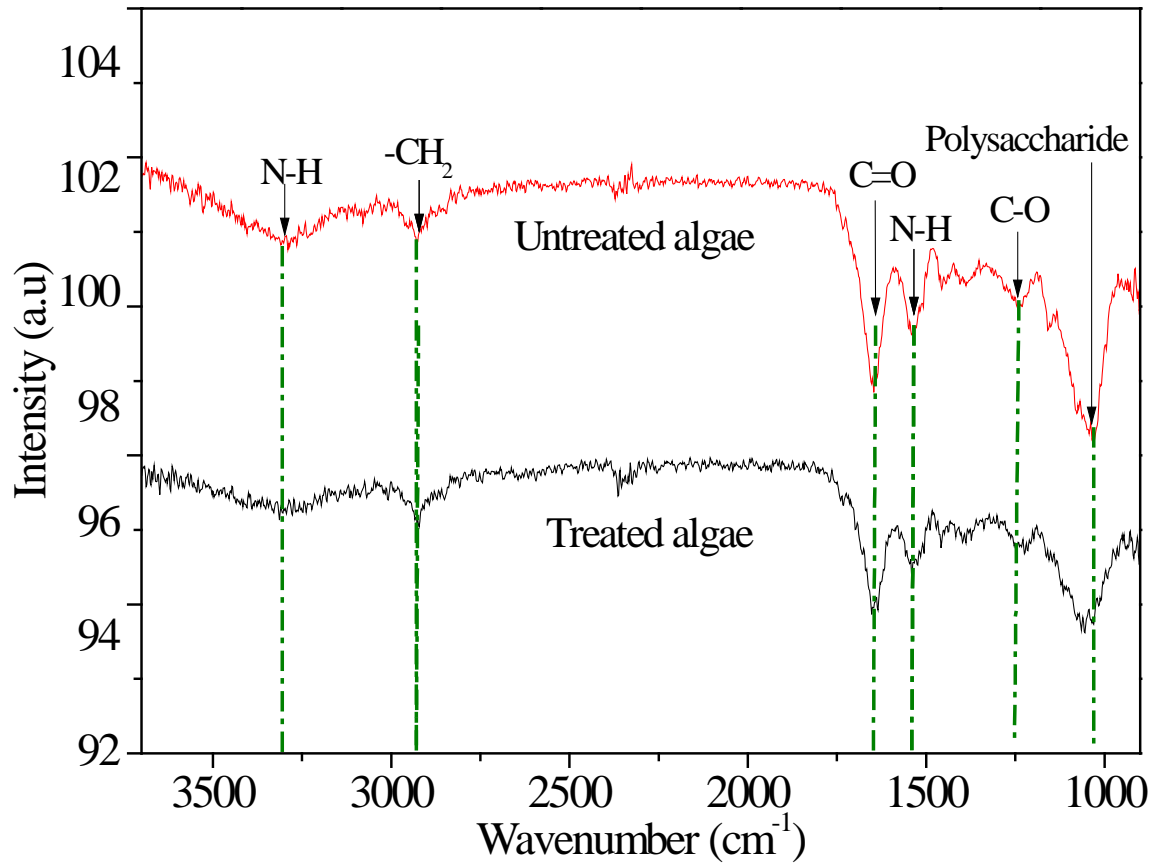
Figure 2.10 FTIR spectra for algal surface with and without REM treatment under the condition (72 J·ml^{-1}): 500 mA (≈20 mA·cm^{-2}), 20 V and 60 min for 500 ml of algal suspension at the initial concentration of 1.8 g·L^{-1} (unless indicated, the same treatment condition applied to the following data comparison).

2.3.4 Algal photosynthetic activity changes

Figure 2.12 compares four photosynthetic efficiency curves for untreated and treated algae under three different treatment times of electrical treatment (500 mA and 20V) in 500 ml. The photosynthetic efficiency declined from 0.5 to 0.2 fv·fm^{-1} with the increase of the treatment time from 0 to 120 min (2.0 A·h·L^{-1}). Figure 2.11 compares three DO regeneration curves for untreated and treated algae under two different conditions. Clearly, the DO curve for untreated algae was quite linear at a rate of *c.a.* 2.7 mg·L^{-1}·h^{-1}, which is the greatest among all. By applying 100 mA and 10 V to the REM to treat algae

suspension of 500 ml for 60 min (equivalent to the energy input of 7.2 W·ml^{-1} or 4 W·mg-algae^{-1}), the treated algae maintained the similar photosynthetic activity with the untreated algae. However, further increasing the DC charging level to 500 mA and 20 V (or 72 W·ml^{-1} or 40 W·mg-algae^{-1}), the REM exposure significantly inhibited DO regeneration because of the perceivable cell damage as shown in Figure 2.6 and Figure 2.7.
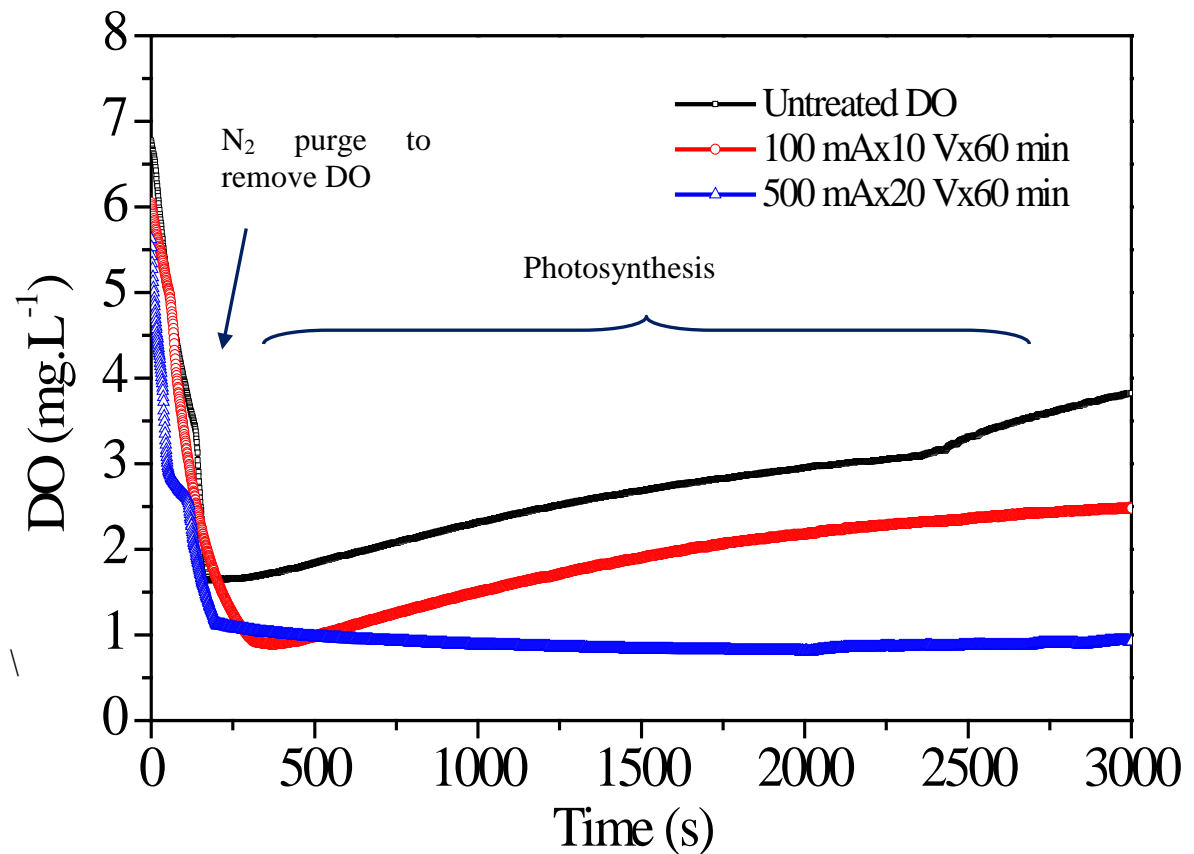
Figure 2.11 DO curves versus time for the untreated and treated algal cells in 500 ml algal suspension with the algal concentration of 1.8 g·L^{-1}.
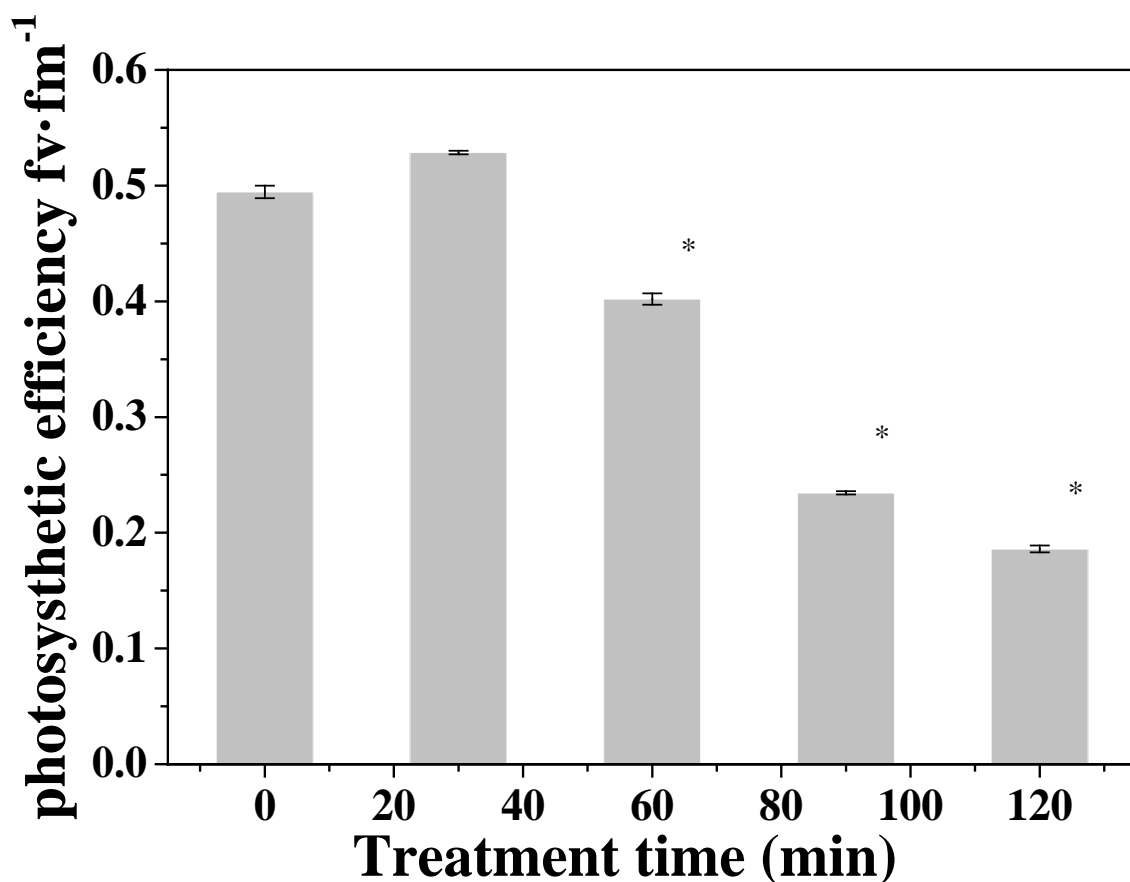
Figure 2.12 Photosynthetic activity for the untreated and treated algal cells under the condition: 500 mA (current density≈20 mA·cm^{-2}) and 20 V for 500 ml of algal suspension at the initial concentration of 1.4 g·L^{-1}. * denotes significant differences ($p<0.05$) between the values of treatment groups and the initial value.

2.3.5 Characterization of DOM in algal suspension

Polysaccharide-like and protein-like substances found on the algal surfaces were likely the major components of algogenic organic matter (AOM) released from algae due to surface oxidation. In addition, cell lysis by oxidation may also be induced with a release of intracellular organic matter (IOM) that is considered as hydrophilic substances with high SUVA$_{254}$, the ratio of UV$_{254}$ to dissolved organic carbon (DOC).[109] To evaluate the possible algal surface oxidation by DC-charged REM, the UV-vis spectra for the

supernatant collected from untreated and treated algal suspension were obtained and presented in Figure 2.13, which shows little difference between the samples, which is likely due to the low concentrations of AOM in the algal suspensions.

However, the EEM spectra obtained by the fluorescent spectrophotometer in Figure 2.13 were particularly useful for revealing information on protein and humic- or fulvic-like substances.[29] There are two major peaks at Ex/Em of 245/400 nm and 340/400 nm. After the treatment, a peak at (Ex/Em of 350 nm/400 nm) emerged, which is likely ascribed to humic substances.[110] This may indicate the production or release of AOM from algae was due to anodic oxidation. It was previously reported that DOC in the solution increased as contact time of ozonation increased.[104] Ozone exposure further reduced the algal mass and the size of algal cells due to the release of AOM from algal surfaces. Consequently, the fluorescent intensity of the observed peaks in EEM also decreased, which agreed with the FTIR results as shown in Figure 2.10.
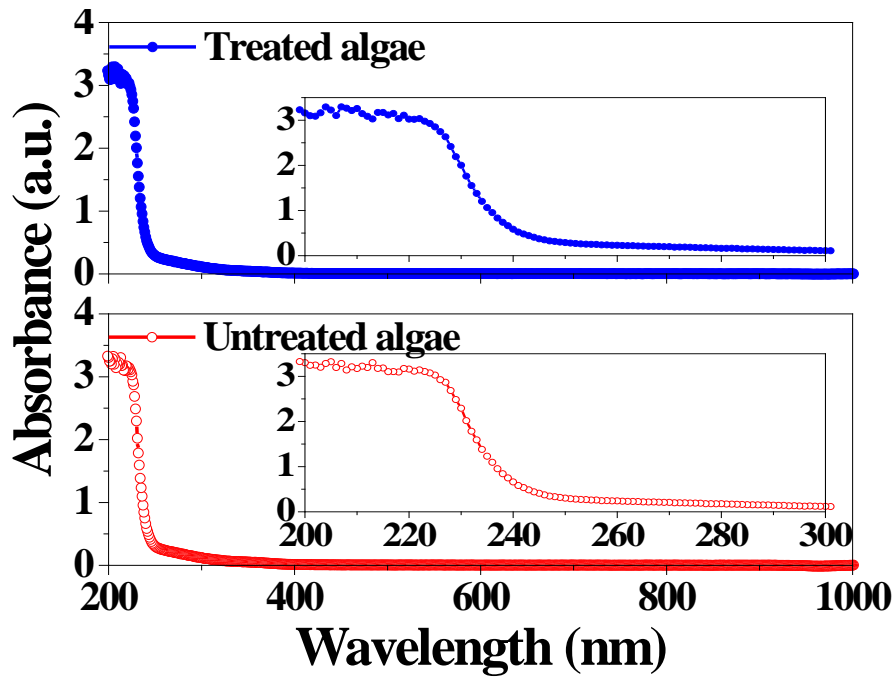
Figure 2.13 UV-vis spectra for supernatant from untreated and treated algal suspension under the same condition as **Figure 2.10**.
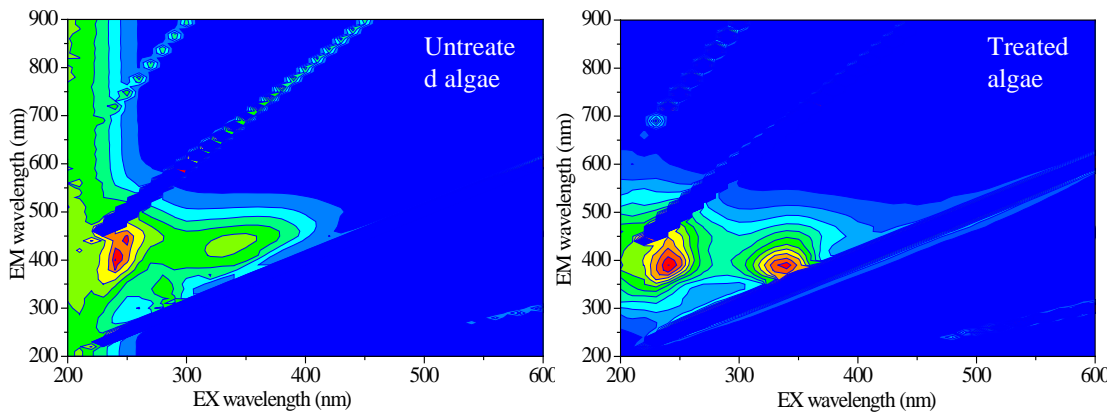
Figure 2.14 EEM spectra for the supernatant from untreated and treated algal suspension under the same condition as Figure 2.10. The intensity of EEM is represented by contour lines.

Molecular weight (MW) distribution within samples was assayed using gel filtration chromatography. The MW distribution of AOM usually exhibits a significant heterogeneity (high polydispersivity) due to an array of different components such as glycolic acid, carbohydrates, polysaccharides, amino acids, peptides, organic phosphorus, enzymes, and vitamins.[105] The untreated AOM may consist of high MW carbohydrates or proteins (>20 kDa), medium-MW components (i.e., humic like substances, ~1,000 Da and building blocks, 350–500 Da), and low-MW substances (<350 Da).[111-113] Our data in Figure 2.15 shows that the peaks of 2.6 kDa and 1.8 kDa both decreased, indicative of the decomposition of typical AOM. The increase in the peak of 2.1 kDa suggested the possible conversion from larger organic matters to small ones. The MW distribution in Figure 2.15 did not reveal any high MW biopolymers, probably because the UV detector could not detect all organics. A shift of MW from high to low region was also observed previously when applying ozone to algae.[114] This shift could be supported by the calculation of the UV absorbance ratio index (URI), which corresponds to the ratio of UV absorbance at 210 nm to that at 254 nm (UVA_{210}/UVA_{254}). URI can provide information on the relative proportions between UV-absorbing functional groups and unsaturated compounds in DOM.[115] Based on the results in Figure 2.13, URI for untreated and treated algal suspension were 11.8 and 12.7 respectively, which means a smaller MW of DOM existed in treated algal suspension. Furthermore, $S_{275-295}$, a spectral absorption index, is the spectral slope coefficient in the spectral range of 250–365 nm. $S_{250-365}$ can be used for tracing DOM sources and indicating DOM molecular weights (a higher $S_{275-295}$ indicates a lower MW of DOM).[116] $S_{250-365}$ can be calculated from a linear regression of log-transformed absorption coefficient in Equation (2.1):[117-118]

$$a(\lambda) = 2.303A_\lambda \ / \ L = a(\lambda_{ref})e^{-S(\lambda-\lambda_{ref})} \tag{2.1}$$

where a(λ) is the absorption coefficient at the wavelength of λ nm, λ_{ref} is the reference wavelength (nm), A_λ is the absorbance at λ nm, and L (m) is the cell path length. Using the data in Figure 2.13, we compared the values $S_{250\text{-}365}$ for untreated (0.0179 nm^{-1}) and treated (0.0196 nm^{-1}) algal suspension, which also indicates the shift of MW from large to small ranges.
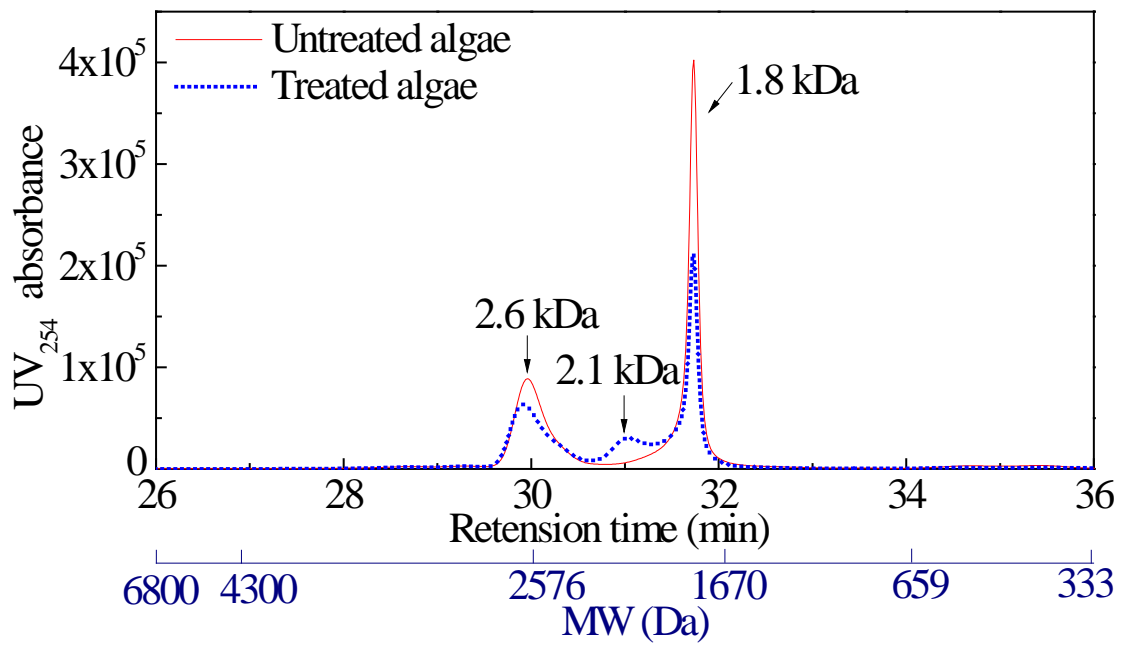
Figure 2.15. MW distribution measured by DLS (a) and by gel chromatography (b) under the same condition as Figure 2.11.

2.3.6 The role of the radicals production on algal pretreatment and filtration

Under an applied electrode potential, the electrochemical reaction on the REM surface include direct electron transfer reactions (R $\rightarrow$ R$^{\bullet+}$ + e$^-$) and the formation of hydroxyl radicals (OH•) via water oxidation ($H_2O \rightarrow OH \bullet + H^+ + e^-$).[78] OH• radicals are short-lived intermediates that self-decay with a second-order reaction rate of 5.5×10^9 M$^{-1}\cdot$s^{-1}. Therefore, reactions occurred to algal cells could only occur in a thin layer near the REM

surface. The production of ROS (primarily OH•) and the removed chemical oxygen demand (COD) in the algal suspension could both be estimated by the Faraday's law:[119]

$$R = \frac{COD}{8} = \frac{i \cdot t \cdot M}{V \cdot F} \tag{2.2}$$

where R is the moles of OH• produced the REM electrode (mole), i is the current density ($A \cdot cm^{-2}$), t is the elapsed (s), M is the surface area of the REM electrode (25.4 cm^2), V is the volume of the algal suspension (500 ml), and F is the Faraday's constant (96500 $C \cdot mol^{-1}$). Under the current treatment (20 $mA \cdot cm^{-2}$ for 60 min), the total produced OH• was approximately 0.038 $mol \cdot L^{-1}$, which may lead to the reduction of COD by 0.303 $mol \cdot L^{-1}$ (9.7 $g \cdot L^{-1}$ or 1.2 $eq \cdot L^{-1}$). However, the algal concentration was 1.8 $g \cdot L^{-1}$, which corresponds to only 0.2 $eq \cdot L^{-1}$ if the empirical formula for algae is assume to be $C_{106}H_{263}O_{110}N_{16}$ (419 $eq \cdot mole^{-1}$).[120] Clearly, the ROS production is the maximum level that could be achieved theoretically. In reality, not all electrons transferred are converted into OH• radical, but they may also lead to O_2 production (i.e., $2H_2O \rightarrow O_2 + 4H^+ + 4e^-$), thereby reducing the chances of algal surface oxidation.

The role of the produced ROS on REM surface may have additional benefits besides the pretreatment of algae. The algal culture media usually contain hormonal substances, inhibitors, and toxins while algae grow and may accumulate these substances, especially when reusing the culture media. Thus, the oxidation power by REM may also enable the treatment of culture media with significant reductions in AOM and inhibiting compound accumulation, which makes the reuse of culture media more feasible and saves water consumption for algal cultivation. However, to better preserve the quality of algal biomass/extracted lipid and reduce energy consumption, the DC charging conditions shall also be optimized to avoid the excessive formation of free radicals that

could cause oxidation and proteins denaturation and consequently reduce the biolipid quality or production. [17]

2.3.8 Lipid extraction from untreated and treated algal cells

Microalgae (*S. dimorphus*) used in this study are oleaginous. Treated cells are presumably broken and easy to extract and produce more lipid with the same extraction method compared to the untreated ones. Figure 2.16a shows that the specific extracted lipid increased from 15.2 ± 0.6 to 23.4 ± 0.7 g-lipid·g-cells^{-1} ($p<0.05$) as the REM treatment intensity increased from 0 to 0.75 A·h by increasing the exposure time at 500 mA. Figure 2.16b shows that the extracted lipid increased from 6.3 ± 0.13 to 20.0 ± 0.14 g-lipid·g-cells^{-1} ($p<0.05$) as the REM treatment intensity increased from 0 to 0.75 A·h by increasing the exposure time at 500 mA. However, once REM treatment intensity increased from 0.75 to 1.25 A·h, extracted lipid decreased down to 3.1 ± 1.2 g-lipid·g-cells^{-1}. Clearly, the REM treated cells allowed greater lipid extraction efficiencies presumably due to the oxidative cell damage. But if the treatment intensity get too high, lipid extraction efficiencies may decrease presumably due to the lipids themselves were oxidized. Similar improvement in lipid extraction was previously reported when other algal pretreatment such as pressure-assisted ozonation (PAO), Fenton oxidation, and peroxone treatment were applied.[121-123]
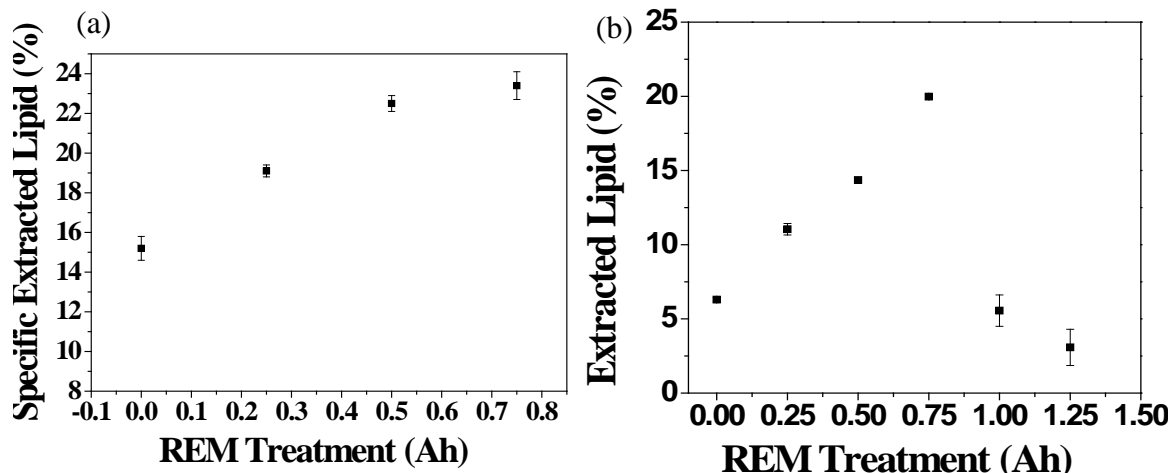
Figure 2.16 Result of Heterogeneous lipid extraction (a) and homogeneous lipid extraction (b) efficiency by REM treatment under the condition: 500 mA (current density≈20 mA·cm^{-2}), 20 V for 500 ml of algal suspension at the initial concentration of 1.4 g·L^{-1}. *t*-test suggested that there is a significant difference between the extracted amounts of lipid from untreated and treated cells.

2.3.9 Comparison of energy consumption with other algal harvesting and treatment techniques

Algal pretreatment by anodic oxidation of REM is comparable to some of the above-mentioned techniques such as ultraonication, microwave, or pulsed electric field (PEF) charging, which employ oxidative stress or an electrical field to induce membrane compression and pore/cavity formation to facilitate lipid extraction.[91] Mechanical techniques, such as bead mill, high-pressure homogenization (HPH) and high speed homogenizer (HSH), consume nearly the same amount of energy to process a unit of volume, independent on whether the feed is diluted or concentrated.[92, 124-126] Thus, for these methods, processing higher DCW concentrations per unit of time is more cost effective. Energy consumption not only varies with processes but also design parameters. For example, Doucha and Lívanský reported that the specific energy consumption (kWh/kg-disrupted cells) of bead milling can be reduced from 10.3 to 0.86 kWh·kg^{-1} by changing the process parameters.[127] A recent study on the disruption of *Tetraselmis*

suecica through AFM measured an energy consumption of 0.000187 kWh·kg^{-1} to break up a single cell on analytical scale.[128] Several authors compared different methods at low DCW concentrations, i.e., ultrasonication, HPH, bead milling and microwave treatment.[15, 129-130] Generally, HPH has the highest specific energy consumption (kWh·kg^{-1}), followed by microwave treatment and ultrasonication as shown in Table 2.1. Ultrasonication has the specific energy consumption ranging from 36.67 kWh·kg^{-1} (inefficient disruption) to 100 kWh/kg (efficient disruption).[15, 130] For continuous PEF treatment processes, the specific energy consumption almost linearly decreases with the biomass treatment rate (kg·h^{-1}), i.e., biomass disrupted per unit of time.[124, 131-132] In other words, specific energy demand strongly depends on the concentration of the suspension and ranges from 0.42 kWh·kg^{-1} for 10% DCW to 239 kWh·kg^{-1} for 0.03% DCW.[124-125, 131] A recent literature review suggested that algal biomass pre-processing should not exceed a threshold level of energy consumption (5.8 kWh·kg^{-1} or 21 kJ·g^{-1}) in order to be cost effective.[17] Our current bench scale algal treatment by REM had a relatively high-energy consumption of approximately 14 to 28.6 kWh·kg^{-1} to achieve improved lipid extraction. However, it is worth mentioning that the REM treatment can further be optimized (e.g., reducing the electrode spacing from 2.5 cm to 0.5 cm), which may reduce the needed cell voltages from 20 V to 4 V while maintaining the same current density. Moreover, the applied DC current potentially reduces membrane fouling and thus improves algal harvesting efficiency, which is an additional benefit that largely offsets the cost and needs further exploration. Overall, REM filtration and pretreatment could reduce energy demand for algal harvesting and pretreatment that is relatively easy to scale up at industrial applications.

Specific energy requirements vary from 33 megajoule (MJ) per kg of dry algae cells for hydrodynamic cavitation to 860 MJ per kg of dry algae cells for pulse electric field, refer to Table 2.2. The energy available by the combustion of the entire algal biomass was estimated to be about 22 MJ per kg of dry cells. Therefore, the existing ell disruption methods result in a negative net energy balance. This fact has been already demonstrated through an energy return of investment (EROI) analysis performed for various algal bioproducts extraction and upgrading pathways resulting in EROIs in the ranges of 9.2×10^{-5} to 0.36.

The energy required for the indentation and disruption of a single algae cell was estimated as 17 picojoule (pJ) with an atomic force microscope, which is equivalent to 670 J per kg of dry algae cell, demonstrating that the existing cell disruption methods are highly inefficient in transferring energy to the individual algae cells. In the hydrodynamic cavitation, the most "efficient" of the existing methods, only about 0.002% of the energy input is used for cell disruption. This clearly shows that any incremental or evolutionary improvement in the efficiencies of the existing cell disruption methods will not bring about a significant change in the algae biofuels industry. Therefore, an outside-the-box and transformative solution is necessary for the development of a sustainable algae biofuels industry.

Table 2.1 Comparison of Different Algal Cell Treatment Techniques (DCW: 1 %≈10 mg·ml^{-1})

Cell treatment techniques	Preferred algal concentration	Specific energy consumption (kWh·kg^{-1}) under different algal concentrations (DCW %)	Overall energy consumption	Reference
Bead Milling	Concentrated	10 for 3.5 %	High/medium	[87, 133]
HPH	Diluted/concentrated	0.25–147 for 15%–0.85%	High/medium	[133-134]
HSH	Diluted	0.125 for 0.14%	High/medium	[135-136]
Ultrasonication	Diluted	0.06–37 for 15%–0.85%	Medium/low	[137-142]
Microwave	Diluted	17–117 for 0.14%–0.5%	High/medium	[143-145]
Enzymatic lysis	Diluted	N.A.	Low	[146-147]
Chemical treatment	Diluted/concentrated	N.A.	Medium/low	[23, 90, 130, 148-150]
PEF	Diluted	0.07 for 25%	High/medium/low	[151-158]
REM	Diluted	11 for 0.18%	High/medium	This study

Table 2.2 Summary of Existing Algae Cells Disruption Methods (adapted from Lee *et al.* 2012)

Methods	Material and experimental conditions (disruption volume, concentration, power consumption, disruption duration)	Calculated energy use (GJ/m3 cell suspension)	Energy use MJ/kg dry mass	Scale of use
Sonication	*Chlorococcum* sp. (0.2 L, 8.5g/L, 750 W, 5 min)	1.125	132	Laboratory, industrial
High Pressure Homogenizer	*Chlorococcum* sp. (0.2 L, 8.5g/L, 2.5 kW, 6 min)	4.5	529	Laboratory, industrial
High Speed Homogenizer	*Saccharomyces cerevisiae* (0.8 L, 10g/L, 0.6 kW, 15 min)	0.675	67.5	Laboratory, industrial
Bead mills	*Botryococcus, Chlorella, Scendesmus* (0.1 L, 5g/L, 840 W, 5 min)	2.52	504	Laboratory, industrial
Microwave	*Botryococcus, Chlorella, Scendesmus* (0.1 mL, 5g/L, 700 W, 5 min)	2.1	420	Laboratory, industrial
Freeze Drying	Mathematical modeling on an industrial scale	1.4	140	Laboratory, industrial
Pulsed Electric Field	*Synechocystis* PCC 6803 (5 mL, 0.3 g/L)	0.26	860	Laboratory, pilot scale
Hydrodynamic cavitation	*Saccharomyces cerevisiae* (50 L, 10g/L, 5.5 kW, 50 min)	0.33	33	Laboratory, pilot scale

2.4 Conclusion

This work demonstrated for the first time the use of a novel REM to oxidize algal cells, which resulted in an increase in the lipid extraction yield. Particularly, algal cells underwent significant disruption in morphology due to surface oxidation, as evidenced by microscopic images and FTIR analysis. The REM-treated algae had reduced photosynthetic activity and oxygen production rates compared to untreated algal cells. Algal lysis was confirmed by the release of AOM that was analyzed by EEM, HPLC, and UV-vis spectrometry. Lipid extraction from the compromised algae

(23.4 ± 0.7 g-lipid·g-algae^{-1}) was proved to be higher than that from untreated algae (15.2 ± 0.6 g-lipid·g-algae^{-1}), highlighting the potential to integrate algal harvesting and pretreatment together in REM processes. Our batch REM system certainly deserves intensive optimization to improve the cost efficiency. The present work employed relatively low algal concentrations to facilitate the algal disruption and observation, more systematic work is clearly needed to optimize REM operations to deal with greater concentrations of algal feed at larger or industrial scales, which would provide important insight into the cost effectiveness of this novel technique. The results also offered new insights into the design of innovative REM systems for sustainable biomass separation or treatment for biofuel production.

Overall, REM as a novel membrane filtration process holds great potential in efficient biomass separation, reduction of membrane fouling, biomass oxidation, ease of scaling up at industrial applications. This work particularly demonstrated the use of REM to oxidize and break down cells that increased the extraction yield. Although the batch results showed a great level of energy consumption to achieve algal destabilization and improved lipid extraction, future reactor optimizations clearly can reduce the energy demand. Moreover, additional benefits of REM such as reduced membrane fouling potential, reduction of organic (toxic) solvent and energy consumption for downstream lipid processing, and removal of aqueous algal growth inhibitors that enables water and nutrient reuse of algal media may largely offset the associated costs. Ultimately, the results also shed new insights into the sustainable design of innovative REM systems for broader energy and environmental applications such as biomass separation, water, wastewater treatment, pathogen removal, and inactivation.

Originality: The reported results are new and original, which are not under consideration for publication elsewhere. Reactive electrochemical membrane, Ti_4O_7, was demonstrated for the first time in algal destabilization for lipid extraction. This finding lays the groundwork for integrating algal harvesting and pretreatment in one step using REM filtration systems, which holds great potential to lower the algal or other biomass separation and biofuel cost.

Scientific Merit: Extraction of biolipid from algae requires the use of chemical solvents such as n-hexane, chloroform and methanol or other mechanical treatment to break down cell walls, which increases significant costs and negatively affects the environmental safety. The presented REM treatment may not only serve as an efficient biomass separation (to be studied in the future research) but also be proven effective in algal destabilization or pretreatment, which improves the lipid extraction. The pretreatment process is completely chemical free and potentially reduces the cost or demand of downstream treatment for algal biofuel extraction. Therefore, the presented research well aligns with the principles of green chemistry and engineering.

Environmental importance: In addition to biomass engineering and bio-fuel industrialization, rapid and high efficient algal harvesting or removal is clearly critical for water or wastewater treatment. Reactive electrochemical membranes (REMs) or electrochemical advanced oxidation processes (EAOPs) are next-generation membrane technologies holding great promise in revolutionizing water and wastewater treatment. REM pretreatment could lower the operating cost and increase the economic viability of products (biomass and cleaned water). Furthermore, unlike hollow fiber membranes which are generally subject to severe fouling, resulting in flux decline and an increase in

transmembrane pressure, REM could oxidize organic foulants via the anodic oxidation due to the radical production on anode surface and increase the operation cycles. Our ongoing work is currently investigating the algal harvesting efficiency, fouling/defouling processes, and removal organics in algal medium with REM, which should further our understanding in the design of sustainable reactive membrane systems for complex environmental matrix.

This research is original and transformative because it was the first time that the use of REM for disrupting algae cells, making the proposed research innovative, novel, and unique. The findings from the research are expected to provide fundamental knowledge on the kinetics and mechanism of actions, optimal dose and contact time, influence of operational parameters on the process (e.g., pH, temperature and algal cell concentration), among others. The findings will also advance scientific knowledge and build a knowledge base on the use of electrochemistry for algae cells disruption. These in turn would move the algae biofuels industry forward by reducing the costs associated with the disruption and separation of algae bioproducts used as feedstock for biofuels production. Currently, there are 100 plus companies involved in the algae biofuel's arena worldwide, with 36 plus of them based in the U.S. Thus, algae biofuels companies based in the U.S. and elsewhere in the world are expected to adopt the findings from this research. The adoption of the process would help the U.S. meet its biofuel goals, which calls for the production of 136 billion liters of biofuels annually by 2022.

CHAPTER 3

ASSESSMENT OF ELECTROCHEMICAL CERAMIC MEMBRANE FOULING MITIGATION IN ALGAL BIOMASS HARVESTING

3.1 Introduction

Microalgae are one of the typical water contaminants that affect water quality and drinking water security. Meanwhile, microalgal biomass is deemed as a third-generation feedstock for biofuel production. Harmful algal bloom (HABs) threats freshwater resource and human health in the past decades. Numerous toxic metabolites that produced by HABs heavily accelerates the severity of the public human health issues (e.g., global water shortage).[159] On the other hand, microalgae have been realized as a good resource of the third-generation biofuel feedstock due to its high lipid content and efficient biomass production. According to some researches, microalgae produce more than 20 times oil per hectare than the former biofuel feedstock.[160-161] Therefore, efficient microalgal harvesting technology is not only critical for freshwater reservation, but also important to biofuel production in the future. However, the prohibitive cost of harvesting process is the major obstacle to the commercialization of biofuel production using microalgae. It has been reported that the process of microalgae harvesting typically accounts 20-30% of the total cost microalgal biofuel production.[162] Among current biomass harvesting methods (e.g., sedimentation, centrifugation, filtration), membrane filtration is believed to be one of the most efficient processes for microalgal separations due to its advantages in complete retention of biomass, simplicity in operation and less consumption in energy.[163-165] In addition, the absence of chemicals allows the integration

of membrane technology into the biorefinery of microalgae which does not complicate product extraction from the biomass and culture media.[166] It is more suitable for fragile cells and small-scale production processes. Therefore, membrane filtration reveals a promising technology for microalgal harvesting. Figure 3.1 shows the hierarchy characterization of different membrane filtration technologies.
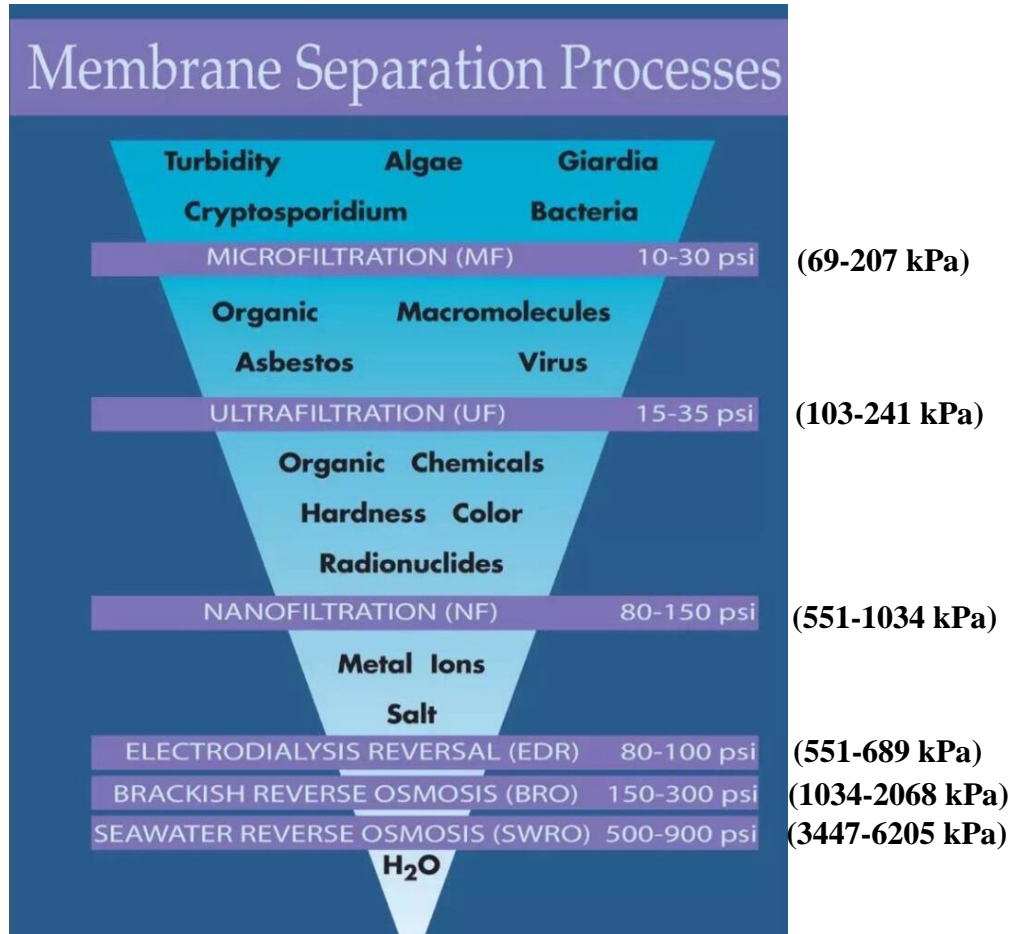
Figure 3.1 Filtration pore size, the transmembrane pressure requirement and the particle in permeate.

Notwithstanding traditional membrane filtration has been discovered to have some advantages for microalgal harvesting, there are still many unsolved problems that impede its industrial applications. One of the problems that cause considerable energy consumption and system downtime is membrane fouling and associated membrane

cleaning and maintenance. Membrane fouling is a process whereby a solution or a particle is deposited on a membrane surface or in membrane pores in a process.[167] Throughout the filtration harvesting process, microalgae and some other particles (e.g., microalgal metabolites, colloids, dissolved organic matters) tend to deposit and condense by gradually thickening on the filtration membrane surface, causing the decrement of permeation flux and constant drop of pressure.[165, 168] This phenomenon induces the main drawback associated to the improvement of the filtration efficiency, thereby hampers the development and commercialization of this technology. Traditional membrane filtration development has encountered unprecedented challenges in nowadays. Different membrane technologies and their applications and molecular cutoff ranges are shown in Figure 3.1. Thus, developing an innovative method that can efficiently address the fouling problems is an imperative task in present membrane filtration technology.

Reactive electrochemical membranes (REMs) based on electrochemical advanced oxidation processes (EAOPs) are a cutting-edge class of membranes that holding great promise in revolutionizing water and wastewater treatment and bioseparation.[78-79] Combining membrane filtration with electrochemical oxidation may effectively reduce filter fouling, extending membrane life, and enabling continuous operation. REMs are often made as porous, conductive, and chemically and mechanically stable. REM acts as both filters and electrodes.[78, 80] Past research with REMs has focused more on dissolved compound oxidation, but their ability to provide efficient biomass separations is limited. Therefore, there is a pressing need to apply REM to biomass separation and to evaluate its technical feasibility and cost effectiveness, compared to traditional membranes or

other biomass harvesting methods. Application of potential bias transfers the electro-generated electrons from the conduction band of the REM anode to the external circuit and then to the cathode. There are two possible mechanisms for microalgae destabilization through REM, namely, (1) direct anodic oxidation, where microalgae cells are oxidized after adsorption on the REM surface, which served as anode, without involvement of any substances other than the electron or (2) indirect electrolysis, in which organic pollutant oxidation is mediated by REM-generated species.[169-170] For the second mechanism, radicals such as hydroxyl radicals (•OH) could be formed via water oxidation at an anode surface when the electric potential is supplied.[81-82] During this indirect oxidation, the agents produced on the anode, which are responsible for oxidation of inorganic and organic matters, may be chlorine and hypochlorite, hydrogen peroxide, and ozone.[171] Moreover, during electrolysis, two species of active oxygen can be electrochemically produced on oxide anodes (MO_x). One is the chemisorbed "active oxygen" (oxygen in the oxide lattice, MO_{x+1}), while the other is the physisorbed "active oxygen" (adsorbed hydroxyl radicals, •OH).[172-173] Microalgae cells are, to a large extent, destroyed through indirect oxidation by oxidants (such as hypochlorite) generated from the anodic oxidation of chloride, which is abundant in the cultivating medium.[174-175] Thus, the antifouling potential of REM is promising, as organic foulants could undergo electrochemical adsorption and rapid oxidation by •OH.[176-177] Past research with REMs has focused largely on dissolved compound oxidation, but their anti-fouling ability in harvesting and inactivating microorganisms such as bacteria and algae is unexplored.

In this study, a reactive electrochemical ceramic membrane, in which stainless steel mesh/rod acted as cathode and Ti_4O_7 as anode/filter was developed for efficient

algal separation while maintaining high flux during filtration and excellent stability under anodic and cathodic polarization. Ti_4O_7 ceramic membrane was synchronized from TiO_2, which becomes an n-type semiconductor with donor impurities (i.e., electrons) after heat treatment in a reducing atmosphere due to the thermodynamically favored formation of under-coordinated Ti^{3+} species associated with oxygen vacancies and titanium interstitials.[178-182] These changes lead to the formation of mediator trap states or ionized surface states, shifting the E_F to more positive potentials. When thermally reduced in the presence of hydrogen, additional trap states are produced as a result of H dissociation into a proton bound to a lattice oxygen, creating Ti^{3+}-OH species.[183-184] The prepared conductive Ti_4O_7 REM can be directly used as not only a cathode but a separation membrane. Our device were expected to show no loss of efficacy, surface deactivation or corrosion after the treatment of over a 1000 L of water, which are all issues that have been reported for the Magnéli phases after prolonged anodic polarization.[180] To substantiate this research, we designed, fabricated, and tested both dead-end and cross-flow filtration systems to evaluate the separation efficiencies of algal biomass in algal medium suspension together with fabricated REM. Key questions addressed in the present work include (1) characterization of Ti_4O_7 REM such as inherent membrane resistance and porosity; (2) critical flux, filtration efficiency, fouling kinetics and backwash efficiency of different membrane configurations; (3) model development, fitting and simulation of different membrane filtration processes.

3.2 Method and Materials

3.2.1 Cultivation of algae

Details of cultivation and characterization are provided in Chapter 2 section 2.1. Briefly, the algal suspension was cultivated for 11 days at 20 °C. The algal concentration in the feed suspension was adjusted to 0.05 $g \cdot L^{-1}$ with algae medium.

3.2.2 Synthesis and preparation of Ti_4O_7 filter

Ceramic TiO_2 tubes (Vector Corrosion Technologies, Inc.) were firstly soaked into 0.625M sodium hydroxide solution for 24 hours to remove the most organic compounds, and then rinsed with DI water. The cleaned electrodes were placed into a tube furnace (MTI OTF-1200X), which was then placed in a hood for safety. As shown in Figure 3.2, the furnace was purged with highly pure N_2 (Airgas, 99.99%) for 30 minutes to completely remove oxygen. The N_2 was slowly reduced by swirling the valve until it was shut down. At last, the N_2 gas was by H_2 gas (Airgas, 99.99%) by turning on the H_2 outlet valve. The furnace was heated to 200 $^\circ$C for 1 hour in order to desorb water from membrane and the system, and then maintained the temperature at 1050 $^\circ$C for 10 hours. Then the system was shut down and cooled for at least 1 hour. After the temperature of the membrane recovered to room temperature, H_2 flow was then closed. The TiO_2 in the tubular membrane was considered to be transformed to Ti_4O_7 or REM, which was verified by XRD in our previous study.[176]
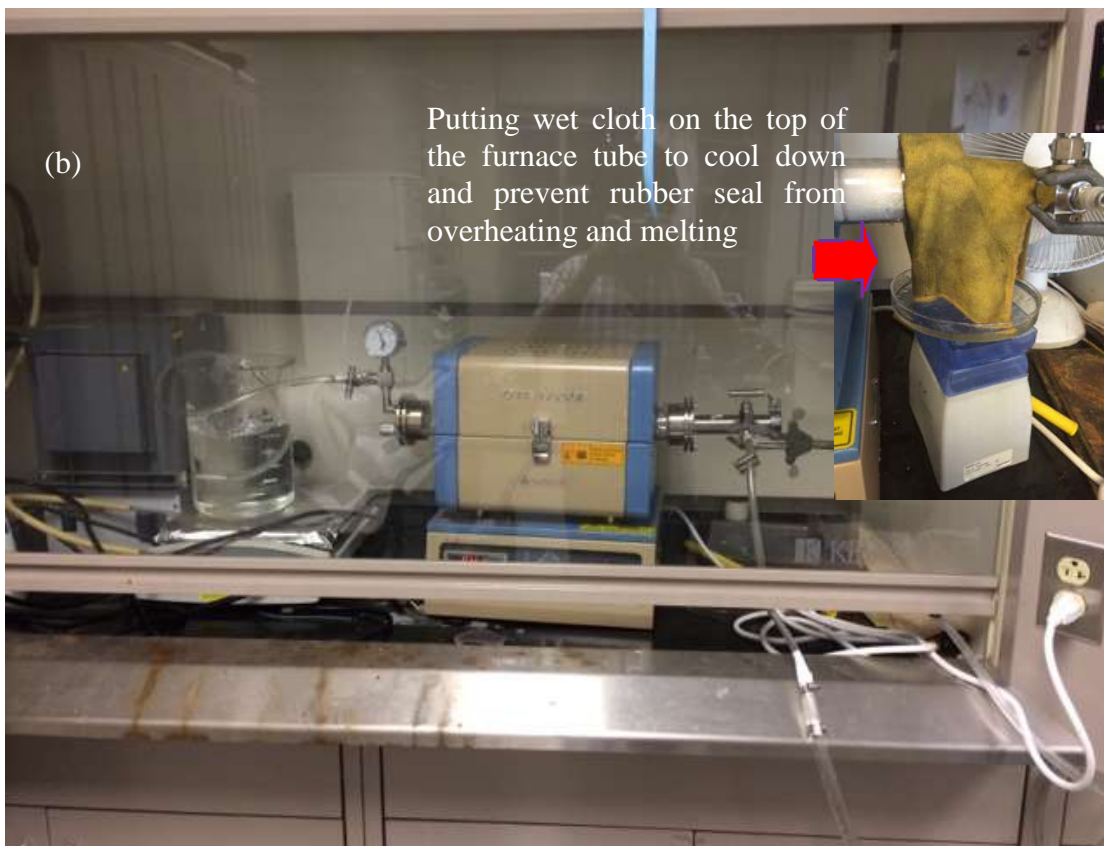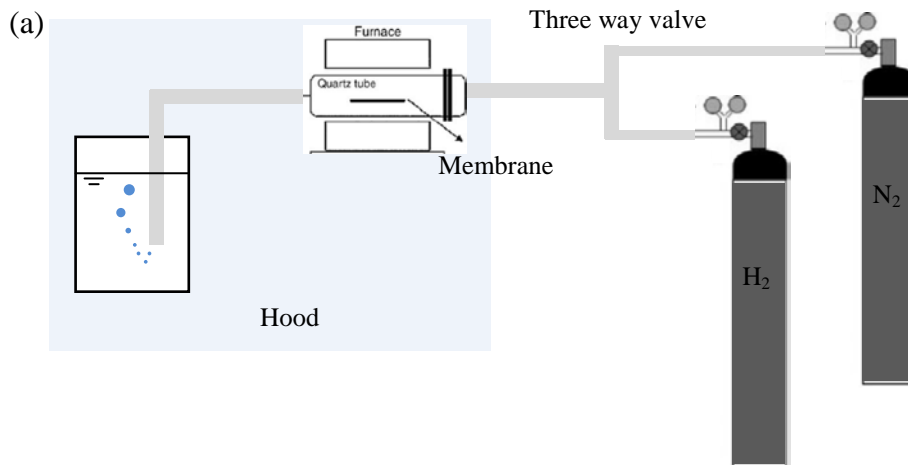
Figure 3.2 (a) Schematic of furnace system for REM thermal treatment synthesis. Not drawn to scale. (b) Actual setup of furnace system for REM thermal treatment

3.2.3 Characterization

3.2.3.1 Electrical resistivity of REM. The total electrical resistance (R) was measured by Multi-meter (EXTECH INSTRUMENTS, MN26T) before and after the thermal treatment. Electrical resistivity of REM was calculated by the Pouillet's law:

$$R = \rho \frac{l}{A}$$

where R is the electrical resistance (Ω), ρ is the electrical resistivity ($\Omega \cdot cm$), l is REM length (cm) and A is the area of REM cross section (cm^2).

3.2.3.2 Voltage distribution of REM anode. Details of voltage distribution of REM anode are provided in Chapter 4.

3.2.3.3 Zeta potential of algal cells. Algal size distribution and zeta potential of algae in culture medium was measured by the dynamic light scattering (DLS) technique performed with a Malvern Instruments Zetasizer Nano ZS at 25 $^\circ$C using the folded capillary cell (DTS1060, Malvern Instruments).[185-186] The same Zetasizer Nano ZS instrument was also used to measure electrophoretic mobility which can be converted to ζ potential using the Smoluchowski's approximation.

3.2.3.4 Surface zeta potential of REMs. Surface zeta potential of our samples was investigated by a surface zeta potential cell equipped on the Malvern DLS. The surface zeta potential cell is an accessory for the Zetasizer Nano instrument. The samples are attached by double coated adhesive tapes (Tedpella) to the cell (See Figure 3.3). The cell was placed in a cuvette filled with the dispersant (i.e., 0.001 $mol \cdot L^{-1}$ NaCl solution within

the pH range 4–11) and tracer particles (300 nm carboxylated latex tracer). The cuvette and cell are then placed in the temperature controlled Zetasizer instrument at a temperature of 25 $^{\circ}$C. An electric field is applied and the subsequent motion of tracer particles, of arbitrary material dispersed within the electrolyte, is detected. By measuring the electrophoretic mobility of the particles at varying distances from the planar surface, the magnitude of the particle electrophoresis and the electro-osmosis generated by the wall zeta potential can be used to calculate the zeta potential at the wall surface using the Henry's equation.[187] Henry's equation:

$$U_E = \frac{2\varepsilon f(Ka)}{3\eta}$$

where U_E is the electrophoretic mobility, ε is the dielectric constant, z is the zeta potential, $f(Ka)$ is Henry's function, and η is the viscosity. Henry's function generally has value of either 1.5 or 1.0. For measuring zeta potential in aqueous solutions of moderate electrolyte concentration, a value of 1.5 is used and this is referred to as the Smoluchowski approximation.[188]
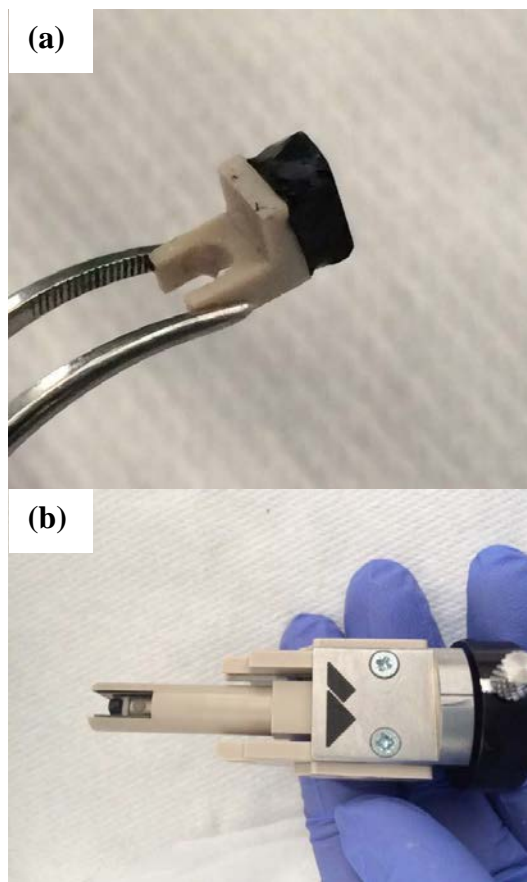
Figure 3.3 Zetasizer Nano accessory for surface zeta potential. The samples are attached by double coated adhesive tapes (Tedpella) to the cell.

3.2.3.5 SEM/ XRD. The REM surface was imaged by scanning electron microscopy (SEM) previously by Dr. Brian P. Chaplin with Hitachi S-4800 cold field emission SEM.[177, 189] XRD analysis was reported by Yin Jing, Lun Guo and Brian P. Chaplin with Siemens D5000 X-ray diffractometer.[190]

3.2.3.6 Porosity and mean pore size.   The overall porosity (P_r) was determined by a gravimetric method. Briefly, the REM membranes were immersed in water and fully soaked (or ran filtration to allow water to flow through all pores and channels. Then wet membrane weight (m_w) was measured and the difference from the dry membrane (m_d)

was determine. This difference represents the weight of pure water in the REM pores, which can be used to calculate the overall porosity as defined in the following equation:[191]

$$P_r = \frac{m_w - m_d}{\rho S L}$$
(3.1)

where m_w is the weight of the wet membrane; m_d is the weight of the dry membrane; S is the membrane effective area (m^2), ρ is the water density (0.998 g·cm^{-3}), and L is the membrane thickness (m).

In addition, to determine the membrane mean pore radius (r_m), the Guerout–Elford–Ferry equation in Equation 3.2 on the basis of the pure water flux and porosity data was utilized:[192-193]:

$$r_m = \sqrt{\frac{(2.9 - 1.75 P_r) \times 8\eta L Q}{P_r \times S \times \Delta P}}$$
(3.2)

where η is the water viscosity (8.9×10^{-4} Pas), Q is the volume of permeate water per unit time (m^3·s^{-1}), and ΔP is the operation pressure.

3.2.3.7 Electrochemical impedance spectrometry (EIS)

To analyze electron transfer-initiated chemical reactions, cyclic voltammetry (CV) were carried out on a CHI 660 electrochemical workstation (CH Instrument, USA).[194] A traditional three-electrode system was employed, including a 3-mm platinum wire as the counter electrode, an Ag/AgCl electrode as the reference electrode, and an REM filter as the working electrode. All the measured electrochemical potentials were referenced to the Ag/AgCl electrode potential, which is assumed to be zero. The electrolyte solution was 10 mM $K_3Fe(CN)_6^{3-}$ (a redox mediator) in 0.5 M KCl as a supporting electrolyte.[195] The REM filter was cut to 5 cm in length to fit into the container, and was immersed in the

supporting electrolyte as shown in Figure 3.4. The CV curves were obtained by sweeping voltages from -1.5 to 1.5 V versus Ag/AgCl at a scan rate of 0.5 V·s^{-1}. Based on the acquired CV data, the electroactive surface area of the Ti_4O_7 REM can be estimated from the calculation of the double layer capacitance (C_{dl}):[190] $(I_a - I_c)/2 = C_{dl} \cdot v$, where I_a and I_c are the measured anodic and the cathodic plateau currents at a given potential, respectively, and v is the scan rate (V·s^{-1}). The electroactive surface area was determined by dividing the measured capacitance by 60 $\mu F \cdot cm^{-2}$, a standard value for metal oxides.[190]
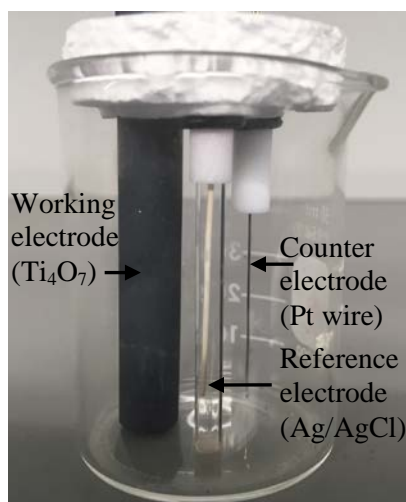
Figure 3.4 Placement of three electrode system in EC station.

EIS is a non-invasive and non-destructive characterization technique for membrane fouling.[190] Due to the foulant adsorption onto the REM surface, the interfacial polarization processes on REM will be affected. To reveal surface fouling on the REM surface and analyze the electrical resistance changes on fouled REM,[190] EIS measurements were made at the OCP in an electrolyte solution containing 10 mM $K_3Fe(CN)_6$, where the clean and fouled REM membranes were immersed, with an amplitude of 5 mV in the sinusoid perturbation and over a frequency range of 1 MHz

to10 mHz. EIS is a non-invasive and non-destructive characterization technique for membrane fouling.[190] Due to the foulant adsorption onto the REM surface, the interfacial polarization processes on REM were affected. To obtain the fouled REM, the membrane was installed into a dead-end filtration system and submerged into 0.05 g·L^{-1} algae suspension for filtration until 90% flux was lost. The configuration of dead-end filtration was described in Section 3.2.4.2). The initially applied voltage was the peak voltage achieved from the CV measurements. The fouled REM was obtained by filtering algal suspension through the REM filter, through which the algal cells and extracellular organic matters deposited on the REM surface and thus, induced surface fouling. To avoid the potential interfrence from the adsorption of the redox active species onto the REM surface on the impedance measurements by changing the interfacial polarization processes, the EIS measurements were conducted over a short time-scale (i.e., ~15 min) and the REM was thoroughly rinsed afterwards to minimize adsorption of the redox active species. A previosu study conducted by Yin Jing, et al. has indicated that these redox active species were not found to significantly react with REM during this EIS measurement.[190]

3.2.4 Dead-end filtration

3.2.4.1 Determination of intrinsic resistance (R$_m$)

The dead-end filtration unit has a cell volume of 1 L,[189] in which there is an Ebonex REM as anode and a 57 mm diameter stainless steel cylinder case as cathode.[18, 19] The REM filter was sealed up on one end by acrylonitrile butadiene styrene (ABS) plastic and reinforced by Epoxy as shown in Figure 3.5f. The other end was also filled with the same ABS plastic and Epoxy but one stainless steel tube or copper tube (1.1 mm in diameter)

were punched through the gel to permit permeate flow and electric conductivity. The Sealing process was shown in Figure 3.5. The REM as anode is at the center of stainless-steel cathode, with approximately 23 mm spacing and their concentric placement creates an isopotential surface on the outer surface of the REM. As shown in Figure 3.6, the solution was vacuum sucked through the surface of the REM at a constant transmembrane pressure (75 kPa) using an adjustable check valve and a vacuum pressure gauge, which forced flow through the REM pores. The constant transmembrane pressure was obtained by imposing a constant vacuum pressure as indicated in Figure 3.6. Flux measurements were made volumetrically by collecting the permeate weight data per minute using WinWedge software and an Ohaus Adventurer Pro Balance AV8101 (Ohaus, USA). (See Figure 3.7b) The clean water flux j_w ($kg \cdot m^{-2} \cdot h^{-1}$) is calculated using the following equation:

$$J_w = \frac{V}{At} \tag{3.3}$$

where V is the volume of permeated water, A (m^2) is the membrane area, and t (h) is the permeation time.

DI water was pumped through both the pristine TiO_2 and Ti_4O_7 filters under the same TMP levels to compare the flux permeability and porosity differences. Inherent membrane resistance was calculated with TMP and permeate flow rate using Equation 3.13.
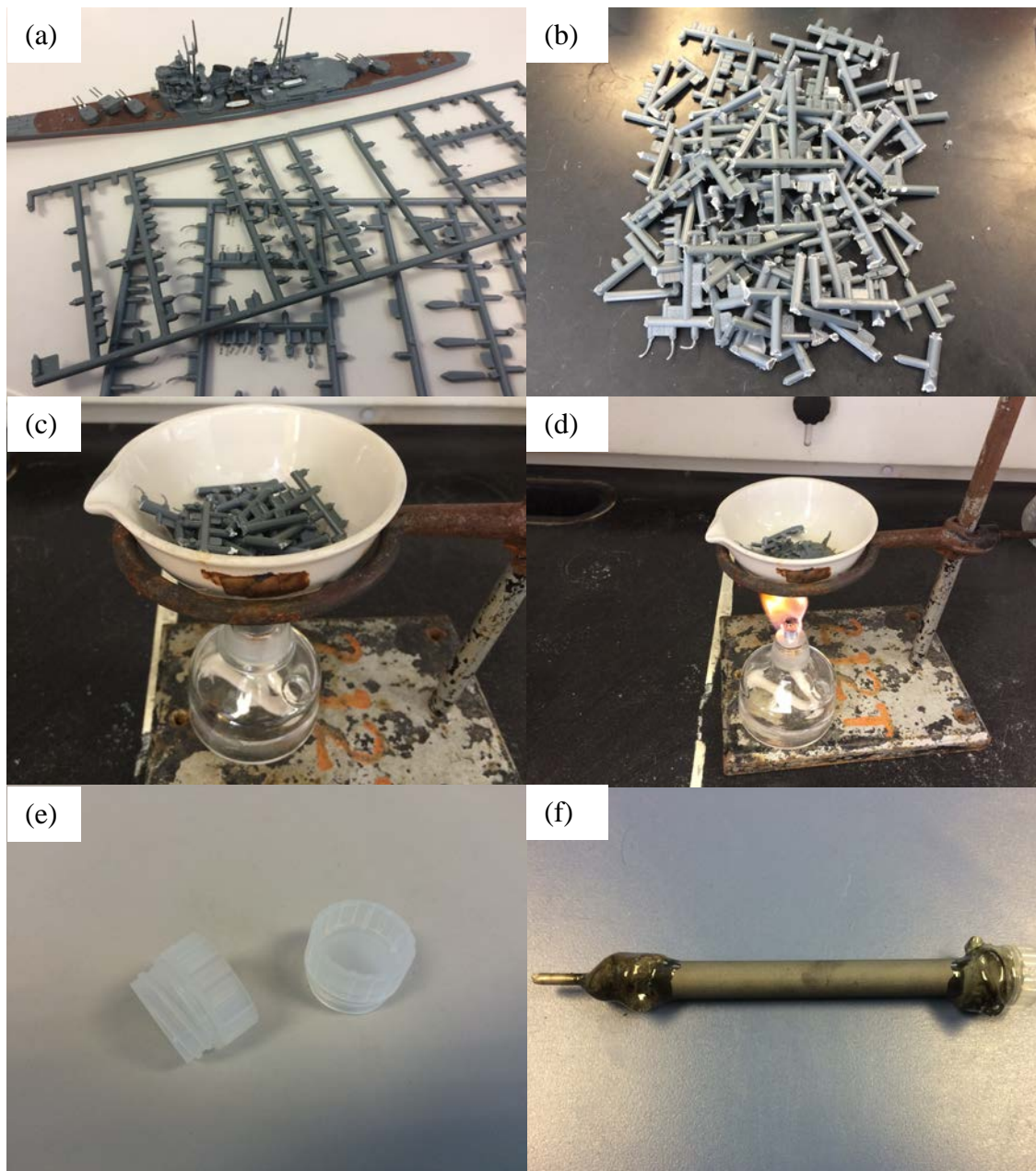
Figure 3.5 Dead-end REM filter sealing process. (a) ABS plastic plate frames were collected from used model parts. (b) ABS plastic plate frames were cut into small pieces so they would be easier to contain. (c) ABS plastic pieces were put into an evaporating dish and an ethanol light is used to heat and liquefy them. (d) With ethanol light, the ABS plastic pieces were starting to melt. (e) Sample tube caps were use as the bottom of the sealing for reinforce. (f) Liquid ABS plastic is poured on both end of REM, and Epoxy is covered after the ABS plastic became solid.
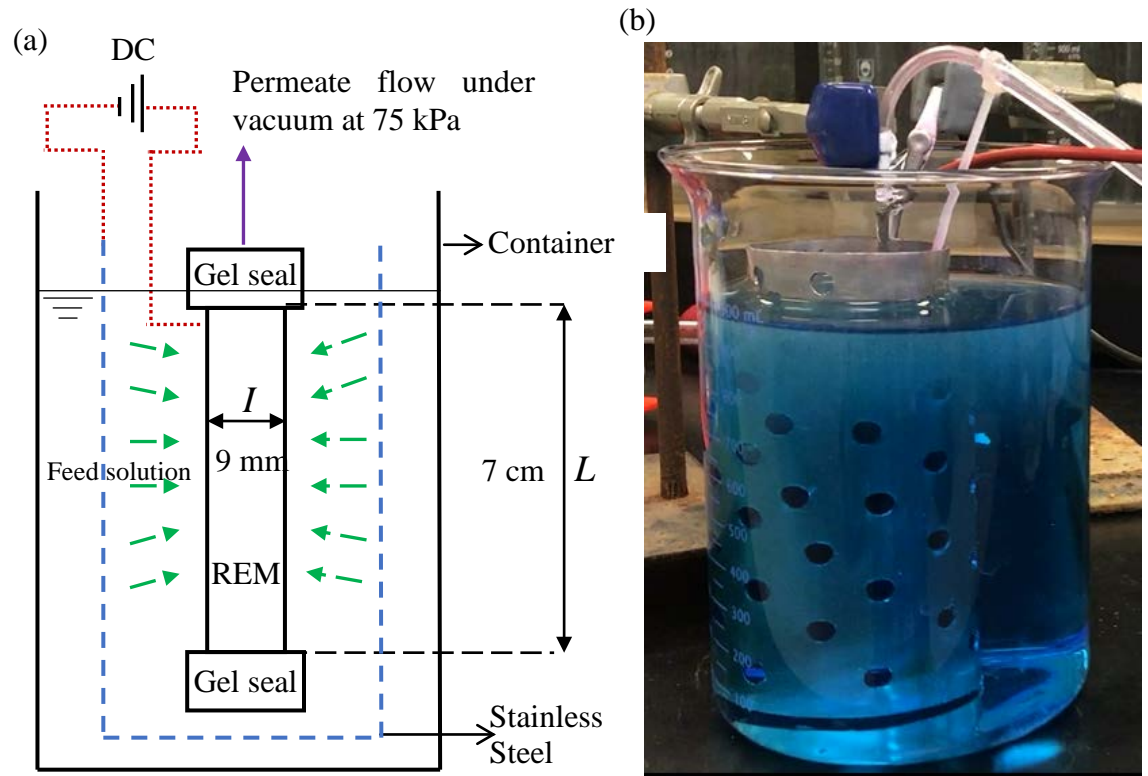
Figure 3.6 (a) Schematics of the REM filtration under a DC application; (b) dead-end filtration setup used in this research.
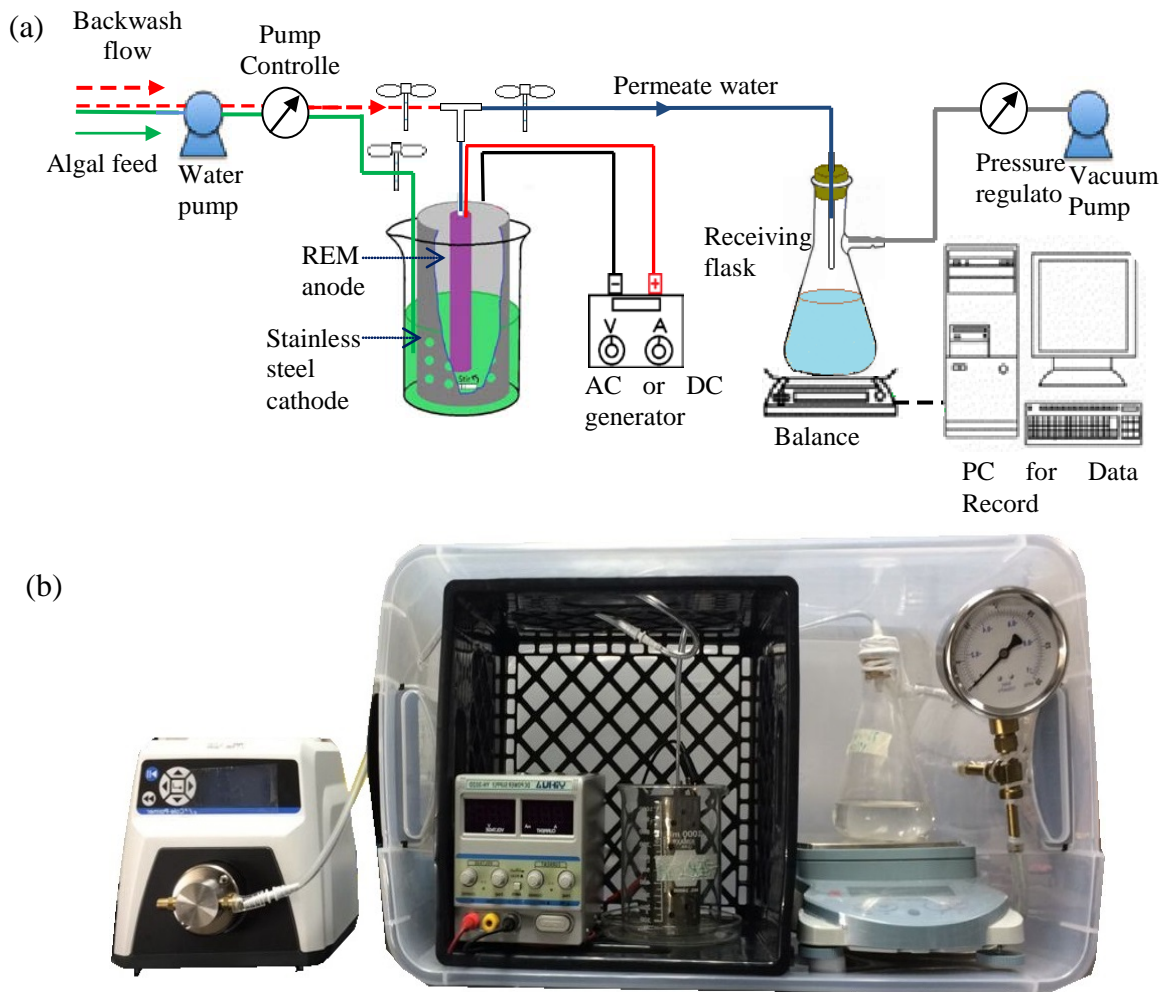
Figure 3.7 (a) Schematic and (b) picture of experiment setup for dead-end filtration in this chapter.

3.2.4.2 Filtration of algal suspension for fouling kinetics study under dead-end filtration.

The fouling kinetics test was performed at a TMP of 75 kPa with the same equipment the used in clean water test as shown in Figure 3.7a. The only difference is that the clean water was replaced by algal suspension. The REM was fully submerged in the algal suspension. Briefly, the REM was first chemically rinsed by 200 mg·L^{-1} NaClO. The DI water tank was replaced by an algal suspension tank with the same cell density of 0.05 g·L^{-1}. After turning a booster pump (aquatic® CDP8800), the permeate water was

immediately collected and measured using WinWedge software and an Ohaus Adventurer Pro Balance AV8101 (Ohaus, USA). Three different DC current densities (0, 1.25 and -1.25 mA·cm^{-2}) were applied. The fouling kinetics data was further interpreted by the flux model as described in Section 3.2.6.

3.2.4.3 Comparison of backwash efficiency with hydraulic rinsing, chemical rinsing and DC current applications for dead-end filtration

The fouled REM was obtained from the above fouling experiments and was subjected to the following three backwash treatment to compare the flux recovery and defouling efficiency. Backwash efficiency (r) was calculated using Equation 3.13 and compared with each other.

(1) Hydraulic backwash.

When the flux is close to zero, the clean water backwash was conducted at a backpressure of 137.90 kPa with a booster pump (aquatic® CDP8800).[189] The backwash flushing was conducted for 60 min, 120 min and 240 min to effectively remove reversible and some irreversible foulant. Clean water flux tests were conduct under a TMP of 70 kPa, 75 kPa, and 80 kPa to compare the recovery of flux permeability.

(2) Chemical backwash

While all other parameters remained the same, the backwash flushing was conducted using 200 mg·L^{-1} NaClO as commonly used for membrane disinfection and biofouling control.[196-198] After washing, REM was backwashed with DI water until pH in the wash water returned to neutral.

(3) Hydraulic backwash under DC currents (or electrochemical backwash)

Electrochemical backwash was implemented using clean water to backwash fouled membranes under the application of DC current at a constant current density (25.3 mA·cm^{-2}) corresponding to a cell voltage of 18-22 V. The backwash flow was maintained at a backpressure of 137.90 kPa for 30-90 min.

3.2.5 Cross-flow filtration

The cross-flow filtration unit was prepared following the design published previously.[29, 34] As illustrated in Figure 3.8, the membrane module consists of an Ebonex REM as anode and a 1.1-mm diameter 316 stainless steel rod as cathode. The REM anode is a hollow cylinder in shape with outer and inner diameters of 1 cm and 0.5 cm, the length is 20 cm and the volume in the filter was 3.925 ml, respectively. The cathode crosses through the center of the REM anode with approximately 4 mm spacing between the cathode and the inner surface of the anode. The resulting hollow space within the REM filter has a volume of 300 ml.[189] With this concentric placement, an isopotential surface can be created on the outer surface of the REM when DC is applied. A bench analog drive gear pump (75211-70 Cole Parmer, USA) was used for injecting the feed influent. The flow meter #1 reads the influent flow rate; Flow meter #2 reads the retentate flow rate; and Flow meter #3 reads the permeate flow rate. An adjustable check valve on flow meter #1was used to control and modulate the flow rate of the permeate flux. Two pressure gauges was installed before and after the crossflow filtration unit to monitor the pressure of the inflow and cross-flow, respectively. Cross-flow velocity and

transmembrane pressure (TMP) are two major parameters affecting cross-flow microfiltration process. Cross-flow velocity was calculated by:

$$\text{Cross flow velocity } (\text{m}\cdot\text{s}^{-1}) = \frac{\text{Flow rate of the influent } (\text{m}^3\cdot\text{s}^{-1})}{\text{Flow channel cross sectional area } (\text{m}^2)}$$

where the flow channel cross sectional area was 1.96×10^{-5}cm in this study. TMP was calculated by:[199]

$$TMP = \frac{P_{in} + P_{cr}}{2} - P_{out} \tag{3.4}$$

where P_{in} denotes the influent pressure, P_{cr} denotes the crossflow pressure and P_{out} denotes the permeate flow pressure. P_{out} is equal to 0 in this case due to the permeate flux was in connection to air.
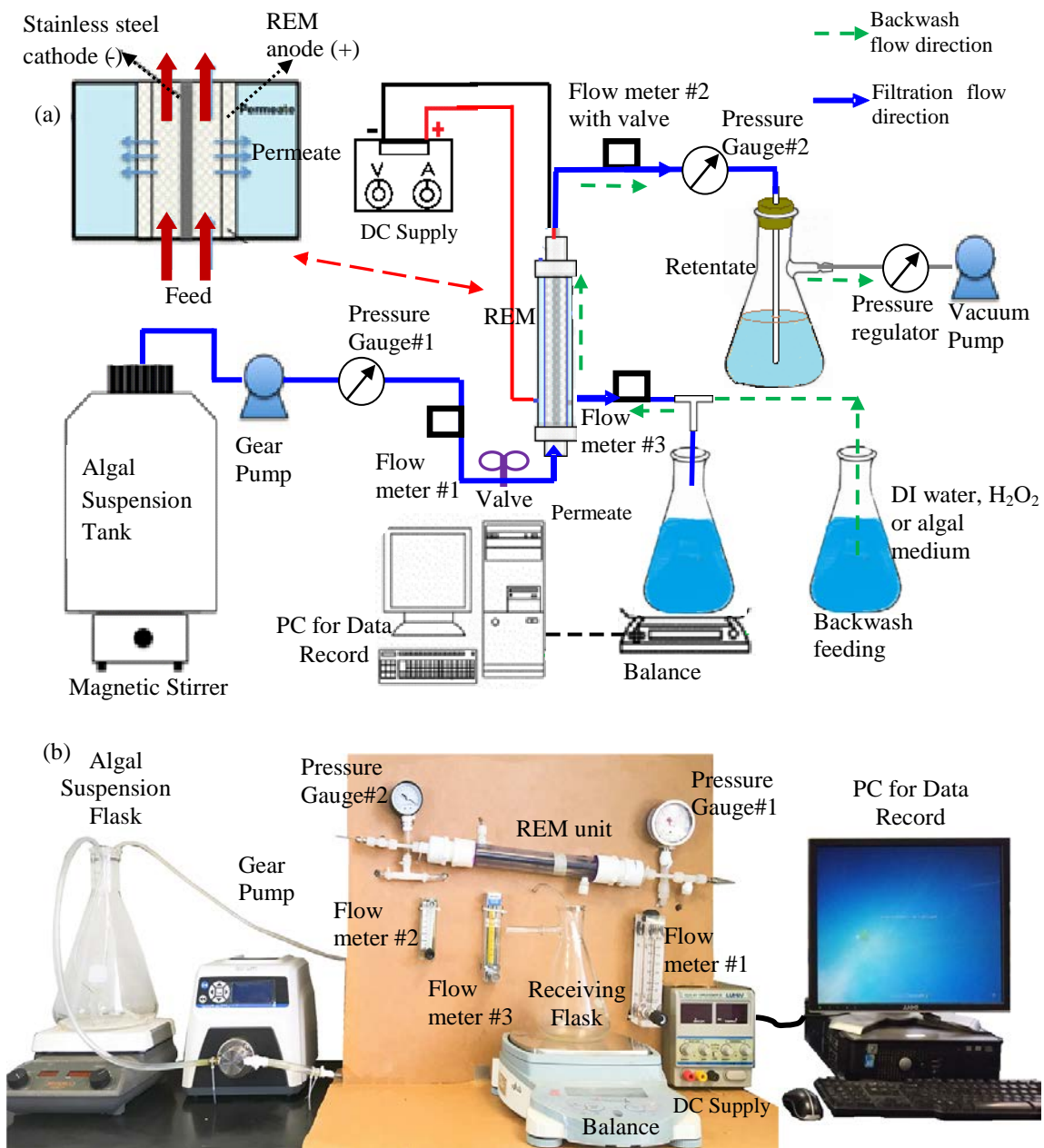
Figure 3.8. (a) Schematics of the cross-flow filtration unit and (b) Real setup of the cross-flow filtration apparatus.

3.2.5.1 Determination of intrinsic resistance (R_m). To evaluate the intrinsic resistance (R_m) of Ti_4O_7 REM, DI water was pumped through the REM anode at five different permeate flux ranging from 5 ml·min^{-1} to 25 ml·min^{-1}. In our current cross-flow configuration, the DI water was pumped from one port with the other port sealed such

that all DI water must permeate through REM (in a dead-end mode). The step height and duration were set to be $2.07 \times 10^{-5} \cdot m^3 \cdot m^{-2} \cdot s^{-1}$ (5 $L \cdot m^{-2} \cdot min^{-1}$) and 15 min, respectively. The pressures of inflow (P_{in}) and crossflow (P_{out}) were directly recorded from the pressure gauges and recorded once every minute. TMP was calculated with the corresponding observed P_{in} and P_{out} by using Equation 3.4 and R_m was then calculated using Equation 3.13.

3.2.5.2 Critical flux determination. Critical flux is the permeate flux above which the membrane fouling rate becomes aggravated and thereby a sharp decline of permeate flux or increase of TMP may be immediately observed.[200] Operation under critical flux enables a longer filtration time due to a lower potential of membrane fouling. In addition, critical flux can also be employed to compare the fouling propensities between different membranes or operation conditions.[200]

Critical flux was obtained from flux-TMP measurements by flux or pressure stepping.[201] In this study, critical flux was determined by varying the permeate flux using an improved flux-step method (IFM).[202] The step height and duration were set to be $2.07 \times 10^{-5} \cdot m^3 \cdot m^{-2} \cdot s^{-1}$ (5 $L \cdot m^{-2} \cdot min^{-1}$) and 15 min, respectively. The initial cell density of the algal suspension was 0.05 $g \cdot L^{-1}$. A magnetic stirrer was used to mix the algal suspension to avoid significant sedimentation and maintain good distribution or dispersion of algal cells in the feed tank. The permeate was continuously returned to the feed tank to keep the algal suspension at a constant concentration. The pressures of inflow (P_{in}) and crossflow (P_{out}) were observed and recorded once every minute. The filtration process lasted for at least 1 h until the pressures shown on the gauges #1 and #2 increased significantly. When the increase in the TMP ($\Delta P/\Delta t$) is 20 $Pa \cdot min^{-1}$ or higher, it

is commonly regarded as the occurrence of a pronounced membrane fouling. Accordingly, the permeate flux at the onset of the TMP increase corresponds to the critical flux.[203]

Different DC densities were also applied on the REM to compare the possible changes of critical fluxes. Both positive and negative currents were separately applied to the REM to gain anodic or cathodic polarization at 1.25, 2.5 and 5 $mA \cdot cm^{-2}$ using a programmable direct current (DC) power supply (Proteck P6035). These DC current densities were chosen based on commonly reported levels in literature, which are anticipated to produce sufficient electrode potentials and radicals on REM, while not significantly cause undesirable side reactions such as water splitting.

3.2.5.3 Fouling kinetics of cross-flow filtration with algal suspension under different DC currents

Fouling kinetics was assessed under different levels of DC currents applied on the REM under a fixed TMP of 10 psi (68.94 kPa) to examine the impact of EAOP on fouling kinetics and fouling mitigation. Three different DC densities (0.625, 1.25 and 2.5 $mA \cdot cm^{-2}$) were applied. Permeate flux under different DC current applications were measured respectively. The fouling kinetics data was further employed in the flux model as described in Section 3.2.6 to analyze the fouling mechanisms.

3.2.5.4 Comparison of backwash efficiency with hydraulic, chemical and electrochemical backwash for fouled membranes after cross-flow filtration

Similar to dead-end filtration, three backwash treatment was used to compare the flux recovery and defouling efficiency.[177] Clean water flux tests were conducted under TMP from 5 to 25 psi (34.47 to 172.37 kPa) to compare the recovery of flux permeability.

(1) Hydraulic backwash.

When the permeate flux is close to zero, the hydraulic backwash was conducted by sucking DI water at a vacuum pressure of 80 kPa from the outside chamber of the membrane module into or across the REM surface as illustrated in Figure 3.8a. The backwash flushing was conducted for 60 min, 120 min and 240 min to allow the filtered DI water to cross the membrane from outside to inside and effectively rinse off the attached algal biomass or other foulants on the inner surface of the REM.

(2) Chemical backwash

In chemical backwash, while all other parameters remained the same, the DI water solution was replaced by a chemical reagent solution (200 mg·L^{-1} H$_2$O$_2$ as used in membrane disinfection and biofouling control[196-198]). After washing, REM was backwashed with DI water until pH in the wash water returned to neutral.

(3) Electrochemical backwash

Electrochemical backwash was implemented using clean water to backwash fouled membranes under the application of DC current at a constant current density (2.5 mA·cm^{-2}) corresponding to a cell voltage of 3-3.3 V. The backwash flow was maintained at a backpressure of 20 psi for 15-30 min.

3.2.5.5 Evaluation of biomass concentration performance. Volumetric reduction factor (VRF) and concentration factor (CF) are commonly used to assess algal harvesting efficiency in membrane filtration processes:[204-206]

$$VRF = \frac{V_0}{V_f} \tag{3.5}$$

$$CF = \frac{C_f}{C_0} \tag{3.6}$$

where V_0 and C_0 are, the initial volume (L) and initial algal concentration (dry weight, $g \cdot L^{-1}$), respectively; V_f and C_f are final volume (L) and concentration ($g \cdot L^{-1}$) of the concentrated algal suspension, respectively.

To evaluate the harvesting efficiency per unit membrane surface, the recovery rate (R_{ec}), the productivity of the physical cleaning (η_m, $g \cdot m^{-2} \cdot min^{-1}$) and the retentate in the membrane tank (η_t, $g \cdot m^{-2} \cdot min^{-1}$) were calculated using the following equations:

$$R_{ec} = \frac{C_f V_f}{C_0 V_0} \times 100\% \tag{3.7}$$

$$\eta_m = \frac{C_f V_f}{A \cdot t} \tag{3.8}$$

$$\eta_t = \frac{(C_t - C_0) V_t}{A \cdot t} \tag{3.9}$$

where V_t and C_t were the volume of the algae culture (m^3) and algae density ($g \cdot m^{-3}$) of the membrane tank at the membrane filtration time; A is the membrane filtration area (0.004 m^2 for the cross-flow membrane) and t is the filtration time (min).

Moreover, the algal distributions on the membrane (Wm) and in the membrane tank (Wt) were also calculated as:

$$W_m = \frac{C_f V_f}{(C_t - C_0)V_t + C_f V_f} \tag{3.10}$$

$$W_t = \frac{(C_t - C_0)V_t}{(C_t - C_0)V_t + C_f V_f} \tag{3.11}$$

In addition, I propose a new indicator of recovery efficiency that is named as specific biomass recovery efficiency (SBRE). In this definition, we evaluate the biomass harvesting or recovering efficiency by considering the total energy consumption for harvesting certain amount of biomass.

$$SBRE = \left(\frac{C_f V_f}{C_0 V_0} \right) W^{-1} \tag{3.12}$$

where W is the total energy applied to concentrate algae (J) in the suspension, and

W=Q·t·TMP (Q: flow rate, m^3·s; t: filtration time, s; and TMP is the transmembrane

pressure, Pa).

Finally, we also computed the uptime, which is equal to (Volume of treated

wastewater)/(Volume of available wastewater or the stock algal suspension) × 100% (Not

including chemical cleaning). In industrial membrane operations, system uptime is often

used as an indicator of membrane operation stability and residual waste to manage.

3.2.6 Membrane fouling kinetics modeling using resistance-in-series model

The resistance-in-series model was used to calculate the permeate flow rate according to

the Darcy's law:[207-208]

$$Q = \frac{A\Delta P}{\mu(R_m + R_r + R_{ir})} \tag{3.13}$$

All parameters are explained in Table 3.1. Particularly, R_m is the inherent

membrane resistance that was determined with filtration of DI water as mentioned above

in section 3.2.4.1 and 3.2.5.1. The calculation of irreversible membrane resistance (R_{ir}) is

shown in Equation 3.15 and reversible membrane resistance (R_r) is described in

Equation 3.16.[204]

3.2.6.1 Calculation of backwash efficiency (*r*) and irreversible fouling resistance (*R_{ir}*)

Backwash efficiency is calculated using the following equation:

$$r = \frac{Q_n}{Q_{n-1}} \tag{3.14}$$

where r is backwash efficiency, and Q_{n-1} and Q_n are the flow rates after the $n-1$ and n backwashes.

The flow rates after the $n-1$ and n backwashes can be calculated by:

$$R_{irn} = \frac{1-r}{r}R_m + \frac{1}{r}R_{ir(n-1)}$$
(3.15)

where $R_{ir(n-1)}$ and R_{irn} are the irreversible fouling resistances after the $n-1$ and n backwashes. At the beginning of the filtration, $R_{ir0} = 0$, and r can be determined via the backwash experiment. Thus, Equation 3.15 can be used to calculate the irreversible fouling resistance.[204]

3.2.6.2 Calculation of reversible fouling resistance. The cake layer is usually an immobile layer of retained particles packed on the membrane surface. Neglect the polarization effect, reversible fouling resistance R_r could be equal to the resistance of the cake layer R_c, is given as:

$$R_c = k_c \cdot \delta_c$$
(3.16)

The specific resistance per unit of cake thickness (k_c) and cake layer thickness (δ_c) were calculated by Equation 3.17 and Equation 3.18 with experimental data of t and V_t under different conditions.[209]

$$\frac{t}{V_t} = \frac{\mu k_c C_b}{2A^2 \Delta P}V_t + \frac{\mu R_m}{A\Delta P}$$
(3.17)

For dead-end filtration, δ_c can be calculated from Equation 3.13 to 3.18 (See the logic chart in Figure 3.9a).[210]

$$\delta_c = \frac{-R_m + \sqrt{R_m^2 + 2k_c \frac{\Delta P}{\mu}\frac{C_b}{C_w}t}}{k_c}$$
(3.18)

For cross-flow filtration, Equation 3.19 and Equation 3.20 were used to describe the cake growth kinetics instead of Equation 3.18.

$$-\frac{\Delta P}{J_s \mu k_c k_{cr}} \ln\left(1 - \frac{J_s \mu k_c \delta_c}{\Delta P - J_s \mu (R_m + R_{ir})}\right) - \frac{\delta_c}{k_{cr}} = t \tag{3.19}$$

$$k_{cr} = \frac{J_s}{J_0 - J_s} \cdot \frac{C_b}{C_w} \cdot J_0 \tag{3.20}$$

where J_s is the flux at steady state and J_0 is the initial flux, both could be obtained by filtration experiment.

3.2.6.3 Calculation of flux at steady state using the force balance model. In the cross-flow membrane filtration process, negative direction forces such as permeation drag (F_d) move algae toward the membrane surface, while positive forces such as Brownian diffusion (F_B), shear-induced diffusion (F_s), and lateral inertial lift (F_l) shift algae away from the membrane surface. The net force exerted on an algal particle, F, is the sum of all forces listed above. At a steady state, the flux (J_s) can be calculated using the following equation:[211-212]

$$J_s = V_B + V_S + V_I \tag{3.21}$$

$$V_B = \frac{0.807 D_B^{2/3} \gamma^{1/3}}{L^{1/3}} \ln\left(\frac{C_w}{C_b}\right) \tag{3.22}$$

$$V_s = \frac{0.807 D_S^{2/3} \gamma^{1/3}}{L^{1/3}} \ln\left(\frac{C_w}{C_b}\right) \tag{3.23}$$

$$V_I = 0.577 \frac{d_P^3 U_m^2}{I^2 \nu} \tag{3.24}$$

The wall shear rate (γ) can be calculated from the following formulas:[212]

$$\gamma = \frac{8 U_m}{I} \tag{3.25}$$

Some related studies misused wall shear stress (τ_w, Pa) with wall shear rate (γ, s^{-1}) and in Equations 3.22 and 3.23, which may lead to calculation error or misunderstanding. The wall shear stress (τ_w) is in fact calculated by:

$$\tau_w = \frac{8 U_m}{I} \mu \qquad\qquad (3.26)$$

3.2.6.4 Simulation of membrane fouling kinetics in dead-end mode using Matlab

Figure 3.9a shows the algorism schematics using above mentioned equations for dead-end membrane filtration. Briefly, ExpQ, were firstly calculated the linear interpolation method from experimental data (t and V_t). ExpQ was then used to calculate a set of C_w with the input value of μ, R_m, A, R_{ir}, C_b and ΔP, with Equation 3.13 and 3.18. R_{ir} was obtained from backwash experiment (descried in Section3.2.4.3). Then, C_w was used to calculate a set of Q with Equation 3.13 and 3.18. R^2 method was used to compare Q and ExpQ. The Q with the R^2 was output as the simulated flow rate with the corresponding C_w. The simulation code is provided in Appendix 3.5.1. This model was not only used for the fitting of experimental data, but also used to predict the flow rate without experimental data and evaluate the dependence of the flow rate on factors such as volume concentration of algal cells at the membrane surface (C_w), inherent membrane resistance (R_m), specific resistance per unit of cake thickness (k_c) and bulk concentration (C_b).

3.2.6.5 Simulation of membrane fouling kinetics in cross-flow mode using Matlab

Figure 3.9b presents the calculation processes using above mentioned equations for cross-flow membrane filtration. Briefly, Q, J_0 and J_s were firstly calculated the linear interpolation method from experimental data (t and V_t). Q was then used to calculate a set of R_c (or R_r) with the input value of μ, R_m, A and ΔP. R_{ir} was ignored for cross-flow filtration experiments as only one filtration cycle was operated after which chemical

backwash was used to remove all membrane foulants. Thus, the irreversible membrane foulants or resistance was minimized before the start of new filtration tests. Then, with Equations 3.16 and 3.17, we can determine the specific resistance per unit of cake thickness (k_c) and the time-dependent cake layer thickness (δ_c). Finally, C_w was calculated using Equations 3.19 and 3.20 with the input of k_c, δ_c and other parameters that already known or determined. The full Matlab code is provided in the appendix 1.1.

(a)

Input t, V_t.

↓

Calculate experimental Q by a linear interpolation fit method.

↓

Input experimental Q, μ, R_m, C_b, A, ΔP, r, R_{ir}.

↓

Use Equation 3.13 to 3.18 to calculate a set of C_w.

↓

Use C_w vector and Equation 3.13 to 3.18 to determine a set of Q

↓

Use R^2 method to compare Q and ExpQ — Low R^2

↓ Highest R^2

Output Q vector, C_w

(b)

Input t, V_t.

↓

Calculate Q, J_0 and J_s by a linear interpolation fit method.

↓

Input μ, R_m, A, ΔP, R_{ir}.

↓

Calculate R_c from Q using Equation 3.13

↓

Input C_b.

↓

Use Equation 3.13 to 3.20 to calculate a set of kc' and C_w'.

↓

Use C_w and kc vector and Equation 3.13 to 3.20 to output a set of R_c'.

↓

Use R^2 method to compare R_c and R_c' — Low R^2

↓ Highest R^2

Output Q, C_w, k_c and R_c'

Figure 3.9 Logic chart of Matlab algorithm. (a) Dead-end filtration; (b) cross flow filtration.

Table 3.1 Parameter Nomenclature

	Parameters	Physical meanings and values
*	Q	Permeate flow rate ($m^3 \cdot s^{-1}$), which is determined by Equation 3.13
	ΔP	Transmembrane pressure (Pa), which is the trans-membrane pressure (TMP) defined as:[213] $TMP = \Delta P = P_{feed} - P_{permeate}$ ΔP remained constant in our filtration experiments and was determined by pressure gauges 1 and 2 as labeled in Figure 3.6.
	μ	Dynamic viscosity (Pa·s)(for water, 8.90×10^{-4} Pa·s at 25 $^{\circ}$C).
	R_m	Inherent membrane resistance (m^{-1}), which is constant (to be determined by filtration experiment using pure water.
*	R_r or R_c	Reversible fouling resistance or resistance of the cake layer (m^{-1}), determined by Equation 3.16
*	R_{ir}	Backwash irreversible resistance (m^{-1}), determined by Equation 3.15
	A	Membrane filtration area (m^2), known parameter, approximately 0.004 m^2 for cross flow REM filter
	r	Backwash efficiency, determined by Equation 3.14 via experiment
*	k_c	Specific resistance per unit of cake thickness (m^{-2}); To be determined by Equation 3.18
*	δ_c	Cake thickness (m); To be determined by Equation 3.19
	C_b	Algae bulk concentration (v/v, %), defined as algal volume divided by volume of water. Constant, variable around 0.0005% (or 0.05 $g \cdot L^{-1}$) in cross flow experiment
	t	Filtration time (s)
	V_t	Permeate volume at time t (m^3), which is a variable factor (to be determined by experiment), vary by time
*	J_s	Permeation flux at steady state ($m^3 \cdot m^{-2} \cdot s^{-1}$); To be determined by Equation3.21
*	k_{cr}	Cake growth rate constant ($m \cdot s^{-1}$); To be determined by Equation3.20
	J_0	Initial permeate flux ($m^3 \cdot m^{-2} \cdot s^{-1}$); Constant (to be determined by each experiment)
	C_w	Volume concentration of algal cells at the membrane surface (%); To be determined by Equation 3.20
*	V_B	Algal transport velocity due to Brownian diffusion ($m \cdot s^{-1}$); To be calculated by Equation 3.22
*	V_S	Algal transport velocity due to shear-induced diffusion ($m \cdot s^{-1}$); To be calculated by Equation 3.23
*	V_I	Algal transport velocity due to lateral inertial lift ($m \cdot s^{-1}$); To be determined by Equation 3.24
	D_B	Brownian diffusion coefficient ($m^2 \cdot s^{-1}$), which is a constant ($D_B = k_B T/6\pi\mu d_p^2$) used in Equation 3.22
	T	Temperature (K), a constant (298 K or 25 $^{\circ}$C), used for D_B
	k_B	Boltzmann constant ($1.38064852 \times 10^{-23}$ m^2 kg s^{-2} K^{-1}), used for D_B
	γ	Wall shear rate s^{-1}; To be determined by Equation3.25
	L	Membrane module channel length (m), a constant (approximately 0.2m),
	D_S	Shear-induced diffusion coefficient, a constant ($D_S = 0.03\ d_p^2 \tau_W$)
	d_p	Equivalent volume radius of the algae (m), (approximately 1.7×10^{-6} m)
	v	Kinematic viscosity ($m^2 \cdot s^{-1}$)(for water, 1.0×10^{-6} at 25 $^{\circ}$C)
	I	Channel height (m) or diameter of the tubular REM (approximately 0.009m)
	U_m	Cross-flow velocity ($m \cdot s^{-1}$), which is the linear rate of flow of fluid parallel to the membrane (m·s) and $U_m = 4Q \cdot (\pi \cdot I^2)^{-1}$

The * highlighted are unknown key factors.

Table 3.2 Parameters in Matlab Codes

Parameters	Matlab symbols	Property		value
Q	Q			
ΔP	deltaP	Global	Constant	68947.6
μ	Mu	Global	Constant	8.90×10^{-4} Pa·s
R_m	R_m	global		3×10^{11}
R_c	R_c, R_c1			
R_{ir}	R_ir			
A	A	global	Constant	4×10^{-3}
r	R	global		
k_c	k_c, realk_c, k_c1		Constant	
δ_c	delta_c, delta_c1			
C_b	C_b	global	Constant	0.1%
t	t			
V_t	V_t			
J_s	Js			Determine by experiment
k_{cr}	Kcr			
J_0	J0	global		Determine by experiment
C_w	realC_w, C_w	global	Constant	92.5%
V_B	VB			
V_S	VS			
V_I	VI			
D_B	D_B		Constant	
T	T	global	Constant	298
k_B	KB	global	Constant	$1.38064852 \times 10^{-23}$
γ	Gama		Constant	
L	L	global	Constant	0.07
D_S	DS			
d_p	DB	global	Constant	1.7×10^{-6}
v	V		Constant	1.0×10^{-6}
I	I	global	Constant	0.009
U_m	Um			

3.2.7 Viscosity effects on algal filtration

The three major factors affecting fouling are biomass and feed characteristics, membrane operation and membrane module characteristics as shown in Figure 3.10 for submerged MBRs.[213] Non-Newtonian fluid does not have a constant viscosity, in particular biomass suspension such as activated sludge, which has a decreasing apparent viscosity with increasing applied shear rate[214-215] The behavior of MBR viscosity has also been referred to as pseudoplastic, i.e. the particles tend to flocculate in a large network that, when disrupted, by increasing the applied shear rate, results in a decrease in viscosity.[214] Several models were proposed where the apparent viscosity of the MBR activated sludge was calculated as a function of MLSS concentration, shear rate and temperature. [214, 216-217] The models proposed by the abovementioned authors are presented in Table 3.3. In our simulation of the impacts of suspension viscosity, we assumed algal suspension is subjected to viscosity increase when their concentration is increased after repeated membrane filtration. We adopted three models with a fixed level of shear rate. Permeability (P), the ratio between the flux and TMP [$L·m^{-2}.h^{-1}·bar^{-1}$] was calculated as follows:

$$P = \frac{J}{TMP} \qquad (3.27)$$

Permeability can be corrected for temperature by incorporating viscosity, as follows:

$$P_c = \frac{J}{TMP} \cdot \frac{\eta_{act}}{\eta_{ref}} \qquad (3.28)$$

where: P_c = permeability corrected for reference temperature [$L·m^{-2}.h^{-1}·bar^{-1}$]; η_{act} = actual viscosity [Pa·s]; η_{ref} = viscosity at reference temperature [Pa·s].
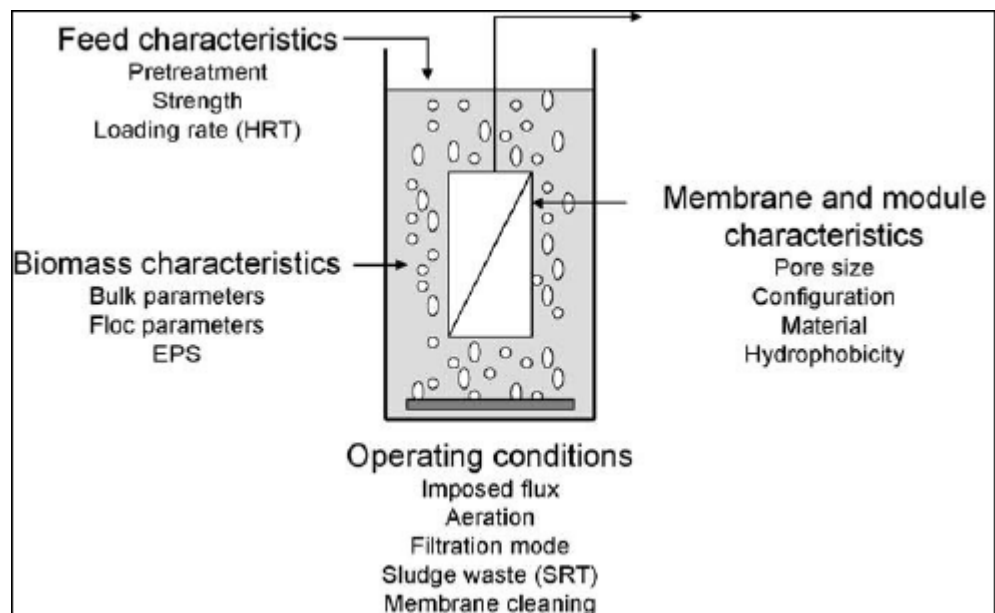
Figure 3.10 Factors affecting fouling in submerged MBRs.[218]

Table 3.3 Models for Determining the Viscosity of MBR Activated Sludge at 20°C

Model types	Equation	Reference
Model 1	$\eta = e^{2 \times C_{MLSS}^{0.41}} \times \gamma^{-0.23 \times C_{MLSS}^{0.37}}$	214
Model 2	$\eta = e^{0.882 \times C_{MLSS}^{0.494}} \times \gamma^{-0.05 \times C_{MLSS}^{0.631}}$	216
Model 3	$\eta = 32.36 \times C_{MLSS}^{1.359} \times \gamma^{-0.807}$	217

H: apparent viscosity of biomass suspension [mP·s];

C_{MLSS}: biomass concentration [g·L^{-1}];

γ : shear rate [s^{-1}].

3.2.8 Compressibility coefficient for the cake layer

Compressibility can be understood as the compress potential of a certain cake layer

expressed by the compressibility coefficient or index (*n*), varying between 0 and 1. A

compressibility coefficient of 0 is obtained when no compression occurs, i.e., when the

resistance is independent from compression. In contrast, a compressibility coefficient of 1

is obtained when the resistance is dependent from compression, therefore when the cake

layer is highly compressible. When permeate flux is fixed and TMP is changing, the compressibility index (n) and resistance coefficient (α) can be calculated if the cake resistance (R_c) are known.

$$\log(R_c) = \log(\frac{m_{cake} \times \alpha}{A}) + n \log TMP \qquad (3.29)$$

where A is the membrane filtration area (m^2), TMP is transmembrane pressure and m_{cake} is the mass of cake layer (g). When TMP is fixed while the permeate flux is changing, Equation 3.29 can be modified as follows:

$$\log(R_c) = \log(\frac{m_{cake} \times \alpha}{A}) - n \log J \qquad (3.30)$$

where J is the permeate flux (m^3·m^{-2}·s^{-1}). m_{cake} can be estimated as $m_{cake} = \rho \cdot (\delta_c \cdot A \cdot C_W)$, where C$_W$ is the cell density on the membrane wall (%, v/v) and ρ is the algal density (approximately 0.05 g·L^{-1}). This equation was used to fit the experimental result in Figure 3.27.

3.2.9 Surface energy calculation based on EDLVO theory

The REM-algae interactions were modeled as particle–surface geometry.[219] In our calculation, the total interaction energies, U_{Total}, between Ti$_4$O$_7$ REM and algae are equal to:

$$U_{Total} = U_{vdW} + U_{EL} + U_{AB} \qquad (3.31)$$

where U_{vdW}, U_{EL}, and U_{AB} are the van der Waals, double-layer and and acid-base interaction energy (k_BT), respectively..[220]

$$U_{132}^{vdw} = -\frac{A_{132}}{6}\left[\frac{a}{h} + \frac{a}{h+2a} + \ln\left(\frac{h}{h+2a}\right)\right]$$

$$U_{132}^{EL} = \pi\varepsilon_0\varepsilon\left(\xi_1^2 + \xi_2^2\right)\left[\frac{2\xi_1\xi_2}{\xi_1^2 + \xi_2^2}\ln\frac{1+\exp(-\kappa h)}{1-\exp(-\kappa h)} + \ln\left\{1-\exp(-2\kappa h)\right\}\right] \qquad (3.32)$$

Although surface hydrophobicity changes may induce the changes to van der Waals, electrostatic and steric interaction energies, to simplify the EDLVO calculation, the effect of surface hydrophobicity changes is only attributed to the change of acid-base interaction energy in Equation 3.33 in this study:[221]

$$U_{AB}(h) = \pi a\lambda\Delta G_{132,D_0}^{AB}\exp\left(\frac{h_0-h}{\lambda}\right) \qquad (3.33)$$

$\Delta G_{132,D_0}^{AB}$ can be estimated by following equations:[222-223]

$$\Delta G_{132,D_0}^{AB} = -\frac{K_{132}}{2\pi h_0\lambda} \qquad (3.34)$$

$$\log K_{132} = -7.0\left(\frac{\cos\theta_1 + \cos\theta_2}{2}\right) - 18.0 \qquad (3.35)$$

where $\Delta G_{132,D_0}^{AB}$ is the standard polar or acid-base free energy (J m^{-2}) at the minimum equilibrium distance (h_0=0.157 nm) due to Born repulsion can be estimated by the hydrophobicity determination using water contact angles,[222-223] K_{132} is the hydrophobic force constant (J). The contact angles (θ) were measured on plain surfaces of different samples at room temperature by liquid drops and ImageJ software. The results of contact angles using three different probe liquids are shown in Table 3.4.

The extended Young's equation is used to calculate the surface tension:[224]

$$(1+\cos\theta)\cdot\gamma_L = 2(\sqrt{\gamma_i^{LW}\gamma_L^{LW}} + \sqrt{\gamma_i^+\gamma_L^-} + \sqrt{\gamma_i^-\gamma_L^+}) \qquad (3.36)$$

where γ_L is the probe liquid surface energy (mJ·m^{-2}), which is known for the three probe liquids as shown in Table 3.4. γ_i^{LW} is the apolar part of surface tension of condensed

material (i) caused by dispersion energy between molecules, and to γ_i^+ or γ_i^- are the polar part of surface tension of condensed material (i) caused by dipole interaction included dipole moments and hydrogen bonds. The surface tension results are summarized in Table 3.5, which are further used to compute the Hamaker constant for interaction between algae and Ti_4O_7 REM in water using the method of van Oss:

$$A_{132} = 24\pi h_0^2 \left(\sqrt{\gamma_1^{LW}} - \sqrt{\gamma_3^{LW}} \right)\left(\sqrt{\gamma_2^{LW}} - \sqrt{\gamma_3^{LW}} \right) \tag{3.37}$$

where h_0 is the minimum equilibrium distance (0.157 nm). The subscript 1, 2, and 3 corresponds to Ti_4O_7 REM, algae, and water, respectively. The calculated Hamaker constant is 2.2×10^{-21} J, which is incorporated in the EDLVO calculation in Table 3.6.

Table 3.4 Contact Angles Data

	Contact angle (º)		
	Water	**Formamide**	**Glycerol**
Thermally reduced REM	0	59.44±8.89	58.08±8.93
Untreated REM	0	46.58±2.47	77.42±5.24
Scenedesmus dimorphus	19.3±3.1	26.1±3.7	24.2±2.4

Table 3.5 Surface Energy Components of Untreated and thermally reduced REM, Algae, and the Three Probe Liquids [225-226]

	Surface energy (mJ·m^{-2})	**Polar surface tension components** (mJ·m^{-2})	**Polar surface tension components** (mJ·m^{-2})	
	γ_L	γ^{LW}	γ_i^+	γ_i^-
Untreated REM	N.A.	6.142086667	3.83703333	114.84908
Thermally reduced REM	N.A.	14.39811591	10.189025	74.22501818
Scenedesmus dimorphus	N.A.	8.8±8.3	7.9±7.2	86.1±2.2
Water	72.8	21.8	25.5	25.5
Formamide	58		2.3	39.6
Glycerol	64		3.9	57.4

Table 3.6 Parameters used in EDLVO Theory Equations

a_1	The radius of Ti_4O_7 REM taken as 27 nm.[227]
a_2	The radius of algal cells taken as 4000 nm, which is the average radius of *Scenedesmus dimorphus* characterized by the Multisizer 3 Coulter Counter instrument previously.[228]
A	The reduced particle radius, $a = a_1 a_2/(a_1+a_2)$.
A_{132}	Hamaker constant for interacting subject 1 and subject 2 in the medium 3. 2.2×10^{-21} J (calculated above)
ξ_1 and ξ_2	Zeta potential. -1.03 ± 0.4 and -29.0 ± 1.3 mV for Ti_4O_7 REM and algae, respectively, in algal medium (assuming no changes in zeta potential of the nanocomposite during UV irradiation).
h_0	The minimum equilibrium distance due to the Born repulsion, 0.157 nm.
H	The separation distance between the two interacting particles (nm).
Λ	The correlation length, or decay length, of the molecules of the liquid medium. For pure water, it is approximately 0.6 nm [229].
θ_1	the water contact angles of algae, (19.3 ± 3.1) °
θ_2	the water contact angles of thermally reduce REM
Λc	The "characteristic wavelength" of the interaction, often assumed to be 100 nm.[230]
κ	The inverse Debye length (m^{-1}) defined as $\kappa = \left(N_A e^2 \sum c_i z_i^2 / \varepsilon_0 \varepsilon_r k_B T \right)^{1/2}$.
N_A	Avogadro's number, 6.02×10^{23} mol^{-1}.
e	Unit charge, 1.602×10^{-19} C.
c_i	c_i is the molar concentration of one species ions (i), mol·L^{-1}.
ε_0	The dielectric permittivity of a vacuum, 8.854×10^{-12} C·V^{-1}·m^{-1}.
ε	The dielectric constant of water, 78.5 (dimensionless).
z_i	The valence of the ith ion.
k_B	Boltzmann constant, 1.38×10^{-23} J·K^{-1}.
T	The absolute temperature taken as 298 K.
n	The molar concentration of ionic species in the medium (mol·m^{-3}) multiplied by Avogadro's number (#·mol^{-1}).
D_{Sc}	Scaling length, 1 nm.
$\alpha S_c k_B T/a_m^3$	3×10^5 N·m^{-2}.[231]
δ	Adsorbed SA layer thickness, 2 nm (measured from the SEM images in Figure 3.13).
Φ_{S0}	SA volume fraction at a single saturated surface, 0.2.
Γ/Γ_0	Fractional SA surface coverage, 0.5*
μ_0	The magnetic permeability of vacuum ($\mu_0 = 1.26\times10^{-6}$ Tm A^{-1}).[232]
R_R	The reduced particle radius, $R_R = a_1 a_2/(a_1+a_2)$.

*The surface coverage was assumed in this EDLVO analysis.

3.3. Results and discussion

3.3.1 Characterization of Ti_4O_7 REM

3.3.1.1 Conductivity change before and after thermal reduction.

There is a conductivity change from the original TiO_2 REM to thermally treated ones that are reduced to Ti_4O_7. The electrical resistivity changed from 4-6 $\Omega \cdot cm$ to 1.5-3.5 $\Omega \cdot cm$, which agrees with previous studies.[233] Figure 3.11 shows the tubular filters had negligible appearance change before and after the thermal treatment.
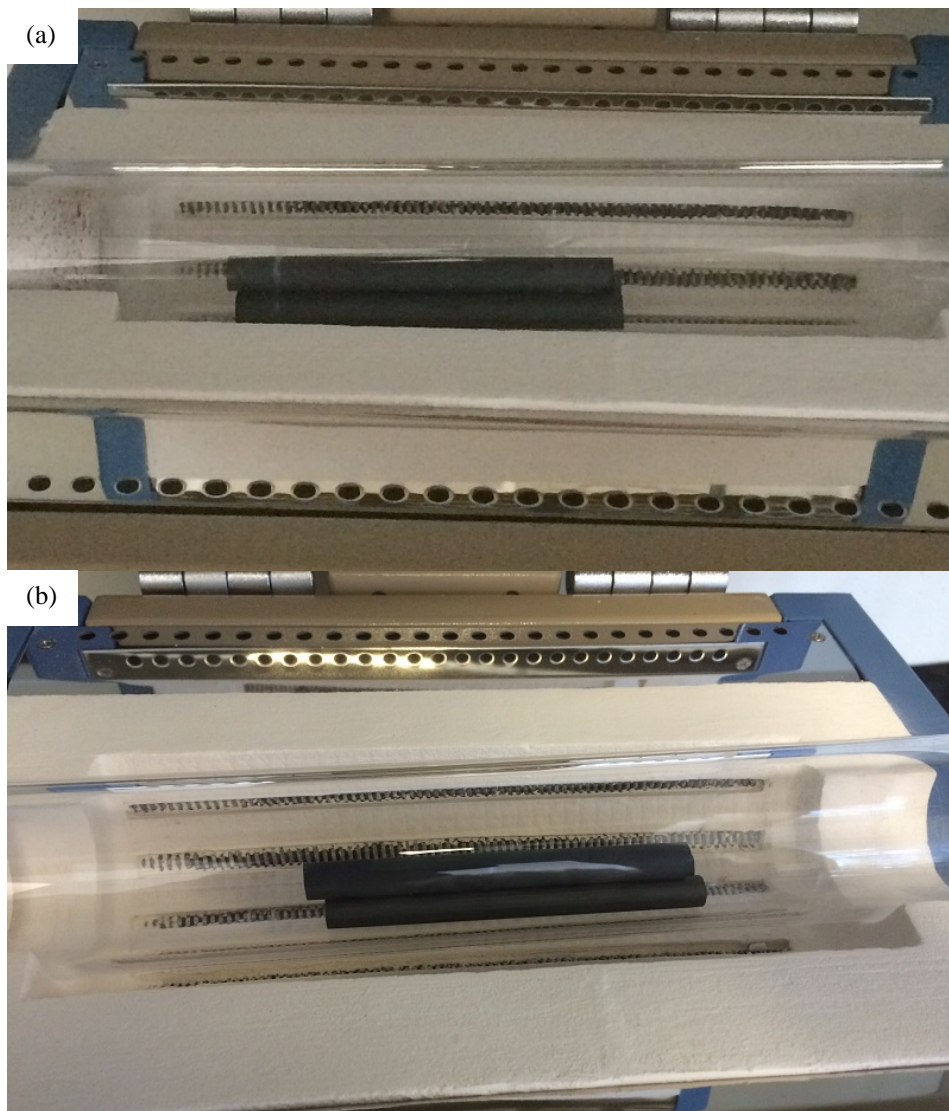
Figure 3.11 Original TiO_2 tubular filter (a) and thermal treated TiO_2 (Ti_4O_7) filter (b).

3.3.1.2 FTIR analysis . FTIR analysis was also conducted to verify the change of surface composition or functional groups. As shown in Figure 3.12, the green spectrum corresponds to TiO_2 (rutile) while the red spectrum has a shift of the first peak at 721 cm^{-1} due to TiO_2 changed to Ti_4O_7 after the thermal treatment. This result is consistent with previous research.[234]
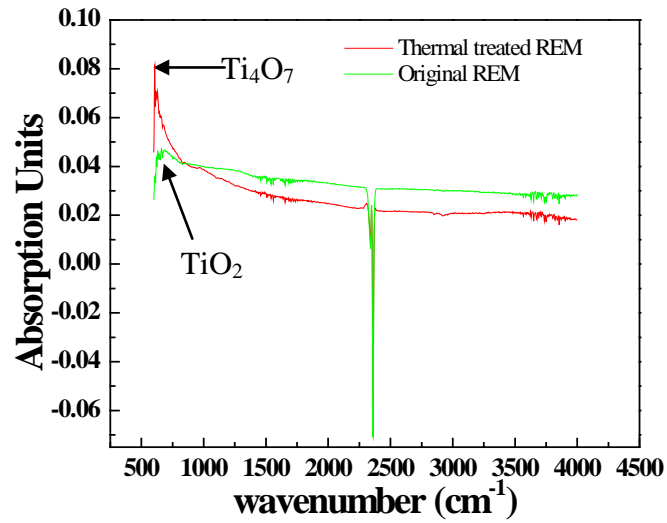
Figure 3.12 FTIR spectra of rutile TiO_2 and Ti_4O_7.

3.3.1.3 Zeta potential of algae and REM. Figure 3.13 shows the zeta potentials and

surface zeta potentials of suspended algae cells in water, untreated REM and thermally

reduced REM as a function of pH. As pH increases, the zeta potential and surface zeta

potentials both decreases, which agrees with most colloidal behavior.[235] The zeta

potentials of algae and REMs were also measured in the algal cultivation medium. In the

presence of medium suspension, both algae and REMs were negatively charged at around

-30 mV. The original TiO_2 filter was more negative (-55 mV) than the thermally reduced

REM (-30 mV), probably because the Ti_4O_7 REM has reduced surface oxygen atoms

after hydrogen reduction, which reduces the number of the negatively charged hydroxyl

groups on REM surface.
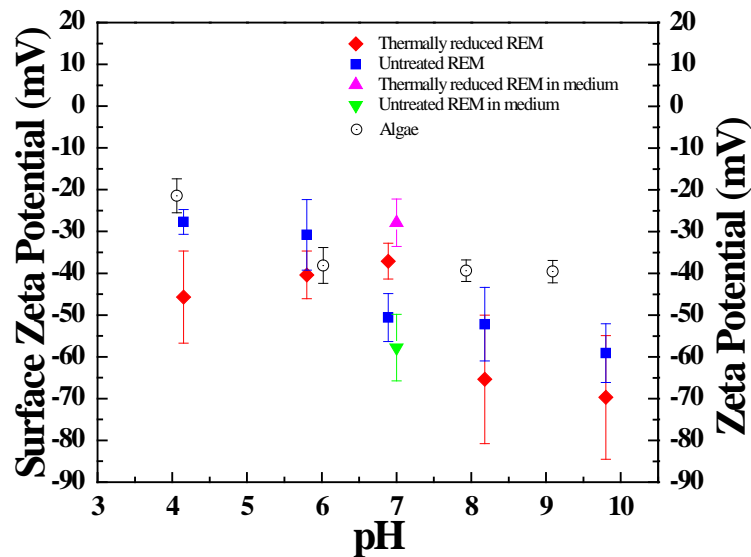
Figure 3.13 Zeta potential of REM and algae in DI water at different pH.

3.3.1.4 SEM/XRD. The SEM image in Figure 3.14a shows an asymmetrical and

porous structure of the REM. The XRD characteristic peaks for Ti_4O_7 and Ti_6O_{11} are

located at 2 theta angles of 20.78° and 22.84°, respectively.[236] The two peaks in Figure

3.14b indicates that the REM consists primarily of Ti_4O_7 and Ti_6O_{11}.[190] Peaks

characteristic of TiO_2 were not present, which indicates a full conversion from TiO_2 to the Magnéli phases was accomplished.[190]
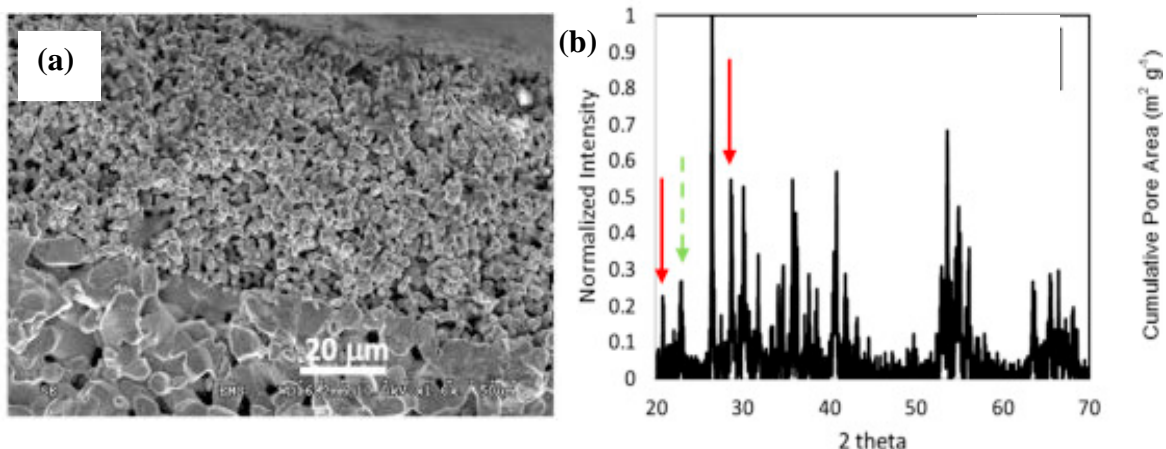
Figure 3.14 (a) Overall SEM image. (b) XRD of substoichiometric TiO_2 membrane with red (solid) and green (dash) arrows representing standard characteristic peaks of Ti_4O_7 and Ti_6O_{11}. Data cited from ref.[190].

3.3.1.5 Porosity and mean pore size. Table 3.7 summarizes the measurement of mean flow rates under different TMPs for untreated and thermally treated REM. The overall porosity and pore sizes were calculated with Equation 3.1 and 3.2. Clearly, the porosity for untreated and thermally treated REM remained almost unchanged at 14-15%. The mean pore size, however, was shown to reduce slightly from 524±32 nm to 408±7 nm for untreated and treated REM respectively, which agrees with previous studies.[237] The minor change of the mean pore size could result from the thermal sintering process that may melt some TiO_2 and lead to reorganization of porous structures.[237]

Table 3.7 Results of Pore Sizes of Untreated and Treated REM Filters.

	TMP (Pa)	Mean flow rate $(m^3 \cdot s^{-1})$	Surface area (m^2)	Membrane thickness (m)	Overall porosity (%)	Pore size (m)	Mean pore size (m)
Untreated REM	31000	6.07×10^{-08}				4.91×10^{-07}	
	40000	7.24×10^{-08}	0.00283	0.002	15.08	5.22×10^{-07}	5.24×10^{-07}
	60000	7.07×10^{-08}				5.43×10^{-07}	
	70000	8.88×10^{-08}				5.38×10^{-07}	
Thermally reduced REM	31000	8.50×10^{-08}				5.00×10^{-07}	
	40000	1.24×10^{-07}	0.00197	0.002	14.91	4.40×10^{-07}	4.08×10^{-07}
	60000	2.01×10^{-07}				3.60×10^{-07}	
	70000	2.30×10^{-07}				3.32×10^{-07}	

3.3.1.6 Cyclic voltammetry and EIS. The increase in the size of the peaks and the shift toward the oxygen-evolution region with increasing scan rate indicates that these peaks correspond to irreversible reactions. Likewise, the decrease in the size of the reverse peaks corresponding to peaks P1 and P2 (Figure 3.15a) suggests the occurrence of a later chemical reaction involving the electrochemically formed products (EC mechanism). In fact, the voltammetry behavior observed is characteristic of the anodic oxidation of $K_3Fe(CN)_6$ on REM electrodes, and it has been previously reported for 4-chlorophenol.

Figure 3.15b shows the EIS comparison of original Ti_4O_7 membrane and fouled membrane. Membrane fouling was represented by the backward shift on Figure 3.15(c), which is consisted with previous report.[190] Therefore, EIS could be used as an indicator of membrane fouling in the future studies.
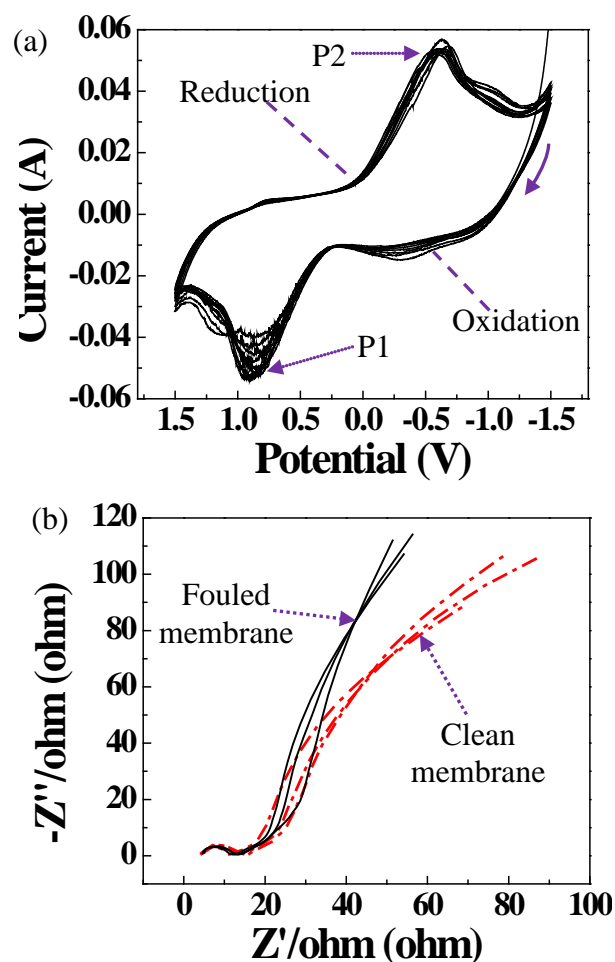
Figure 3.15 (a) I/V curves for REM filters in 0.5 M KCl solution when exposed to 20 mM $K_3Fe(CN)_6^{3-}$ and (b) EIS spectra in complete frequency range for clean and fouled REM.

3.3.2 Dead-end filtration
3.3.2.1 Measurement of membrane resistance (R_m) and permeate flux (J_0) for dead-end filtration.

Figure 3.16 shows that the fluxes of untreated and treated REM both increased with the

increasing TMP. As the porosity and means pore size both decreased slightly, the fluxes

of the treated REM under different TMPs were generally lower than those of untreated

REM, specially under high TMPs. The levels of membrane resistance (R_m) fluctuated

between 0.8×10^{12} m^{-1} and 1.2×10^{12} m^{-1}, which is at similar order of magnitude with that of ZrO_2/Al_2O_3 ceramic membrane (0.43 to 1.24×10^{12} m^{-1}) as reported previously.[238]
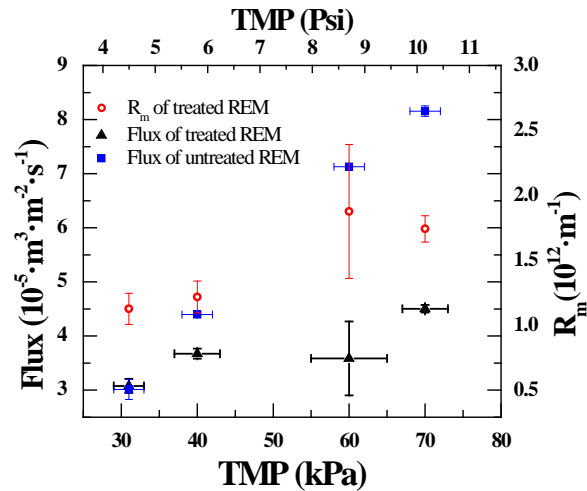
Figure 3.16 Flux and membrane resistance (R_m) under different TMPs in Psi and kPa in clean water test.

3.3.2.2 Membrane fouling kinetics in dead-end filtration. Figure 3.17 presents the dynamic change of permeate flow rate in continuous dead-end filtration. Three filtration cycles were executed in 12 hours. Hydraulic backwash without applying DC currents was conducted between each cycle. Clearly, the membrane fouling occurred rapidly as the permeate flow rate decreased with filtration time, primarily due to the algal cake layer formation and irreversible fouling mechanisms. Hydraulic backwash was not effective to reverse the fouling process. Figure 3.19 compares the fouled REM (left) that is covered by a green film of algal cake layer on the surface and the cleaned REM that is dark black (right).

As shown in Figure 3.18, the permeate flow rates was also simulated using the membrane fouling kinetics model mentioned in Section 3.2.6 using Equation 3.13 to Equation 3.18 according to the algorism in Figure 3.9a, which requires the determination of a key parameter, the volume concentration of algal cells at the membrane surface (C_w),

which was determined to be 83%. The Matlab code for the determination is provided in Section 3.5.1.
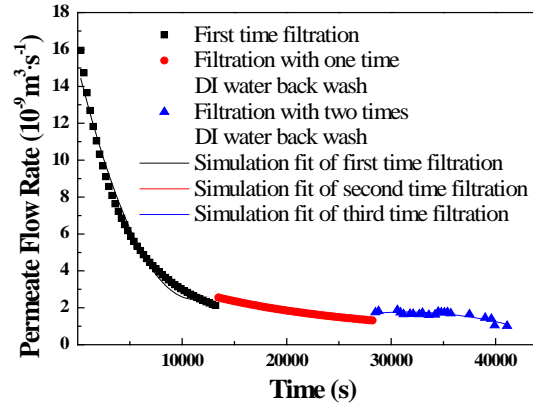
Figure 3.17 Change of permeate flow rate in dead-end filtration and fittings (Initial algal concentration: 1 g·L^{-1} and TMP: 75 kPa).
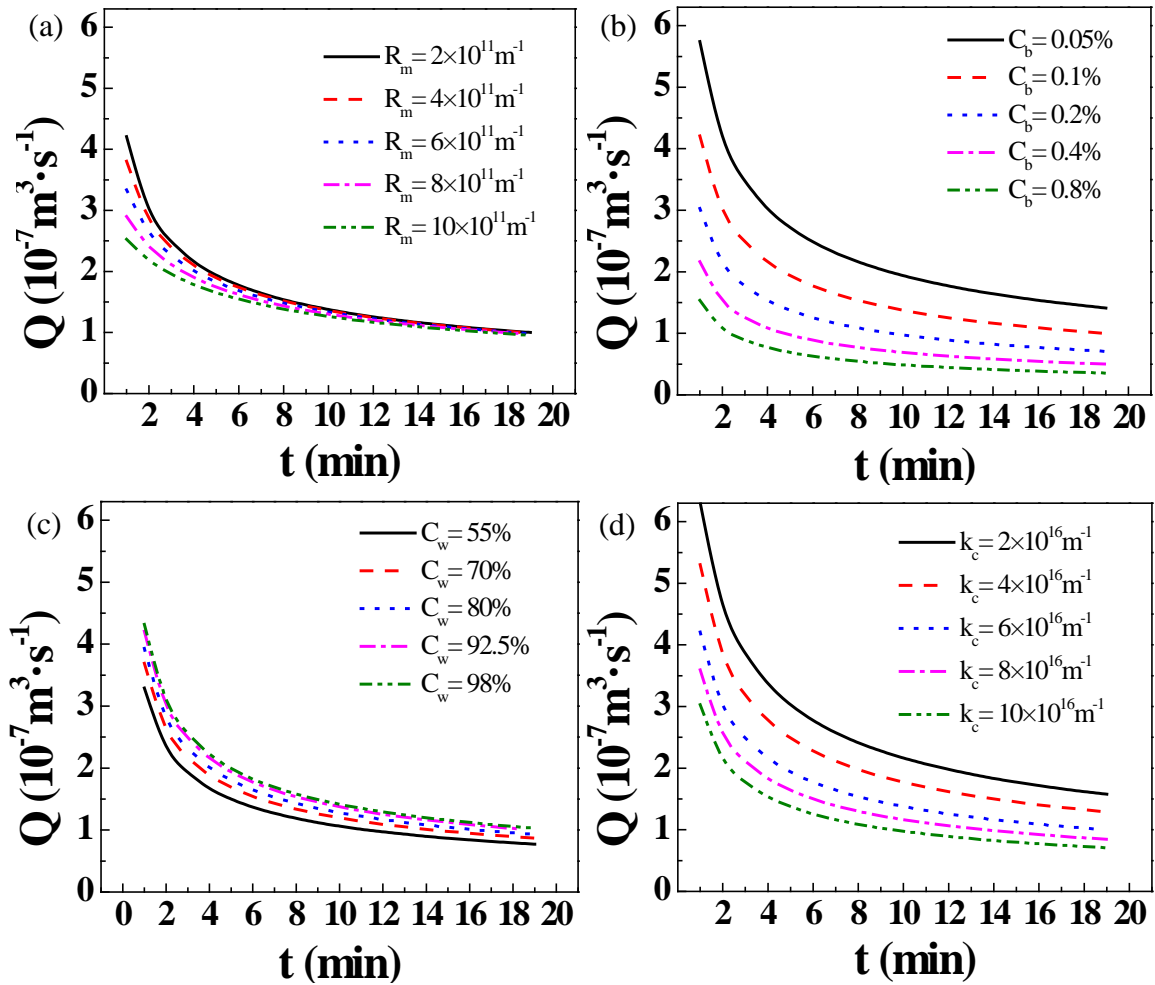
Figure 3.18 (a) to (d) Simulations of permeate flow change in dead-end filtration with the change of different parameters (R_m, C_b, C_w and k_c).
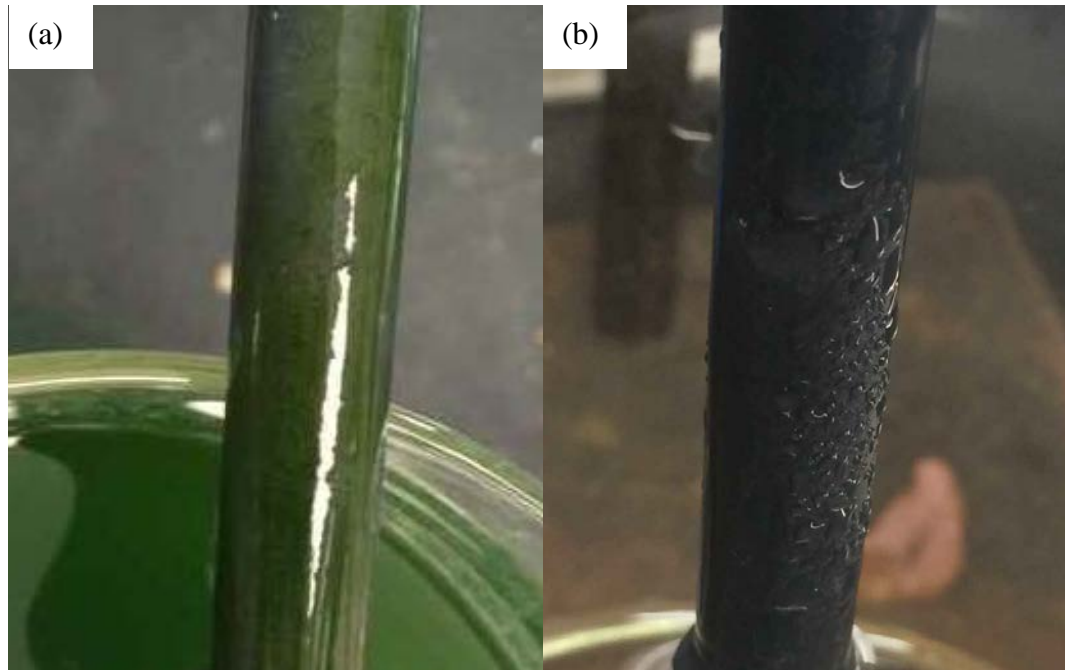
Figure 3.19 (a) REM with a fouling cake layer. (b) REM after chemical backwash.

3.3.2.3 Assessment of backwash efficiency and flux recovery after dead-end filtration using three different backwash methods

As mentioned in the Section 3.2.4.3, backwash studies were performed after the permeate flux was close to zero, indicating that the REM membranes had significant surface fouling. Flux recoveries under different duration of hydraulic backwash with and without DC currents were measured. Figure 3.20 indicated that (1) hydraulic backwash under DC currents (electrochemical backwash) for a longer duration time (90 min) led to a better flux recovery as shown in blue triangle data; (2) hydraulic backwash alone without DC resulted in very limited flux recovery, though the flux recovery was increased as the backwash time increased; (3) chemical backwash led to a lower flux recovery than electrochemical backwash did. Moreover, chemical backwash not only involved the use of corrosive chemicals but took longer times to achieve the comparable flux recovery. Backwash efficiency (r) for each backwash method was calculated by dividing the fluxes

at different TMPs by the original flux in Figure 3.16. Figure 3.21 shows that the highest

flux recovery by electrochemical backwash was 35%-40% of the original fluxes for the

clean REM membrane.
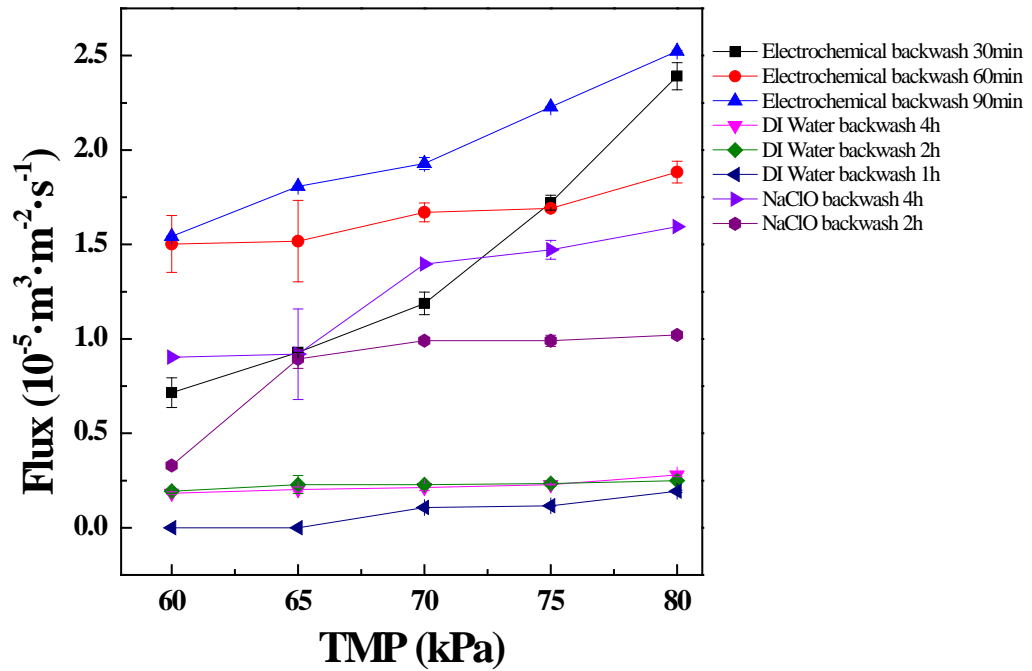
Figure 3.20 Comparison of flux recovery under hydraulic backwash with and without DC current (25.3 mA·cm^{-2} corresponding to a cell voltage of 18-22 V) and chemical backwash (2 g·L^{-1} NaClO).
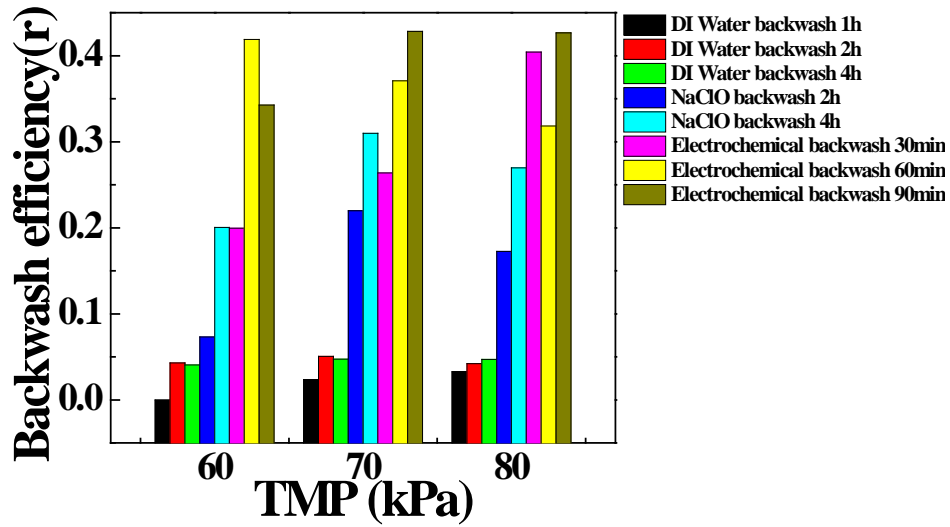
Figure 3.21 Backwash efficiency (*r*) for three different backwash methods at different TMP levels.

3.3.2.4 The dead-end filtration performance with and without DC currents

Membrane fouling is typically caused by surface accumulation of inorganic particles, biomass, and organic matter (OM), which has seriously hampered membrane applications forwater purification.[29] It was previously reported that chemical treatment such as preozonation improved performance of microfiltration because surface oxidation reduced cake compressibility and the biomass loading.[104] EAOP on REM surfaces has shown to inhibit membrane fouling through swift oxidation of organic matters.[239-240] To understand this effect, we performed a dead-end filtration experiment using clean REM membranes and DI water under different DC currents. Figure 3.22 shows that bubbles formed on the REM surface under high DC currents (e.g., 25.26 mA·cm^{-2}), which induces strong anodic oxidation reactions. The electrode potential at REM surface may reach 22 V when the current density was 25.26 mA·cm^{-2}. Thus, water may be oxidized as

$$O_2 + 4H^+ + 4e^- \rightleftharpoons 2H_2O \ \ E_H(pH=0) = +1.23 \text{ V}$$, and oxygen is produced and rise up as

bubbles. The bubble formation may also scour the REM surface and physically remove

surface foulant. However, excessive bubbling on REM surface was shown to negatively affect the dead-end filtration efficiency as shown in Figure 3.23a, which shows that the permeate flux declined with high DC currents (e.g., 25.26 mA·cm^{-2}).

Figure 3.23b shows the normalized ratio of permeate flux (J) to their respective initial permeate flux (J_0) of dead-end filtration with and without DC currents were almost identical. Figure 3.23c compares the flux decline or fouling processes when a lower level of DC current density was applied to avoid oxygen production. The electrode potential at REM surface was ±3.3 V when the current density was ±2.5 mA·cm^{-2}. Positive or negative DC currents cause anodic oxidation or cathodic reduction, which shows limited impacts on permeate flow decline rate or fouling kinetics. This suggests under dead-end filtration, the EAOP on REM may not be effective for membrane fouling mitigation probably because the anodic oxidation or electrostatic repulsion against algal cells or organic matters could not overcome their deposition rates driven by TMP.
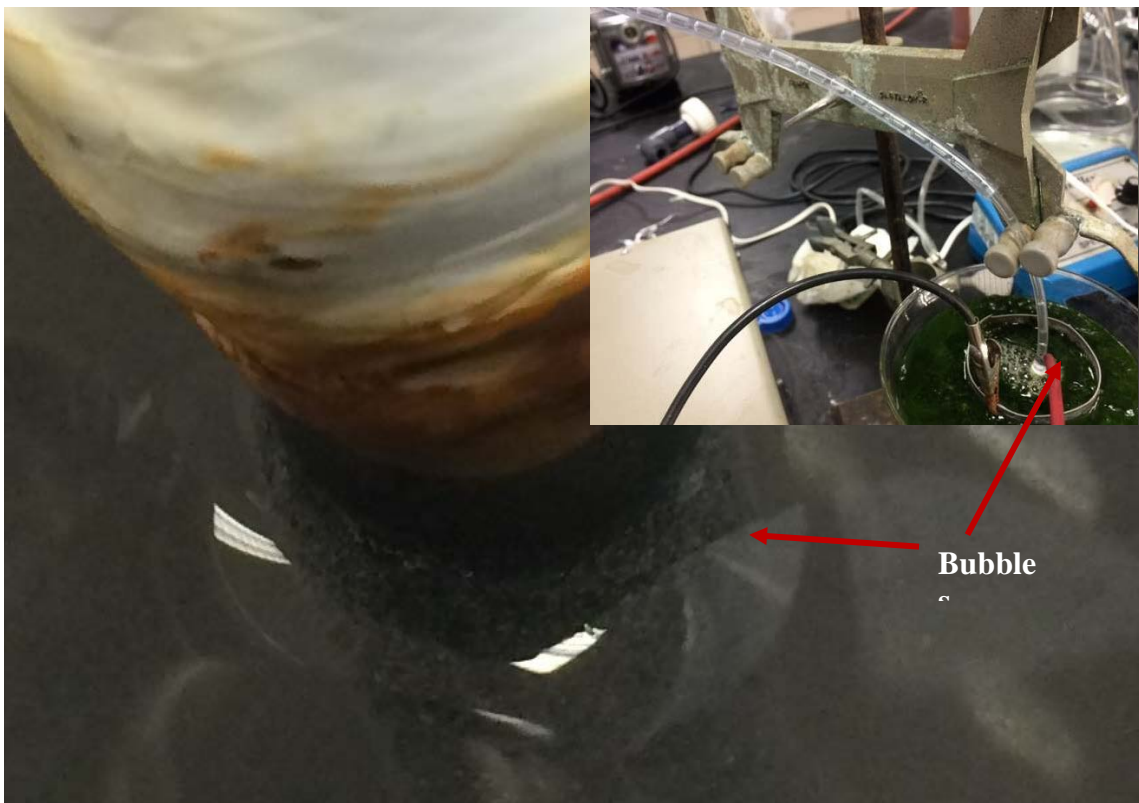
Figure 3.22 Significant bubble generated on REM surface under current density at 25.26 mA·cm^{-2}. See our lab video at: https://youtu.be/J5YdyaF3sSw.
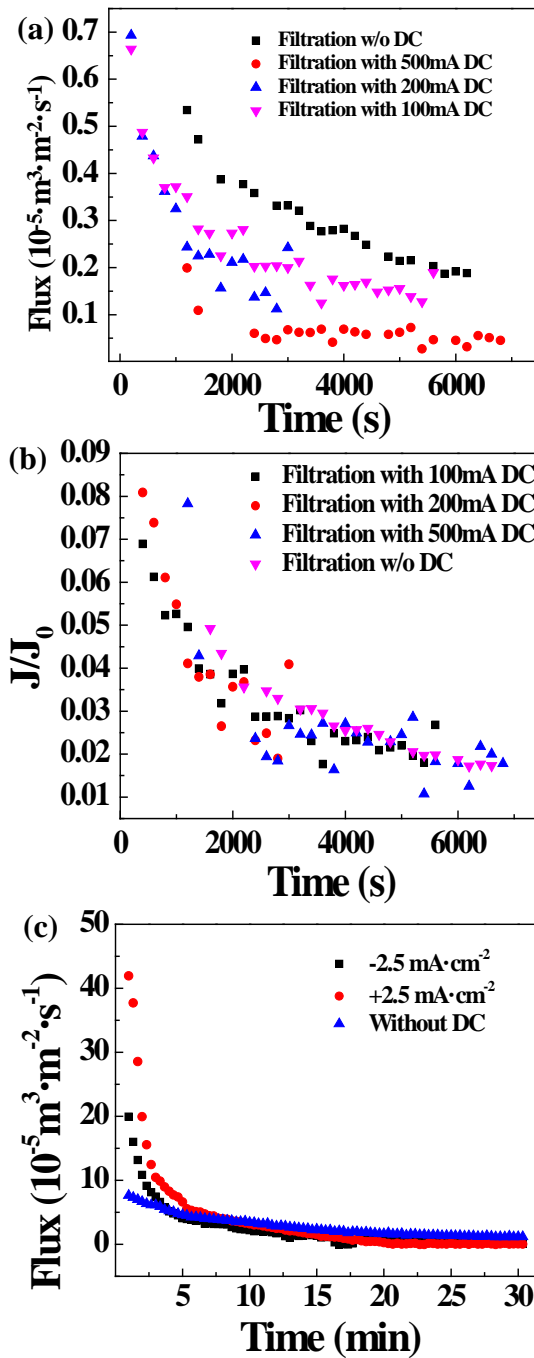
Figure 3.23 Permeate flux decline of permeates flux under a constant TMP of 10 psi (68.9 kPa) during dead-end filtration with different DC current density (algal concentration in the influent: 0.05 g·L^{-1}). **(a)** Current density was 0, 5.05, 10.10 and 25.26 mA·cm^{-2} and potential was ranging from 0-22 V. **(b)** Ratio of permeate flux (J) to initial permeate flux (J$_0$) of **(a)**. **(c)** Current density was 0, -2.5 and 2.5 mA·cm^{-2}.

3.3.3 Cross flow filtration

3.3.3.1 Measurement of inherent membrane resistance (R_m) and permeate flux (J_0) for cross flow filtration.

As verification, R_m and J_0 were both determined using the cross-flow filtration unit in a dead-end filtration mode as mentioned in Section 3.2.5.1. Figure 3.24 shows the permeate flux almost linearly increased with the increasing TMP. The membrane resistance (R_m) calculated by Equation 3.12 is an inherent membrane property that should be independent on TMP. Our result shows that R_m fluctuates slightly under different TMP with a mean level of around 1.0×10^{11} m^{-1}. This result is at similar order of magnitude with the reported membrane resistance of ZrO_2/Al_2O_3 ceramic membrane (0.43 to 1.24×10^{12} m^{-1}).[238]
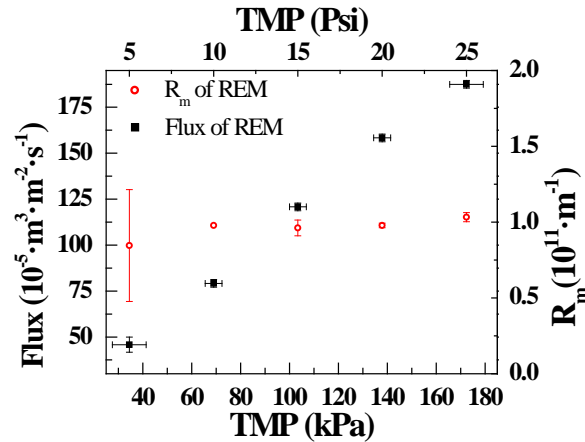
Figure 3.24 Permeate flux and membrane resistance (R_m) under different TMPs in the clean water test. The upper and lower axes are TMPs in the units of psi and kPa, respectively.

3.3.3.2 Critical flux determination with and without different DC currents.

Figure 3.25a shows the change of TMP with the filtration time under different DC currents. Without DC currents, no significant change was observed in the TMP during the first ($2.08 \times 10^{-5} \cdot$ m$^3 \cdot$ m$^{-2} \cdot$ s^{-1}) and second flux steps ($4.17 \times 10^{-5} \cdot$ m$^3 \cdot$ m$^{-2} \cdot$ s^{-1}) during the first 15 min and the interval of 15 min to 30 min. However, after the permeate flux reached

$6.25\times10^{-5}\cdot m^3\cdot m^{-2}\cdot s^{-1}$, the TMP suddenly increased from 112 kPa to 207 kPa in the first 7 min in the third 15-min step. Accordingly, the increase rate of TMP ($\Delta P/\Delta t$) reached 226 $Pa\cdot s^{-1}$, which means the turning point of TMP corresponds to the critical flux. Therefore, the permeation flux of $6.25\times10^{-5}\cdot m^3\cdot m^{-2}\cdot s^{-1}$ was the critical flux of the Ti_4O_7 ceramic membrane in the filtration of algal suspension (0.05 g L^{-1}) without DC current as pointed in Figure 3.25b.

With the same determination method, the critical fluxes were also determined when positive and negative DC currents run through REM at different current densities (1.25, 2.5 and 5 $mA\cdot cm^{-2}$), which are expected to induce different electrode potentials or oxidation or reduction reactions. For example, when applying 1.25 $mA\cdot cm^{-2}$ current density (the electrode potential=1.803 V), the TMP increased from 11.72 kPa to 164.79 kPa starting from the 16 min to 45 min and then dramatically increased to 226.84 kPa at the 30 min, which corresponds to the occurrence of critical flux as $\Delta P/\Delta t$ was 166 $Pa\cdot s^{-1}$. Thus, the critical flux was approximately 4.16×10^{-5} $m^3\cdot m^{-2}\cdot s^{-1}$ under the positive DC current at 1.25 $mA\cdot cm^{-2}$. Compared to the critical flux without DC, the critical flux slightly decreased when applying a low level of positive DC currents, probably because the positive surface charge on REM favored the deposition of negatively charged algal cells and deteriorated the membrane fouling.

With applications of higher DC currents at 2.5 $mA\cdot cm^{-2}$ (the electrode potential=2.803 V) and 5 $mA\cdot cm^{-2}$ (the electrode potential=9.803 V), the TMP increase occurrence was apparently delayed to over 40 min. The estimated critical flux was about the same ($6.25\times10^{-5}\cdot m^3\cdot m^{-2}\cdot s^{-1}$) for both DC levels. The shift of critical flux indicates that

the membrane fouling under DC polarization could be reduced due to the anodic surface oxidation of surface foulants.

By contrast, cathodic polarization was achieved by applying negative DC current to REM. Different from the anodic polarization, the negatively charged REM surface may repel negatively charged algal cells and thus mitigate membrane fouling, which is verified by our results in Figure 3.25a. For example, at the DC density of -1.25 mA·cm^{-2}, the TMP level was relatively stable under 43.8 kPa in the first 60 min of the four different flux steps. An increase of TMP from 43.8 kPa to 62.0 kPa occurred at 61 min after the permeate flux increased $10.41 \times 10^{-5} \cdot m^3 \cdot m^{-2} \cdot s^{-1}$. Thus, the critical flux was approximately $8.33 \times 10^{-5} \cdot m^3 \cdot m^{-2} \cdot s^{-1}$ and $14.56 \times 10^{-5} \cdot m^3 \cdot m^{-2} \cdot s^{-1}$ for the DC densities of -1.25 mA·cm^{-2} and -2.5 mA·cm^{-2} respectively. When applying -5 mA·cm^{-2}, the TMP remained stable in the first three flux steps and increased very mildly, which made it difficult to estimate the critical flux. Apparently, the membrane fouling mitigation was obtained under cathodic polarization.

Figure 3.25b shows that the critical flux determined under -2.5 mA·cm^{-2} was $14.56 \times 10^{-5} \cdot m^3 \cdot m^{-2} \cdot s^{-1}$, which is two times that of 2.5 mA·cm^{-2} ($6.25 \times 10^{-5} \cdot m^3 \cdot m^{-2} \cdot s^{-1}$). This result suggests that in anodic polarization, EAOP could be the main anti-fouling mechanism, whereas the electrostatic repulsion against algal cell deposition on REM was the main anti-fouling mechanism in cathodic polarization. Critical flux without EAOPs on membrane filters has previously been studied.[200, 206, 241] For example, the critical flux of 47-mm Anopore Inorganic disc membranes (Anodisc, Whatman) were 17 LMH ($4.7 \times 10^{-6} \cdot m^3 \cdot m^{-2} \cdot s^{-1}$) when filtering algal suspension (*C. sorokiniana*) at a mass concentration of 0.29 g·L^{-1}.[241] Different anti-fouling approaches (e.g., vibrating

membranes[203]) were reported to improve algal harvesting and increase the critical flux from 22 to 64 LMH (6.1×10^{-6} to 1.7×10^{-5} $m^3 \cdot m^{-2} \cdot s^{-1}$) when filtering 0.2 $g \cdot L^{-1}$ *C. pyrenoidosa* suspension.
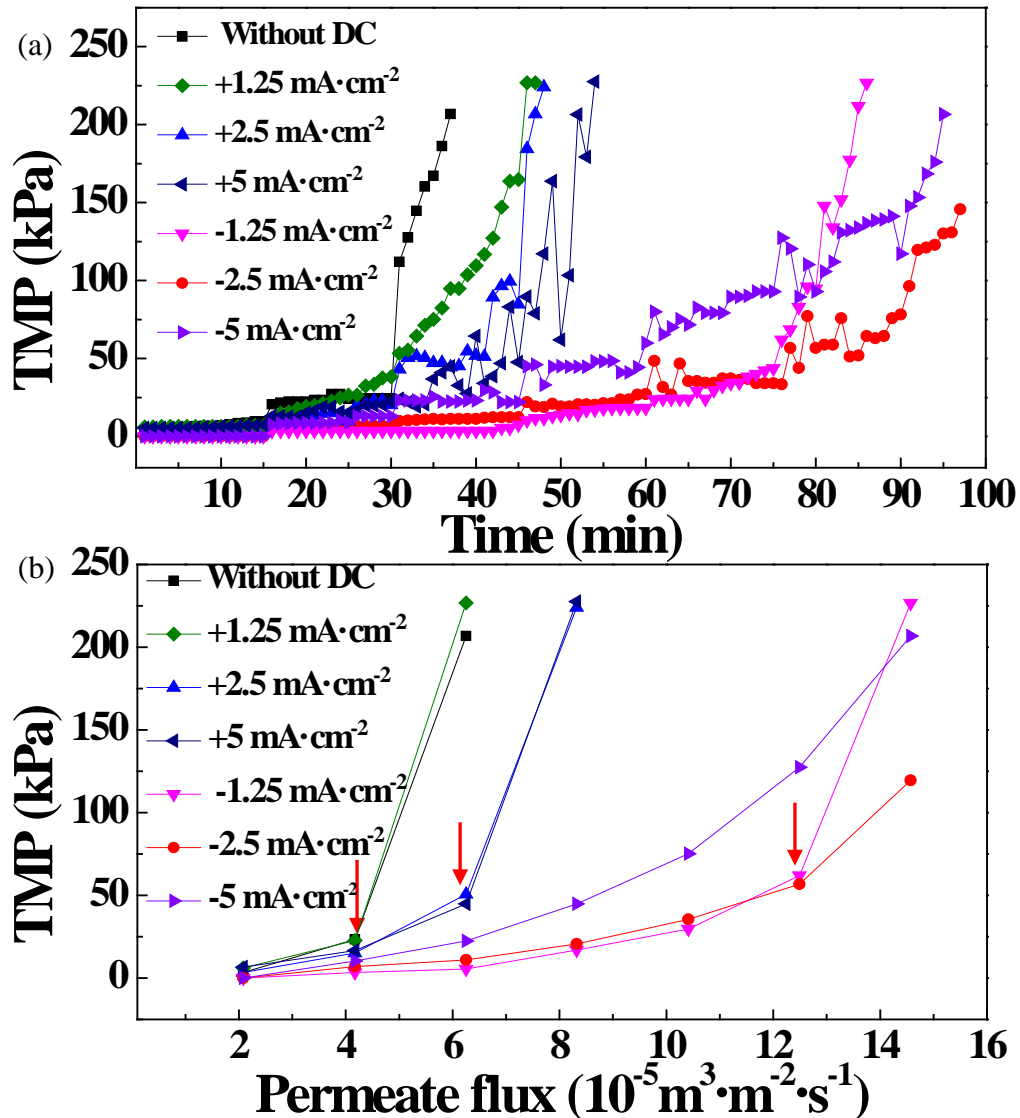
Figure 3.25 (a) TMP and Flux profiles of membrane filtration with *S. dimorphus* of 0.05 $g \cdot L^{-1}$ under an initial permeate flux of 2.08×10^{-5} $m^3 \cdot m^{-2} \cdot s^{-1}$ in the cross-flow filtration test with different DC current densities according to the conditions described in section 3.2.5. (b) TMP versus permeate flux for REM filtration. The red arrow shows the possible critical flux at 4.17×10^{-5}, 6.25×10^{-5} and 12.48×10^{-5} $m^3 \cdot m^{-2} \cdot s^{-1}$.

3.3.3.3 Membrane fouling kinetics in the cross-flow filtration under different DC currents.

Due to membrane fouling, the specific rate of permeate flux changes can generally be divided into three stages: the rapidly declining stage, the slowly declining stage and the stable stage.[242] Figure 3.26a shows for the REM filtration without DC current, the permeate flux experienced a sharp decrease stage within the initial 5 min followed by a relatively slow declining period, which is similar to the observations of some other membrane filtration systems.[243-244] The stabilized permeate flux was 1.18×10^{-5} $m^3 \cdot m^{-2} \cdot s^{-1}$ with a decline rate of 89% of the initial level. When applying positive or negative DC currents, the decline of permeate flux was apparently became less significant than that of no DC currents. Moreover, the stabilized fluxes reached approximately 5.50×10^{-5} when applying +2.5 or -2.5 $mA \cdot cm^{-2}$, which confirms the above-mentioned antifouling ability empowered by anodic oxidation or cathodic repulsion against negatively charged foulants respectively.

Figure 3.26b provides the profiles of the cake layer resistance (R_c) calculated by Equation 3.12 with the experimental data of permeate flux and TMP shown in Figure 3.26a. Moreover, the kinetics of the R_c increase can be simulated with the model equations Equation 3.15-3.19 shown in Section 3.2.6, which requires the determination of three key parameters: the specific resistance per unit of cake thickness (k_c), the volume concentration of algal cells at the membrane surface (C_w) and cake layer thickness (δ_c). The Matlab code for the determination is provided in Section 3.5.1. The cake layer resistance increased gradually as the deposited algal biomass formed a cake layer on the membrane surface. The cake layer resistance was about 4×10^{12} m^{-1} after 40 min filtration without DC currents. Under DC currents, the increase rate of cake layer

resistance decreased with the increasing intensity of DC currents, indicative of the antifouling feature of REM. For example, R_c increased to approximately 9×10^{11} m^{-1} when applying +2.5 or -2.5 mA·cm^{-2} after 40 min. The simulated cake resistance is shown in Figure 3.26b in continuous lines, which were calculated using Equations 3.15, 3.16, 3.18 and 3.19, and the mean values of the specific resistance per unit of cake thickness (k_c) and the volume concentration of algal cells at the membrane surface (C_w). The simulated results well fitted the experimental data ($R^2 > 0.9$).
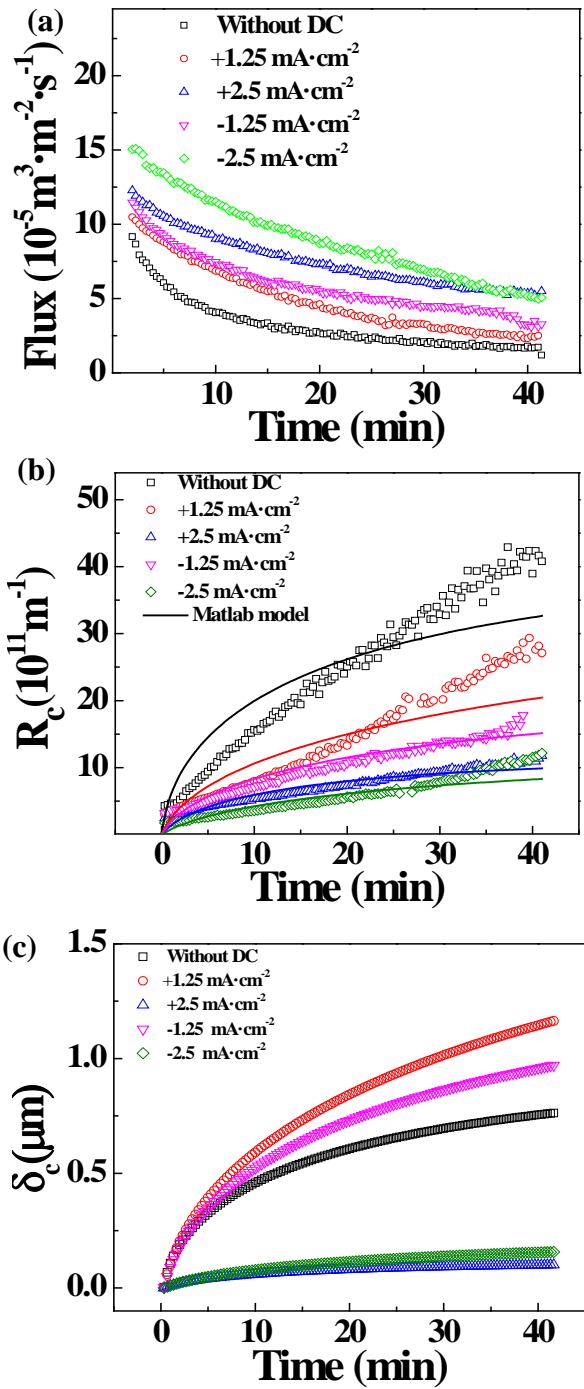
Figure 3.26. **(a)** Variations in permeate flux under a constant TMP of 10 psi (68.9 kPa) during continuous filtration with different DC current density (algal concentration in the influent: 0.05 g·L⁻¹). **(b)** Cake layer resistance (R_c) increase in the membrane filtration process with different DC current densities over 40 min time period, where dots represent the experimental values and continuous lines represents the model calculation values. **(c)** Cake layer thickness (δ_c) increase over time of filtration.

Figure 3.27 shows the fitted results of k_c and C_w, which both fluctuated under different DC conditions (-2.5 to 2.5 mA·cm^{-2}). For example, k_c fluctuated from 2×10^{16} to 10×10^{16} m^{-2}, which is comparable to the reported values in literature.[204] Moreover, k_c exhibited no clear dependence on DC currents, which may be reasonable because k_c represents an inherent material property that describes the cake layer resistance for specific types of algal biomass or foulant on REM surface. C_w ranged from 60% to 110% with the lowest levels when no DC was applied, which means that the positive or negative DC currents on REM may increase the volume concentration of algae on the membrane wall. This value was fluctuated because of all calculation were based on the best fitting result.
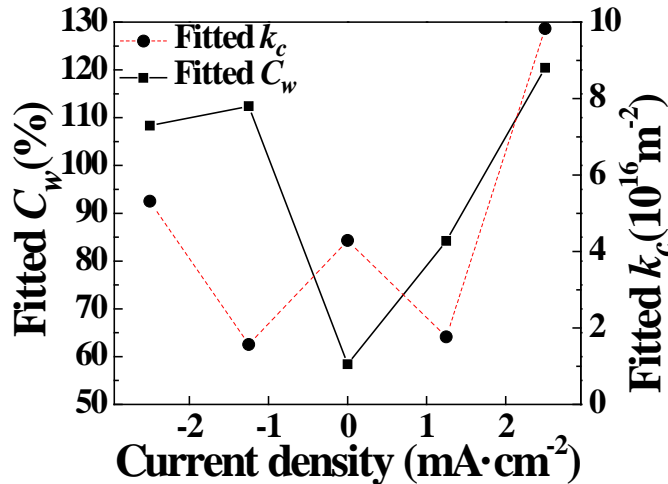
Figure 3.27 Variations of specific resistance per unit of cake thickness (k_c) and cake concentration on the membrane wall (C_w) in the membrane filtration process under different DC current densities.

3.3.3.4 Influences of different backwash methods on backwash efficiency and flux recovery in cross-flow filtration.

Flux recovery under different duration of hydraulic backwash (TMP = 85 kPa) with and without and DC were tested by clean water under TMP from 5 psi to 25 psi (34.5 kPa to 172.4 kPa). The DC current was 200 mA and the density was 5 mA·cm^{-2}. As shown in

Figure 3.28, (1) hydraulic backwash with DC by longer duration time had a better flux recovery in clean water test; (2) hydraulic backwash with DC by the same duration time had a better flux recovery than hydraulic backwash without DC; (3) 30 min hydraulic backwash without DC had a better flux recovery than 15 min backwash without DC. The affinity of algal foulants to membrane surfaces is strongly affected by their nature. In reversible fouling, the weak affinity of foulants to the membrane surface due to external deposition suggests that the foulants can be removed by hydraulic backwash alone. However, hydraulic backwash process without additional chemical could not remove adsorbed, or chemical bonded algogenic organic matter, which can only be removed by chemical and electricity backwash.[245]
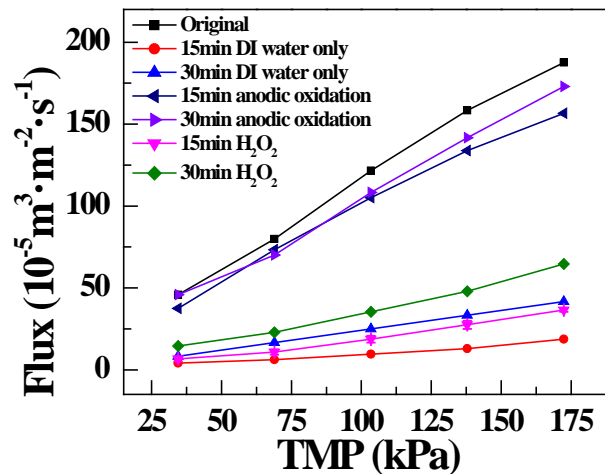
Figure 3.28 Comparison of flux recovery under hydraulic backwash (80 kPa) with and without DC current and chemical (0.2 g·L^{-1} H$_2$O$_2$) backwash. The power setting of DC is 100 mA, 3.0-3.3 V and the current density was 2.5 mA·cm^{-2}.

3.3.3.5 Determination of cake layer compressibility and resistance coefficient

Based on the results in Figure 3.26a-3.26b, we plotted the logarithm values of cake layer resistance (Log R_c) over permeate flux (Log J) under different current densities in Figure 3.29. The compressibility index (n) and resistance coefficient (α) were determined by

fitting this log-log plot with Equation 3.30. To determine n and α from the fitting equation shown as an inset in Figure 3.29, an average value of C_w (96.75%) in Figure 3.27 was chosen. The cake layer thickness (δ_c) was taken from Figure 3.26c. Table 3.8 shows the results of compressibility indexes and resistance coefficients under different current densities. Clearly, the fitted values of compressibility indexes were all greater than 1, indicating that algal cake layers on various filtration conditions were possibly compressible and the flux resistance is dependent on the cake layer compression state. Moreover, the compressibility index increased slightly when positively or negative DC currents were applied, suggesting that the algal cake layer may become more compressible than that under no DC current. This compressibility increase may be attributed to the possible surface oxidation and destruction or repulsion of algal cells by REM under anodic oxidation or cathodic reduction.

The resistance coefficient (α) is not the same as the above analyzed specific resistance per unit of cake thickness (k_c). However, they both indicate that degree of flux resistance from algal cake layer. From the result in Table 3.8, the resistance coefficient appeared to increase when DC currents run on REM, which suggests that the flux resistance per unit mass of the accumulating cake layer may be higher, especially under negative DC currents.
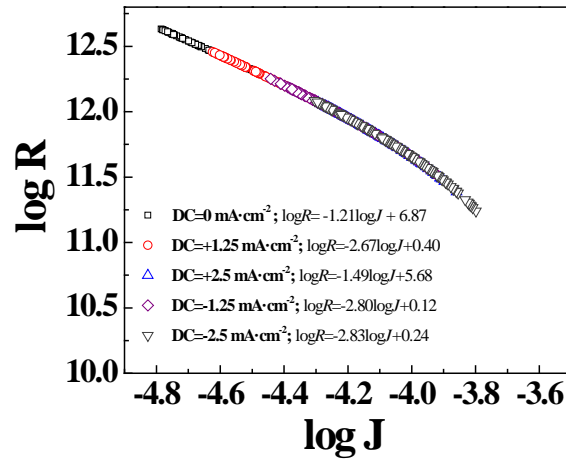
Figure 3.29 Log (R_c) and Log (J) relationship. Compressibility index (n) and resistance coefficient (α) was fitted by Equation 3.30.

Table 3.8 Compressibility Index (n) and Resistance Coefficient (α) Determined by Equation3.30 with Curve Fitting.

Current density (mA·cm^{-2})	Compressibility index (n)	Resistance coefficient (α)
0	1.2	1.6×10^9
+1.25	2.6	1.2×10^{10}
+2.5	1.49	1.2×10^{11}
-1.25	2.8	1.4×10^{10}
-2.5	2.8	9.5×10^{10}

3.3.3.6 Impacts of viscosity increase in algal suspension on membrane permeation

Figure 3.30 shows that the simulation results about the dependence of viscosity and permeability corrected for reference temperature (P_c) on algal concentrations using the three models in Table 3.3. Flux and TMP used in simulation were chosen from the experimental data in Section 3.3.3.3. The reference viscosity was the viscosity of water at 25 °C. The result shows that as the algal concentration increases, the viscosity almost linearly increases. The permeability of membrane decreased as predicted by the model 1 and 2, which is reasonable due to the increase of viscosity and membrane fouling. However, the model 3 revealed an increasing permeability, implying that the model 3 may not be suitable for explaining our membrane filtration.

124
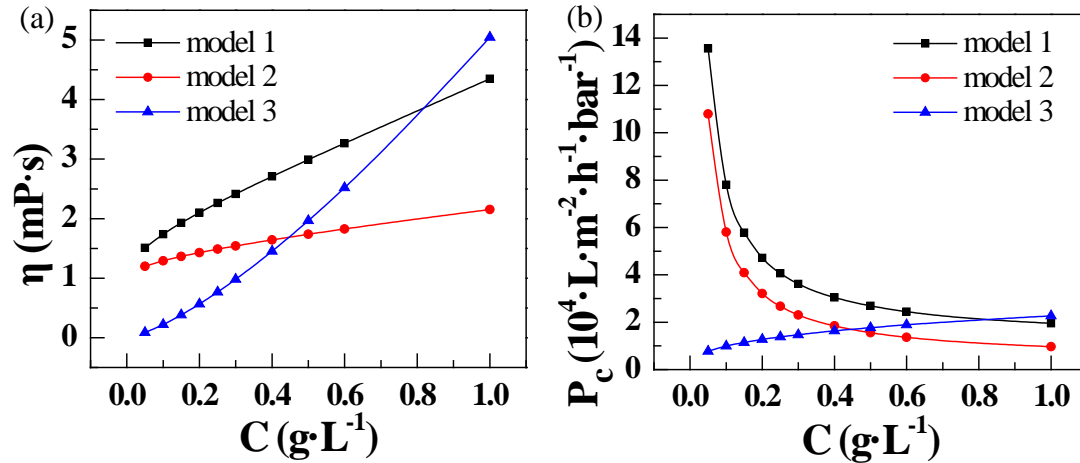
Figure 3.30. (a) Simulation of actual viscosity (η_{act}) by the thre models in Table 3.3 at differetn algal concentrations; (b) calculated permeability corrected for reference temperature (P_c) from actual viscosity.

3.3.3.7 Biomass concentration in continuous filtration under different DC currents

Table 3.9 shows the different indicators of algal harvesting efficiencies at three DC conditions (0, +2.5 and -2.5 mA·cm^{-2}) in one cross-flow filtration cycle with the algal suspension of 1.8 L and 0.05 g·L^{-1}. For these three conditions, relatively lower volumetric reduction factors (VFR) and concentration factors (CF) were obtained when applying DC currents, because of the cell damage or oxidation by REM as we characterized previously.[176] As comparison, the VFR of Millipore 0.45μm filter has a VFR of 5 to 40, 40 kDa polyacrylonitrile filter has a VFR of 10 and 50 kDa PVC UF membrane has a VFR of 154.[204, 246] For the same reason, algal distribution on the membrane (W_m) and retentate (η_t) in the membrane tank have shown negative value. However, negative

charged membrane shows high uptime of 76.3%, which is higher than the 57.3% uptime when membrane was served as anode.

Table 3.9 Algal Harvesting Concentration Performances at Three DC Conditions.

Current density $(mA \cdot cm^{-2})$	VRF	CF	R_{ec} (%)	η_m $(g \cdot m^{-2} \cdot min^{-1})$	η_t $(g \cdot m^{-2} \cdot min^{-1})$	W_m	W_t	*Uptime* (%)
0	5.06	0.89	17.6	0.0011	-0.03	1.14	-0.14	19.4
+2.5	4.12	0.51	12.4	0.0007	-0.18	21.33	-20.3	57.3
-2.5	3.24	0.78	24.1	0.0014	-0.10	1.39	-0.39	76.3

3.4 Conclusion

In this study, the microalgae biomass separation performance of reactive electrochemical membranes, using different current density during dead-end and cross flow membrane filtration, was systematically investigated through experiments performed under different operating conditions (such as flux and TMP). According to the critical flux calculations, the membrane with the best filtration flux performance was the one with 1.25 $mA \cdot cm^{-2}$ current density, when the REM served cathode. The characteristic properties of the membranes (e.g., pore diameter, morphology, and hydrophilic affinity) might all have an effect on the critical flux values.[247] However, the loss of algal integrity was significant when the filtration system was running. The cake layer formation can be easily removed by electrochemical cleaning and the irreversible membrane fouling was insignificant during this process.

In order to examine microfiltration behaviors of REM for micro algae under both constant flux and constant pressure conditions with direct current. Micro algae were

filtered with REM in both dead-end and cross flow mode.[248] The model for describing the pore blocking of the membrane and the buildup of the cake layer that proceed simultaneously during the course of filtration has been developed by integrating the intermediate blocking law and the cake filtration model sophisticatedly. The model calculations well described not only the pressure rising behaviors in constant flux filtration but also the flux decline behaviors in constant pressure filtration. The adjustable parameters such as R_{ir}, and R_c, which were measures of pore blocking, as well as k_c and δ_c, which was a measure of cake formation, were little influenced by the filtration rate in constant flux filtration, the filtration pressure in constant pressure filtration, and the solid mass fraction in suspension. Moreover, the model calculations well evaluated the negative slope occurring in the plots of the characteristic filtration curve based on the classical blocking filtration law.

CHAPTER 4

Ti$_4$O$_7$ REACTIVE ELECTROCHEMICAL MEMBRANE (REM) FILTRATION FOR RECALCITRANT POLLUTANTS REMOVAL AND MICROBIAL DISINFECTION

4.1 Introduction

4.1.1 Challenges of emerging micropollution in aquatic environments

Emerging water contaminants in natural waters such as rivers and groundwater aquifers is a widespread problem. These emerging contaminants could be persistent in the environment and pose adverse effects on ecosystems and human health. Environmentally persistent organic micropollutants may include polyromantic hydrocarbons (PAHs), organophosphate flame retardants, endocrine disrupting compounds (EDCs), pesticides, herbicides, pharmaceuticals and personal care products (PPCPs).[249-250] For example, poly- and perfluoroalkyl substances (PFASs) such as perfluorooctanoic Acid (PFOA) and perfluorooctanesulfonic acid (PFOS), as an example of emerging water contaminants, are potentially carcinogenic and persistent in the environment. The Water Research Foundation (WRF) has released findings of a study addressing effective methods for removing PFASs on waters collected from 13 water and wastewater treatment plants in the United States. The research report (WRF project #4322) demonstrated that conventional treatment at wastewater treatment plants and most drinking water treatment plants (e.g., aeration, chlorine dioxide, dissolved air flotation, coagulation, flocculation, sedimentation, granular filtration, and microfiltration) were all ineffective for removing PFASs. Carbon–fluorine bonds make PFASs extremely stabile. PFCs repel and resist oil, water, and degradation at high temperatures. Activated carbon and anion exchange can

remove most of PFASs but are less effective at removing shorter chain PFASs. The most effective treatment technologies are nanofiltration and reverse osmosis, which are characterized by high initial capital investment and costly operation and maintenance. A combination of multiple treatment technologies will likely be required to effectively degrade PFAS and their different forms.

4.1.2 Challenges of membrane filtration in the removal of micropollutants

Membrane separation such as ultrafiltration (UF) and nanofiltration (NF) have gained increased attention in the water treatment industry due to their high selectivity, high throughput, and reduced chemical usage.[1-2] For example, UF membranes can selectively remove not only large molecules such as proteins, viruses, and microorganisms through size sieving mechanisms but can also substantially reduce emulsion to improve the successive solvent extraction efficiency. However, traditional membrane separations suffer from membrane fouling due to either the formation of a cake layer of biomass, or more commonly due to organic matter or salt adsorption onto the membrane surface.[10-11] Moreover, membrane filtration is not effective to remove small molecular weight compounds such as nitrate or nitrite, phosphate, metal ions and trace-level micropollutants.[204, 251] Therefore, post-treatment is necessary before or after membrane filtration is essential.

4.1.3 Integration of AOP into for reactive membrane systems

Advanced oxidation processes (AOPs) are widely studied to effectively treat biorefractory organic substances[252] or resistant microbes.[253] Three categories of AOPs

exist: (1) UV/O_3; (2) Photocatalysis (TiO$_2$ or other semiconductor particles under UV-vis illumination); (3) Fenton process (Fe^{2+} / H$_2$O$_2$), Photo Fenton process (Fe^{2+} / H$_2$O$_2$ / UV) and Photo-Fenton-like processes of homogeneous nature (Fe^{3+}/ H$_2$O$_2$ / UV, Fe^{3+}/ APS / UV and Fe^{2+}/ APS / UV) and heterogeneous nature (Fe^0 / oxidants) (where APS is (NH$_4$)$_2$S$_2$O$_8$).[254] AOPs such as photocatalytic oxidation, photochemical oxidation, electrochemical oxidation, photochemical reduction, persulfate radical treatment, thermally induced reduction, and sonochemical pyrolysis involves the production of hydroxyl radicals (•OH) as potent, nonselective oxidants to degrade recalcitrant pollutants.[255] However, continuous UV irradiation and consumption of chemical reagents (e.g., H$_2$O$_2$, O$_3$, and ferrous iron) cause potentially high operation and maintenance costs. [256]

Coupling AOP with physical membrane filtration has been extensively studied to enable the destruction of organic pollutants by free radicals (mainly hydroxyl radicals or •OH) and antifouling capabilities.[257-260] For instance, photocatalytic ceramic membranes (PCMs)[261-265] utilize semiconducting inorganic materials, such as TiO$_2$ and ZnO, as photocatalysts to enable surface reactions on water-permeable porous membranes. Along with the physical separation of contaminants in water through the porous structure of PCMs, the contaminants are chemically decomposed by reactive radical species generated on the PCMs under UV radiation. However, there are still some practical challenges when implementing the PCMs technology, including: (1) difficulty in providing effective UV illumination; (2) the reduced light penetration in tabular and spiral membrane surfaces; (3) the reduced active surface on catalyst and membranes accessible to chemicals and photons. Therefore, other than photo irradiation, an

alternative irradiation source that can evenly pass through membrane modules and distribute energy to water, catalysts and membrane surface is highly needed.

4.1.4 EAOP and electrochemically reactive membrane development

Recent studies shows electrochemical advanced oxidation processes (EAOPs) also known as electrolytic treatment have emerged as promising technologies for the destruction of recalcitrant and complex waste.[82] EAOPs mineralize persistent organic pollutants (POPs) primarily through direct electron transfer at the electrode surface and through mediated oxidation by electro-generated reactive oxygen species (ROS), such as •OH radicals produced from the electrolysis of water:[25-26, 78, 266]

$$H_2O \rightarrow OH^{\bullet} + H^+ + e^-$$

OH• is a powerful and unselective oxidant with a high oxidation potential (E^o = 2.6 V), which could mineralize most organics at near diffusion-limited rates.[267-268] Additional reactions at the anode surface will produce several other stable oxidants. These may include, H_2O_2, Cl_2, and $S_2O_8^{2-}$ (depending the presence of ionic species in the feed solution) as shown below:

$$2OH^{\bullet} \rightarrow H_2O_2$$

$$Cl^- \rightarrow Cl^{\bullet} + e^- \qquad\qquad 2Cl^{\bullet} \rightarrow Cl_2$$

$$SO_4^{2-} \rightarrow SO_4^{-\bullet} + e^- \qquad\qquad 2SO_4^{-\bullet} \rightarrow S_2O_8^{2-}$$
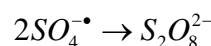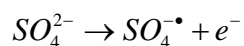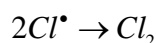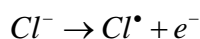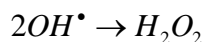
The standard reduction potentials for H_2O_2 (E^o = 1.8 V), Cl_2 (E^o = 1.48 V), and $S_2O_8^{2-}$ (E^o = 2.01 V) are high enough to oxidize typical organic compounds and inorganic substances such as H_2S and NH_3 efficiently, and are currently used for aquifer remediation.[269]

Many studies have demonstrated high conversion rates of to CO_2 or readily biodegradable products. Electrochemical processes have been reported to be effective for recalcitrant organic pollutants such as PFASs (Table 4.1), as well as microbial inactivation (Table 4.5 and Table 4.6). Most previous studies have focused on the electrochemical generation of active chlorine species (>2.5 V; HOCl, Cl_2) or electrochlorination that can result in the formation of harmful disinfection byproduct.[270] However, recently the anodes without electrochlorination was also studied (e.g, BBD, porous carbon.). The low driving potentials of these materials will reduce energy requirements and avoid disinfection byproduct formation.[271]

Reactive Electrochemical Membranes (REM) or electrochemically reactive membranes combined electrochemistry with ceramic membranes may provide a solution by *in situ* and real-time production of chemical oxidants, higher flux, and less maintenance. This combination may help overcome some of limitations of traditional EAOP such as the intrinsic mass transport limitations associated with organic pollutants required to interact with the electrode surface,[272-275] high cost of electrodes, and low current densities without high concentrations of electrolyte.[276] Because the radicals can be generated *in-situ* via electrochemistry, which means the oxidation process can be driven by electricity rather than by chemicals to produce radicals.[277] The reduced chemical consumption potentially leads to a more environment-friendly approach.[278] For example, Doped-SnO_2 electrodes has resulted in an electrode with high conductivity and a potential for O_2 evolution of 1.9 V versus SHE. However, Sb is a toxic substance with an EPA drinking water limit of 6 $\mu g \cdot L^{-1}$.[82, 279] PbO_2 and doped PbO_2 electrodes are also

utilized in packed-bed reactors containing oxidized Pb pellets, which may cause safety concerns in water treatment due to the release of Pb element.[8]

4.1.5 Applications of EAOP in the removal of different micropollutants

4.1.5.1 Industrial solvent additives-1,4-dioxane. 1,4-Dioxane is a semivolatile, cyclic ether historically used as a stabilizer in chlorinated solvents and currently still used in the manufacturing.[280-283] 1,4-dioxane causes liver damage and kidney failure with carcinogenic effects on animals and human beings.[284] Thus, EPA has classified 1,4-dioxane as a hazardous and priority pollutant.[252] Its water miscibility and low potential for sorption to soil promote the formation of large and dilute plumes and environmental transport.[275] 1,4-dioxane is not readily biodegradable in the environment due to the strong internal chemical bonding of its heterocyclic ether ring.[281-282, 285-286] Table 4.2 summarizes electrochemical processes applications on 1,4-dioxane with different electrode materials. For example, boron-doped diamond (BDD) electrodes demonstrated that 1,4-dioxane can be completely mineralized by anodic oxidation.[256, 275, 287] The high cost of BDD electrodes, however, precludes their application in large-scale operations at this point. In addition, many electrochemical studies are conducted in stirred-batch reactors with elevated electrolyte concentrations that favor high mass-transfer rates and current densities, creating increased contaminant degradation rates that may not be achieved in realistic conditions.

4.1.5.2 Persistent dye micropollutants.   Synthetic dyes are extensively used in textile, leather, painting and printing processes because of their uniquely high brilliant shades, and relatively simple, low cost production methods. More than 10–15% of synthetic dyes produced are lost as effluent and pose a major threat to the health of ecosystem.[288] Industrial effluents discharged from dyeing industries are highly colored, of low BOD and high COD. Disposal of this colored water into receiving waters can be toxic to aquatic life. The dyes upset the biological activity in water bodies. They also pose a problem because they may be mutagenic and carcinogenic and can cause severe damage to human beings, such as dysfunction of kidney, reproductive system, liver, brain and central nervous system.[289] Dye-contaminated water is usually chemically stable, non-biodegradable, and potentially carcinogenic.[290] Furthermore, dyes inhibit photosynthesis because they reduce light penetration. These dyes diminish the amount of dissolved oxygen because they block the oxygen interchange at the surface while simultaneously increasing the biochemical oxygen demand.[290] Therefore, the treatment of dye wastewater is one of the growing needs.[291]

Among the various dyes, methylene blue (MB), rhodamine B (RB) and orange II (OGII) are three of the most commonly used coloring agents. Methylene blue is an important basic dye widely used for printing calico, printing cotton and tannin, dyeing leather, and in purified zinc-free form.[291] Rhodamine B has been often used as a tracer dye, fluorescent staining dye and also used in fluorescence instruments. Orange II dye is mainly used in textiles, plastics, tanneries, pharmaceuticals, leather, packed food, pulp, paper, paint, and electroplating.[292] MB, RB and OGII are toxic and highly water soluble. RB causes irritation to skin, eyes and respiratory tract. The carcinogenicity, reproductive

and developmental toxicity, neurotoxicity and chronic toxicity of these dyes towards humans and animals have been experimentally proven.[291]

Common treatment of dye wastewater include activated carbon adsorption, chemical oxidation, reverse osmosis and ion exchange.[293] Different AOPs such as photo/Fenton, photocatalysis, and UV/H_2O_2/O_3 have also been applied for degradation of azo dyes.[294] Ozonation is effective in decolorizing the textile wastewaters. But the cost of operation is rather high.[294] In recent years, electrochemical treatment processes, especially electrochemical oxidation and electrocoagulation, have been studied as alternatives for degradation of various types of organic dyes in wastewater.[295] A summary of electrochemical processes for different dyes and their effectiveness was listed in Table 4.3. For example, electrochemical oxidation on conductive diamond was used to discolorize Azoic Dyes, such as methyl orange (MO) and congo red (CR).[103] However, the high cost of electrodes and high energy consumption often make this technology unsuitable in industrial productions. Additionally, many studies have employed different types of electrodes (e.g., TiO_2/Ti, Ti/Pt, Ti/MnO_2, and Ti/PbO_2) in the electrocatalytic process of dyes. However, lower removal efficiency limit them in practical application.[105,106,107]

4.1.5.3 Cyanotoxins and harmful algal blooms (HABs) related micropollutants.

Oxygen depletion or hypoxia and anoxia in coastal and estuarine, resulted from excessive phytoplankton growth and decay, have major deleterious impacts on fish and other living resources. In particular, the occurrence of HABs is increasingly common in inland freshwater (lakes, ponds, reservoirs and rivers) across all 50 states in the US[296] and

globally.[297] Algal blooms are caused by an expeditious growth and aggregation of microalgae in the surface waters, such as cyanobacteria, dinoflagellates and diatoms.[298] In some cases, accumulation of these organisms (mainly dinoflagellates) can cause a discoloration of water, giving rise to the name "red tides".[299] HABs form naturally and are triggered by slow water movement or droughts. They can also form as a result of the nutrients from the environment and contaminants from human activities such as storm water runoff, runoff from agricultural activities that release pesticides, and salinization[300]. HABs negatively affect the environment, ecosystems and human health.[300-301] The accumulation of HABs reduce water quality and change color, taste, odor, turbidity of the surface water.[298]

HABs pose a serious threat to public health also because many HAB species produce potent toxins. Cyanobacteria release cyanotoxins such as anatoxin, cylindrospermopsin, nodularin, saxitoxin, and microcystin that are responsible for illness and death of animals and human.[302] In 2007, 11 states reported 70 pet, livestock, and wildlife mortality and morbidity cases related to freshwater HABs.[303] Yet basic questions of HAB occurrence, extent, intensity, and timing are largely unanswered.[304-306] The increase in HAB occurrences has triggered the need to track health issues related to HABs, investigate the formation mechanisms of HABs, and develop effective mitigation and control measures.[303]

Incorporating a chemical oxidation process to treat cyanobacteria cells is shown to produce toxic metabolites (e.g., microcystin, anatoxin, cylindrospermopsin) and/or odorous metabolites (e.g., Methyl-Isoborneol (MIB) and geosmin).[307] For example, the effect of chlorination on cell lysis, toxin release, and disinfection byproduct (DBP)

formation has been observed on a few aquatic organisms and algae.[308] Clearly, the potential physicochemical interactions with reactive NBs and oxidation of algae may also lyze algal cells and release intracellular toxins, which has not been investigated and reported. It is therefore interesting and imperative to investigate the release and removal mechanisms of cyanotoxin such as microcystins. For example, Microcystin-LR (MCLR), a cyclic heptapeptide produced by the blue-green algae Microcystis aeruginosa, is a common cyanotoxin in water.[309-310] In MC degradation, the conjugated diene bond, benzene ring, and methoxy group of the side chain of MCLR can be attacked by •OH and produce byproducts such as dihydroxylated-MCLR, aldehyde or ketone peptide residues, benzene hydroxylation and formic acide-MCLR.[311] The degradation mechanisms of cyanotoxin by NBs remain largely illusive and deserve extensive research. The objectives of our project are (1) to further examine the release characteristics of cyanotoxins following cell damage and lysis after treatment by different NBs; and (2) quantitatively compare the efficacy of degradation of a few model cyanotoxins (e.g., MC-LR, CYN, ANTX) in their dissolved form (extracellular) in water by different NBs.

In addition to cyanotoxin, many studies indicated that both NH_3 and H_2S are produced by algae may be inhibitory toward other aquatic organisms.[312-313] Previous studies indicated that both NH_3 and H_2S can be oxidized on different electrodes as shown in Table 4.7.[314-315] For example, Ti/IrO_2 electrodes demonstrated complete removal of ammonia ions by anodic oxidation.[115] BDD can remove 90% of H_2S at high current densities.[121] Similarly, the high cost of BDD electrodes and high current density in operation, however, precludes their applications in large-scale operations. Such oxidation could be enhanced in the presence of Cl^-, due to the oxidation of chloride ion to chlorine

gas at the anode and then conversion to hypochlorous acid and hypochlorite (strong oxidizing reagents).[315-316]

4.1.5.4 Removal of NOM and precursors of disinfection byprdoucts.   Natural organic matter (NOM) constitutes a complex mixture of organic compounds with varying molecular weights, charge densities, and hydrophobicity. The presence of NOM or dissolved organic matters in drinking water primary affects the aesthetic quality such as taste, color,and odor issues. Moreover, NOM serve as a carrier of toxic metal ions and organic micropollutants in water bodies, promote the microbial re-growth and corrosion problems in the water distribution systems.[317] Finally, NOM is one of the precusor of disinfection byproducts (DBPs), which cause adverse human health impacts.[318] Thus, removal of NOM is critical for the safety of drinking water supply.

Currently, no single process alone can be used to treat NOM due to its high variability. The most common and economically feasible processes available are coagulation and flocculation followed by sedimentation/flotation and filtration. Numerous bench-scale studies have demonstrated the ability of electrochemical processes to remove organic contaminants, chemical oxygen demand (COD) and dissolved organic carbon (DOC),[319-320] as summarized in Table 4.4.

4.1.5.5 Removal of Antibiotic resistant bacteria (ARB) and antibiotic resistance genes (ARG)

Bacterial contamination is one of the greatest global problems for drinking water security. Recent occurrences of pathogenic microorganisms such as pervasive SARS, Ebola virus, avian influenzas, and pneumonia causes severe diseases and poses threat on general

public safety and human health. In the USA, each year 560,000 people suffer from severe waterborne diseases, and 7.1 million suffer from a mild to moderate infections, resulting in estimated 12,000 deaths a year.[321] Majority of waterborne diseases in the US are associated with the opportunistic pathogen *Legionella*, which may originate from drinking water contamination in distribution systems and premise plumbing. Conventional disinfectants (e.g., chlorine, chlorine dioxide, or ozone) can eliminate a wide spectrum of undesirable microorganisms; however, they also render the rise of more than 600 different disinfection byproducts (DBP)[322-325] and increase microbial resistance to disinfectant chemicals.[326-328] Most DBPs (e.g., trichloromethane, brominedichloromethane, dibromomethane and tribromomethane) are potentially carcinogenic.[329] Conventional disinfection methods are becoming less efficient due to the evolution of antibiotic-resistant strains or genes.[330-331] UV irradiation is an effective, safe, and environmentally friendly disinfection method but the lack of persistent antibacterial capacity generally causes high risk of regrowth, particularly in poor sanitation. Due to recent changes in water quality regulations, particularly the Long-Term 2 Enhanced Surface Water Treatment Rule (LT2ESWTR) and the Stage 2 Disinfectants and Disinfection Byproducts Rule (D/DBPR), water utilities may need to implement alternative treatment technologies to remain in full regulatory compliance.

Besides regular microbial pathogen, antibiotic resistant bacteria (ARB) and antibiotic resistance genes (ARG) in the aquatic environment have also become an emerging contaminant issue, which has implications for human and ecological health. As antibiotics are widely applied to treat bacterial infections and due to the environmental accumulaiton and magnficaition, there is growing concern that unused antibiotics in the

surface water may be causing a risk to human health by promoting ARB and ARG.[253] ARB and ARG are formed due to the intensive application of antibiotics in pharmaceuticals and agriculture worldwide, which are not fully removed by wastewater treatment and released to the environment.[253] Table 4.4 and 4.5 summarizes the reported perfomrane of EAOPs on bacterial and viral removal or inactivation. For example, Ti/RuO$_2$ electrodes showed the ability to remove 96% of the *Microcystis aeruginosa* by anodic oxidation. BDD was also reported 98% removal of *E.coli* cells.

4.1.6 Research objectives of this chapter

To advance the electrochemically reactive membrane applications in micropollution treatment, this study employed a monolithic tubular ceramic membrane made of a Magneli phase suboxide of TiO$_2$ (primarily of Ti$_5$O$_9$ and Ti$_4$O$_7$ [85]) to assess the degradation performances of a few biorefractory contaminants (i.e., 1,4-dioxane, dyes and algal metabolites) and bacteria in both dead-end and continuous filtration conditions. The Magneli phase TiO$_2$ membrane or typically termed as reactive electrochemical membrane (REM) can generate •OH from water oxidation under anodic and cathodic polarization.[26, 332] At the same time, the monolithic porous structure results in a high water flux in filtration (e.g., 5000-6000 L m^{-2} h^{-1} bar^{-1} or LMH bar^{-1}), which makes the REM filtration an ideal platform for sustainable water treatment and chemical separation. In the past research, the Magneli phase REM has been demonstrated in the degradation of various micropollutants (e.g., tetracycline,[333] p-substituted phenol,[177] and *N*-nitrosodimethylamine*[334]). In this study, we first examined the DC voltage drop or decline along the REM surface experimentally and developed a mathematical model of electrical resistance using Matlab to provide new insight into in the future design of up-scaled

REM filters. We also measured the electrode potentials of REM under different DC current densities to explain the formation of potential oxidative species or radicals. For degradation performance assessment, we ran batch and continuous flow filtration experiments, in which the effects of DC current density and the initial pollutant concentration on the degradation efficiency were analyzed.

Table 4.1 Summary of Electrochemical Oxidation of PFASs Pollutants.

Reference	Pollutant	Catalyst	Electrode Potential (V)	Current Density (mA·cm^{-2})	Removed (%)
276	1,4-dioxane	TiO$_2$	8.0 - 14.0	3.5 - 8.3	70
335	1,4-dioxane	Ti/IrO$_2$−Ta$_2$O$_5$ with Aerobic Biodegradation	3.0 - 8.0	0.2 - 2.3	41 - 62
336	1,4-dioxane	Boron-doped diamond (BDD)	-	12	> 85
337	1,4-dioxane	Activated carbon electrode	-	-	> 98.8

Table 4.2 Summary of Electrochemical Oxidation of 1,4 dioxane.

Reference	Pollutant	Catalyst	Electrode Potential (V)	Current Density (mA·cm^{-2})	Removed (%)
338	Perfluorooctanoic acid (C$_7$F$_{15}$COOH, 98%)	Ti/SnO$_2$-Sb	1.492	5 - 40	76.9 - 98
339	6:2 Fluorotelomer sulphonic acid	BDD anode and a stainless-steel cathode	14	50	80
340	Perfluorooctanoic acid (96%)	UNCD - tungsten	8	10 - 20	70.6 - 81.8
71	PFOS (40% in H$_2$O)	UNCD - tungsten	4.6 - 12	3 - 50	60 - 98
274	PFOA and PFOS	stainless steel and Ti/RuO$_2$	4 - 13	0 - 20	90

Table 4.3 Summary of Electrochemical Oxidation of Dyes.

Reference	Pollutant	Catalyst	Electrode Potential (V)	Current Density (mA·cm^{-2})	Removed (%)
341-342	Azoic Dyes (Naphthol and Diazo-compound) Such as Methyl Orange (MO)	Conductive Diamond	2.8	30	80 - 85
343	Methyl Orange (MO)	TiO$_2$	1.5	0.055	53
344-345	Methylene Blue (Cationic dye)	Ni and Fe bimetallic catalyst	0.01	0.06	40
346	chromate Cr (VI) and azo dye Acid Orange 7	Brevibacterium casei	1.5	1.47	25 - 30
347-348	Cationic Red X-GRL	Hydrothermal Synthesis of PbO2/RGO Nanocomposite	1.0	1.77	30

Table 4.4 Summary of Electrochemical Oxidation of Bacteria/Genes

Reference	Pollutant	Catalyst	Electrode Potential (V)	Current Density (mA·cm^{-2})	Removed (%)
349	*Escherichia coli*	Platinum-tipped copper	5	-	100
349	*Pseudomonas aeruginosa*	Platinum-tipped copper	5	-	100
271	*Escherichia coli*	Carbon nanotubes	2 - 3	-	87 - 99
350	*Microcystis aeruginosa*	Ti/RuO$_2$	9.2	10	96
351	*Escherichia coli*	BDD	2.8 - 3.1	1.5 - 13.3	98

Table 4.5 Summary of Electrochemical Oxidation of Ciruses

Reference	Pollutant	Catalyst	Electrode Potential (V)	Current Density (mA·cm^{-2})	Removed (%)
349	Bacteriophage MS2	Platinum-tipped copper	5	-	98
349	PRD1	Platinum-tipped copper	5	-	98
271	Bacteriophage MS2	Carbon nanotubes	2 - 3	-	99 - 100
352	Bacteriophage MS2	Ti pellet with a thin layer of IrO2 –Sb2O5 – SnO2 coating	18	21.7	95

Table 4.6 Summary of Electrochemical Oxidation of Ammonia, H_2S or Na_2S.

Reference	Pollutant	Electrode	Electrode Potential (V)	Current Density (mA·cm^{-2})	Removed (%)
353	Ammonia ion	Cu as cathode, Ti/IrO$_2$ as anode	-1.8 - 0.2	45.13	100
354	Ammonia ion	Pt roughened	2.8 - 3.0	0.4	98
355	Ammonia ion	Cu/Zn as cathode, Ti/RuO$_2$-Pt as anode	50	30	100
356	Ammonia ion	Ti/RuO$_2$ as anode	0-50	20	88.3
357	Ammonia ion	Ni(OH)$_2$	0.3 - 0.54	5 - 10	58
357	Ammonia ion	Ni$_{0.8}$Cu$_{0.2}$LHs	-0.2 - 1.0	34 - 40	84
358	Na$_2$S	Ru MMO	0.92 - 0.17	20	4.8
359	H$_2$S	Boron-(BOD) diamond as anode, graphite as cathode	0.44	33.3	90
360	H$_2$S	Carbon felt porous	0.01 - 0.1	19 - 57	83.4

4.2 Method and Materials

4.2.1 Preparation of REM filtration system

The bench top REM filtration system was assembled as we reported previously.[176] Briefly, a 10-cm long Ebonex one-channel tubular REM with the outer and inner diameters of 10 mm and 6 mm respectively were purchased from Vector Corrosion Technologies, Inc.[85] This Ebonex REM has a median pore diameter of 1.7 μm with pore diameters of <10 nm accounting for >90% of the surface area. The Ti_4O_7 electrode had porosity of $30.7 \pm 2.8\%$ and a specific surface area of 2.8 ± 0.7 $m^2 \cdot g^{-1}$, and a roughness factor of 619. To increase conductivity of REM and obtain a higher Ti_4O_7 content, the received REM electrodes was first soaked in a 0.625-M sodium hydroxide solution for 24 hours to remove possible organic contaminants, and then rinsed with DI water. The clean electrode was reduced under a H_2 flow at 1050 ^{o}C for 10 hours with a heating and cooling rate of 5^oC·min^{-1} in a tube furnace (MTI OTF-1200X). Other important characterization data were reported elsewhere.[78, 83, 189]

The REM filtration unit has a total liquid volume of 0.5 L, in which the Ebonex REM was placed in the center with a 57-mm diameter stainless steel cylinder case as the counter electrode.[18, 19] There were approximately 23 mm spacing between REM and the counter electrode, which creates an isopotential surface on the outer surface of the REM. The REM filter was sealed up on one side by acrylonitrile butadiene styrene (ABS) and reinforced by Epoxy as shown in Figure 3.5 or Figure 4.3. The other end was also sealed with the same ABS plastic and Epoxy but one stainless steel tube or copper tube (1.1 mm in diameter) were inserted through the plastic gel to permit the permeate flow out.

The continuous filtration was run in a dead-end mode by filtering the feed solution through the REM surface under a constant vacuum pressure (75 kPa) using a check valve and a vacuum pressure gauge. Permeate flux was measured volumetrically by collecting the permeate weight data per minute using the WinWedge software and an Ohaus Adventurer Pro Balance AV8101 (Ohaus, USA).

4.2.2 Porosity and mean pore size

See Chapter 3 for details.

4.2.3 Voltage drop measurement and calculation

A conceptual model of membrane electrical resistance was established to compute the voltage distribution and drop along the length direction of the REM. As shown in Figure 4.1, the REM filter is divided into multiple layers of circular discs with a thickness of dl. The electrical resistance is composed of water resistance (R_W) and membrane resistance (R_M), which can be integrated along the radial direction:

$$dR_W = \int_{r_1}^{r_2} \frac{\rho_W dr}{2\pi r dl} = \frac{\rho_W}{2\pi dl} \ln \frac{r_2}{r_0} \tag{4.1}$$

$$dR_M = \frac{\rho_M dl}{\pi(r_1^2 - r_2^2)} \tag{4.2}$$

where dR_W and dR_M are the fluid resistance and the REM resistance at a depth of dl (e.g., dl = L/n and n = 10^8); L is the length of the REM (10 cm); r_1 and r_2 are the outer and inner radius of REM; r_0 is the radius of the stainless steel rod; ρ_W is the resistivity of water ($\Omega \cdot m$); and ρ_M is the resistivity of REM ($\Omega \cdot m$). Along the different distance (x) from the top of the REM, the applied voltage decline (α_n) is equal to:

$$\alpha_n = \frac{\dfrac{dR_W R_x}{dR_W + R_x}}{\Bigg/ dR_M + \dfrac{dR_W R_x}{dR_W + R_x}} \qquad (4.3)$$

where R_x is the total resistance from point x to the bottom of REM. Using recursive algorithm to express the resistance at point x:

The 1st *dl* layer: $R_1 = dR_W + dR_M$

The 2nd *dl* layer: $R_2 = dR_M + R_1 // dR_W$

The 3rd *dl* layer: $R_3 = dR_M + R_2 // dR_W$

At point x: $R_x = dR_M + R_{x-1} // dR_W$ $\qquad (4.4)$

where $R_x // R_y = \dfrac{R_x R_y}{R_x + R_y}$. The corresponding voltage decline from point x to the bottom

of REM could be expressed as:

$$x+1dl: \ \alpha_1 = \frac{R_x // R_W}{dR_u + R_x // R_W} \ . \ R_{x+dl} = dR_M + R_x // R_W$$

$$x+2dl: \ \alpha_2 = \alpha_1 \frac{R_{x+dl} // R_W}{dR_M + R_{x+dl} // R_W} \ . \ R_{x+2dl} = dR_M + R_{x+dl} // R_W$$

$$x+3dl: \ \alpha_3 = \alpha_2 \frac{R_{x+2dl} // R_W}{dR_M + R_{x+2dl} // R_W} \ . \ R_{x+3dl} = dR_M + R_{x+2dl} // R_W$$

$$\text{At the bottom of REM: } \alpha_n = \alpha_{n-1} \frac{R_{L-dl} // R_W}{dR_M + R_{L-dl} // R_W}$$

$$R_{total} = R_L = dR_M + R_{L-dl} // R_W \qquad (4.5)$$

A set of Matlab calculation code was developed based on Equation 4.1 to Equation 4.5 to calculate the voltages at different axil locations when connecting the DC power to one end or the top of the REM as shown in Figure 3.5. The Matlab code is

provided in appendix. This model allows us to evaluate the dependence of the voltage distribution on factors such as radius of stainless-steel cathode (r_0), inner and outer radius of REM (r_2 and r_1), the applied voltage ($U_{initial}$) and resistivity of liquid medium (ρ_W) and REM (ρ_M). The voltage decline at different locations of REM was also measured in the tap water with a DC power (the cell potential of 20 V or 15 mA·cm^{-2}) applied to REM.
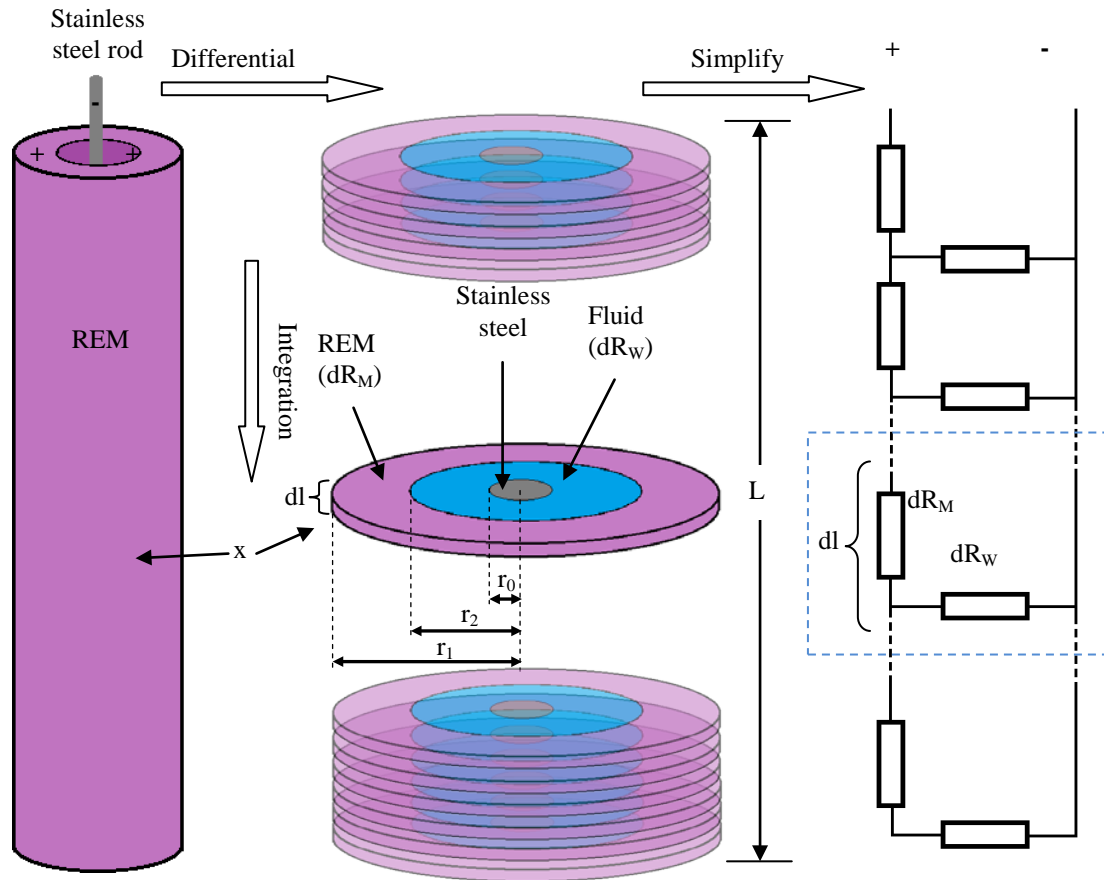
Figure 4.1 The conceptual model of electrical resistance along axil and radial directions of a hollow REM filter as well as the corresponding electric circuit diagram.

4.2.4 Electrode potential measurement in relevant aqueous environment

A two-electrode system was set up where the working electrode (REM) and the reference electrode are equipotential. Modified Bold's Basal Medium (MBBM) solution was used

as the electrolyte as shown in **Figure 4.2.** The MBBM contains Na^+, K^+, Mg^{2+}, Fe^{2+}, Zn^{2+},

Mn^{2+}, Cu^{2+}, Co^{2+}, Ca^{2+}, H^+, OH^-, NO_3^-, $H_2PO_4^-$, HPO_4^{2-}, SO_4^{2-}, Cl^-, MoO_4^{2-} and

$EDTA^{2-}$.[73-75] A cylinder-shaped stainless-steel mesh as the counter electrode was placed

around the REM in the center. A Silver/Silver chloride (catalog# 930-00015; Gamry) was

the reference electrode.[361] The reference electrode was immersed in the solution and the

voltage between the reference and the working electrode was measured by a Multi-meter

(EXTECH INSTRUMENTS, MN26T). The experimental temperature was kept at 21 ±

1 °C. The conductivity of MBBM solution was measured by a Pasco conductivity meter

(Model: #699-06621). All potentials were reported versus the standard hydrogen

electrode (SHE).

$$U_c = U_a + U_r + U_{rf} \tag{4.6}$$

where the U_c is the cell voltage between anode and cathode, U_a is the electrode potential

for anode, U_r is the voltage loss by the liquid resistance, and U_{rf} is the potential between

anode and reference electrode. The Ag/AgCl reference electrode potential is +0.197 V at

25 °C compare with Standard Hydrogen Electrode (SHE).

4.2.5 Redox potentials of different reactive species

The redox potentials of different reactive species that are involved in EAOPs on

REM were indicated by the half reaction (E_H) using the Nernst equation. For a redox

reaction,

$$aA + bB + n[e^-] + h[H^+] = cC + dD \tag{4.7}$$
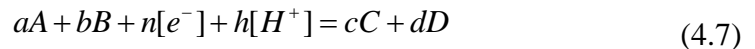
The E_H can be calculated by Equation 4.8:

$$E_H = E_0 + \frac{0.05916}{n} \log\left(\frac{\{A\}^a \{B\}^b}{\{C\}^c \{D\}^d} \right) - \frac{0.05916}{n} pH \tag{4.8}$$

where E_0 is the standard potential at pH=0. In standard condition, E_H can be simplified as follows:

$$E_H = E_0 - \frac{0.05916}{n} pH$$

(4.9)
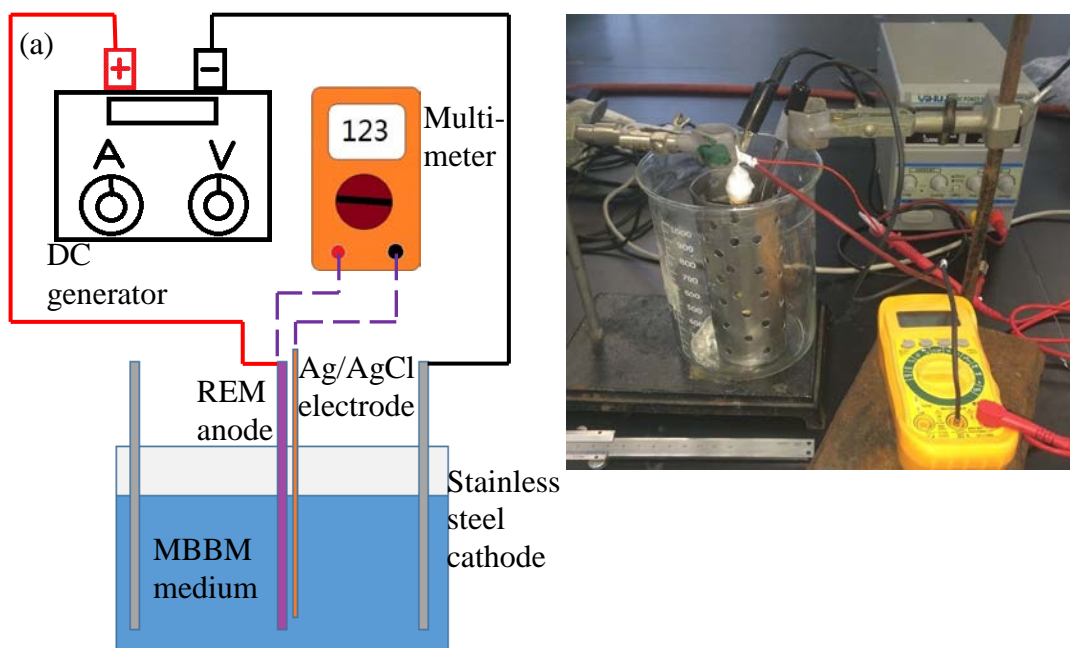
Figure 4.2 Experimental setup for electrode potential measurement (a) Schematic and circuit diagram. (b) The setup of this electrochemical cell.

4.2.6 Assessment of chlorine species generation on REM

Chlorite and chlorate production appears to involve oxidation of HOCl or $HClO_2$ via direct electron transfer from the medium solution containing Cl^-, followed by reactions of $ClO\bullet$ or $ClO_2\bullet$ with $\bullet OH$, which may react with $\equiv C\bullet$, $=C\bullet H$, $\equiv C\text{-}O\bullet$ and $=C\bullet HO$ from anodic polarization, and generate chlorine oxyanions (ClO^- or ClO_2^-).[362] These chlorine oxyanions could further react with $\bullet OH$ and generate higher oxidized states (ClO_2^- or ClO_3^-).

To generate and measure chlorine species via surface electrochemical reactions at the REM and stainless-steel cathode, an electrochemical batch reactor (500 ml glass beaker) were used (Figure 4.3). The reactor was filled with the MBBM medium (the green liquid in Figure 4.3a), where the REM was immerged as the anode (the dark gray rod in the center) and a stainless-steel circular mesh as the cathode surrounded the REM with a spacing distance of 2.5 cm. The REM was applied under a constant current (100–500 mA) using a DC power supply (Proteck P6035, Tempe, AZ) corresponding to cell voltages between 10–20 V and for different times (30–120 min) to generate different levels of chlorine species. The effective exposed surface area of the REM was 25.4 cm^2. The conductivity of the MBBM medium was 1040±5 μm·cm^{-1}.

The concentration of active chlorine and the other combined chlorine species generated was determined as the total Cl$_2$ by a N, N-diethyl-p-phenylenediamine (DPD) colorimetric method, which included free chlorine, hypochlorous acid (HClO) and hypochlorite ion (ClO$^-$). DPD is oxidized to form a red-violet product, which was measured by the total chlorine test kit (CN-70, HACH Co., Loveland, USA) (Figure 4.4a).[363] For a low range (0-0.7 mg·L^{-1}) of the total Cl$_2$, 25 ml of the electrically treated MBBM medium was taken from the 1-L beaker and mixed with the DPD Total Chlorine Reagent Power Pillow. After 3 minutes, 15 ml of the mixed sample was filled into a test tube (Figure 4.4b), while another test tube was filled with DI water as a blank. Then, the lengthwise viewing adapter was placed into the color comparator (Figure 4.4c). The above-mentioned test tubes were then inserted into the color comparator and viewed through the openings in the front of the comparator. To obtain the reading, the disc was rotated to make two tubes have a color match. When the tubes had the same color from

the openings, the total chlorine concentration could be read from the scale window (Figure 4.4d). The value was divided by 5 to obtain the total chlorine in $mg \cdot L^{-1}$ unit. For a high range (0 - 3.5 $mg \cdot L^{-1}$) of the total Cl_2, the lengthwise viewing adapter was not used, and the final value did not need to be divided by 5. Other procedure was the same as that for the low range total Cl_2 method. Concentrations of ClO^{2-} and ClO^{3-} were determined by ion chromatography (Dionex ICS-3000; Dionex IonPac AS16 column; KOH eluant; 1 $mL \cdot min^{-1}$ eluant flow rate).[362]
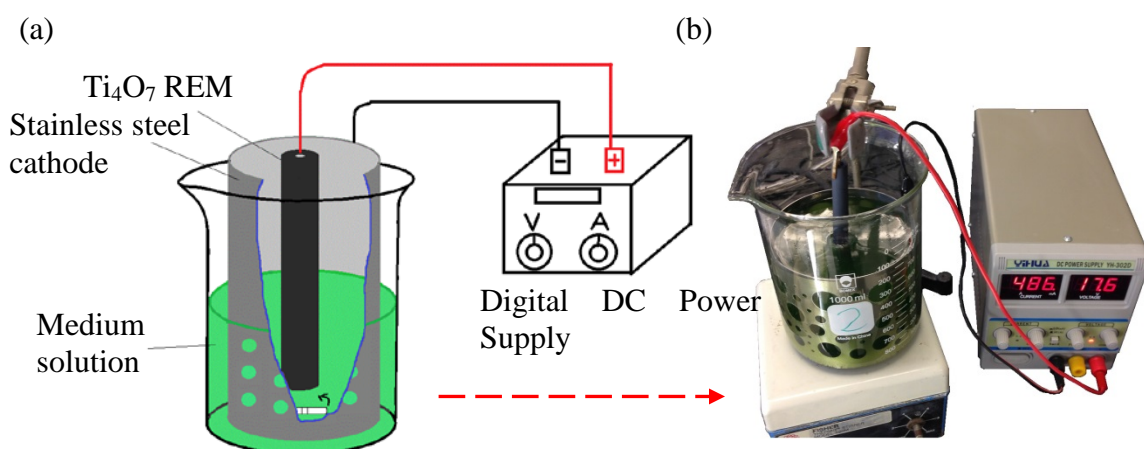
Figure 4.3 (a) Schematic and (b) experimental setup for the chlorine species generation detection.
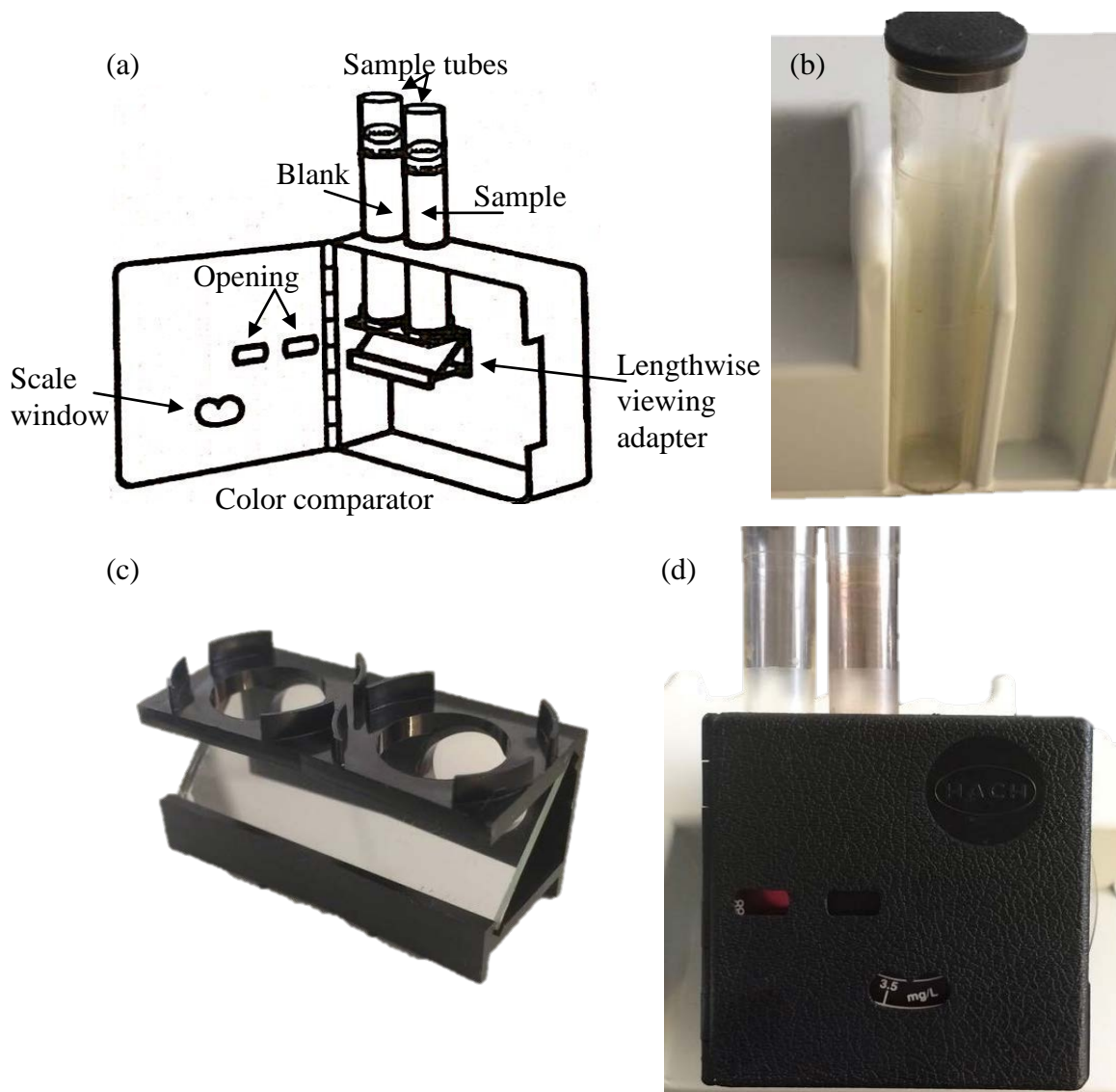
Figure 4.4 (a) The schematic of HACH total chlorine test kit. (b) 15 ml test tube used for color comparator. (c) Lengthwise viewing adapter used for low range total Cl_2 measurement. (d) Chlorine concentration reading from the scale window.

4.2.7 Assessment of other ROS generation on the REM surface and stainless steel cathode and in the solution

ROS, such as O_3, H_2O_2, and •OH, $O_2^{•-}$, and $^1O_2$ were identified by direct or indirect methods. Same batch reactor and the same DC configuration for of chlorine species generation assessment was used. The concentration of O_3 was measured using the indigo

method (EMD Millipore™ MColortest™ Ozone Test Kits) with an UV–vis spectrophotometer (Hewlett-Packard 8453, USA) and 10 cm cuvettes. This method is based on the quantitative decolorization of indigo trisulfonate as a result of its reaction with O_3, which is observed at 600 nm and whose detection limit is about 0.01 mg·L^{-1}.[2] All experiments for O_3 generation were conducted at low temperature (10 °C), since our previous study revealed that the electrochemical generation of O_3 is strongly dependent upon the temperature of electrolytic solution, such that a higher O_3 concentration is achieved at lower temperature.[364-365]

For $O_2^{\bullet-}$, 100 μM XTT (2, 3-Bis(2-methoxy-4-nitro-5-sulfophehyl)-2H-tetrazolium-5-carboxanilide) was used as the indicator.[366-367] The XTT stock solution (5.25 mM, Sigma-Aldrich) was stored for no longer than one week at 4°C. After UV illumination for different periods of time, 1 mL of the suspension was sampled and injected into a quartz vial. The concentration of the orange-colored XTT-formazan (the product resulting from the reduction of XTT by $O_2^{\bullet-}$) was measured using a UV-Vis spectrophotometer (Thermo Scientific Evolution 201) at 470 nm. Exposure tests were run for different time periods up to 48 h until indicator degradation equilibrium was reached. Superoxide anion radicals ($O_2^{\bullet-}$) can be formed from potassium superoxide (KO_2). Positive tests can be run with KO_2 solution. Krebs-Ringer phosphate buffer (pH 7.4) containing a fluorescence probe (1 μM of APF or 2 μM of DCFH) was added and vigorously mixed with the KO_2 powder in the centrifuge tube. After reacting with KO_2 for 5 minutes, the fluorescence intensity was determined. To detect the reaction of APF with $O_2^{\bullet-}$, we compared the fluorescence increase of probes using the buffer with and without hydrogen NBs.

p-Chlorobenzoic acid (*p*CBA, 20 μM, Sigma-Aldrich) and furfuryl alcohol (FFA, 0.85 mM, Sigma-Aldrich) were used as indicators for •OH and $^1O_2$, respectively.[366-367] Standard solutions with different concentrations (0-150 μM) of pCBA (HPLC-grade, SPEX CertiPrep, USA) were prepared, and used to generate the calibration curve. The average, standard deviation, and limit of detection (LOD) were obtained from triplicate experimental results. LOD was calculated by:

$$LOD = 3 \times STYX / \text{slope of the standard curve}$$

where STYX is the standard error of the predicted y-value for each x in the regression.[368-369] The concentrations of *p*CBA were analyzed by Alliance high performance liquid chromatography (LC/MS) waters 2695 system with Waters 2489 UV/visible detector, according to the published methods. The mobile phase was acetonitrile/Direct-Q UV Millipore water 65:35 (v: v), and the used UV detector, flowrate, and injection volume was 234 nm, 1 ml.min-1, and 10 μl, respectively.[370-371] All tested samples were filtered with 0.2-micron filter (Whatman Anotop 25 Plus syringe filter - Sigma Alorich, USA) prior to testing by LC/MS system. 500 ml MBBM solutions with 25 μM of pCBA in the beaker setup (same as Figure 4.3) were exposed to REM anode oxidation for 1h.[366] Applied current density was 0.4 mA·cm^{-2} (electrode potential 4.803 V as the result in Table 4.7a), according to radical formation requirement in Table 4.7a. Samples were collected at different reaction time and tested immediately.

Alternatively, we can use the fluorescence probes to detect most of the probes for radicals. The fluorescence probes are reduced dyes, such as 2'7'-dichlorodihydrofluorescein (DCFH), 3'-(p-aminophenyl) fluorescein (APF), 3'-(p-hydroxyphenyl) fluorescein (HPF) and mitochondrial superoxide indicator (MitoSOX).

The reduced dyes exhibited little or no fluorescence due to disrupted π conjugation. However, upon reaction with radicals, the reduced dyes were oxidized, regenerating the extended π conjugation, which substantially increased the fluorescence intensity. For example, APF (final concentration 1 μM) was added to the Krebs-Ringer phosphate buffer (0.1 M, pH 7.4) and mixed with the electrochemical reactor. Then, the efficiencies of •OH production can be assessed by the increase of fluorescence intensity of oxidized APF.

The formation of hydroxyl radicals (•OH) on the surface of REM can be detected by a photoluminescence (PL) technique with terephthalic acid as a probe molecule. Terephthalic acid readily reacts with •OH to produce highly fluorescent product, 2-hydroxyterephthalic acid.[372-373] The intensity of the PL peak of 2-hydroxyterephtalic acid is in proportion to the amount of OH radicals produced in water. This method relies on the PL signal at 425 nm of the hydroxylation of terephthalic acid with •OH generated at the water/REM interface with DC. Experimental procedures are as follows:[374] The REM with its stainless steel cathode is inserted into a 500 mL of the 5×10^{-4} M terephthalic acid aqueous solution with a concentration of 2×10^{-3} M NaOH in a glass beaker. Connect with DC (5V) for 60 min. PL spectra of the generated 2-hydroxyterephthalic acid are measured on a Hitachi fluorescence spectrophotometer. After DC connection every 10min, the reaction solution was filtrated to measure the increase in the PL intensity at 425 nm excited by 315 nm light.

Thermo Scientific™ Pierce™ Quantitative Peroxide Assay Kits were used to detect and measure hydrogen peroxide levels (H_2O_2) in samples using an iron (Fe) and xylenol orange (XO) reagent for microplates or tubes. The working reagent (WR) was

prepared by mixing Fe reagent and XO reagent at the ratio of 1:100 (v/v). Before measuring hydrogen peroxide levels, a calibration curve is required for Quantitative Peroxide Assay Kits. 30% (8.8 M) H_2O_2 stock solutions are serially diluted to achieve 10 standards in the range of 1-1000 μM. WR was added into these standards at the ratio of 1:10 (v/v). After 15-20 minutes incubation at room temperature, 700 μL of each sample was extracted and filled into plastic cuvette for UV-vis spectrum scan to find the peak of absorbance at 590 nm. Then, the wavelength of the peak was used as a fixed value for establishing the calibration curve.

The production of oxidants other than ROS and active chlorine, such as $S_2O_8^{2-}$, $C_2O_6^{2-}$, and $P_2O_8^{4-}$, was also investigated because the importance of these oxidants in the chlorine-free disinfection process has been frequently reported.[375]

To detect the reaction of hydrogen with Nitric oxide (NO•), NO donor 1-hydroxy-2-oxo-3-(N-methyl-3-aminopropyl)-3-methyl-1-triazene (NOC7) (Dojindo Molecular Technologies, Inc. Japan) was dissolved in 0.1 M NaOH solution (Kanto Chemical Co., Inc. Japan) and was freshly prepared prior to each use. APF was added to the buffer with and without hydrogen NBs; 10–80 μM NOC7 was then added and the mixture was incubated for 30 minutes at 20 °C.

4.2.8 Degradation of 1,4-dioxane by REM under different electrode potentials

4.2.8.1 Analytical detection. The concentration of 1,4-dioxane was determined by gas chromatography (Trace 1300, Thermo Scientific, US) using an TG-624 capillary column (Thermo Scientific, 30 m length×0.25 mm ID×1.4 μm film) equipped with a flame ionization detector (FID) with auto sampler (Thermo Scientific, A11310, US) and

GC/MS system (Agilent 7890A/5975C, Santa Clara, CA, USA). An HP-5MS capillary column (30 m × 0.25 mm × 0.25 µm) was utilized for separation on GC/MS system. The liquid samples from the REM filtration tests were obtained and subjected to liquid/liquid extraction using methylene chloride (MC). The extraction procedure is shown in **Figure 4.5**.10 mL of water sample was placed in a 60 mL separatory funnel spiked with 20 µL surrogate (1,4-dioxane-d_8). 2 g of sodium chloride was added and dissolved in the water sample to improve the extraction efficiency.[376] Then, 20 mL of methylene chloride (MC) was added and shaken vigorously. A 2 µL of this organic phase was injected and analyzed by GC/MS.[376] Purge flow set as 5.0 mL; the inlet temperature of 200 °C; the flow rate was constant at 6.0 mL min^{-1} with He as the carrier gas; the oven temperature program started at 110 °C for 1 min, then ramped to 180 °C at 15 °C·min^{-1}, held for 4 min. The detector temperatures were maintained at 250 °C. 5 standard samples with different concentrations from 0.39 to 100 ppm were prepared and injected to GC/MS. The standard curve based on GC/MS readings was used for concentration calculation in the following experiments.

```
10 ml sample
        │ Add 2g NaCl, 20 μL surrogate
        │        and 20 mL MC
        ▼
   Extraction ──────────────────────▶ Aqueous layer
        │                                  │
        │                                  ▼
   Organic layer                       Discard
        │ Add 2g NaCl and 10 ml sample
        ▼
   Extraction ──────────────────────▶ Aqueous layer
        │                                  │
        │                                  ▼
   Organic layer                       Discard
        │ Concentrate to 1ml
        ▼
     GC/MS
```
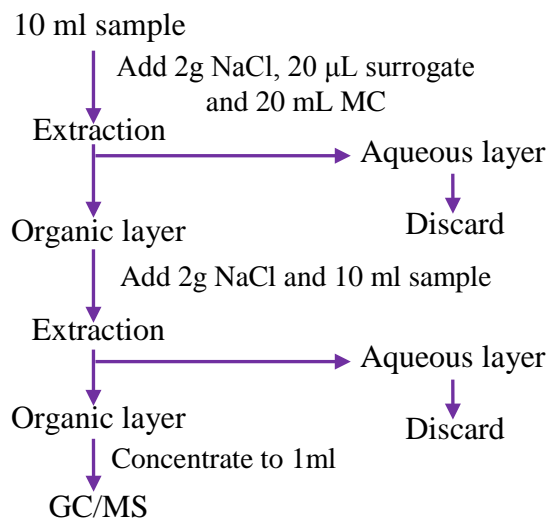
Figure 4.5 Sample preparation procedure of 1,4-dioxane by liquid–liquid extraction.

4.2.8.2 Batch reaction

(a) The effect of current density.

The concentration of 1,4-dioxane in DI water was 60 ppm. The batch reaction was operated in a 500-ml beaker as described in Section 4.2.1. The REM was operated at 3 levels of electrode potentials (approximately 1.3 V-5 V) using a DC power supply (Proteck P6035, Tempe, AZ) corresponding to the current density between 1.17-9.34 mA·cm^{-2} and for different times (10–40 min).

Theoretically, to completely degrade 50 ppm dioxane in 500 ml solution under 23 mA current, a reaction time of 20 min is required, which is computed as follows: First, according to the half-reaction of 1,4-dioxane degradation in Equation 4.10, each 1,4-dioxane molecule provides 20 electrons. The molecular weight of 1,4-dioxane is 88.11 g·mol^{-1}. If the total volume of 1,4-dioxane was 500 ml, the total electrons that can be transferred to REM can be calculated:

$$\frac{1}{20}C_4H_8O_2+\frac{3}{10}H_2O=\frac{1}{5}CO_2+H^++e^- \qquad (4.10)$$
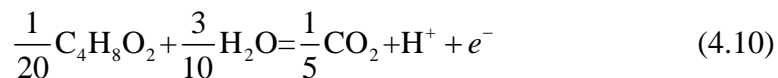
$$\frac{500\ \text{ml}\times 50\ \text{mg}\cdot\text{L}^{-1}}{88.11\ \text{g}\cdot\text{mol}^{-1}}=2.837\times 10^{-4}\text{mol}$$

Given that one electron has 1.6×10^{-19} C of charge and the Avogadro constant is 6.02×10^{23} mol^{-1}, the total transferrable amount of charges could be calculated as following:

$$2.837\times 10^{-4}\ \text{mol}\times 6.02\times 10^{23}\ \text{mol}^{-1}\times 1.6\times 10^{-19}\ \text{C}=27.326\ \text{C}$$

The reaction time (t) is equal to 20 min (=Q/I), where Q is the total charge (27.326 C) and I is the DC current (23 mA).

(b) The COD changes.

To measure the COD changes under batch reactions with REM, 500 ppm 1,4-dioxane was present in the reaction solution, which was treated under three current densities from 5 – 15 mA·cm^{-2}. COD was calorimetrically tested according to the USEPA Reactor Digestion Method 8000 (DOC316.53.01099)[377] using a Hach COD kit (HR+) on a UV-vis spectrophotometer (model Evolution 201, Thermo Scientific).[378] Briefly, liquid sample was added in to Hach COD vials and heated to 150 $^{\circ}$C for 2 hours in Hach COD reactor (16000 series). After cooling down, the absorbance of the samples in the vials were tested on the UV-vis spectrophotometer at 620 nm. Sample's COD levels could be calculated from a standard curve using samples with known COD values.

4.2.8.3 Continuous dead-end filtration.   Filtration unit was prepared following the design in Chapter 3, as illustrated in Figure 3.8. The 1,4-dioxane solution was filtered through the surface of the REM under a constant pressure of 10psi using an adjustable

check valve and a a booster pump (aquatic® CDP8800) in dead-end filtration mode. The resulting permeate flux was approximately 0.213 $m^3 \cdot m^{-2} \cdot h^{-1}$. Every 10 minutes the permeate solution was collected and stored in a cleaned container, which was sent to GC/MS for analysis. Three initial concentrations of 1,4-dioxane were chosen (500 ppb, 250 ppb, and 125 ppb). The filtration was operated with a constant current density of 15 $mA \cdot cm^{-2}$ starting from 10 min.[256] The aqueous samples were taken every 10 minutes and analyzed by GC/MS.

4.2.6 Degradation studies with Dyes

4.2.6.1 Analytical detection. Two cationic dyes, Rhodamine B (RB) and Methylene Blue (MB), and one anionic dye, Orange II (OGII) were selected for the degradation studies. A UV/vis spectrophotometer (Thermo Scientific Evolution 201) was used for the determination of dye discolorization kinetics. All samples were analyzed by a UV-vis spectrometer and a TOC analyzer, along with the untreated dye solution and physically filtered solution (without DC) as control tests. The corresponding absorbance wavelength is at 550 nm for RB, 664 nm for MB and 486 nm for OGII.[379-380] Five different concentrations (10 ppm, 5 ppm, 2 ppm, 1 ppm, and 0.25 ppm) of each dye were used to build the calibration curves.

Fluorescence spectroscopy is a relatively low-cost and easily handled analysis, providing emission-excitation matrices (EEMs) that identify different fluorophores and helps analyze the species of organic matters and their degradation byproducts. EEMs of Rhodamine B samples with/without REM treatment were measured in a 1 cm quartz cuvette (4 mL volume) using a Hitachi FL4500 fluorescent spectrophotometer. EEMs

were measured for excitation wavelengths of λ_{ex} = 200-400 nm at 5 nm increments across an emission range of λ_{em} = 280-500 nm at 2 nm intervals.[381]. Excitation and emission slit widths were set to 5 nm, with a photomultiplier tube (PMT) voltage of 700 V.[381]

4.2.6.2 Batch reaction.   Similar to the 1,4-dioxane batch test, 500 ml dye solution with an initial concentration of 5 ppm for three kinds of dyes was prepared in the same REM filtration unit. 12.52 mA·cm^{-2} (250 mA) and 25.3 mA·cm^{-2} current density (500 mA) were used to examine the current density effect.

4.2.6.3 Continuous dead-end filtration

In continuous filtration tests, 25.3 mA·cm^{-2} current density (500 mA) was selected and inlet concentration of dyes was fixed at 5 ppm. TMP was maintained constant at 75 kPa. The resulting permeate flux was approximately 0.213 m^3·m^{-2}·h^{-1}. Filtration was lasted for one hour. Every 10 minutes filtered solution was collected and the collection container was cleaned for next sample.

4.2.6.4 Continuous dead-end filtration with extended reaction time

Besides the above regular dead-end filtration test, we also conducted a dead-end filtration with repeated filtration or treatment of the collected permeate solution. The intent was to analyze the degradation of dyes and their byproducts in a continuous dead-end filtration for an extended treatment time as opposed to that for the filtrate water to pass through the REM membrane once, which might be too short to achieve substantial degradation of dyes. To evaluate the degradation kinetics in in this continuous dead-end filtration with

external circulation of the collected permeate, we first defined and calculated the treatment time, which is related to the hydraulic retention time (HRT):

$$\text{HRT} = \frac{V_{membrane}}{Q}$$

where $V_{membrane}$ is the void volume in the REM membrane (2.827×10^{-6} m^3); and Q is the flow rate (6.99×10^{-6} m$^3 \cdot$min^{-1}). In this experiment, we prepared 500 ml of the Rhodamine B (RB) solution with an initial concentration of 20 ppm. Other conditions were the same as above mentioned in section 4.2.6.3. The 500-ml solution was first filtered and the concentration of Rhodamine B (RB) was measured in the permeated. Then, the treated 500 ml solution was filtered for the second round under the same condition to measure the further decline of the Rhodamine B (RB) concentration as well as the TOC level changes. The result of the dye concentration was plotted against the number of filtration times with each filtration cycle accounting for a reaction time of one HRT (0.4 min).

4.2.7 Degradation of geosmin and MIB

4.2.7.1 Analytical detection

For sample extraction, purification and concentration, a liquid-liquid extraction method was adopted.[382] Briefly, 50 mL of the water sample and 5 g of sodium chloride were placed in a 50-mL extraction glass flask. The sample was mixed thoroughly and then filled with 1 mL n-Hexane, followed by mechanical shaking for 60 min. 0.5 mL of sample in hexane was taken out after extraction and 1 µL of extracted sample solution was injected into the GC–MS system (Agilent 7890A/5975C, Santa Clara, CA, USA) to measure the concentrations of 2-MIB and geosmin.[383] An HP-5MS capillary column (30 m × 0.25 mm × 0.25 µm) was utilized for separation. The GC operating conditions

were as follows: the temperature of the injector was 270 °C; the carrier gas was helium at a flow of 1 mL min^{-1}; the oven was programmed to start at 60 °C with a 4 min hold, and then the temperature was increased at a rate of 10 °C min^{-1} to 200 °C, followed by 20 °C min^{-1} to 280 °C. The electron impact (EI)-MS conditions were as follows: ion source temperature of 230 °C; MS transfer line temperature of 280 °C; solvent delay time of 5 min; ionizing voltage of 70 eV; a splitless mode was selected due to the low amount of analytes. Selected ion monitoring (SIM) mode for 2-MIB and geosmin were selected to monitor specific ions: m/z = 112 (GSM), m/z = 95 (2-MIB). The ions monitored in SIM were m/z 111, 112, 125 amu for geosmin, 95, 107, 108 for 2-MIB, respectively. The full scan mass spectra were obtained at an m/z range of 50–350 amu to analyze all potential degradation byproducts.[382]

The molecular weight of GSM is 182.3 g·mol^{-1}. If the total volume of GSM was 500 ml, the total electrons that can be transferred to REM can be calculated:

$$\frac{1}{68}C_{12}H_{22}O + \frac{23}{68}H_2O = \frac{3}{17}CO_2 + H^+ + e^-$$
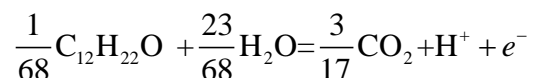
$$\frac{500 \text{ ml} \times 50 \text{ μg·L}^{-1}}{182.3 \text{ g·mol}^{-1}} = 9.3 \times 10^{-6} \text{mol}$$

Given that one electron has 1.6×10^{-19} C of charge and the Avogadro constant is 6.02×10^{23} mol^{-1}, the total transferrable amount of charges could be calculated as following:

$$9.3 \times 10^{-6} \text{mol} \times 6.02 \times 10^{23} \text{mol}^{-1} \times 1.6 \times 10^{-19} \text{C} = 0.89 \text{ C}$$

4.2.7.2 The degradation performance in continuous dead-end filtration

The geosmin and MIB solutions at an initial concentration of 200 ppb were filtered through the surface of the REM under a vacuum pressure of 75 kPa and a resulting permeate flux of approximately 0.213 $m^3 \cdot m^{-2} \cdot h^{-1}$ using the same unit as shown in Figure 4.3. At the initial 5 min, no DC current was applied to examine the rejection of geosmin and MIB by physical filtration on REM. Then, a positive DC current at 25.3 $mA \cdot cm^{-2}$ run through REM beginning from 10 min. The permeate solution was collected and was sent to GC-MS to measure the residual concentrations of geosmin and MIB as well as the speciation of their degradation byproducts.

4.2.8 Cyclic voltammetry

To analyze electron transfer-initiated chemical reactions, cyclic voltammetry (CV) were carried out on a CHI 660 electrochemical workstation (CH Instrument, USA).[194] The traditional three-electrode system was the same setup as described in Chapter 3. All the measured electrochemical potentials were referenced to the Ag/AgCl electrode potential, which is assumed to be zero. The electrolyte solution was 10 mM $K_3Fe(CN)_6^{3-}$ (a redox mediator) in 0.5 M KCl as a supporting electrolyte.[195] The REM filter was cut to 5 cm in length, 1 cm in outer diameters and 0.5 cm in inner diameters to fit the container, and was immersed in the supporting electrolyte as shown Figure 3.4. The CV curves were obtained by sweeping voltages from -1.5 to 1.5 V versus Ag/AgCl at a scan rate of 0.5 $V \cdot s^{-1}$. Based on the acquired CV data, the electroactive surface area of the Ti_4O_7 REM can be estimated from the calculation of the double layer capacitance (C_{dl}):[190] (I_a - I_c)/2 = $C_{dl} \cdot v$, where I_a and I_c are the measured anodic and the cathodic plateau currents at a given potential, respectively, and v is the scan rate ($V \cdot s^{-1}$). The electroactive surface area

was determined by dividing the measured capacitance by 60 μF·cm^{-2}, a standard value for metal oxides.[190]

We measured CV in the presence of a few model water pollutants (i.e., 1,4-dioxane, Rhodamine B (RB) and Methylene Blue (MB), and Orange II (OGII), geosmin and MIB). These pollutants were spiked into the 0.5 M KCl solution at 20 ppm except at 200 ppt for geosmin and MIB. Control tests were conducted in 0.5 M KCl solution. Several cycles were run for each pollutant. These CV curves will help determine the proper levels of applied electrode potentials for explore the activity of the anode for the oxidation of different pollutants.

4.2.9 Bacterial inactivation and removal studies.

Chlorine is generally applied to disinfect water because it is readily available and effective.[253] To quantify the effect of *E. coli* concentration, 60 petri dishes with Luria broth-agar (LB Agar) layer were prepared for culturing. Efficiency of inactivation was tested by batch reaction and continuous filtration. The batch reaction test used the same instrument in Sub-Section 4.2.5.1, in which REM was submerged in 500 ml *E. coli* suspension with approximately 10^3 and 10^4 cfu·ml^{-1} concentration under current density from 5.02 mA·cm^{-2} to 25.26 mA·cm^{-2} (current at 100 mA to 500 mA) for various time. A magnetic stirrer was put in the container to insure mixing.

The continuous filtration test used the same instrument in Sub-Section 4.2.5.2, where *E. coli* suspension (approximately 10^3 and 10^4 cfu·ml^{-1}) was forced flow through the REM pores by 75 kPa vacuum. REM was also charged with 5.02 mA·cm^{-2} to 25.26 mA·cm^{-2} density of current. The result was indicated by colony counting on LB-Agar petri dishes after spreading and 24 hours culturing.

4.2.10 Degradation of NOM

Several analytical techniques have been applied for the characterization of NOM and for monitoring the changes occurring during the application of different water treatment stages (Matilainen et al.2011).[384] Dissolved organic carbon (DOC) and absorbance at 254 nm (UV_{254}) are the most commonly controlled parameters, utilized for the optimization of respective treatment processes. The ratio of UV_{254} to DOC concentration (SUVA) is also used as a surrogate for NOM molecular weight, aromatic content, and hydrophobic/hydrophilic characterization. Fluorescence spectroscopy is a relatively low-cost and easily handled analysis, providing emission-excitation matrices (EEMs) that can constitute an identity of NOM origin and recognize the different fluorophores. EEMs coupled with multi-way data analysis (e.g., PARAFAC) can be also used to quantify different NOM fractions, such as humic-like and protein-like (Fellman et al. 2010, Stedmon and Bro2008).[385-386] Size exclusion liquid chromatography combined with organic carbon detector (LC-OCD) is possibly the most sensitive and reliable technique for the detailed NOM characterization. LC-OCD fractionates NOM, based on molecular weight, into five separate groups: biopolymers, humic substances, building blocks, low molecular weight humic substances and acids, and low molecular weight neutrals (Huber et al. 2011).[317, 387]

4.2.11 Bacteriophage removal studies

Bacteriophage male specific type 2 (MS2) (ATCC 15597-B1) and its host bacterium *Escherichia coli* (*E. coli*) cells (ATCC 15597) were obtained from the American Type Culture Collection (ATCC, Rockville, MD). *E. coli* cells in log phase of growth in tryptic soy broth solution were collected as the host cells. MS2 were grown in *E. coli*

suspensions and purified by sequential centrifugation and filtration with minor modifications (Li et al., 2008).[388] Briefly, after cell lysis and virus release, debris was removed via microfiltration through 0.2-mm and 0.05-mm low-protein-binding polycarbonate track-etched membranes (Whatman Nucleopore, USA). Virus was concentrated on a 100-kDa membrane (Koch Membranes, USA) in a Millipore ultra-microfiltration unit (Whatman Nucleopore, USA). The virus accumulated on the membrane surface was washed extensively with sterilized 1 mM NaCl solution to remove nutrients and organic matters. The final MS2 stock was stored in 1-mM phosphate buffered saline solution (PBS, pH 7.3) at 4 °C. MS2 was enumerated by the double agar layer procedure USEPA Method 1602. Briefly, concentrated MS2 were sequentially diluted with the same PBS and cultivated with *E. coli* cells at 37 °C for 16 h. Plates with between 20 and 200 plaques were used for calculating the concentration of MS2. The average MS2 concentration in the stock suspension was 1.5×10^8 PFU·mL^{-1}.

4.3 Results and Discussion

4.3.1 Voltage decline and influencing factors

Figure 4.6a shows the voltage decline on the REM with 10 cm in length when immersed in tap water with a cell potential of 20 V DC power applied. Resistivity of tap water and the wetted Ti_4O_7 REM were 290 Ω·m and 0.24 Ω·m respectively as measured by a PASCO conductivity probe. According to Equation 4.1 to Equation 4.5, when applying the following conditions (20 V DC power was applied to the top of REM; the radius of the stainless steel rod (r_0) was 0.15 cm, the outer and inner radius of REM (r_1=0.5 cm and r_2=0.3 cm), the voltage may decline from 20 V to 19.5 V from the top to the bottom part

of the REM filter as shown in blue solid line in Figure 4.6a due to the electrical resistance of REM. The experimental data points in Figure 4.6a showed a similar extent of voltage drop along the length distance with the prediction from the model calculation.

Other configurations were also calculated by the Matlab code to observe the influences of different factors. Figure 4.6b-4.6d shows the calculated voltage decline when varying the REM's outer or inner diameters and the diameter of stainless-steel rod (r_0). The result shows the increasing r_0 from 0.05 to 0.2 cm, although not significant, can increase the voltage drop. The reason of this phenomenon is due to the resistance increasing of liquid between membrane and cathode according to Equation 4.1. As the inner radius of membrane (r_2) was fixed, the cross-sectional area of liquid was decreased with the increasing r_0, which caused the increasing resistance according to Pouillet's law. Since resistivity of simulated liquid was far higher than cathode, resistance decrease of cathode was ignorable compare to resistance increasing of liquid, which could explain Figure 4.6b.

Decreasing the REM's outer diameter (r_1) from 0.8 to 0.4 cm caused a greater extent of voltage decline because of the decreasing resistance of REM according to Pouillet's law. For the same reason, increasing the REM's inner diameter from 0.2 to 0.4 cm slighted increased the voltage decline. Figure 4.6e shows under different input cell potentials, the voltage decline was similar and does not significantly depend on the applied voltage.

Figure 4.6f and Figure 4.6g shows the dependence of voltage decline on ρ_W and ρ_M. Obviously, increasing the liquid medium's resistivity can lead to substantial voltage drop due to the increasing electrical resistance from liquid. Likewise, increasing the

REM's resistivity also significantly reduce voltage along the length of REM due to the increasing energy loss by the internal resistance of REM. These results as well as the mathematical model calculations provide new potential insight into the rational design of REM filtration unit of different scales or configurations of electrodes/electrolyte.
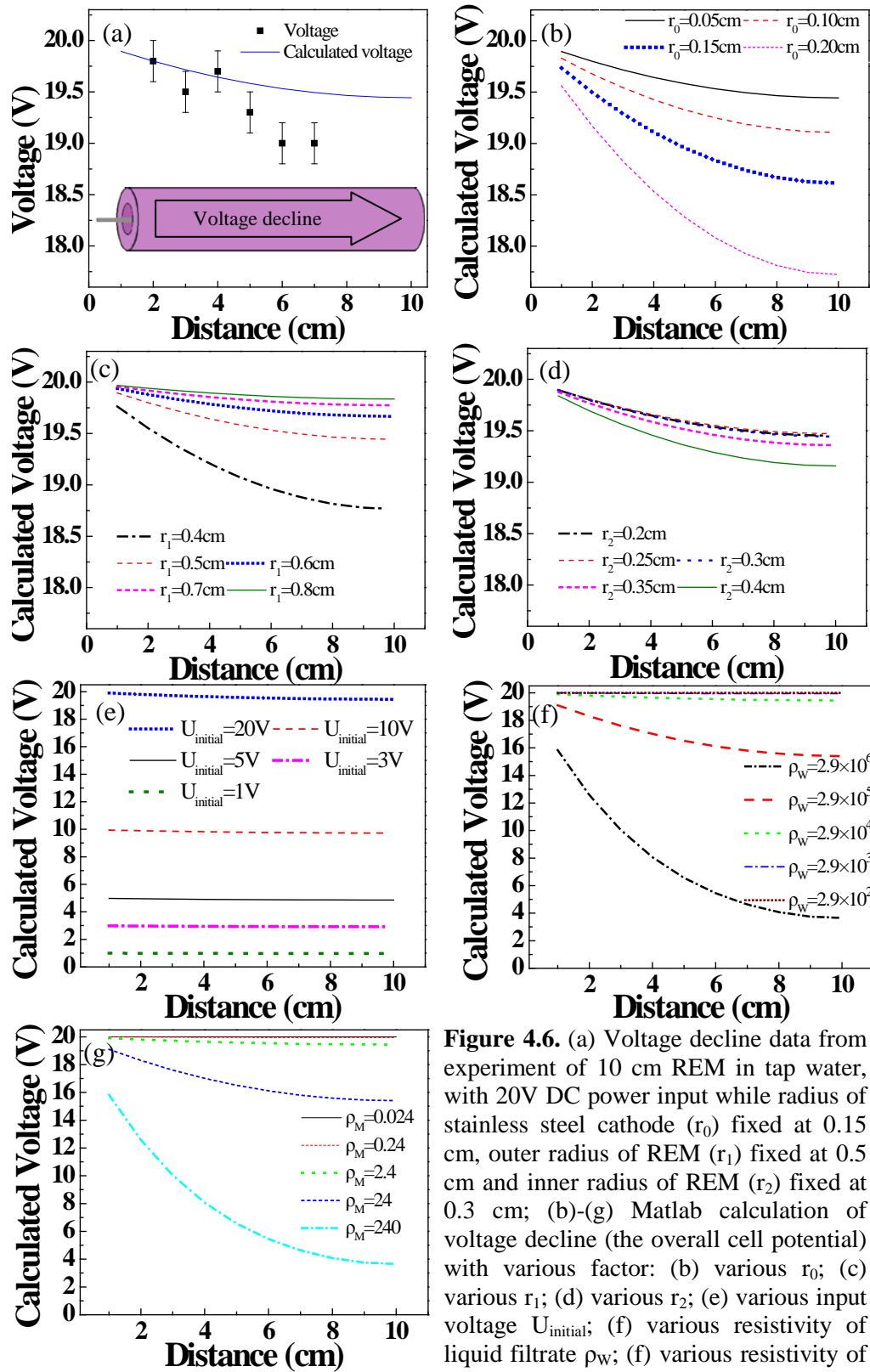
Figure 4.6. (a) Voltage decline data from experiment of 10 cm REM in tap water, with 20V DC power input while radius of stainless steel cathode (r_0) fixed at 0.15 cm, outer radius of REM (r_1) fixed at 0.5 cm and inner radius of REM (r_2) fixed at 0.3 cm; (b)-(g) Matlab calculation of voltage decline (the overall cell potential) with various factor: (b) various r_0; (c) various r_1; (d) various r_2; (e) various input voltage $U_{initial}$; (f) various resistivity of liquid filtrate ρ_W; (f) various resistivity of REM ρ_M.

4.3.2 All potential radicals and non-radicals and their redox potentials/free energies.

Table 4.7 shows the redox potentials of all possible radicals and non-radicals at standard conditions. The redox potentials at pH 7 were calculated by the Nernst equation in Equation 4.9.

Table 4.7a Half-reactions and redox potentials of different radicals at pH 0 and pH 7

Radical species half-reaction	E_H^0 (pH 0)	ΔG/n (kJ·mol^{-1})	E_H^0 (pH 7)
$^3O_2 + e^- \rightleftharpoons O_2^-\cdot$	-0.16	+15.42	0.83
$^3O_2 + H^+ + e^- \rightleftharpoons HO_2\cdot$	+0.12	-11.57	-0.293
$^1O_2 + e^- \rightleftharpoons O_2^-\cdot$	+0.83	-80.01	0.83
$O_2^+ + e^- \rightleftharpoons O_2$	+3.20	-308.45	3.2
$\cdot OH + e^- \rightleftharpoons {}^-OH$	+1.90	-183.14	-0.224
$\cdot OH + H^+ + e^- \rightleftharpoons H_2O$	+2.72	-262.19	2.307
$O^-\cdot + H^+ + e^- \rightleftharpoons HO^-$	+1.77	-170.61	1.357
$HO_2 + e^- \rightleftharpoons HO_2^-$	+0.75	-72.29	0.75
$HO_2 + H^+ + e^- \rightleftharpoons H_2O_2$	+1.50	-144.59	1.087
$H_2O_2 + 2H^+ + 2e^- \rightleftharpoons 2H_2O$	+1.77	-170.61	1.357
$H_2O_2 + e^- \rightleftharpoons \cdot OH + H_2O$	+0.72	-69.40	0.72
$O_3 + 2H^+ + 2e^- \rightleftharpoons O_2 + H_2O$	+2.08	-200.50	1.667
$O_3 + e^- \rightleftharpoons O_3^-\cdot$	+1.00	-96.39	1
$O_3 + H^+ + e^- \rightleftharpoons O_2 + \cdot OH$	+1.34	-129.17	0.927
$SO_4^-\cdot + e^- \rightleftharpoons SO_4^{2-}$	+2.437	-235.13	2.437

Table 4.7b Half-reactions and redox potentials/free energies of non-radical species

Non-radical species half-reaction	E_H (pH 0)	$\Delta G/n$ (kJ·mol^{-1})	E_H (pH 7)
$O_2 + 4H^+ + 4e^- \rightleftharpoons 2H_2O$	+1.23	-118.56	0.817
$O_2 + 2H^+ + 2e^- \rightleftharpoons H_2O_2$	+0.70	-67.47	0.287
$O_3 + 2H^+ + 2e^- \rightleftharpoons O_2 + H_2O$	+2.076	-200.30	1.663
$ClO^- + H_2O + 2e^- \rightleftharpoons Cl^- + 2OH^-$	+0.841	-81.14	0.427
$HClO + H^+ + 2e^- \rightleftharpoons Cl^- + H_2O$	+1.482	-142.99	1.069
$ClO_2(aq) + e^- \rightleftharpoons ClO_2^-$	+0.954	-92.05	0.954
$ClO_4^- + 8H^+ + 8e^- \rightleftharpoons Cl^- + 4H_2O$	+1.389	-134.02	0.976
$Cl_2(g) + 2e^- \rightleftharpoons 2Cl^-$	+1.358	-131.03	1.358
$MnO_4 + 4H^+ + 3e^- \rightleftharpoons MnO_2 + 2H_2O$	+1.679	-162.00	1.128
$MnO_4 + 8H^+ + 5e^- \rightleftharpoons Mn^{2+} + 4H_2O$	+1.507	-145.40	0.8462
$FeO_4^{2-} + 8H^+ + 3e^- \rightleftharpoons Fe^{3+} + 4H_2O$	+2.20	-212.27	1.099
$SO_4^{2-} + 4H^+ + 2e^- \rightleftharpoons SO_2(aq) + 2H_2O$	+0.17	-16.40	-0.656

4.3.3 Electrode potential measurement in relevant aqueous environment.

Table 4.8 shows the measured electrode potential. The MBBM conductiviy was 27000 ± 280 μS·cm$^-$1. Calculated solution resistivity was 3.7×10^{-11} Ω·cm. Since the distance between anode and reference electrode was 1mm, the resistance between them was the 3.7×10^{-12} Ω. The voltage output of the DC generator was selected between 0.5 V to 29 V. The corresponding current density was 0.00616 mA·cm^{-2} to 25.263 mA·cm^{-2}. The calculated electrode potential for both anode and cathode was from 0.303 V to around 29 V. However, the voltage measure from reference electrode shown that the potential dropped dramatically on the anode when the output voltage raised, while stay almost the same on the cathode (Figure 4.7). By comparing Figure 4.7 to Table 4.7, it can be concluded that if cell voltage was maintained above 5V, all half reactions in Table 4.7 could proceed and generate ROS.

Table 4.8a Electrode potentials for REM anode under different current densities.

Step	Operation and measurement items	Data							
1	Distance between reference electrode and anode (mm)	1 ± 0.1							
2	Solution conductivity ($\mu S \cdot cm^{-1}$)	27000 ± 280							
3	Solution resistivity ($\Omega \cdot cm$)	3.7×10^{-11}							
4	The resistance between anode and reference electrode (Ω)	3.7×10^{-12}							
5	Current flow between anode and reference electrode (mA)	0.0123	0.33	8	100	200	300	400	500
6	Current density ($mA \cdot cm^{-2}$)	0.00616	0.016	0.4	5.053	10.105	15.158	20.210	25.263
7	Voltage loss in resistance, U_r, (V)	4.551×10^{-16}	1.221×10^{-14}	2.96×10^{-13}	3.7×10^{-12}	7.4×10^{-12}	1.11×10^{-11}	1.48×10^{-11}	1.85×10^{-11}
8	Cell voltage, U_c, between anode and cathode (V)	0.5	2	5	10	14	20.4	25	29
9	Insert reference electrode near anode at the distance as shown above. Measure the potential between anode and reference electrode, (V)	0.4 ±0.05	1.54 ±0.06	4.2 ±0.1	7.2 ±0.1	8.45 ±0.15	11.5 ±0.3	12.3 ±0.2	13.5 ±0.1
10	Electrode potential for anode, U_a (V)	0.303	1.803	4.803	9.803	13.803	20.203	24.803	28.803

Table 4.8b Electrode potential for the stainless steel cathode.

Step	Operation and measurement items	Data							
1	Distance between reference electrode and cathode (mm)	1 ± 0.1							
2	Solution conductivity ($\mu S \cdot cm^{-1}$)	27000 ± 280							
3	Solution resistivity ($\Omega \cdot cm$)	3.7×10^{-11}							
4	The resistance between anode and reference electrode (Ω)	3.7×10^{-12}							
5	Current flow between anode and reference electrode (mA)	0.0123	0.33	8	100	200	300	400	500
6	Current density (mA·cm^{-2})	0.00616	0.016	0.4	5.053	10.105	15.158	20.210	25.263
7	Voltage loss in resistance, U_r, (V)	4.551×10^{-16}	1.221×10^{-14}	2.96×10^{-13}	3.7×10^{-12}	7.4×10^{-12}	1.11×10^{-11}	1.48×10^{-11}	1.85×10^{-11}
8	Cell voltage, U_c, between anode and cathode (V)	0.5	2	5	10	16.5	21	26	29.5
9	Insert reference electrode near cathode at the distance as shown above. Measure the potential between cathode and reference electrode, (V)	0.425 ±0.1	1.75 ±0.2	4.5 ±0.2	9.2 ±0.1	15.4 ±0.15	18.89 ±0.24	24.74 ±0.32	28.28 ±0.14
10	Electrode potential for anode, U_a	0.303	1.803	4.803	9.803	16.303	20.803	25.803	29.303
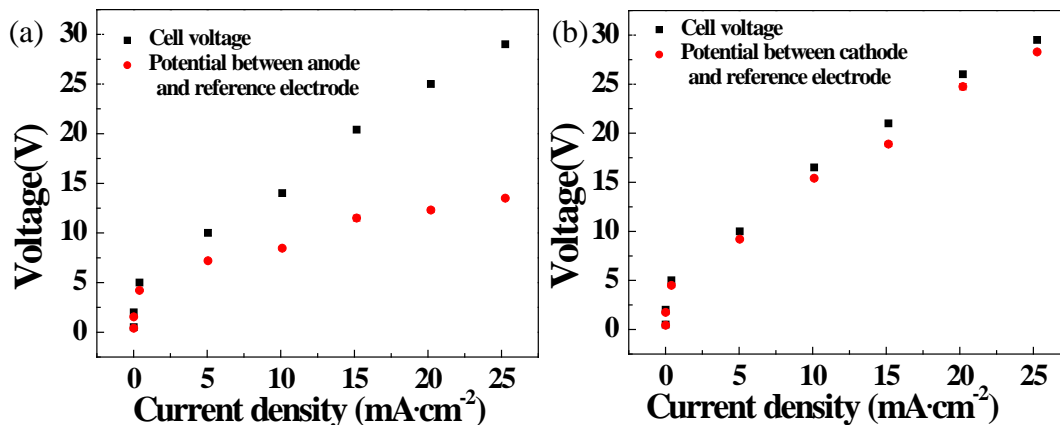
Figure 4.7. Electrode potentials for REM anode (a) **and** stainless steel cathode (b) in MBBM medium. Black dots are the applied cell voltage (U_c) and red dots are the electrode potential (U_{rf}).

4.3.4 Assessment of the ROS.

4.3.4.1 Measurement of hydroxyl radical

Calibration curve/LOD , according to the following Equation 4.11:

$$\text{LOD} = \frac{S_b \times k}{m} \tag{4.11}$$

where k is a factor with the value of 3, S_b is the standard deviation of the blank and m is

the slope of the calibration graph in the linear range.
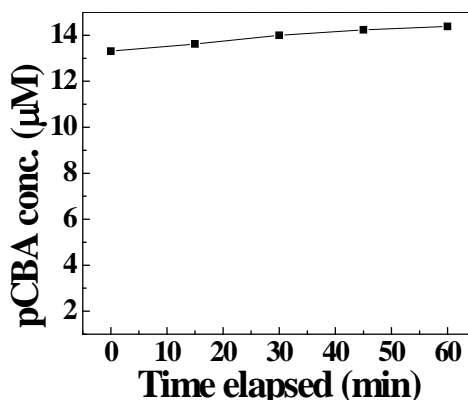
Figure 4.8 The pCBA concentration changes over the treatment time on REM under a current density of 25.3 mA·cm^{-2} in algal medium.

4.3.4.2 Measurement of H_2O_2

Figure 4.9a shows the characteristic absorbance of the solution where H_2O_2 reacted with an iron (Fe) and xylenol orange (XO) reagent at 590 nm, which indicates the presence of H_2O_2. Figure 4.9b is a calibration curve with different concentrations of H_2O_2 spiked in the solution to react with the reagent. Before 300 µM of H_2O_2, the curve is linear and after that leave, the curve levels off and declines at high H_2O_2 concentrations, which may resulted from the rapid self-decay of H_2O_2. The LOD for the linear range is determined to be 4.413±1.07 µM.
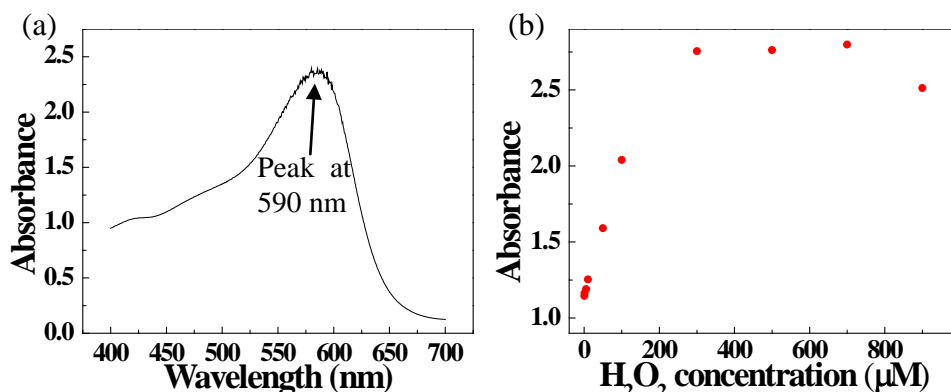
Figure 4.9 (a) Spectral and peak position of H_2O_2. (b) The calibration curve for the H_2O_2 concentration versus absorption.

Figure 4.10 shows the H_2O_2 production in REM unit under anodic polarization when two different current densities were applied to REM. At a high current density (25.26 mA·cm^{-2}), up to 55 µM of H_2O_2 was produced, whereas the H_2O_2 production reached only 10 µM at 5.02 mA·cm^{-2}. Clearly, higher current densities lead to greater electrode potentials, which promotes the formation of more powerful radicals such as •OH and catalyze the production of H_2O_2. As comparison, a modified graphite electrode could produce 26.27 mM H_2O_2 under 5.02 mA·cm^{-2} in an electro-Fenton reaction.[389]
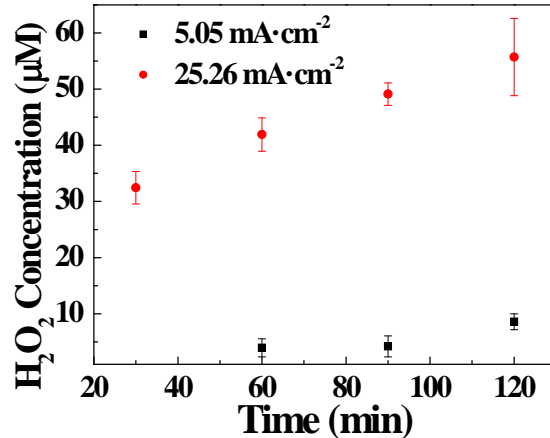
Figure 4.10 Concentrations of the produced H_2O_2 over time when the REM was subjected to DC currents of 5.02 mA·cm^{-2} and 25.26 mA·cm^{-2}.

4.3.5 Detection of the chlorine species generation electrochemical processes.

Figure 4.11 compares the total chlorine concentrations versus reaction time under two different current densities. Applying the lower current density of 5.02 mA·cm^{-2}, the total chlorine production was 0.35 mg·L^{-1} in two hours. This result indicates that it is possible to promote oxidation of small amounts of chlorine species even at low current densities. As expected, at a higher current density of 25.26 mA·cm^{-2}, the total chlorine production was 1.5 mg·L^{-1} in two hours.[390] This result is comparable with boron-doped diamond (BDD), which was reported has 0.25 to 0.33 mg·L^{-1} with 167 mA·cm^{-2} by one hour electrochemical reaction in synthetic conductive waters.[391]
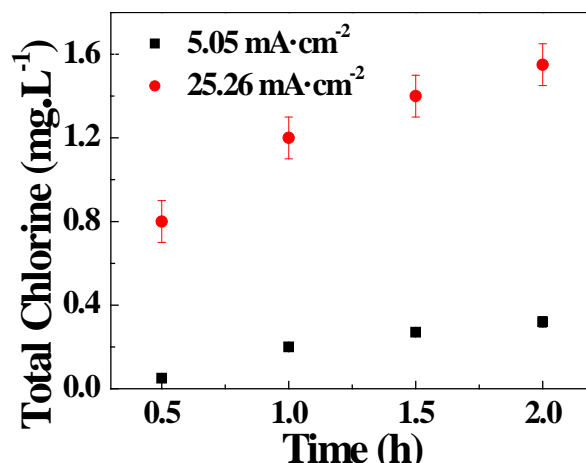
Figure 4.11 The total chlorine concentrations versus reaction time in MBBM medium solution under 5.02 mA·cm^{-2} and 25.26 mA·cm^{-2} density.

4.3.6 Assessment of 1, 4-dioxane degradation

4.3.6.1 Calibration curve of 1,4-dioxane. Figure 4.12 shows the standard curve of 1,4-dioxane detected by GC-FID with the fitting equation shown in the graph. The fitting result in an correlation coefficient (R^2) of 0.997, indicating that the calibration equation could account for 99.7% of the errors. The LOD of 1,4-dioxane by GC-FID is calculated from the date in the linear range of the calibration plot, according to the following Equation 4.11:

$$LOD = \frac{S_b \times k}{m} \tag{4.11}$$

k is a factor with the value of 3, S_b is the standard deviation of the blank and m is the slope of the calibration graph in the linear range. The LOD in this experiment was 988.7 ppb.
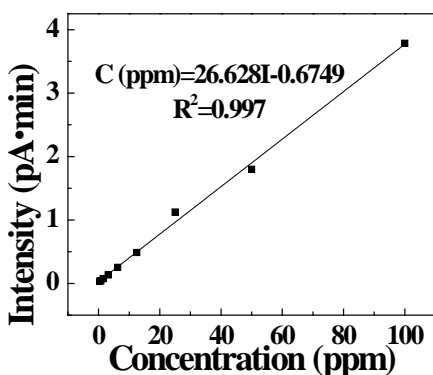
Figure 4.12 Calibration curve of 1, 4-dioxane.

4.3.6.2 Batch degradation test. Figure 4.13a shows the degradation of 1,4-dioxane by anodic oxidation under different current densities almost followed a zero order of kinetics as indicated by the linear concentration decline.[392] Linear regression coefficients (R^2) were 0.93 - 0.95 for the three fitting equations. The corresponding electrode potentials were 1.3 V-5 V (1.17 to 9.34 mA·cm^{-2} current density), which means that electrode potential from 1.3 V became effective to degrade 1,4-dioxane with REM anode.

Figure 4.13b shows the 1,4-dioxane concentration decrease with three different initial concentration (50 ppm, 25 ppm, and 12.5 ppm) under a fixed current density of 15 mA·cm^{-2}. The concentration remained unchanged during the first 10 min with no DC currents and began to decrease progressively for three conditions. Figure 4.13c compares the removal of 1,4-dioxane expressed as the COD reduction after 60 minutes of anodic reaction with current densities from 0 - 15 mA·cm^{-2}. The initial concentration of 1,4-dioxane was 500 ppm, which has a corresponding COD of approximately 1100 mg·L^{-1}.[393] At 15 mA·cm^{-2} current density the 1,4-dioxane concentration dropped to approximately 990 mg·L^{-1}.
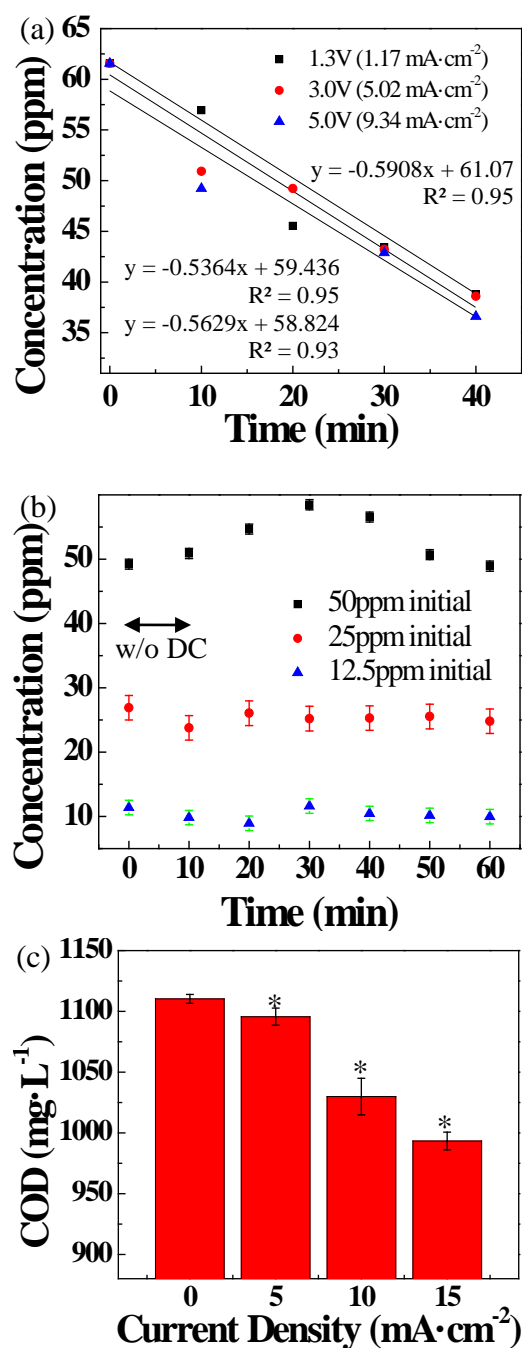
Figure 4.13 (a) The concentration decrease of 1,4-dioxane under different current densities over 40 min of batch reactions with an initial concentration of 60 ppm. (b) The 1,4-dioxane concentration decrease with different initial concentrations and a constant current density of 15 mA·cm^{-2} starting from 10 min. (c) COD decline in the 1,4-dioxane solution after 60 min of batch reactions under different current densities. * labels the results that are significantly different from the control group (no DC) according to the *t*-test (*p*<0.05).

4.3.6.3 Continuous dead-end filtration. Figure 4.14 shows C/C_0 value of 1,4-dioxane concentration after continuous dead-end filtration with current density from 0 to 15 mA·cm^{-2} with REM served as anode and cathode. The result indicated physical filtration without DC could remove 40% of 1,4-dioxane, which could also the result of REM structure absorption. When REM served as anode, as the current density increasing from 5 to 15 mA·cm^{-2}, appreciable decrease of 1,4-dioxane concentration up to 90% and there was no significant flux decline during the filtration process. Even though the idea of REM served as cathode with the same current density was to repel the 1,4-dioxane molecules in order to prevent fouling, the removal rate was low according to the result. As comparision, TiO$_2$ pellet was reported have 85.2% degarded rate with 7.0 mA·cm^{-2} current density on 1,4-dioxane when served as anode.[276]
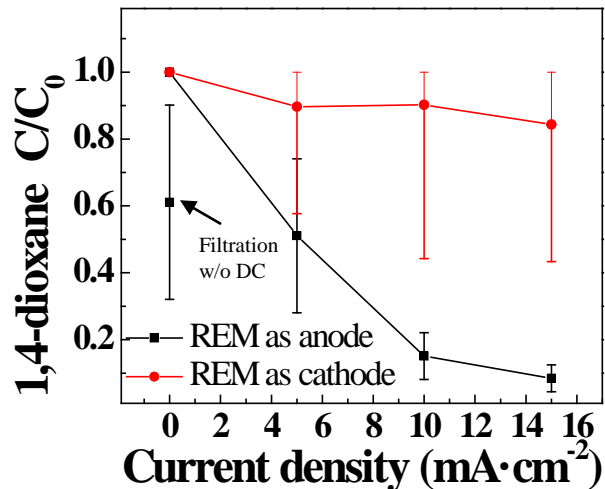
Figure 4.14 The stable 1,4-dioxane concentration (C) in the permeate under different current densities in continuous membrane filtration process. The results is expressed as the ratio of C/C_0, where C_0 is the initial 1,4-dioxane concentration (49.52 ppm). The TMP or influent flux was 75kPa.

A model was developed in 2018 by Lan et al to calculate limiting current density in Equation 4.12: [394]

$$J_{\text{lim}} = n \cdot F \cdot k_m \cdot C \qquad (4.12)$$

where J_{lim} is the limiting current density (A·m^{-2}), n is the number of exchanged electrons per molecular of pollutant degraded (e.g., 20 electrons of 1,4-dioxane), F is the Faraday constant (96,485.33 C·mol^{-1}), k_m is the average mass transfer coefficient (m·s^{-1}), and C is the pollutant concentration (mol·m^{-3}) that readily react on the electrode surface.[394] The average mass transfer coefficient (k_m) could be estimated with the results in Figure 4.12a and 4.13. For example, in the batch reaction, we estimated by:

$$k_m = \frac{J_{\text{lim}}}{n \cdot F \cdot \Delta C}$$

where ΔC is the changes of the concentration in the solution, which represents the mean 1,4-dioxane concentration that readily react on the electrode surface. Thus, k_m is estimated to be 9.14×10^{-6} m·s^{-1} (assuming $J_{lim}= 5$ A·m^{-2}) in batch reaction. Similarly, in continuous filtration, the estimated k_m is 5.43×10^{-6} m·s^{-1}. Clearly, in continuous filtration, the mass transfer coefficient is significantly higher than that in batch reaction, which confirms that integrating EAOPs into membrane filtration processes could lower mass transfer resistance and enhance surface reaction due to the flow pressure.

The experimental results have also been compared with instantaneous current efficiency (ICE). As a function of time during electrolysis, ICE is estimated by the following equation:

$$\text{ICE} = \frac{n \cdot F \cdot V}{I} \frac{\left[\text{COD}_t - \text{COD}_{t+\Delta t} \right]}{\Delta t}$$

where F is the Faraday constant 96,485.33 C·mol⁻¹, V is electrolyte volume (m³), I is applied current (A), Δt is time interval(s), COD is chemical oxygen demand (mol $O_2 \cdot m^{-3}$). n is mole electron transferred per mole pollutant degrade. The stoichiometric quantity of O_2 needed for combustion of 1 mol 1,4-dioxane is 5 mol. And 20 mole electron is transferred per mole 1,4-dioxane. So n = 4 in this case. Based the equation of ICE COD method, we modified it to:

$$ICE = \frac{n \cdot F \cdot V}{I} \frac{\left[C_t - C_{t+\Delta t}\right]}{\Delta t}$$

C is the pollutant concentration (mol·m⁻³), and n is mole electron transferred per mole pollutant degrade (20 mole electrons per mole for 1,4-dioxane)

Table 4.9 ICE calculation in batch reaction mode and continuous dead-end filtration mode

Mode	current density (mA·cm⁻²)	I (A)	ICE (%)
Batch reaction	1.17	0.023049	450.90
	5.02	0.098894	106.00
	9.34	0.183998	61.94
Continuous dead-end filtration	5	0.0985	62.74
	10	0.197	54.45
	15	0.2955	39.13

The result showed a decrease of ICE when current increases. However, Fig 4.12(a) and Figure 4.13, shows that processes operating at higher current density had much better degradation rate. This could be a consequence of secondary reaction (such as oxygen evolution) when the applied current density is higher than the limiting current density and electrolysis is under mass transport control.[256] Thus, it can be concluded that a compromise must be made to balance energy consumption with the time required to achieve the desired removal efficiency. The more amount of current supplied into the system is used up for oxidation of more 1,4-dioxane, showing faster degradation rate.

185

However, the system becomes to meet the limit of mass transport earlier due to the low concentration of 1,4-dioxane. Therefore, the process using higher current density can show faster degradation rate while the current efficiency decreases.[256]

4.3.6.4 Mechanism analysis. Initial concentration of 1,4-dioxane influences pH variation during the electrochemical reaction. Major reaction intermediates produced during oxidation of 1,4-dioxane by hydroxyl radicals are acidic species such as oxalic acid, glycolic acids, acetic acid.[256, 395] These reaction intermediates are finally degraded into carbon dioxide and water. Thus, if the rate that 1,4-dioxane is degraded into acidic intermediates is higher than that acidic intermediates are mineralized perfectly, it can be expected that pH decreases during the reaction due to a buildup of acidic intermediates, and then recovers its origin point after complete mineralization of acidic intermediates into carbon dioxides and water.[256] Also, the initial concentration affects initial limiting current density. When limiting current density is higher than the applied current density of the system, electrochemical reaction would begin from current control regime and the concentration of 1,4-dioxane decreased linearly with time as shown in Figure 4.12(b).[256] Otherwise, the reaction began from mass transport control regime with a non-linear decrease of 1,4-dioxane due to a secondary reaction (such as oxygen evolution).[256]

4.3.7 Assessment of MB, RB and OGII dye degradation

4.3.7.1 Calibration curves. Five different concentrations of each dye were prepared in DI water and scanned by a UV-vis spectrometer to determine the characteristics absorbance wavelength. Figure 4.15a-4.15c show the characteristic absorption peaks and the intensity shift for different dye concentrations, which agrees with other literature.[379-380] Figure 4.15-4.15d are the calibration curves with the fitting equations and R^2 shown in the graphs. The LOD values for MB, RB and OGII were determined to be 100ppb, 25ppb, and 20ppb respectively using the current detection method.
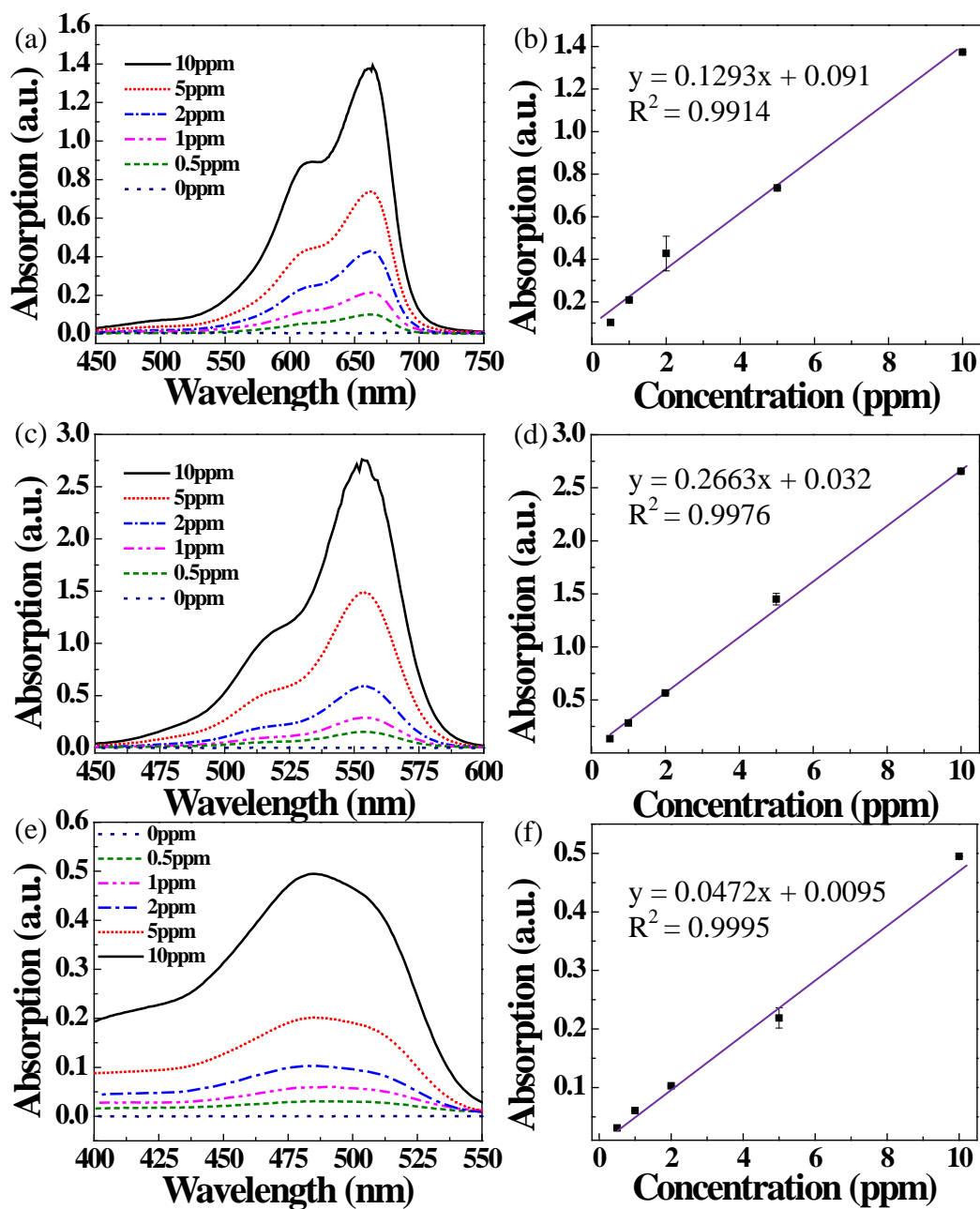
Figure 4.15 Absorption spectra of MB at 664 nm, RB (c) at 550 nm and OGII (e) at 486 nm. Calibration curves for MB (b), RB (d) and OGII (f).

4.3.7.2 Discoloration in batch reaction and continuous filtration modes

Figure 4.16a and 4.16b compare the visual color changes of MB and RB solutions after REM filtration with DC in batch reaction treatment, which shows that MB and RB solutions had a transition from dark to lighter color after batch reaction treatment. Figure

4.17c and Figure 4.17d show the visual color changes after continuous filtration of MB and RB. With physical filtration alone, the solutions turned to lighter color which was not obvious in visual. With DC filtration in one hour, all the samples turned clear. The dye solutions were then tested in a quartz cuvette by the UV-vis spectrophotometer. As shown in Figure 4.16a and 4.16b, in batch reaction, MB concentration was brought down from 5.12 ppm to 3.33 ppm in 60 minutes with 12.53 mA·cm^{-2} current density and from 5 ppm to 0.118 ppm in the same time with 25.3 mA·cm^{-2} current density. Similar to MB, the initial RB concentration was brought down from 5.049 ppm to 1.914 ppm with lower current density and from 5.339 ppm to 0.152 ppm with higher current density. With higher current density, REM showed more than 95% reduction in concentration for both dyes. Figure 4.18c to 4.18e show the removal of dyes in filtration. With physical filtration only, REM obtained 60% removal rate on MB and 50% on RB. Filtration with 25.3 mA·cm^{-2} current density DC could reach 100% removal for both dyes in 10 min dead-end filtration. As reference, it was reported activated carbon could gain 100% removal of RB with 120 min contact time.[379]

Figure 4.19 shows the TOC change of RB and MB solutions during continuous filtration. The initial concentrations of both dyes were 5ppm. Since the carbon mass is 70.14% in RB and 60.03% in MB. The initial TOC of concentrations RB and MB solutions were 3.5 and 3 ppm. There was no significant disappearance TOC on both RB and MB after filtration, which may indicated even though dye solutions were degraded during the electrochemical filtration, the products still contain organic compounds.
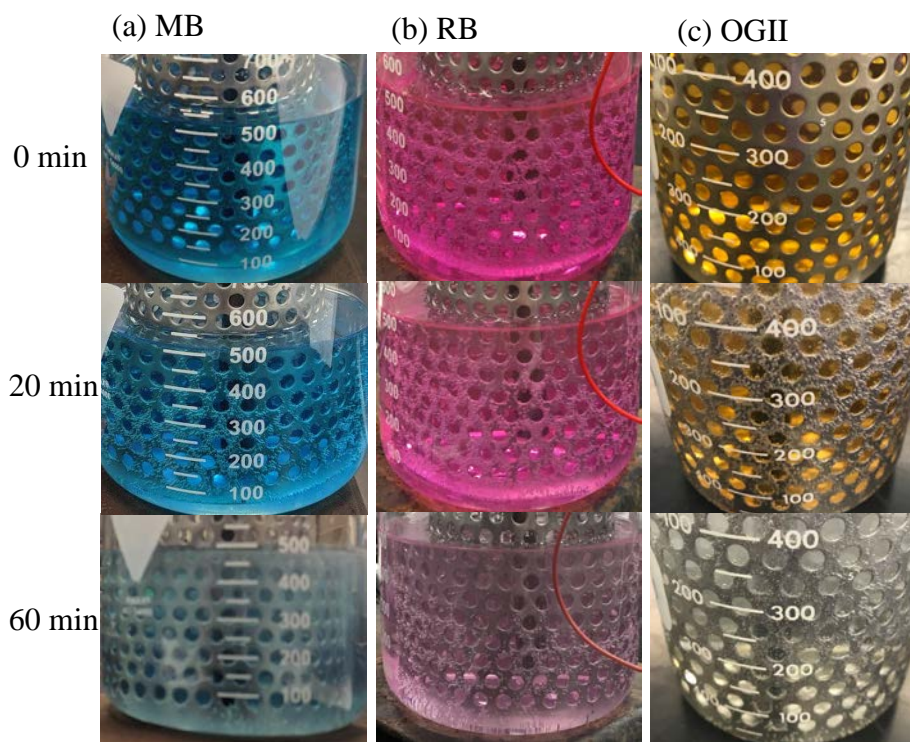
Figure 4.16 (a), (b) and (c) The visual color changes of MB, RB and OGII solutions under anodic oxidation of 25.3 mA·cm^{-2}.
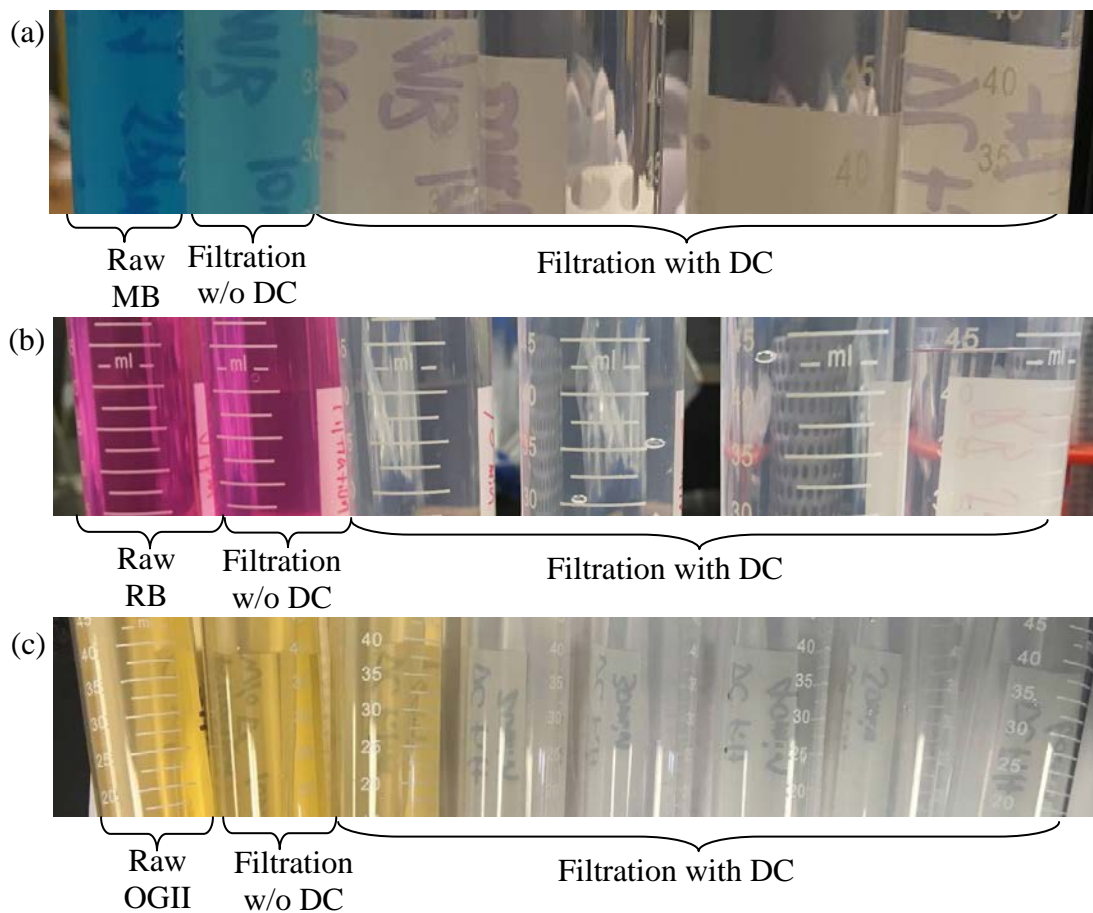
Figure 4.17 (a), (b) and (c) show color changes after continuous filtration (with and without DC currents of 25.3 mA·cm^{-2}) of the MB, RB and OGII solution. Sample time interval was 10 min. The video of filtration process could be accessed at https://youtu.be/K6iTSSV6rvI.
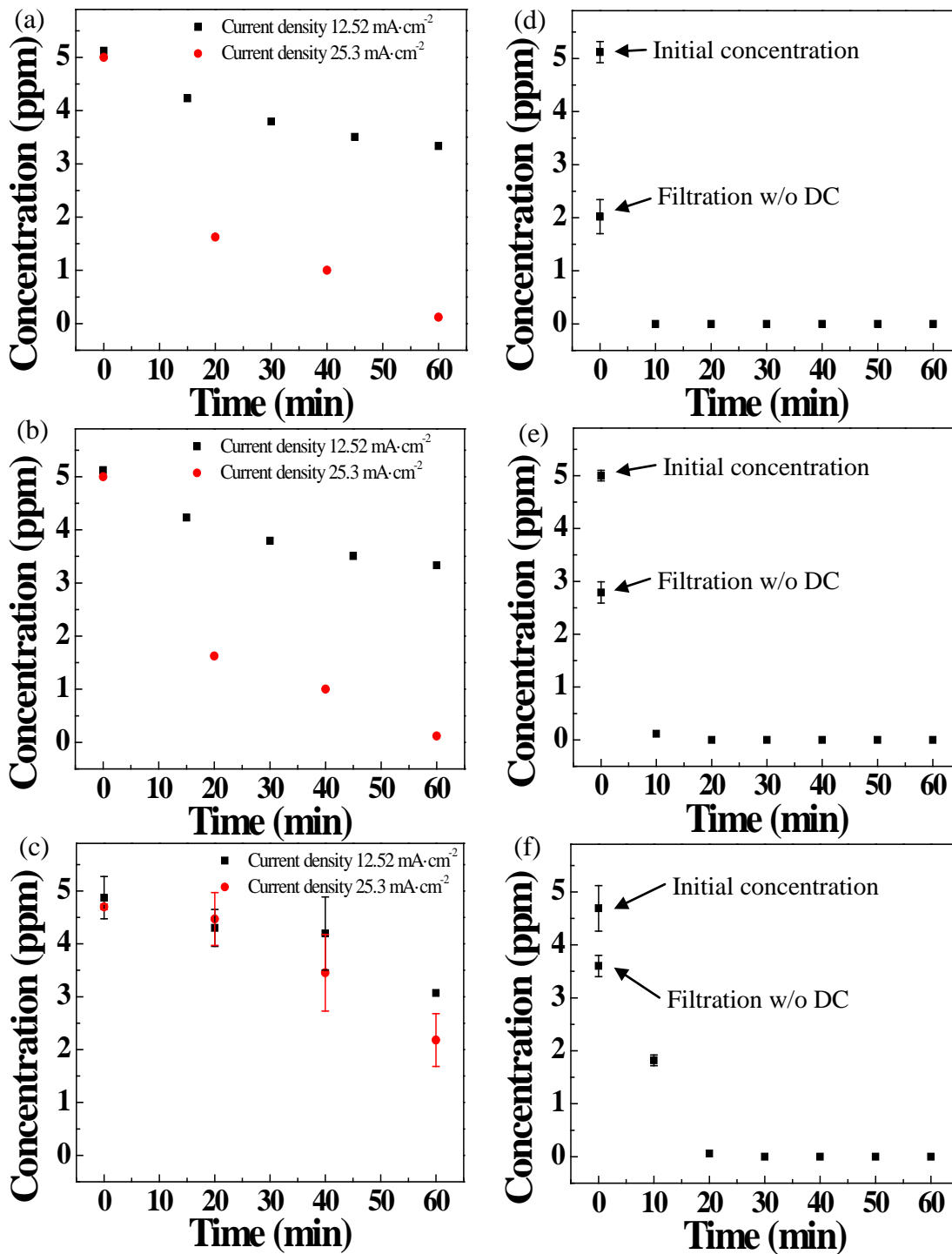
Figure 4.18. (a) - (c): The concentration changes of MB (a), RB (b) and OGII (c) in batch reaction mode under two different current densities; (d) – (f): the concentration changes of MB (d), RB (e) and OGII (f) in the permeate of dead-end filtration under the DC current density of 25.3 mA·cm^{-2}.
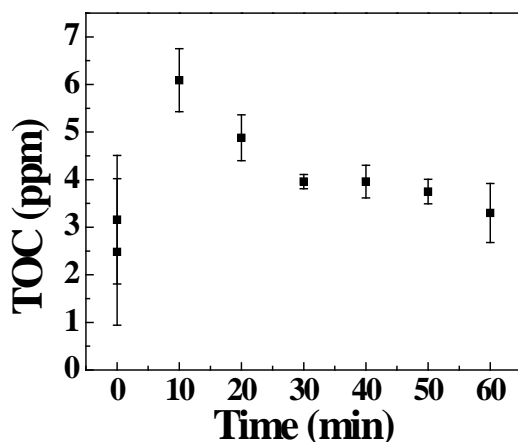
Figure 4.19 TOC change of dyes during continuous filtration.

4.3.8 Assessment of Geosmin and MIB degradation

4.3.8.1 Calibration curves and recovery rates of the extraction method

For 2-MIB and geosmin test, liquid samples were extracted and concentrated for 25 times. Standard solutions with different concentrations of 2-MIB and geosmin were used to obtain the calibration curves as shown in Figure 4.20. The tested extraction efficiency was 74.5% ± 5% for 2-MIB and 84.7% ± 4% for geosmin respectively. The LOD for 2-MIB and Geosmin were 52 ppt and 35 ppt respectively.
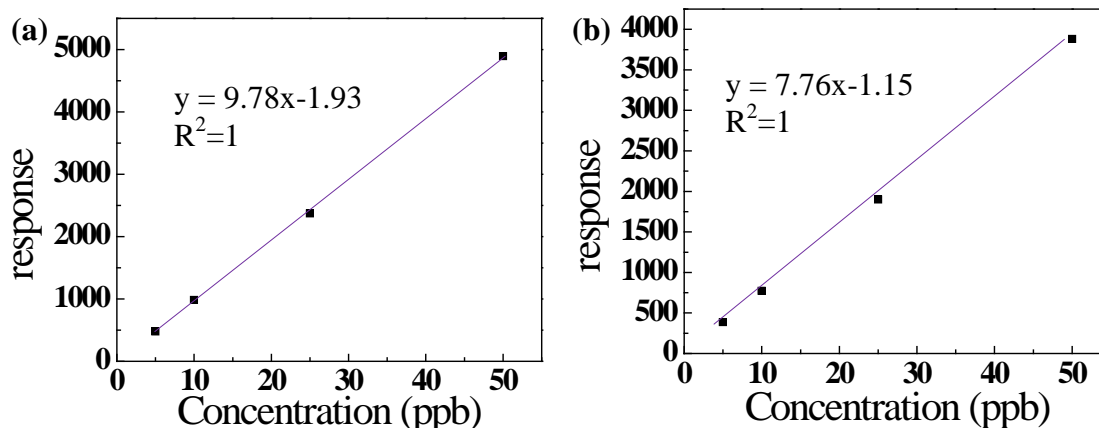
Figure 4.20. Calibration curves for Geosmin and MIB

4.3.8.2 Degradation of Geosmin and MIB in continuous filtration with/without DC current

Figure 4.21 show the removal of Geosmin and MIB in filtration. With physical filtration only, REM obtained 95% removal rate on Geosmin and MIB. Filtration with 12.5 and 25.3 mA·cm^{-2} current density DC could reach 100% removal for both Geosmin and MIB in 5min dead-end filtration.
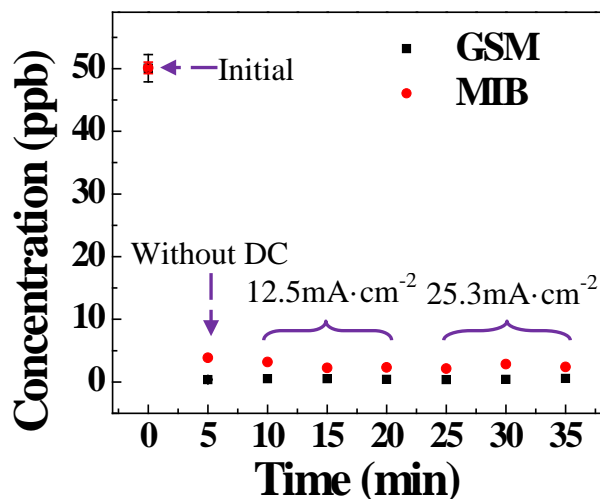
Figure 4.21 The concentration changes of Geosmin and MIB during continuous filtration.

4.3.8.4 Mechanism analysis.

The formation of numerous intermediate products took place were illustrated in Figure 4.22. The majority of the identified intermediates were cyclic ketones which upon ring opening lead to formation of linear saturated and unsaturated products (Scheme 1). The formation of all intermediates is followed by their decay during the photocatalytic process, coming finally to total photodecomposition to CO_2. As presented in Figure 4.22a, part of 2-MIB were directly transformed to P1 and P2 by elimination reaction via dehydration, while others were degraded to ketone-derivatives (P3) by β-scission. Then, P2 was further oxidized to alcohol-derivatives (P4) by addition reaction. These products could be subsequently oxidized to other intermediates with

smaller molecular weight (Figure 4.22a).[400] During the electrochemical degradation of geosmin, CO_2 was assumed to be the final product. However, according to Figure 4.23, as the by-products produced during the electrochemical reaction were not detected, in the further research, it is still needed to be studied to confirm whether toxic by-products exist.[401]
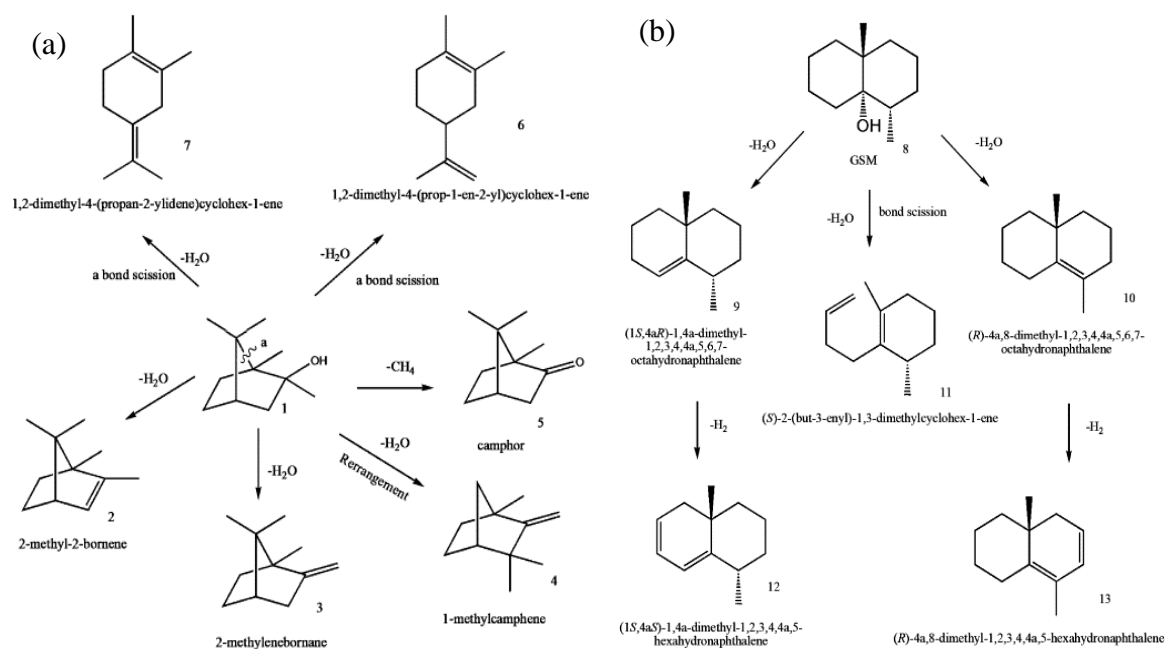
Figure 4.22 Degradation pathways in the oxidation processes of MIB (a) and Geosmin (b) solutions.[400]
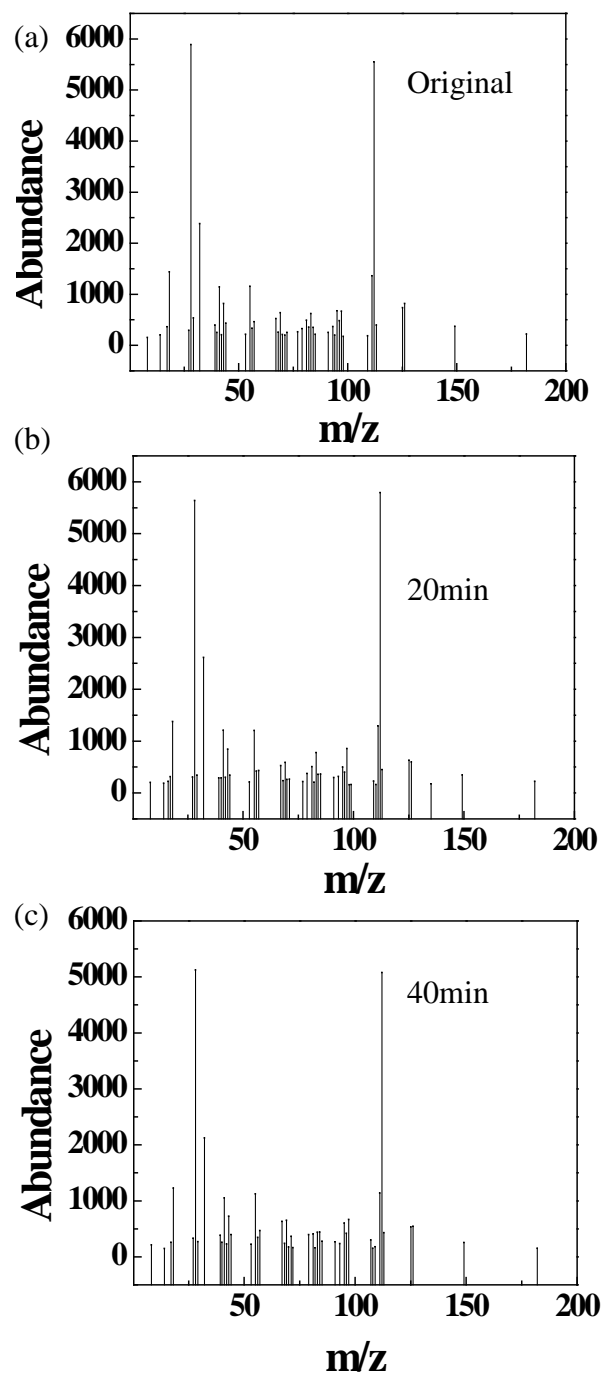
Figure 4.23 The m/z spectrum of the original and electrochemical treated Geosmin (a) and MIB (b) solutions in batch reaction. The current density was 25.26mA·cm^{-2} and treatment time was 40 min.

The voltammograms for the dioxane, MB, RB and OGII containing solutions show no corresponding reduction or oxidation peak (Figure 4.24). This illustrates electrochemical oxidation was not happening in -3 to 3V potential range. Therefore, it was decided to focus on the electrochemical oxidation behaviour of dioxane in higher potential region in further experiments.
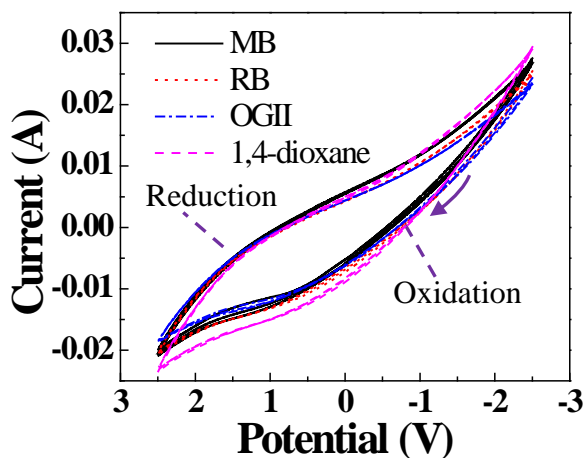
Figure 4.24. 20 ppm of 1,4-dioxane, Rhodamine B (RB) and Methylene Blue (MB), and Orange II (OGII), and geosmin and MIB at 200 ppt. The arrow indicates the beginning and sweep direction of the first segment.

4.3.10 Bacterial inactivation and removal studies

Figure 4.25 shows the plate spreading and counting of two different concentrations of *E. coli* inactivation in REM batch reaction and filtration with different DC current density (5.02 mA·cm^{-2} to 25.26 mA·cm^{-2}). In all four experiments, the result shows *E. coli* was mostly inactivated in the first 20 minutes.

(a)   (b)
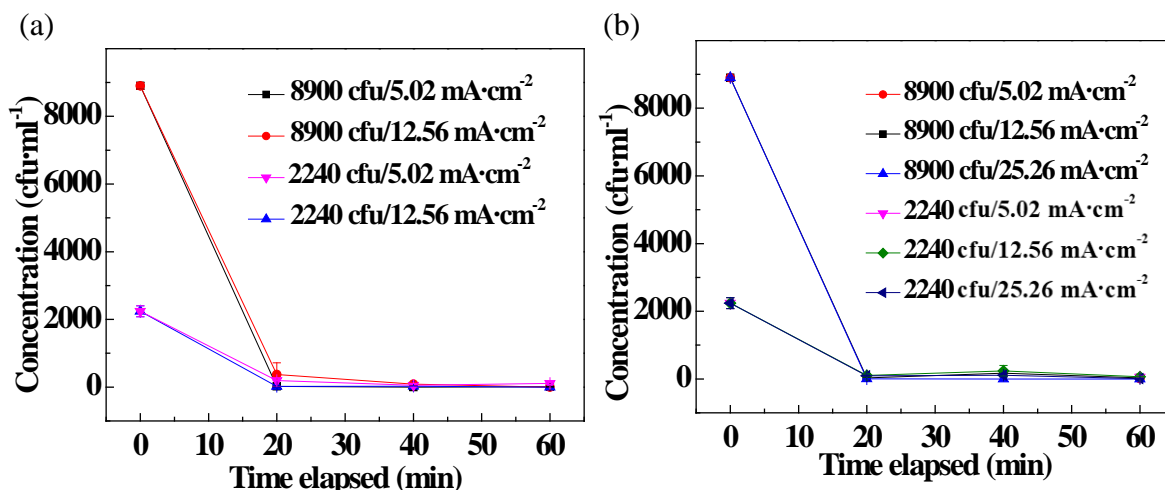
Figure 4.25 *E. coli* inactivation under different DC current density by different elapsed time. (a) 8900 and 2240 cfu·ml^{-1} initial concentration *E. coli* were filtered by REM under 5.02 mA·cm^{-2} and 12.56 mA·cm^{-2} current density. (b) 8900 and 2240 cfu·ml^{-1} initial concentration *E. coli* were reacted with REM in batch under 5.02 mA·cm^{-2} to 25.26 mA·cm^{-2} current density. (c) 8900 and 2240 cfu·ml^{-1} initial concentration *E. coli* were filtered by REM without DC.

4.4 Conclusion

In this study, Ti_4O_7 REM under direct current was demonstrated to be highly effective for the degradation of organic dye in aqueous solution. Batch reaction and filtration studies have been conducted for three different dyes to assess the removal capability of REM to remove in the aqueous phase. All three dyes were successfully decolorized. COD and TOC removal efficiencies during batch reaction and dead-end filtration implied that few intermediate products remained and the organic part was completely converted into CO_2. Ti_4O_7 REM appears as a valuable treatment for purifying and reusing colored aqueous effluents.

The electrochemical oxidation of 1,4-dioxane with Ti_4O_7 electrode was also investigated under a range of major system variables such as initial 1,4-dioxane concentration, current density, electrode potential and current direction. As a result, Ti_4O_7

REM showed a high removal efficiency of 1,4-dioxane in both batch reaction and continues dead-end filtration. The initial concentration of 1,4-dioxane had no effects on removal behavior of 1,4-dioxane with the setting in this study since the reaction was under current control in this study. However, the mass transfer controlled reaction could be investigated in the future study. The voltage decline along the tubular membrane was also investigated and proved that the voltage distribution on Ti_4O_7 electrode did not have significant decline along the surface, which suggested that the reaction efficiency along the membrane surface did not have significant change either. The removal efficiency of COD was shown to be low while the initial COD was high. During the dead-end filtration, no electrode fouling was observed during the reaction. Thus, if several process variables, such as surface area, applied current density and initial concentration, are considered, electrochemical degradation of 1,4-dioxane by Ti_4O_7 REM promises to be both efficient and economically feasible.

CHAPTER 5

COMMERCIALIZATION

5.1 I-Corps Team

5.1.1 Rationale for team formation

The project PI (Wen Zhang) has been advising the PhD student (Likun Hua) as his thesis advisor since January 2015. They started to work on the fundamental research of antifouling and reactive ceramic membranes for water treatment and biomass separation since then. Up to today, they have filed a provisional patent (Reactive Electrochemical Membrane Filtration, 2016, US application: 62/337,940) and published one journal article in ***Bioresource Technology***.[402] They also presented results at different conferences, workshop and technical meetings including New Jersey Technology Council, 251st National American Chemical Society Meeting, New Jersey Entrepreneurial Network (NJEN) meeting at Princeton University, Dana Knox Student Research Showcase, and Otto York Research Center Workshop. Thanks to a number of internal grant support from the Undergraduate Research Innovation (URI) phase I/II grants and NSF I-Corps Site grant (2015 fall-2016 spring), a major research progress was achieved. Particularly, the entrepreneurial lead, Likun Hua, has obtained systematic and intensive training in technology commercialization, foster entrepreneurial leadership, and skills to interface customers and identify marketing challenges. In addition, the PI's research team received a 3-year NSF CBET grant (Award Number: 1603609) starting from September 1, 2016, which could allow for the fundamental investigations of chemical mechanisms of reactive

membranes. This fundamental research could largely support the proof of concept and complement the NSF I-Corps work.

The PI and the industrial mentor (Paul Schorr) are both serving as committee members in American Water Works Association (AWWA) in New Jersey section, where they began to know each other. This committee is formed to facilitate the interactions and foster industry-university collaboration. The PI represents academia to demonstrate institutional resources in research facilities, students, and faculty expertise to local industries. Paul works with the PI to identify current challenges and problems in water industries and seek research opportunities, which is in line with the mission and operation of NSF I-Corps. Moreover, they also collaborated in hosting the national ACS symposiums on water resources, water quality and water treatment technologies. Due to the sustained interactions, Paul has established a deeper understanding of the PI's research group and the ongoing research project related to the reactive electrochemical membrane (REM) technology. Since he retired from New Jersey Department of Environmental Pollution (NJDEP), he has been closely following Wen's research and team members. He now joins the same Department of Civil and Environmental Engineering at NJIT as adjunct professor. Based on his more than 45 years in the water engineering fields, Paul has accumulated unparalleled knowledge, insight and connections with local industries, which is important and highly needed for our research team to move forward on technology transfer, commercialization and business development. Thus, we had a couple of conversation and discussions at different venues and finalized the plan of partnership and application of national NSF I-Corps.

5.1.2 Members' entrepreneurial expertise

The PI, Wen Zhang, is an associate professor in the Department of Civil and Environmental Engineering at NJIT. He is a licensed Professional Engineer (P.E.) registered in the States of New Jersey and Delaware. His research aims to integrate nanotechnology into environmental engineering and develop innovative solutions for environmental sustainability and challenges in water quality and renewable energy. He served as the PI for this I-Corps team and support the team to perform fundamental research, business model development and customer discovery to facilitate technological development and commercialization. He serves as SBIR proposal reviewers for many agencies including USDA, EPA and NSF. He also led SBIR phase I proposals on a few research projects related to renewable energy and nanotechnology. He co-founded a Chinese Young Environmental Professionals Association (CYEPA, http://www.cyepa.org/), a state-registered nonprofit organization providing industrial networking opportunities and peer review and language editing for technical articles.

Likun Hua, majored in environmental engineering, is a second-year PhD student (a full time research assistant) in the Department of Civil and Environmental Engineering at New Jersey Institute of Technology. In this project, Likun acted as the entrepreneurial lead with a leading role of building business models, customer discovery, product development, testing and on-site interview or demonstration. In his previous effort, he was supported by the NSF I-Corps site grant to perform tutorial learning on business planning, technology commercialization, and customer interview. He established connections with local industries ranging from Water Engineering firms such as United

Waters and American Waters to Engineering consulting firms and obtained invaluable feedback and advice toward marketing and commercialization.

Paul Schorr is a licensed Professional Engineer retired from New Jersey Department of Environmental Protection (NJDEP), a state agency responsible for environmental pollution management and remediation. He has over 45 years of experience in the field of water resources with consulting engineering firms of Clinton Bogert Associates and Gerald E. Speitel Associates; with the federal Environmental Protection Agency (EPA). He was the Project Manager on the New Jersey Special Water Treatment Plan, which provided the framework for the State to approve advanced physical chemical and biological processes to achieve stringent drinking and surface water standards. Equipment and processes included ozonation, denitrification, granular activated carbon, and packed aeration towers. As a member of the American Chemical Society, he hosts a number of symposiums on "Advances in Water Monitoring" that focus on new equipment and techniques to measure water quality parameters. His role in this project included mentorship on evaluating water and wastewater equipment to meet Federal standards and construction costs, industrial customer connections, public financing and market demand analysis.

5.1.3 Lineage of the Proposed Innovation

Table 5.1 Relevant Awards before 2016 National I-Corps

	Relevant Awards	Program officer or agency
1	Undergraduate Research Innovation (URI) phase I/II grants (spring 2015 to spring 2016)	Atam Dhawan, NJIT
2	NSF I-Corps Site grant (2015 fall-2016 spring)	Michael Ehrlich and Judith Sheft, NJIT
3	NSF CBET grant (Award Number: 1603609) (2016 fall-2019 fall)	Carole Read, NSF

Physical membrane separation suffers from membrane fouling due to the deposition and adsorption of various foulants. Frequent membrane backwashing and cleaning is required to maintain a desired separation and functional filtration, which elevates the operational cost. Usually, hydraulic flushing, biocides or harsh chemical cleaners are used to recover permeate flux, which are costly and potentially harmful to membrane integrity or life span. The REM technology we developed uses direct current (DC), alternating current (AC) and a combination of DC and AC as an environmentally benign approach to control and mitigate membrane fouling while filtration, backwash or recovering flux. Many prior research including ours demonstrated the use of REM membrane in various forms (i.e., monolithic porous ceramics, electrospun mats of nanofibers, and carbon nanofibers loaded with conductive nanomaterials) as both electrodes and membrane filter could have could have anodic or cathodic polarization under DC current and therefore could efficiently oxidize organic compounds or surface foulants by hydroxyl radical ($\bullet OH$)

produced from water oxidation.[25-27] Compared to regular ceramic membrane filtration, our invention of electrochemical ceramic membranes will bring more measurable synergies, including but not limited to: durable and stable permeate flux across ceramic membrane without significant fouling over a larger period of time, degradation of organic pollutants or compounds in the treated water, and reduction in membrane fouling and energy use for backwash for recovery of flux. These features are usually not all available in one integrated membrane process.

The REM technology holds high commercialization potential because (1) ceramic membranes and conductive membranes are already implemented in many industrial water and wastewater treatment in various fields (e.g., pharmaceutical wastewater, dye and mining wastewater treatment). Thus, REM could be conveniently deployed and upgrade the existing ceramic membrane modules. (2) The increasing demand for high water quality in many industrial applications. For example, semiconductor production requires ultra-high purity water and has a great demand for reliable and high efficient filtration systems to eliminate water pollutants such as salts, particles, and organics. (3) Conventional polymer membrane filtration suffers inherent limitations in fouling, aging, and instability in the treatment of complex water (e.g., corrosive or high salt content waters). (4) A benchmark innovation in reactive ceramic filtration will advance and potentially upgrade the filtration industries from physical separation to versatile and tunable reactive separation, which is interesting and attractive to customers we interviewed in the past.

5.1.4 Description of the Potential Commercial Impact

One of our typical customers in water and wastewater treatment industries is Mr. Kui Zhou, the General Manager of Nanjing Suhuan Environmental Technology Development Co., Ltd, China. This company's primary business is designing and constructing water treatment equipment and facilities. Their treatment targets are recalcitrant organic wastewater. The treatment method they use is a combination of Al_2O_3 ceramic membrane and polymer membrane filtration. The major problems they constantly encounter are expensive operational and maintenance cost in electricity consumption to drive the water pumps, which are attributed to the membrane surface fouling and resultant hydraulic backwash. Additional cost is caused by the polymer filter replacement due to aging and damage after prolonged exposure to corrosive wastewater and repeated uses. Frequent backwash and chemical rinsing to eliminate surface foulants are also observed to damage membrane surfaces and lead to the hole or crack formation on polymer membranes in addition to the cost of energy consumption. Collectively, as one of the treatment examples on phenol-containing wastewater, the overall operation and treatment cost is approximately $150 per ton of wastewater to reach the discharge standard- reducing chemical oxygen demand (COD) from 3000 mg/L in influent to 50 mg/L in treated water. More than of half of this operational cost is related to pump electricity usage and membrane replacement.

Our proposed technology represents a potentially game-changing filtration technology that is designed to improve water filtration efficiency, lower fouling potential (increased durability and stability), enabling high fluxes of water permeate and pre-oxidation of organic substituents. Accordingly, we may provide value propositions in

saving the capital costs on membrane backwash, membrane maintenance, reduce down time or off-line time, and reduce chemical uses for membrane cleaning, and replacement of membranes that are fouled or aged; decrease pumping energy; increase water quality by efficiently removing organic matters in water based on electrochemical oxidation reactions on REM surfaces. Based on the preliminary interview with the customers, they do have desire to substitute current physical filtration with our reactive filtration systems to achieve the identified benefits and long run sustainability. The possible capital investment to upgrade and install new filtration systems may range from $50,000 to $500,000 depending on the treatment capacity need.
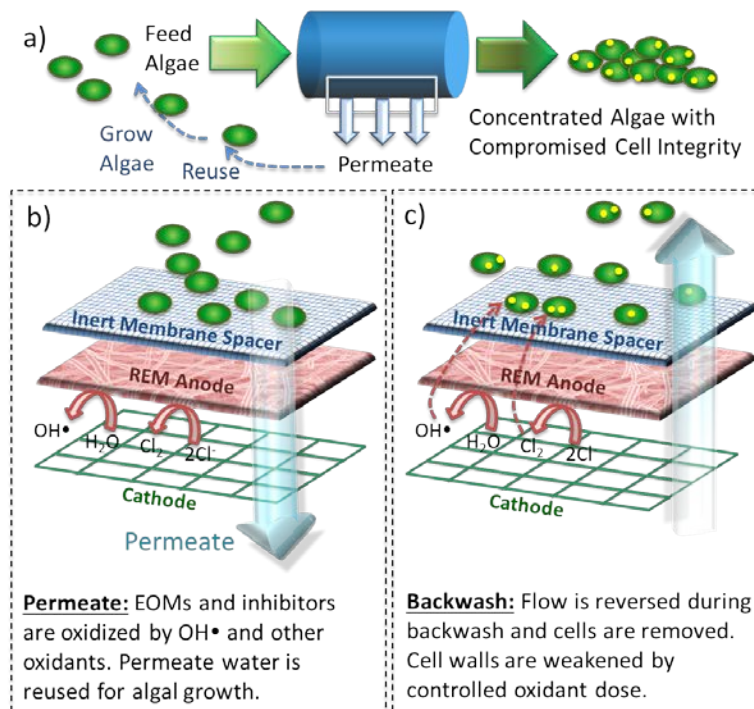
Figure 5.1 Schematic of the REM for algal biomass containing water filtration in cross flow mode (a) Filtration and radical formation for antifouling and biomass degradation (b) and backwash. (c) the dissolved organic matters was oxidized by OH• and other oxidants that are formed electrochemically at the REM surface during backwash.

The innovative REM process consists of conductive and porous Ti_4O_7 material as the anodic filter. Ti_4O_7 is initially selected because of its high performance in generating hydroxyl radical (OH•) from water oxidation, stability under anodic polarization, and low cost.[25-27] The monolithic porous Ti_4O_7 membrane shows a high water flux in filtration (5000-6000 L m^{-2} h^{-1} bar^{-1} or LMH bar^{-1}). These properties make Ti_4O_7 membranes an ideal material for sustainable water filtration and pollutant degradation. By applying a positive DC potential or current to the REM surface, the produced OH• could oxidize organic compounds (surface foulants marked in green) to maintain a clean membrane surface as shown in Figure 5.1. The REM serves as both filter and anode with a stainless steel mesh as a cathode. During filtration (Figure 5.1b) the permeate solution first passes through a 100 µm-thick inert glass fiber membrane spacer with tunable pore sizes (e.g., 1-2 µm) that could effectively filter most microbial contaminants such as bacteria. While passing through the REM, the dissolved organic matters could be oxidized by OH• and other oxidants that are formed electrochemically at the REM surface during backwash (Figure 5.1c). The key physical/chemical processes occurring include *1) Physical Separation;2) Interfacial Electrostatic interactions;* and *3) Electrochemical Oxidation*, which produce hydroxyl radicals (OH•) at the electrode surface:[25-26, 78, 266] $H_2O \rightarrow OH^{\cdot} + H^+ + e^-$. OH• is a powerful and unselective oxidant with a high oxidation potential (E^o = 2.6 V), which could mineralize most organic pollutants at near diffusion-limited rates.[267-268] Major fundamental research has been performed at NJIT to verify the degradation performance while filtering different pollutant-containing waters. As the demand for high water quality increases and wastewater recycling for direct and indirect potable reuse becomes more widespread, REM technologies will further ensure water

quality security and sustainability by effectively eliminating public health risks associated with pathogens and contaminants in addition to taste, odor and color.

5.1.5. Brief description of the project plan

We have completed the part of the proof-of-concept research and assemble a benchtop prototype as shown in Figure 5.2. A provisional patent was filed at NJIT for the novel REM filtration configuration and the designs of REM filtration system. At the end of this I-Corps project, we demonstrated (1) systematic filtration results on various water types; (2) antifouling characteristics compared to the filtration system without DC polarization; (3) relevant operational parameters and their control strategies to achieve antifouling functions, maintain water quality and separation efficiency; (3) disseminate the above information to customers to receive feedback.

The next step is to have the patent licensed by ceramic membrane manufacturers or design companies, filtration industries, algal biofuel companies, water/wastewater treatment consulting firms, pharmaceutical, or chemical engineering industries where efficient bioseparation or treatment processes are needed. Our team may join the licensee company as technical support and consultant. The second route of commercialization is to form a startup company with expected 3-5 personnel in charge of R/D and sales in partnership with NJIT. We will leverage these unique advantages to secure potential off-take agreements with membrane, biofuel, and water/wastewater industries. At the initial stage, REM production will be subcontracted to the manufacturer (Vector Corrosion Technologies Ltd.) and maybe we enter into a joint venture or manufacturing agreement. The core filtration part manufacturing or assembly will be done by our contract manufactures to be sought and determined in the future. To market the product, we may

work with dealers or contract sales through marketing agreements. Regarding financing plans, besides this national I-Corps grant application, we will work with local commercial firms to pursue some non-Federal capital commitments including personal investment, venture capital investment, crowd sourcing, intent to license or collaborate. Moreover, we plan to prepare SBIR and GOALI proposals to submit to NSF, USDA and EPA to secure phase II grants.

The education impacts of this NSF I-Corps project include (1) training of a group of NJIT students (especially the entrepreneurial lead) to develop relevant skills for business planning, team management, customer discovery, technology commercialization, entrepreneurial leadership, and marketing. Moreover, these experiences are important learning materials that could be incorporated in our current curricula to enrich engineering education and motivate students to involve in research innovation. The commercial impacts are expected on end users or markets in, but not limited to, membrane industries, manufacturers and users for water/wastewater treatment industries and algae biofuel industries, renewable energy, bioenergy industries. REM technologies holds promise to transform current physical filtration processes from a chemically inert system to chemically reactive systems that proactively filtrate water with well-defined reactions or reactivity on filter surfaces. In the long term, reactive ceramic membranes, due to their flexible surface modifications and a longer lifetime compared to widely used polymer membranes, will reduce filtration operational cost and increase process stainability.
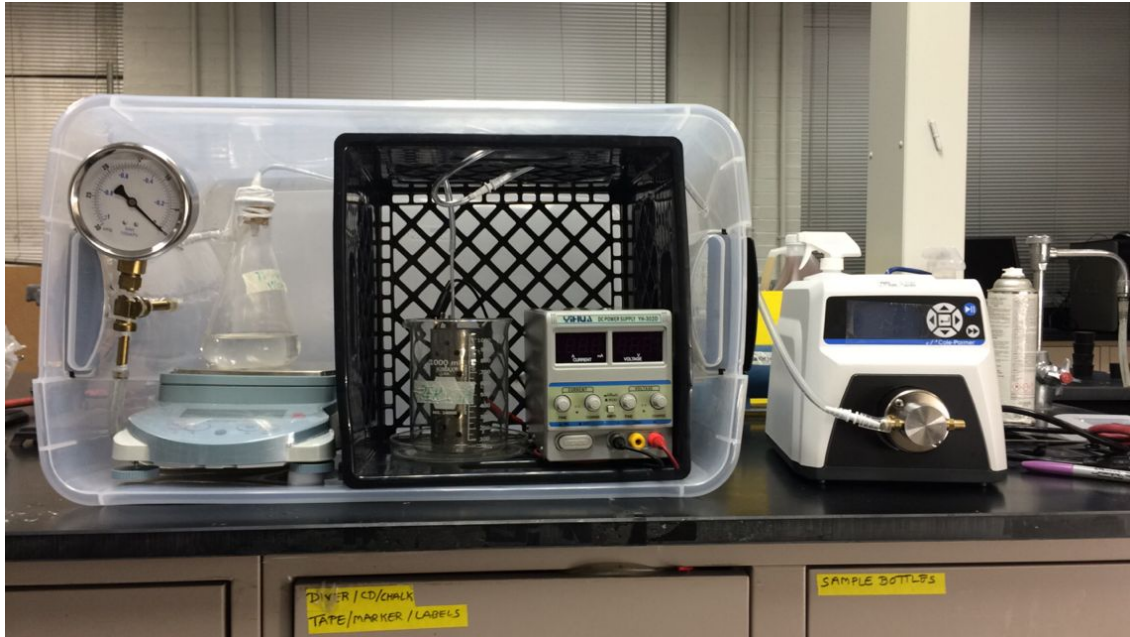
Figure 5.2. Our current REM filtration system apparatus.

5.2. Business Model hypothesis

The business model is defined as the model that describes the rationale of how an organization creates, delivers, and captures value. In this case, business model is described through nine basic building blocks in a "canvas" that show the logic of how a company intends to make money. The nine blocks cover the four main areas of a business: customers, offer, infrastructure, and financial viability. The business model is like a blueprint for a strategy to be implemented through organizational structures, processes, and systems. This concept has been applied and tested around the world and is already used in organizations such as IBM, Ericsson, Deloitte, the Public Works and Government Services of Canada, and many more.[403] The original hypothetical business model canvas (BMC) before any interview is shown in Figure 5.3a. As interviews going further, the

BMC experienced several change/pivot (Figure 5.3b and c) and evolved into the final

version (Figure 5.3d).

(a)

Key Partners	Key Activities	Revenue Streams	Customer relationship	Costs
Advanced Cerametrics Inc. (raw material supplier)

Paul Corporation (Joint ventures to develop new businesses) | REM treatment test. Treatment system Production.

Website development.

Customer consulting.

Key Resources
NJIT lab equipment.

KP's test results.

NSF grant support. | Asset sale, (sale the system itself)

Leasing, (rent the system)

Licensing. (give license for automatic control software) | Personal assistance;

Co-creation.

Channels
Direct sales (on our website)
Indirect sale (from our KP and third-party website) | Material (TiO$_2$ tube and outer case).

Experiment consume (algae/Medium/electricity, etc.)

Labor fee.

Instrumental usage fees.

Long range delivery & transportation fee. |

Customer segments	Value proposition
1. Water/wastewater treatment industries;

2. Beverage companies;

3. Pharmaceutical manufacturers

4. Electronic assemble industries | 1. and 2. REM has a longer lifetime comparing with traditional filters along with effective microbes suppression/removal, which will reduce daily cost.

3. REM provides high selective filtration that is needed for separating specific compounds or biomolecules from the biomass feedstock, which will increase the productive efficiency and lower the risk of defective products.

4. The new filtration system could provide high purity water from semi-conductor parts for electronic device, reduce the defective rate and eventually drop down the recall cost. |

(b)

Business Model Canvas

Key Partners	Key Activities	Value Propositions	Customer Relationships	Customer Segments
Vector Corrosion Technologies, Inc.(ceramic tube supplier)

InRedox LLC.

Meidensha Corporation (Joint ventures)

Pall Corporation

In the swim (NEW)

Eco-lab (NEW) | REM treatment test.

Mobile treatment system production

Product website development for sale and demonstration.

Customer support and technical consulting

Key Resources
NJIT lab facilities and research equipment

Grants from NSF, NJIT and industrial partners

KP's testing facilities | longer lifetime & antifouling features; reduce monthly cost (at least 50%) in backwash or chemical cleaning and reduce downtime; increase water quality and safety (reduce Cl$_2$)

REM provides high selective filtration, which increase the productive efficiency and lower the risk of defective products. (Save for later)

REM provide high purity water which reduce the defective rate and eventually drop down the recall cost. (Save for later) | Personal assistance

Co-creation.

Channels
Direct sales through our website

Indirect sales (referral from our KPs and third-party website) | Swimming pools and landscape (Refit) water in hotels, fitness centers and malls
- General Manager
- Chief Engineer
- Director of Engineering
- Director of facilities

Water treatment companies (Save for later)
Pharmaceutical manufacturers (Save for later)
Beverage industries (Save for later) |

Cost Structure	Revenue Streams
Material cost   Fabrication   Labor fee

Long range delivery fee   Storage fee | Asset sale   Product leasing and rental

Patent and licensing |

Figure 5.3 (a)-(d) The evolution of BMC. (Contioued)

213

Business Model Canvas — (c)

Key Partners
- Vector Corrosion Technologies, Inc.(ceramic tube supplier)
- InRedox LLC.
- Meidensha Corporation (Joint ventures)
- Pall Corporation
- Swimming po... *(NEW)*
- Eco-lab *(NEW)*

Key Activities
- REM treatment test.
- Mobile treatment system production
- Product website development for sale and demonstration.
- Customer support and technical consulting

Key Resources
- NJIT lab facilities and research equipment
- Grants from NSF, NJIT and industrial partners
- KP's testing facilities

Value Propositions *(Refit)*
- longer lifetime & antifouling features; reduce monthly cost (at least 50%) in backwash or chemical cleaning and reduce downtime; increase water quality and safety (reduce Cl_2)
- REM provides high selecti... ...tion, which ... the productive efficiency and lower the risk of defective products. *(Invalidated)*
- REM provide high ... water which ...uce the defective rate and eventually drop down the recall cost. *(Deleted)*

Customer Relationships
- Personal assistance
- Co-creation.

Channels
- Direct sales through our website
- Indirect sales (referral from our KPs and third-party website)

Customer Segments
- Swimming pools and landscape water in hotels, fitness centers and malls *(NEW)*
  - General Manager
  - Chief Engineer
  - Director of Engineering
  - Director of facilities
- Water treatment companies *(Invalidated)*
- Pharmaceutical manufacturers *(Invalidated)*
- Beverage industries *(Invalidated)*

Cost Structure
- Material cost
- Fabrication
- Labor fee
- Long range delivery fee
- Storage fee

Revenue Streams
- Asset sale
- Product leasing and rental
- Patent and licensing

Business Model Canvas — Current (d)

Key Partners
- Vector Corrosion Technologies, Inc.(ceramic tube supplier)
- InRedox LLC.
- Meidensha Corporation (Joint ventures)
- Pall Corporation
- In the swim
- Eco-lab

Key Activities
- REM treatment test.
- Mobile treatment system production
- Product website development for sale and demonstration.
- Customer support and technical consulting

Key Resources
- NJIT lab facilities and research equipment
- Grants from NSF, NJIT and industrial partners
- KP's testing facilities

Value Propositions
- Reduce monthly cost (at least 50%) in backwash or chemical cleaning and reduce downtime; increase water quality and safety (reduce Cl_2)
- Save 20% initial cost by substitute the disinfection system *(NEW)*

Customer Relationships
- Personal assistance
- Co-creation.

Channels
- Direct sales through our website
- Indirect sales (referral from our KPs and third-party website)

Customer Segments
- Swimming pools and landscape water in hotels, fitness centers and malls
  - General Manager
  - Chief Engineer
  - Director of Engineering
  - Director of facilities
- Private pool owner *(NEW)*

Cost Structure
- Material cost
- Fabrication
- Long range delivery fee
- Storage fee
- Labor fee

Revenue Streams
- Asset sale
- Patent and licensing
- Product leasing and rental

Figure 5.3 (Contioued) (a)-(d) The evolution of BMC.

5.2.1 Value proposition

Value proposition solve customer problems and satisfy customer needs. In this case, there were 3 original value propositions and 2 additional value propositions after several interviews:

1. REM filtration system has a longer lifetime comparing with traditional filters along with effective microbes suppression/removal, which will reduce daily cost for water treatment plants and beverage companies.

2. REM filtration system provides high selective filtration that is needed for separating specific compounds or biomolecules from the biomass feedstock, which will increase the productive efficiency and lower the risk of defective products for pharmaceutical industries.

3. REM filtration system could provide high purity water from semi-conductor parts for electronic device manufacturers, reduce the defective rate and eventually drop down the recall cost. High-purity rinse water is needed for microchip manufacturing. Since Microchips are getting more and more compact, with a million transistors per chip, a single micrometer-sized particle can result in a short circuit. The high-purity rinse water from REM will reduce the defective rate and eventually drop down the recall cost.

4. REM filtration system could increase water quality and safety (reduce Cl_2 odor) and will reduce daily cost in backwash or chemical cleaning by at least 50% for swimming pools and landscape water.

5. REM filtration system could increase better water quality for aquarium and fish tank than normal fish tank filters.

5.2.2 Customer segment

Based on the value proposition, the market is divided by 6 different parts: (1) water treatment plants, (2) beverage companies, (3) electronic device manufacturers, (4) pharmaceutical industries, (5) swimming pools and landscape water (e.g., for hotels, schools, fitness centers, residents), and (6) aquariums.

Due to the invalidation of market (1)-(4) in the early stage (see section 5.3.2) and (6) in the latter stage, there are no further customer discoveries in these five markets. The further customer discovery is conducted on the market of swimming pools and landscape water, which gives the following customer segments hypothesis: (1) General Managers, Chief Engineers, Director of Engineering and Director of facilities in hotels and fitness centers; (2) Certified Pool Operator (CPO) of public pools and schools; (3) residential pool owners and designers.

5.2.3 Channels

Channels are the communication, distribution, and sales that delivers value propositions to customers. In the hypothesis, due to the REM system is a physical product; the Physical Distribution Channels is applied, which includes direct sales through our own website and indirect sale from distributors, retailers, value-added resellers (VARs) and system integrators. The relationship between channels is shown in the distribution complexity diagram (Figure 5.4). The detail and validation of channels were obtained by interviews. (See Section 5.3.3)
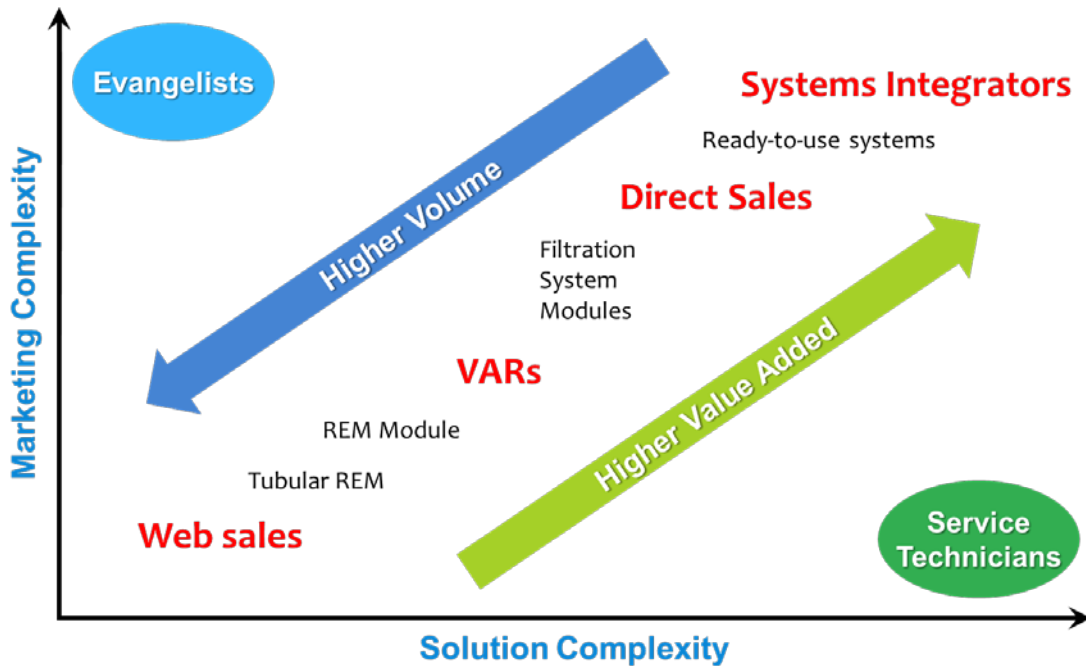
Figure 5.4 Distribution Complexity assumptions. The red texts are different types of channels defined: Web, VARs, Direct Sales, and Integrators. In between that are product types for the range of complexity from these types of channels.

5.2.4 Customer Relationships

Customer relationships are established and maintained with each Customer segment. Three major components of customer relationships are "Get", "Keep" and "Grow" customers. A funnel diagram is used to represent these three components. (Figure 5.5)
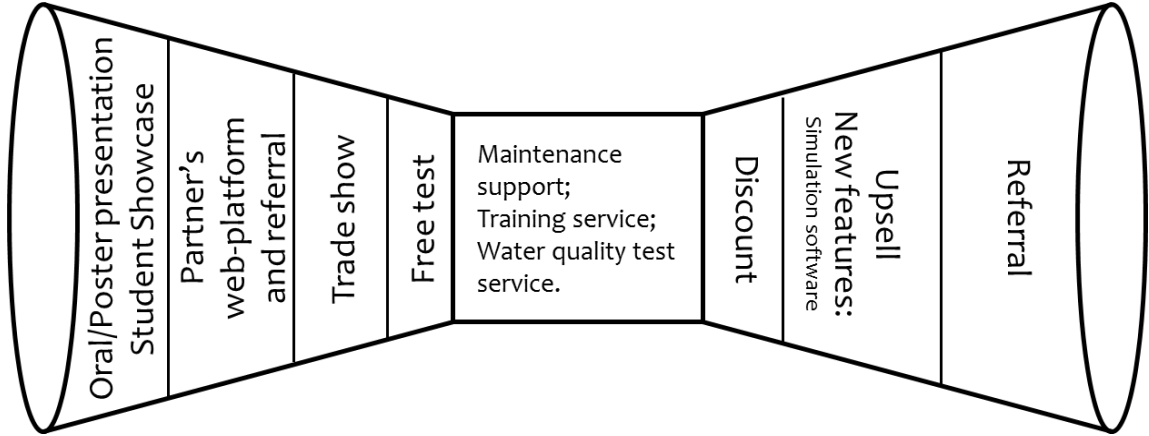
Figure 5.5 Funnel diagram of "Get/Keep/Grow" relationships. Left and right funnels showed the "Get" and "Grow" processes while the square in the middle shows the "Keep" processes.

In the "Get" process, the cost associated in convincing a customer to buy our product or service is called Customer Acquisition Cost (CAC). This cost is inclusive of the product cost as well as the cost involved in research, marketing, and accessibility costs. Our CAC hypothesis is shown in Table 5.2**.**

Table 5.2 Customer Acquisition Cost of the First Year

Item and Activities		Cost
Oral/Poster presentation		$150-300 each
Student Showcase		$0-300 each
Partner's web-platform and referral		Unknown
Trade show		$2,000 each
Free test	Manufacture	$5,000
	Labor fee	$3,000
	Transportation	$500
Total estimate		>$11,000 (first year)

The sum of all the revenue from the beginning of purchase through keeping them and all the grow activities is called customer Lifetime Value (LTV). To make the business practical, the CAC should be less than LTV. In this case, the LTV is shown in Table 5.3.

Table 5.3 Customer Lifetime Value of First and Second Year

Item and Activities	Value
Labor fee for maintenance/ training/ water quality test	$3000/yr.
Labor fee for upsell (1st year)	$8000
Labor fee for upsell (2nd year)	$3000
Profit from each customer	$7000

Assuming the profit from each customer is $7000 and there will be two additional customers per year, the total estimated profit will be: $0 in the 1st year and $20000 in the 2nd year.

5.2.5 Revenue Streams

Revenue streams result from value propositions successfully offered to customers. It represents a strategy for generating revenues (per Customer Segment). Based on the funnel diagram, our revenue model strategy includes three parts, which are:

(1) Asset sale: The REM system, parts.

(2) Freemium: Free use of the REM for a certain period of time (e.g., one month)

(3) Licensing (upsell): The control/simulation software.

5.2.6 Key Partners

A partnership is a two-way street. Both parties have to mutually benefit/share successes and failures. In our hypothesis, there were three kinds of partners: (1) Raw material suppliers are considered to be one of the key partners, by providing/selling essential parts for REM to us, their business could also gain benefit. The cost of this partnership is raw material itself and shipping fee and the risk is quality control. (2) Distributor in the channel section since our product can solve the safety dilemma for their customers. Cost

of the partnership is profit share in the distribution channel while the possible risk is from

Saboteurs in other pool equipment manufacturers and the reliability of the distributor. (3)

Membrane system manufacturer (Joint ventures). By helping us manufacture the system,

they will share the profit, and cooperative research could provide novel ideas for their

R&D department. Cost in this partnership includes manufacturing, shipping, and time

consuming. The risk is potential common customer may turn the partner to competitor,

the possible intellectual property (IP) issue, and the alliance may be affected by the key

person changing.

5.2.7 Key Resources

Key resources include financial, physical, intellectual property and human resources. Our

hypotheses of the key resources are concluded in Table 5.4.

Table 5.4 Key Resources

Financial resources	Federal grant and award, and the investment from key partners.
Physical resources	University lab space and storage, key partners' facility
Intellectual property	A patent which has been already filed
Human resources	Mentors, advisors and qualified employees, which could be the above mentioned team (Section 5.1) or hire additional personnel

5.2.8 Key Activities

The key activities include REM treatment test, mobile treatment system production, obtain certification, product website development for sale and demonstration and customer support/technical consulting.

1. REM treatment test

2. Mobile treatment system production

3. Certification

4. Website development

5.2.9 Cost structure

The assumed cost structure contains the CAC (discussed in section **5.2.4**) plus material cost, fabrication cost, long range delivery fee, storage fee, and labor fee.

5.3 Business model validation

5.3.1 Customer interview questionnaires

There are three questionnaires prepared for users (customers), distributors and manufacturers. Questionnaire for users was focused on value proposition and market size. (See Table 5.4) Questionnaire for distributors was used for channel validation and competitor/partner exploration. (See Table 5.5) Questionnaire for manufacturers was to validate key activity and plan pricing tactics. (See Table 5.6)

Table 5.4 Question List for Users (swimming pool/aquarium owners/operators)

Interview Questions	Purpose
Who is your interviewee (e.g., name, contact phone or email, title, location)	
What are the current technical processes or systems for the water purification for water recirculation and reuse (e.g., filtration or chemical additions)?	To validate the hypothesis that customers are using filtration and/or disinfection technologies.
Do they use chemical for disinfection? If yes, what are those chemicals? (e.g., Chlorine? Bromine?)	To validate the hypothesis that chemical disinfection is the most common method.
What are the major concern, problem, and pain of the current technic/process/system?	To validate the hypothesis that chemical balance and safety is the great concern.
* If there is a technology that could solve the chemical safety issue and obtain the same disinfection effect, will you consider changing the current approach?	* This question will be asked only when the answer of the last question is related to the potential safety issue of chemical use.
Who is the supplier? Who provide service/maintenance (supplier, themselves or a third party)?	To find the distribution channel. And to validate the hypothesis that the end users have limited knowledge of maintenance and operation.
How much does the system cost? the installation cost as well as the operational cost	This information will be used as a reference for price tactics of our own product
What is the daily/monthly cost of the entire process? Cost structure? (e.g., labor fee, electric and water consumption, filter replacement fee, or chemical uses…)	This information will be used as a reference for price tactics of our own product
What is the volume and flow rate?	This information will be used as a reference for prototype build.

Table 5.5 Question List for Distributors (e.g. chain stores, retail stores, designers)

Interview Questions	Purpose
Who is your interviewee (e.g. name, contact phone or email, title, location)?	
What are the current technical processes or systems for the water purification for water recirculation and reuse (e.g., filtration or chemical additions)?	To validate the hypothesis that customers are using filtration and/or disinfection technologies.
Do they use chemical for disinfection? If yes, what are those chemicals? (E.g. Chlorine? Bromine?)	To validate the hypothesis that chemical disinfection is the most common method.
What are the major concern, problem, and pain of the current technic/process/system?	To validate the hypothesis that chemical balance and safety is the great concern.
* If there is a certified technology that could solve the chemical safety issue with the same disinfection effect, will you consider selling this kind of product?	* This question will be asked only when the answer of the last question is related to the potential safety issue of chemical use.
Who is the manufacturer of the product you are selling? Do you need to provide service/maintenance to your customers?	To find the potential partner/competitor. And to validate the hypothesis that the end users have limited knowledge of maintenance and operation.
How much does the system cost? the installation cost as well as the operational cost	This information will be used as a reference for price tactics of our own product. The distributor may not be willing to give answer of this question as well as the next question. If so, write down their price tag.
What is the daily/monthly cost of the entire process? Cost structure? (e.g., labor fee, electric and water consumption, filter replacement fee, or chemical uses…)	This information will be used as a reference for price tactics of our own product
What is the major customer?	To understand the market size.

Table 5.6 Question List for Manufacturers (for different manufacturers, questions may be changed)

Interview Questions	Purpose
Who is your interviewee (e.g., name, contact phone or email, title, location)?	
What is your technical process or systems for the water purification for water recirculation and reuse (e.g., filtration or chemical additions)?	The question is only for system manufacturers.
What chemicals are using for pool/aquarium? (e.g., Chlorine? Bromine?)	The question is only for chemical manufacturers. To validate the hypothesis that chemical disinfection is the most common method.
What are the major concern, problem, and pain of the current technic/process/system?	The question is for all manufacturers. To validate the hypothesis that chemical balance and safety is the great concern. And the alternative method is lacking in the market.
Will you or do you apply technology from institutes and universities? How and Why? If there is a technology in developing that could solve the chemical safety issue with the same disinfection effect, will you consider invest in this kind of product?	Exploring partners. This question is only for system manufacturers. However, these questions need to be asked **very carefully.**
How do you introduce those products to distributors or the customers?	To find the distribution channel.
Are these products certified? Who of authorities issue the certification?	To validate obtain certification is one of the key activities.
What is the major customer?	To understand the market size.

5.3.2 Customer and value proposition validation

5.3.2.1 Water treatment plants and water utilities. Ten interviews have been

conducted on water treatment plants and water utilities which located in Texas and New

Jersey. Some large plants (e.g., 540 MGD capacity) are still using sand filter and dual

media filter in there filtration process, while smaller plants

(e.g., 45 MGD capacity) are applying membrane filtration. The result of these interviews

showed testing a new technology in a large existing plant in which all the components are

interrelated may not be as feasible as testing a new technology such as membrane in a

small facility. The cost of maintenance is not a major concern for water treatment plants

and they are not likely to apply technology from a start-up. So the conclusion of this

market is that there is no room for a start-up in the business of water treatment facilities.

5.3.2.2 Beverage companies. Five interviews have been conducted on Beverage

companies, which included Coco Cola and Nestle Bottle Water. Beverage companies do

use filtration technology. They need to remove the ammonia, chlorine, hardness and other

taste odor which are actually from the water utilities, but this is not their primary "pain",

the current technics are able to handle the problem.

Since the beverage industry operates on a smaller margin of profit than most other

process industries, it was difficult to justify the expense of discarding what had always

worked (e.g., thermal evaporation) and installing a new unit operation) that had not yet

been completely proven to "work" in other industries.

5.3.2.3 Swimming pools and landscape water. More than 50 interviews are focusing

on the owners and users of swimming pool and landscape water. The results show that: (1)

the disinfection is relying on Chlorine and the related odor and safety issue is a major

concern. Half of the hotels rely on third parties to maintain their system because their

own engineers are not qualified to do so. (2) Automatic and simplified system is

preferred. Backwash is occurred once a week or once per two weeks, but the cost of

which is not a major concern. (3) Some of hotels do not have filtration system for

landscape water and instead with manually cleaning the algae.

5.3.2.4 Aquariums.   About 20 interviews were conducted with the aquarium suppliers

in San Francisco, the USA. This segment was invalidated because of fish tank filters have

their special design to make sure the balance of ecosystems in the aquarium fish tanks. A

certain amount of microbes should be maintained in the system; however, REM is

targeting all microbes in the system. This technology does not match the requirement of

aquarium fish tanks

5.3.3 Channel validation.   For channel validation, about 20 interviews were executed

to possible distributors related to pool supplies. As a result, we found retail stores, chain

stores and web-based resellers are the current available distribution channel for pool

supplies. More than half of their customers are from residential swimming pools, though

they also provide supplies to schools, hotels and fitness center. The relationship between

distributor and users are shown in Figure 5.6.
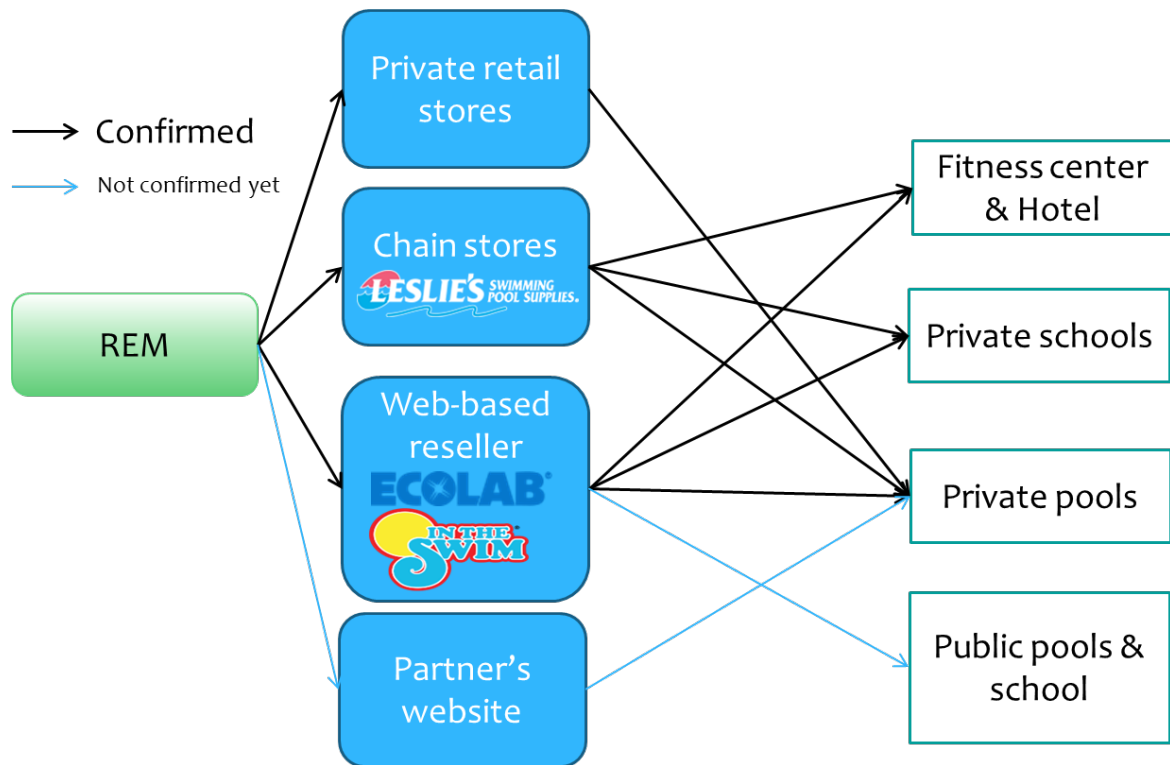
Figure 5.6 Distribution channel diagram. Black arrows show the known channels while blue arrows show the channels not confirmed yet.

5.3.4 Revenue Streams and pricing tactics

Average cost for a residential swimming pool (e.g., 12,000 gallons) is estimated from 80 interviews of users and distributors. The current filtration system uses Sand filter and active carbon. The system costs more than $10,000. For the maintenance, sand costs $110 per 6 months and active carbon costs $120 per three weeks. The current disinfection system uses Chlorine tabs, Chlorine liquid, UV light, Bromine or Copper sulfate. The UV system costs $3,000 and auto chemical system costs $2,800 to $7,100. Maintenance and consumption costs $360 per 6months. Besides, the design fee will be 30% to 50% of total system cost. This makes total system cost to be $35,000 and total maintenance cost to be

$3000 per year. The workflow diagram (**Figure 5.7**) shows how the revenue flowed in the market.

According to the Revenue Streams, Value Based Pricing Tactics is preferred in this business. The value provided are (1) Solve the health risk of Chlorine and the pathogen/bacteria issue at the same time; (2) Drop down the maintenance cost by 50%.
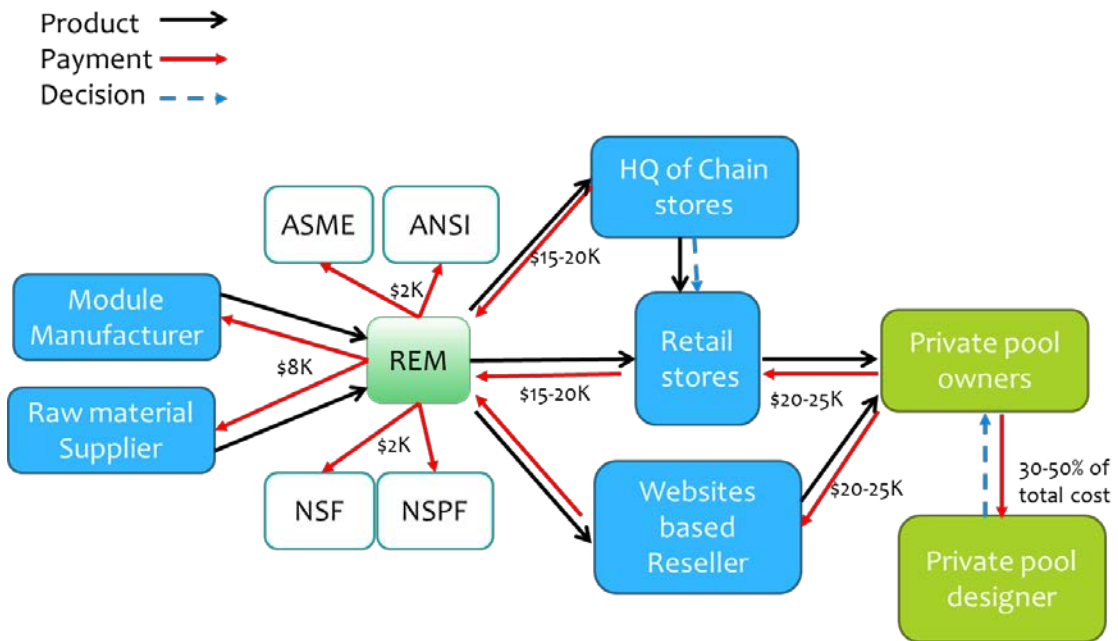
Figure 5.7 Workflow diagrams (private pools), estimation based on interviews.

5.3.5 Key Partners and Key Resources

We have established partnership with industry mentors, including Joseph G. Stanley, Vice President of Hatch Mott MacDonald, an internationally acclaimed Water Engineering firm and Yuhong Jiang, President of BRISEA Group, which is dedicated in

providing environmental and energy professional services, technology and know-how transfer from USA to the developing nations.

5.3.6 Key Activities

After interviewing over 20 manufacturers, the following key activity has been confirmed: Before the product gets into the market, certain organization will test it to make sure it meets the parameter we claimed. If our business is related to membrane manufacturing, ASME and ANSI could issue the certification. In addition, NSF certification #61, #372, and #419 is also required if the business is related to drinking or municipal water. At last, NSPF certification is required for pools supplies.

5.3.7 Cost structure

As hypnotized in Section5.2.4, the cost in the first year would be more than $11,000. What was confirmed is the demo unit structure cost 1100 Chinese Yuan each (about $164.99) if manufacture in China. And a single REM tube cost $25 (purchased from Canada). That makes the demo unit cost about $190. If the larger test unit is also manufacture this way, we except the cost might be lower than hypothesis ($5000).

5.4 SBIR proposal

5.4.1 Executive Summary

Reactive electrochemical membrane (REM) is an emergent technology that offers a novel approach to small scale water purification and disinfection that could be useful for swimming pools, landscape water and small water treatment facilities without access to the capital needed for more traditional means of physical purification and chemical disinfection.

The potential end users or markets for this technology include, but are not limited to, membrane industries, manufacturers, water/wastewater treatment industries, biofuel industries, renewable energy, bioenergy industries as well as residential users. In our initial research, we performed the proof of the concept studies verifying the impacts from REM filtration on pollutant removal (e.g., algal cells) and water quality purification. As our REM system addresses common challenges of water purification and bioseparation, we plan to include additional extensive market surveys and research into a broader spectrum of potential users (e.g., food processing, drinking water treatment, and biomolecule purification) in addition to algal separation or biofuel industries of this work. The value of this technology includes: (1) the membrane filtration technology is free of chemicals, which will save operation costs; (2) it is less vulnerable to fouling and backwash cleaning, which will save energy, cost and reduce overall downtime; and (3) it is easy to install, scale up and flexible to adapt to both small- and large-scale systems without much maintenance.

We have published this research[176] and filed for a provisional patent. In addition, we have initiated collaborations with several entities and will continue to expand our industry collaborations of this commercialization. Second, we have obtained funding from NSF I-Corps which fosters entrepreneurial leadership and skills to commercialize our technology to the market. In this effort, we have established connections with industry mentors, including Joseph G. Stanley, Vice President of Hatch Mott MacDonald, an internationally acclaimed Water Engineering firm and Yuhong Jiang, President of BRISEA Group, which is dedicated in providing environmental and energy professional services, technology and know-how transfer from USA to the developing nations. They will

continue to mentor us with invaluable feedback and advice toward marketing and commercialization.

REM-Ark (a tentative firm name) designed, optimized, and constructed a prototype REM that built upon existing research, making a water purification and disinfection system that is more safe, eco-friendly and cost effective. The final prototype consists of a cell casing made of Polytetrafluoroethylene (PTFE), a reactive electrochemical membrane served as filter and anode, a cylinder-shaped stainless steel mesh as cathode, two pump systems connecting raw water container, REM unit and clean water container by vinyl tubes and a direct current (DC) generator that provides adjustable electric power to REM unit by necessary wires. REM-Ark also designed a simplified and inexpensive mobile platform for on-site convenience.

The functional prototype produces flow rate of 57.6 mL·h^{-1} under 10 psi pump pressure, provides purified and disinfected water and 90 days of use before the REM must have backwash, is portable, operates on a feed obtainable by the user, and proves the validity of the concept of using an REM for safe, inexpensive, small scale water purification and disinfection. The flow rate output of the system can be improved 100 to 1,000 times that of this prototype by the addition of multiple tubular REM and pump with higher pressure. Further research is needed with these cases before implementation; however, this research is beyond the scope of REM-Ark's project.

5.4.2 Anticipated Benefits

This technology represents a potentially game-changing filtration technology that is designed to improve disinfection safety, separation efficiency, lower fouling potential

(increased durability and stability), higher fluxes of water permeate and pre-oxidation of organic substituents and biomass if desirable for downstream processing. We will leverage these unique advantages to secure potential off-take agreements with membrane, biofuel, and water/wastewater industries. The substantial commercial impacts are expected on end users or markets in, but not limited to, membrane industries, manufacturers and users for water/wastewater treatment industries and algae biofuel industries, renewable energy, bioenergy industries. REM technologies holds promise to transform current physical filtration processes from a chemically inert system to chemically reactive systems that proactively filter out water with well-defined reactions or reactivity on filter surfaces. In the long term, reactive ceramic membranes, due to their flexible surface modifications and a longer lifetime compared to widely used polymer membranes, will reduce filtration operational cost and increase process sustainability.

5.4.3 Responsiveness to SBIR Program Priorities

Membrane filtration is one of the most efficient processes for biomass separations and water purification. However, traditional membrane separations suffer from membrane fouling due to either the formation of a cake layer of algal cells, or more commonly due to organic matter adsorption onto the membrane surface. We designed a novel technique to mitigate membrane surface fouling through electrochemical oxidation powered by anodic polarization under a DC current. This invention demonstrated an innovative and multifunctional reactive electrochemical membrane (REM), to act as a model filtration membrane that exhibit great antifouling characteristics and strong surface reactivity. The REM surface acts as both filter and electrode that separate microbes and soluble organic compounds from water and enable water purification in addition to disinfection.

Prior NSF award(s): (1) NSF I-Corps Site grant (2015 Fall-2016 spring); (2) The NSF CBET grant in Chemical Biological Separation program starting from fall 2016.

5.4.4 Technical Objectives

5.4.4.1 Affectivity.   This project is intended to demonstrate the creation of a safe and environmental-friendly method of purification and disinfection. To accomplish this objective, the design must at least produce a standard quality of product water during its operation.

5.4.4.2 Size.   In order to fulfill the design considerations for the intended customers, the working prototype must be transportable from one location to another. Therefore, the size and mobility of the prototype must promote reasonable portability.

5.4.4.3 Cost efficiency.   The tubular membrane used under research conditions for separation is typically for limited flow rate and needs long time synthesize with significant supply consumption. In order to produce a prototype that promotes use in the intended market, REM-Ark must design a membrane that is comparably effective as the laboratory membrane, which should be inexpensive, and can be manufactured with large scale for high flow rate demand.

5.4.4.4 Lifetime.   The design of a final prototype must take into consideration means by which to maximize the functional lifetime of the REM. The prototype REM should be able to last for one year with minimal user intervention or maintenance.

5.4.4.5 Flow rate. The goal set forth by this project is to build upon existing research and improve upon the accomplishments published to date. Since many other objectives have an effect on flow rate, the project goal is to produce at least a comparable flow rate to the least real-life demand.

5.4.5 Design

5.4.5.1 Projected Customers

5.4.5.1.1 Profile. Because of the same purification and disinfection effect, less chemical requirement, low operating costs, low maintenance cost, and low flow rate output associated with a REM system, REM-Ark's main market is focused on the owners and operators of swimming pools and landscape water, especially (1) General Managers, Chief Engineers, Director of Engineering and Director of facilities in hotels and fitness centers; (2) Certified Pool Operator (CPO) of public pools and schools; (3) residential pool owners and designers.

5.4.5.1.2 Resources. Limited resources are available for the construction and maintenance of the REM system in the range of projected use. Since the projected use of the REM system is for people with little engineering background, designing a prototype while maintaining a low cost will result in a much broader impact. The materials for building REM systems should be readily available or easily obtained, inexpensive and simple to construct.

5.4.5.2 Design Norms

5.4.5.2.1 Trust. Gaining the trust of any customer who would purchase and operate an REM system is an important design norm that impacted the prototype design of this

project. Having a reliable disinfection ability and enough capacity are crucial especially when it is the only filtration device available, as the REM system would be for nearly all of the projected customers. Unexpected failures could result in lost time, expensive repairs, frustration by the consumer. If the REM system is not dependable, potential clients will not invest in the technology, rendering the REM ineffective in fulfilling the customer's needs.

5.4.5.2.2 Design Transparency.   The design process of the REM system should be carefully documented. This documentation makes the expressed results reproducible from the documented research and experiments, so further testing and optimization could build upon this research. Aside from replication, this design needed to be transparent so that users can understand the functionality of the product and are able to maintain and use the product to its full potential.

5.4.5.3 Current Design

5.4.5.3.1 Overview.   The first prototype includes a four-compartment design (Figure 5.8). The prototype is designed to be fully enclosed to minimize the bacteria and TDS in the product clean water and provide minimal water head for small scale pool. The design incorporates mobile platform that allows the prototype to be transported easily without dismantling.
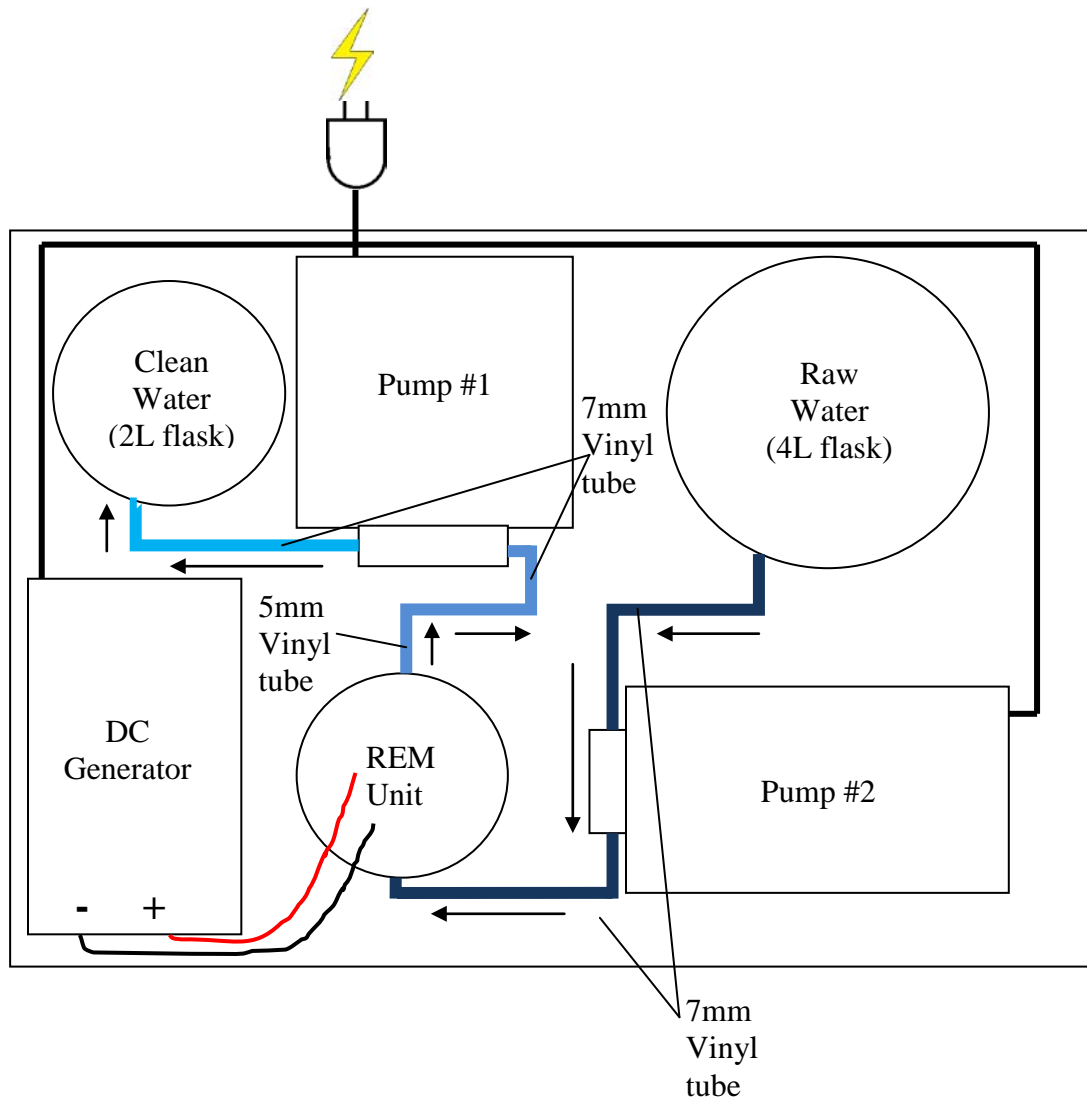
Figure 5.8 First prototype design of REM system.

5.4.5.3.2 Design Component Descriptions. REM Unit is the key component of the entire system (Figure 5.9). Tubular REM anode is attached with stainless steel tube on top for electric connection and water flow, which is sealed on both end with PTFE and waterproof glue. REM is surrounded by cylinder-shaped stainless steel mesh cathode and placed in a PTFE chamber. The chamber has pre-drilled holes for electric wires and vinyl tubes.
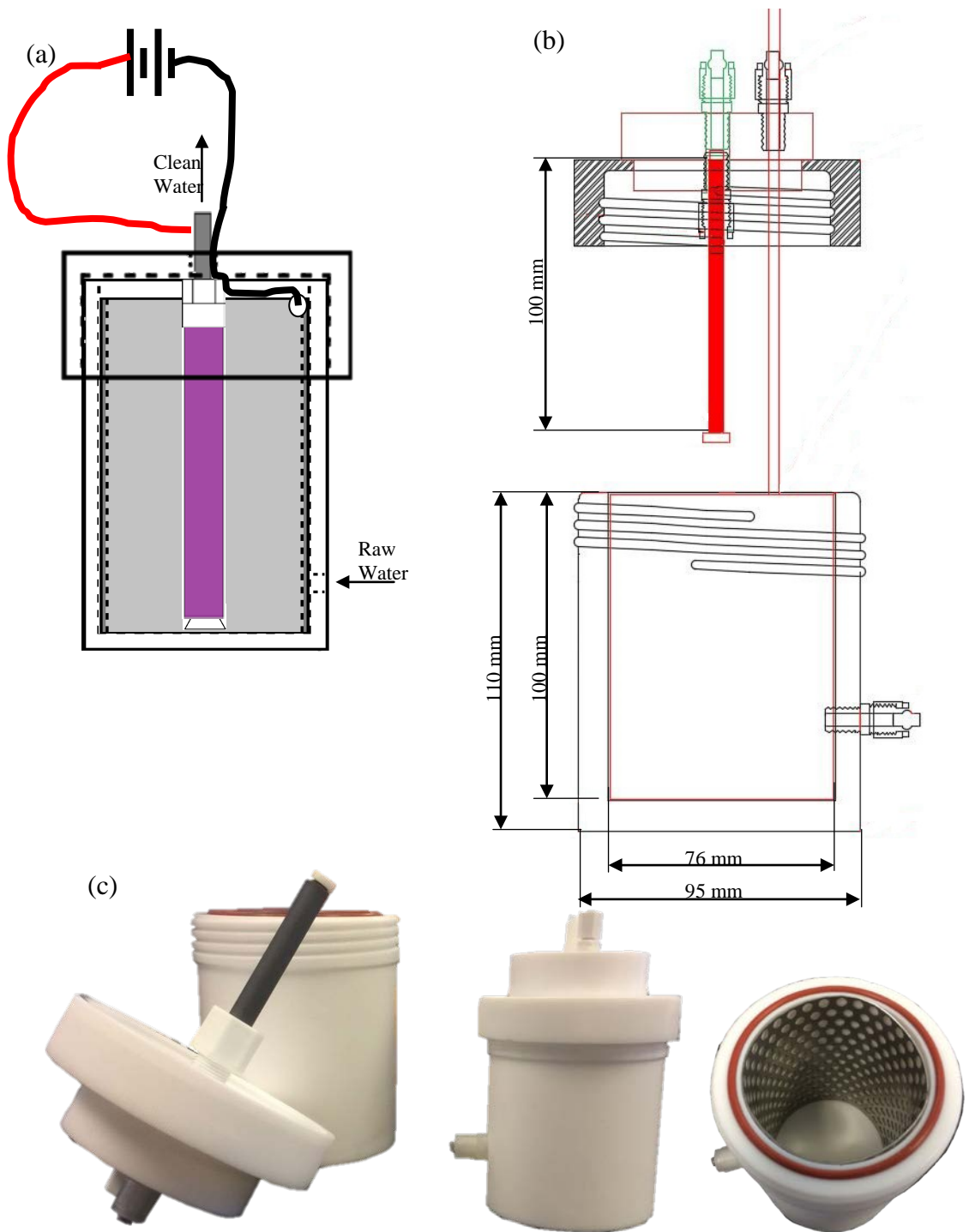
Figure 5.9 (a) Schematic of REM unit; (b) size of module parts; (c) photos of REM parts.

5.4.6 Budget and schedule. Budget information is still under discussion. It will be finished after further contact with our partners.

5.5 Conclusion

This NSF I-Corps project allowed us to comprehensively understand the basis steps and principles of business development, technology transfer and market analysis. In this project, we conducted intensive customer interviews (more than 130 interviews) that covered different sectors of industries such as pure water companies, bottle beverages, swimming pools, landscape water management, chemical processing, pharmaceutical factory, water and wastewater treatment, medical and hospital facilities, and aquarium. Significant and valuable feedbacks were obtained and aided us in the complete business canvas development and some of the key hypothesis validation.

The original value proposition is three fold:

(1) REM filtration system has a longer lifetime than traditional filters along with additional microbial suppression/removal, which will reduce daily cost for water treatment industries and other pure water production facilities such as beverage, food processing companies;

(2) REM filtration system provides high selective filtration that is needed for separating specific compounds or biomolecules from the biomass feedstock, which will increase the production efficiency and lower the risk of defective products for chemical separation industries such as petroleum processing and pharmaceutical industries.

(3) REM filtration system could provide high purity water for semi-conductor and electronic device manufacturers, which reduce the product defect and recall cost. Later a

major pivot was made after the initial 30 customer interviews with local water treatment plants, pharmaceutical factory and beverage companies in Dallas, Texas in January 2017. The interview results indicate that our major value proposition did not meet the pain point of the customer segments.

The new segment of swimming pools and landscape water treatment markets were found and validated in the following interviews. A new value proposition for this new segment was that the REM filtration system could increase water quality and safety (reduce toxic chemical usage such as Cl_2 and also eliminate odor issues) and will reduce daily cost in backwash or chemical cleaning by at least 50% for swimming pools and landscape water. Over 50 interviews with swimming pools owners validated the hypothesis that our product could solve the safety and odor issues coming from the use of chlorine as their major disinfection chemical. The other 20 interviews were conducted with the aquarium suppliers in San Francisco, the USA, invalidated the hypothesis on the potential use in aquarium equipment markets. The ecosystems in the aquarium fish tanks require proper microbes that could be totally removed or inactivated by the reactive filtration systems. The rest of the interviews were focused on channels, key partners and customer relationships. Based on these interview activities, we have pinpointed the most possible areas of industries that may find value propositions from our presented technology. These industries we will focus on the future commercialization process include landscape water quality management, swimming pools and small water treatment facilities (e.g., residential end-point water filtration devices).

We have successfully developed partnership with a technology transfer company (Brisea Group Inc.), located in New Jersey, to jointly promote the commercialization

process (e.g. product design, investment). We have filed non-disclosure agreement (NDA) between NJIT and Brisea. Meanwhile, we have submitted a SBIR type proposal to Shell Company in June, 2017 and also actively prepare another SBIR proposal (see section 5.4 above) to be submitted to NSF and other agencies. Several internal small grants at NJIT (e.g., URI phase I and phase II grants) were raised for building three demo units.

Intellectual Merit. Our current NSF research project (Award Number: 1603609) investigates the multifunctional REM and its synergies in separation of algae as a model microorganism, fouling mitigation, water purification, and cell destabilization and pretreatment. Scientific merits include (1) development and testing of a suite of tailored REMs for efficient biomass separation; (2) evaluation of permeate water quality and removal of water contaminants; (3) elucidation of underlying mechanisms of electrochemical oxidation and contribution to antifouling and high flux properties. The results will not only provide fundamental guidelines as to the rational design of REMs with controlled and efficient performance, flexible structure, and durability of operation for algal separation, but also leads to an avenue for the development of a new generation of reactive membranes. This NSF I-Corps project further enabled us to explore the industrial applications, identify current challenges, problems, and alternative solutions from customer interviews. A number of value proposition hypotheses were proposed and tested through interactions with customers from different industrial segments to achieve new insight into the development of next-generation membrane filtration technologies: for example, a matrix of economic tradeoffs between existing capital and operating costs versus capital and operating costs of REM specifically for different source waters.

Broader Impacts.   Membrane filtration is one of the most efficient processes for separations and water purification. However, traditional membrane separations suffer from membrane fouling due to the formation of foulant layers that may consist of organic matters, biomass debris, salt, and various trapped substances. On the other hand, water disinfection are highly rely on Chlorine or similar chemicals (e.g., hypochlorite and bromine) especially for drinking water plants and swimming pools, which may have hidden safety issue and harm human health. We designed, optimized, and constructed a novel filtration technique to mitigate membrane surface fouling through electrochemical oxidation powered by anodic filter polarization under a DC current. This invention was built upon existing research, making water purification and disinfection system that is more safe, eco-friendly and cost effective. The reactive electrochemical membrane (REM) technology holds a great potential to upgrade current membrane filtration systems that simply rely on physical separation and catalyze many other transformative industrial applications. For example, REM offers a novel approach to small scale water purification and disinfection without using chlorine, which could be useful for swimming pools, landscape water and small water treatment facilities without access to the capital needed for more traditional means of physical purification and chemical disinfection.

In the pursuit of more safe, efficient, flexible, durable, and sustainable membrane technologies, this work will greatly extend REM technologies to many potential areas or fields where high purity water is produced; biomass or biomolecules need to be separated. The research findings will lead to rational designs of REMs with controlled and efficient performance, flexible design, and durability of operation, which therefore radically change and advance the fields of biomass separation and water treatment. Moreover, the

project trains and mentors graduate students and a large number of undergraduate and senior high school students from female and underrepresented groups in STEM. Students represent the future leaders of engineering and science, and their participation in this project will help prepare them for careers in sustainable engineering and establish business development skills. Finally, the substantial commercial impacts are expected on end users or markets in, but not limited to, membrane manufacturers and users for swimming pools, landscape water and small water treatment facilities. In the long term, reactive ceramic membranes have the advantage of higher disinfection safety, higher separation efficiency and lower fouling potential comparing with the traditional filtration-disinfection method. Additionally, due to their flexible surface modifications and a longer lifetime compared to widely used polymer membranes, they will reduce filtration operational cost and increase process sustainability.

The broader impact/commercial potential of this I-Corps project is the commercialization of a potentially game-changing filtration technology based on the synergistic electrochemical reactions created on membrane surfaces. Membrane filtration is indispensable for a wide spectrum of industrial applications such as swimming pools, landscape water and small water treatment facilities.. This project will provide filtration users the value propositions in increasing safety, decreasing the use of hazardous chemicals (chlorine and others) and saving capital costs on membrane cleaning, maintenance, replacement as well as high quality products (e.g., filtered water). This project will also impact membrane manufacturers by increasing the demand for multifunctional and reactive membranes in the global market of membrane filtration, which is estimated to reach $2.64 billion by 2018. Therefore, the ultimate goal of this

project is to upgrade and transform current membrane industries from traditional physical filtration into advanced and chemically reactive membrane systems. This process will also lead to new business opportunities and foster workforce development.

APPENDIX

A.1 MATLAB CODE FOR CALCULATIONS

A.1.1. Matlab Code for Figure 3.17 (calculation and simulation of permeate flow rate, Q and cake layer resistance, R_c, under different experimental conditions)

A.1.1.1 Calculation of ExpQ by linear interpolation method from experimental data

% GetEXPQ is a function based on Interpolation fitting (spline function) to calculate the

derivative of discrete points at any point.

% Example:

%   n = length(t);

%   for i=1:n

%   EXPQ(i) = GetEXPQ (t, V_t, t(i));

%   end

%   Typing the code above, will get a row vector with experimental flow rate (EXPQ),

the input parameters, t and V_t, .

function EXPQ=GetEXPQ(t,V_t,T)

% T is the time points that users are interested to determine the flow rates at.

% creat two points, M(1) & M(2) with tiny distance

M(1)=T-0.001;

M(2)=T+0.001;

% calulate the slop of two points, and obtain the final value we wanted.

diffy=spline(t,V_t,M(1))-spline(t,V_t,M(2));

diffx=M(1)-M(2);

EXPQ=diffy./diffx;

A.1.1.2 Calculation of C_w

% findCw is a function to calculate one of the unknown parameter C_w.

% Example:

% C_w=findCw (t, V_t, EXPQ, DeltaP, R_ir, mu, R_m, C_b, A);

% Typing the code above, will get a row vector with Volume concentration of particles at

the membrane surface (C_w) with the input parameters as defined in file "model equation

for deadend" .

```
function C_w=findCw(t,V_t,EXPQ,DeltaP, R_ir, mu, R_m, C_b, A)
```

% n: the number of data.

 n = length(t);

% initialize vecter k_c, R_c and C_w with zero value in 1 row and n column

% mixtra

% k_c: Specific resistance per unit of cake thickness (m^?2)

% R_c: Reversible fouling resistance or resistance of the cake layer (m^?1)

% C_w: Volume concentration of particles at the membrane surface (%)

 k_c = zeros(1,n);

 R_c = zeros(1,n);

 C_w = ones(1,n);

 % step 1 : get k_c vector, corresponds to equation (4-1) in file "model equation for

deadend"

for loopp=1:n

    k_c(loopp) = 2*DeltaP*A^2*(t(loopp)/V_t(loopp) -

(R_m*mu)/(DeltaP*A))/(C_b*mu*V_t(loopp));

end

% step 2 : get R_c vector, corresponds to equation (3-1) in file "model equation for

deadend"

for loopp=1:n

    R_c(loopp)=(A*DeltaP)/(mu*EXPQ(loopp))-R_m-R_ir;

end

%step 3: get C_w vecter, corresponds to equation (4-2) in file "model equation for

deadend"

for loopp=1:n

  C_w(loopp)=(2*k_c(loopp)*DeltaP*C_b*t(loopp)/mu)/((R_c(loopp)+R_m)^2-

R_m^2);

end

A.1.1.3 Calculation and simulation of permeate flow rate

% Experimental data of permeate volume (V_t), expressed as cubic meter, and time (t), expressed as second, must be

% entered in excel in column vectors. "filename" in the code refers to the name of excell dataset of V_t and t.

% Input: DeltaP: Transmembrane pressure (Pa)

% Input: r: Backwash efficiency (bewteen 0-1)

% Input: R_ir: Backwash irreversible resistance (m^-1)

% output: Q, which is the data of fitted flow rates by varying Cw

% output: EXPQ, which is MATLAB-calculated flow rate from the Vt data

% output: C_W, which is the Cw parameter

% output: Rmax is the correlation coefficient, R2

%Typing the code below in MATLAB will yield several row vectors with simulated flow rate (Q), experimental flow rate (EXPQ), and input data: time& Permeate volume (t, V_t).

function [t,V_t,Q,EXPQ,C_w,Rmax]=Membrane_deadend(filename, DeltaP, r, R_ir, mu, R_m, C_b, A, C_w)

% the following three lines are to determine if it is a first round of filtration without prior membrane filtration (R_ir=0), if not, we need to change the value of R_ir

```
if R_ir ~= 0

   R_ir = (1-r)/r*R_m+R_ir;

end
```

```
% read experimental data of V and t from excel file; number is the matrix exported from
excel file with a name of "filename"
number=xlsread(filename);
```

```
% Extract variables t and V_t from number matrix
t=number(:,1)';
V_t=number(:,2)';
```

```
% n is the number of data
n = length(t);
```

```
% Use the fitted function of V and t to derive a smooth function of flow rate Q and t.
EXPQ=zeros(1,n); % Define the EXPQ vector with value of 0 in the first row and n
column matrix.
for loopp=1:n
   EXPQ(loopp)=GetEXPQ(t,V_t,t(loopp)); % the function (GetEXPQ) could calculate
the value of the experimental flow rate at point time =t(loopp)
end
```

```
if strcmp(C_w,'unknown')

% findCw is a function to determine the value of C_w; see details in the findCw code.

    VecterC_w=findCw(t,V_t,EXPQ,DeltaP, R_ir, mu, R_m, C_b, A); %VecterC_w is a

matrix or vector for all possible C_w


% In the following ten lines we find the best value of C_w by fitting experimental and

calculated V_t at different t

Rmax=0; % Rmax is the variable to memorize the value of R^2, when meet a best value

of C_w.

flag=1; % flag is the subscript of the best C_w value.

for loopp=1:n

    R=compare(t,V_t,EXPQ,DeltaP, R_ir, VecterC_w(loopp),mu, R_m, C_b, A, n); % R

is the correlation coefficient, R^2

% compare the calculated R with Rmax.

    if R>Rmax

        Rmax=R;

        flag=loopp;

    else R=0;

    end

end

C_w = VecterC_w(flag); % the best value of C_w

end

% get the value of Q vecter, the fitted flow rates with t.
```

```matlab
Q = formula_deadend(t,V_t,DeltaP, R_ir, C_w, mu, R_m, C_b, A,n);

R=R_Coefficient(Q,EXPQ);
```

A.1.2. Matlab Code for Figure 3.26 (calculation and simulation of cake layer resistance, R_c, under different experimental conditions)

```matlab
clc;clear;


number =  xlsread('datafile');%read expeirmental data from excel file named 'datafile'

t = number(3:80:10000,1 );%filtration time (s)

V_t = number(3:80:10000,6); %accumulative volume of filtrate or permeate (m^3)

J_0= number(3,11); % Initial flux (m3·m-2·s^-1)

J_s=number(120,11); %Flux at steady state (m3·m^-2·s^-1)


%enter experimental data below

TMP = 68947.6;%TMP (Pa)

A = 4 * 10^-3;%the membrane surface areas (4×10^-3 m^2).

mu = 8.9 * 10^-4;% dynamic viscosity of water at 25 oC (0.8937 ×10^-3 Pa·s).

R_ir = 0; %irreversible fouling resistance

R_m = 3 * 10^11;% the intrinsic resistance of the membrane  ,(m^-1)

C_b = 0.001; %Cb is the algal concentration in the bulk suspension (%).


for i = 1: length(t)

   %Calculation of Q(m3·s^-1)
```

```
M1(i)=t(i)-0.001;

M2(i)=t(i)+0.001;

diffy1(i)=spline(t,V_t,M1(i))-spline(t,V_t,M2(i));

diffx1(i)=M1(i)-M2(i);


Q(i)=diffy1(i)/diffx1(i);


%calculate the cake resistance R_c
R_c1(i) = A * TMP / (mu*Q(i)) - R_m - R_ir;
```

%calculate the specific resistance per unit of cake thickness (m^{-2})

```
k_c1(i) = (t(i)/V_t(i) - mu * R_m / (A * TMP)) * (2 * A^2 * TMP) / (mu * C_b *
V_t(i));
```

```
%calculate the cake layer thickness delta_c
delta_c1(i)= R_c1(i)/k_c1(i);
```

%calculate the cake growth rate constant ($m \cdot s^{-1}$)

```
k_cr1(i)=-TMP/(J_s*mu*k_c1(i)*t(i))*log(1-(J_s*mu*k_c1(i)*delta_c1(i)/(TMP-
J_s*mu*R_m)))-delta_c1(i)/t(i);
```

```
 %the wall concentration of algal, Cw, (%).
C_w1(i) = (J_s*C_b*J_0/(J_0-J_s))/k_cr1(i);
```

```
        i = i+1;


end


% Subtract the real numbers of the calculated k_c and C_w and designated as new
vectors realk_c and realC_w
realk_c=k_c1(imag(k_c1)==0);
realC_w=C_w1(imag(C_w1)==0);


%calculate the mean value of output realk_c and realC_w;
k_c = mean(realk_c(16:110)); % Specific resistance per unit of cake thickness (m⁻²)
C_w = mean(realC_w(31:95)); % Volume concentration of algae at the membrane
surface (%)



% Calculate k_cr using given C_w
k_cr=J_s*C_b*J_0/((J_0-J_s)*C_w);% Cake growth rate constant (m·s⁻¹)



% Denote complex terms
AT = TMP/(J_s*mu*k_c*k_cr);
BT = J_s*mu*k_c/(TMP-J_s*mu*(R_m+R_ir));
```

$k\_c = mean(realk\_c(16:110));$ % Specific resistance per unit of cake thickness (m^{-2})

$k\_cr=J\_s*C\_b*J\_0/((J\_0-J\_s)*C\_w);$ % Cake growth rate constant ($m·s^{-1}$)

```matlab
% Denote delta_c as a matrix

Delta_c = zeros(length(t),2);

% Use solve function to calculate the delta_c;

for i = 1:1:length(t)


ti = t(i);

syms delta_c

delta_c = solve((ti + AT*log(1-BT*delta_c) + delta_c/k_cr) == 0,delta_c);

Delta_c(i,:) = double(delta_c);

end


R_c = k_c * Delta_c(:,2);


plot(t,R_c);title('R_c vs t');xlabel('t');ylabel('R_c');grid;


%manually change the file name output (Rc, kc and Cw):


csvwrite('R_c10psi-100mA.csv',R_c);

csvwrite('k_c10psi-100mA.csv',k_c);

csvwrite('C_w10psi-100mA.csv',C_w);
```

```matlab
1 -    clc;clear;
2
3 -    number =  xlsread('datafile');%read expeirmental data from excel file named 'datafile'
4 -    t = number(3:80:10000,1 );%filtration time (s)
5 -    V_t = number(3:80:10000,6); %accumulative volume of filtrate or permeate (m3)
6 -    J_0= number(3,11); % Initial flux (m3*m-2*s-1)
7 -    J_s=number(120,11); %Flux at steady state (m3*m-2*s-1)
8
9      %enter experimental data below
10 -   TMP = 68947.6;%TMP (Pa)
11 -   A = 4 * 10^-3;%the membrane surface areas (9.8×10-3 m2).
12 -   mu = 8.9 * 10^-4;% dynamic viscosity of water at 25 oC (0.8937 × 10-3 Pa·s).
13 -   R_ir = 0; %irreversible fouling resistance
14 -   R_m = 1 * 10^11;% the intrinsic resistance of the membrane   ,(m-1)
15 -   C_b = 0.001; %Cb is the algal concentration in the bulk suspension (%).
16
17 - ┌ for i = 1: length(t)
18   │      %Calculation of Q(m3/s)
19 - │      M1(i)=t(i)-0.001;
20 - │      M2(i)=t(i)+0.001;
21 - │      diffy1(i)=spline(t,V_t,M1(i))-spline(t,V_t,M2(i));
22 - │      diffx1(i)=M1(i)-M2(i);
23   │
24 - │      Q(i)=diffy1(i)/diffx1(i);
25
26   │      %calculate the cake resistance R_c
27 - │      R_c1(i) = A * TMP / (mu*Q(i)) - R_m - R_ir;
28   │
29   │      %calculate the specific resistance per unit of cake thickness (m-2)
30 - │      k_c1(i) = (t(i)/V_t(i) - mu * R_m / (A * TMP)) * (2 * A^2 * TMP) / (mu * C_b * V_t(i));
31   │
32   │      %calculate the cake layer thickness delta_c
33 - │      delta_c1(i)= R_c1(i)/k_c1(i);
34   │
35   │      %calculate the cake growth rate constant (m?s-1)
36 - │      k_cr1(i)=-TMP/(J_s*mu*k_c1(i)*t(i))*log(1-(J_s*mu*k_c1(i)*delta_c1(i)/(TMP-J_s*mu*R_m)))-delta_c1(i)/t(i);
37   │
38   │       %the wall concentration of algal, Cw, (%).
39 - │      C_w1(i) = (J_s*C_b*J_0/(J_0-J_s))/k_cr1(i);
40   │
41 - │          i = i+1;
42   │
43 - └ end
44
45     % Subtract the real numbers of the calculated k_c and C_w and designated as new vectors realk_c and realC_w
46 -   realk_c=k_c1(imag(k_c1)==0);
47 -   realC_w=C_w1(imag(C_w1)==0);
48
49     %calculate the mean value of output realk_c and realC_w;
50 -   k_c = mean(realk_c(16:110)); % Specific resistance per unit of cake thickness (m-2)
51 -   C_w = mean(realC_w(31:95)); % Volume concentration of algae at the membrane surface (%)
52
53
54     % Calculate k_cr using given C_w
55 -   k_cr=J_s*C_b*J_0/((J_0-J_s)*C_w);% Cake growth rate constant (m*s-1)
56
57
58     % Denote complex terms
59 -   AT = TMP/(J_s*mu*k_c*k_cr);
60 -   BT = J_s*mu*k_c/(TMP-J_s*mu*(R_m+R_ir));
61
62     % Denote delta_c as a matrix
63 -   Delta_c = zeros(length(t),2);
64     % Use solve function to calculate the delta_c;
```

254

```
65 -    ☐for i = 1:1:length(t)
66
67 -        ti = t(i);
68 -        syms delta_c
69 -        delta_c = solve((ti + AT*log(1-BT*delta_c) + delta_c/k_cr) == 0,delta_c);
70 -        Delta_c(i,:) = double(delta_c);
71 -      └end
72
73 -      R_c = k_c * Delta_c(:,2);
74
75 -      plot(t,R_c);title('R_c vs t');xlabel('t');ylabel('R_c');grid;
76
77        %manually change the file name output (Rc, kc and Cw):
78
79 -      csvwrite('R_c10psi-100mA.csv',R_c);
80 -      csvwrite('k_c10psi-100mA.csv',k_c);
81 -      csvwrite('C_w10psi-100mA.csv',C_w);
```

Detailed explanations for each line

Line 1: Clear all data

Line 3: Read experimental data from excel file named 'datafile' that contains the volume of permeate at time t.

Line 4: t is the filtration time (s) that is extracted from in the excel 'datafile'; 1 means data was extracted from the first column; 3 means the vector t started from 3rd cell because the 1st and 2nd row were left for item name and units; 10,000 means the data ended in 10,000 unit cell because the experiment ends in 2500s and each cell was 0.25s; 80 means the data was selected from each 80 cell to avoid too much similar data in short time interval.

Line 5: V_t is the accumulative volume of filtrate or permeate (m^3) under different DC conditions extracted from column 2 to 6; so the number 6 in (3:80:10000,6) may vary depending which column data is to be extracted.

Line 6: J_0 is the initial permeate flux value ($m^3 \cdot m^{-2} \cdot s^{-1}$), (3,11) means the 3rd cell in the 11th column, which may vary depending which column data is to be extracted.

Line 7: J_s is the permeate flux value at steady state ($m^3 \cdot m^{-2} \cdot s^{-1}$), (120,11) means the 120th cell in the 11th column, which may vary depending which column data is to be extracted

Line 9 to line 15: enter experimental data:

Line 10: Input transmembrane pressure value (TMP, 68947.6 Pa in this study),

Line 11: Input membrane surface area value (A, 0.004 m^2 in this study)

Line 12: Input dynamic viscosity of water at 25 ^{o}C (mu, 8.90×10^{-4} Pa·s in this study)

Line 13: Input irreversible fouling resistance (R_ir = 0 in this study, because only single cycle was tested)

Line 14: Input the intrinsic resistance of the membrane (R_m = 1×10^{11} m^{-1} from the experiment data in **3.3.2.1**)

Line 15: Input the algal concentration in the bulk suspension (C_b = 0.001% in this study).

Line 19 to line 24: Calculation of permeate flow rate (Q in m^3·s^{-1}), where spline function was used to obtain the derivation from the relation of t and V_t.

Line 27: Calculate the reversible resistance (R_c1) directly from experimental data (Q, TMP, R_m and R_ir) without fitting.

Line 30: Calculate a set of specific resistance per unit (k_c1) of cake thickness (m^{-2}) from R_c1.

Line 33: Calculate a set of cake layer thickness delta_c from k_c1 and R_c1.

Line 36: Calculate a set of cake growth rate constant k_cr1 (m·s^{-1})

Line 39: Calculate a set of cake (algal) concentration on the membrane wall, C_w1, (%).

Line 46 to line 47: Subtract the real numbers of the calculated k_c and C_w and designated as new vectors realk_c and realC_w. (Because there were imaginary numbers in k_c1 and C_w1 sets)

Line 50 to line 51: Calculate the mean value of output realk_c and realC_w sets. The output value of k_c and C_w were used as model parameters.

Line 55 Calculate cake growth rate k_cr using given C_w

Line 59 to line 60: Denote complex terms

AT = TMP/(J_s*mu*k_c*k_cr);

BT = J_s*mu*k_c/(TMP-J_s*mu*(R_m+R_ir));

Line 62:   Denote delta_c as a matrix

Line 65 to line 70: Use solve function to calculate the delta_c

Line 73: Calculate fitted R_c;

Line 75: plot t verse R_c relationship;

Line 79 to 81: output csv files for t verse R_c relationship, fitted C_w and k_c, file names were manually changed.

A.2 Certification requirement

A.2.1 National Sanitation Foundation (NSF) and American National Standards Institute (ANSI)

A.2.1.1 NSF/ANSI 61.   If we manufacture, sell or distribute water treatment or distribution products in North America, our products are required to comply with NSF/ANSI 61: Drinking Water System Components – Health Effects by most governmental agencies that regulate drinking water supplies. NSF will assign us a project manager as a single point of contact to guide us through the certification process and oversee our certification project every step of the way.

Certification Process:

1. Our company submits an application.

2. We provide product formulation, toxicology and product use information.

3. NSF toxicology department reviews formulations.

4. NSF performs a plant audit and sample collection.

5. NSF laboratory conducts testing.

6. NSF completes a final toxicology evaluation.

7. NSF grants certification for compliant products and we can use the NSF mark on products, packaging and marketing materials.

A.2.1.2 NSF/ANSI 419. NSF/ANSI 419 (Public Drinking Water Equipment Performance – Filtration) is an NSF/ANSI national standard for microfiltration (MF) and ultrafiltration (UF) membrane modules, as well as bag and cartridge filter systems. This standard establishes performance testing protocols that are consistent with the product-specific microbial challenge testing requirements for Cryptosporidium removal credits under the U.S. EPA Long-Term 2 Enhanced Surface Water Treatment Rule (LT2 Rule).

NSF/ANSI 419 allows for a Cryptosporidium removal performance certification to accompany certification to NSF/ ANSI 61, which covers health effects certification for wetted materials.

A.2.2 American Society of Mechanical Engineers (ASME)

The purpose of the review/survey is to evaluate the applicant's quality manual and the implementation of the quality program. The extent of the review/survey will be determined by ASME based on a review of the applicant's intended scope of activities as described in the application.

This assessment ensures that the applicant's quality program has been adequately implemented and that it complies with the requirements in the associated ASME

standard. When the assessment has been completed, the review/survey team leader will submit a written report to ASME. A certificate will be granted by ASME only after the applicant successfully demonstrates the implementation of their quality program to the ASME review/survey team. After ASME reviews the report submitted by the review/survey team, the Society will either authorize the issuance of the certificate or request additional action by the applicant. Certificate holders may request changes to their certificate(s) after issuance. Certification Process is shown in **Figure 6.1**.
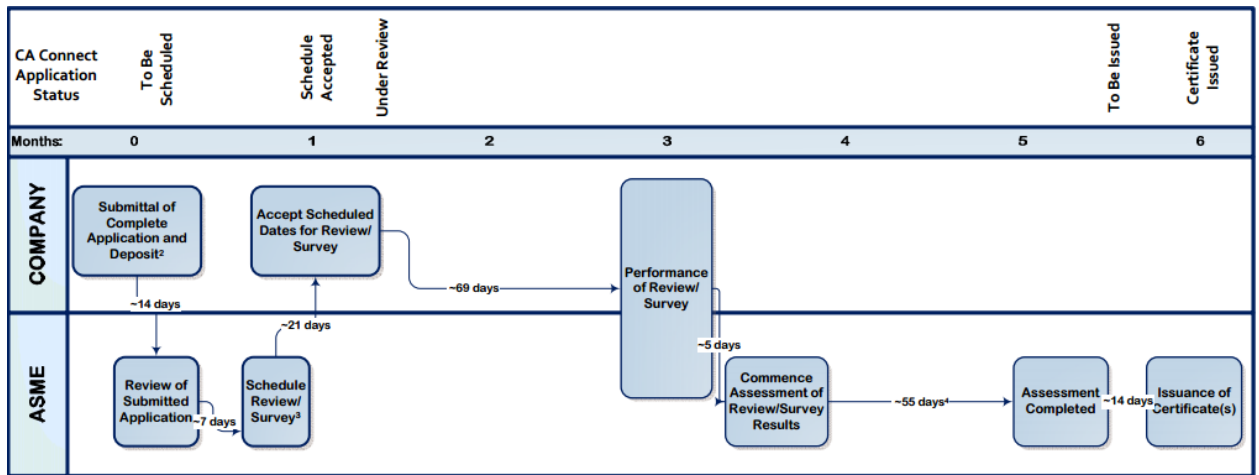
Figure A.1 Certification Process and timeline.

A.3 Interviewee information

The information of some major interviewees is summarized in Table A.1.

Table A.1 Interviewee information

Interviewee's name and title	Company's name	Contact (phone or email; address)	Segment
Kelli Armstrong, owner	JBC Water Treatment Company	support@jbcwatertreatment.com (972)-740-7153	Water Treatment Company
Emily Osta, Administrative Coordinator	Pharmaceutical Research & Consulting, Inc.	emily.osta@daac-prc.com (214) 361-5555	Pharmaceutical Company
Bill, Vanassa Joseph, Chris, Engineer	Trinity River Authority of Texas, Central Regional Wastewater System	(817) 467-4343	Wastewater Treatment Plant
Mark Hughes, Engineer	Aqua-Aerobic Systems, Inc.	mhughes@aqua-aerobic.com	Water Treatment Company (Supplier)
Peter Stencel	Dallas water utilities	peter.stencel@dallascityhall.com (214)670-0906	Water Treatment Company
Pablo Perez, Engineer, Sr. Program Manager	Nestle waters	Pablo.perzteshima1@waters.nestle.com (972)7804066	Beverage companies
Evan, Project manager	City of The Colony Wastewater Treatment Plant	(972)624-4412	Wastewater Treatment Plant
Elizabeth Yarus, Supervisor	Cook/Douglass Recreational Centre	(848)932-0711	Swimming pool owner
Frank, Engineer	Hilton garden inn	(855)618-4697	Swimming pool owner (Hotel)
Wilson, Pool supervisor	Hilton/Princeton	(609)720-0550	Swimming pool owner (Hotel)
Kevin, Chief engineer	Courtyard Marriott/Princeton	(800)207-5499	Swimming pool owner (Hotel)
Alpa Desai, General Manager	Hampton Inn, New Brunswick		Swimming pool owner (Hotel)

Table A.1 Continued

Gary Burrow, Manager	Monarch Dental	(214) 361-2227	Medical (Dental)
Jerry Pressley, Registered Engineering Manager and water reclamation and reuse division	Village Creek Waste Water Treatment Plant	jerry.pressley@fortworthtexas.gov	Wastewater Treatment Plant
Ovi Meret, Chief Engineer	Hightland Dallas Hotel	ovi.meret@thehighlanddallas.com	Swimming pool owner (Hotel)
Kui Zhou, President	Nanjing Suhuan Environmental Technology Development Co., Ltd	511356452@qq.com	Water Treatment Company (Supplier)
John Woodworth, Water Quality Control Officer	Mansfield water utilities	john.woodworth@mansfieldtexas.gov	Water Treatment Company
Sanjav Varma, General Manager	Wingate by Wyndham DFW North	varmazrus@gmail.com	Swimming pool owner (Hotel)
Juan Hurmdo, Chief Engineer	Fairfield Inn&Suites Marriott	(908)938-1550	Swimming pool owner (Hotel)
Daryl Coleman, Chief Engineer	Courtyard Marriott (Edison)	daryl.coleman@concordhotels.com	Swimming pool owner (Hotel)
Mihir Trivedi, General Manager	Holiday Inn	mtrivedi@friendwell.com	Swimming pool owner (Hotel)
Ismael Rivera, Chief Engineer	Hilton Garden Inn	ismael.rivera@hhmlp.com	Swimming pool owner (Hotel)
Jon Fuentes, Chief Engineer	Sheraton Hotel (Edison)	jo.fuentes@sheratonedison.com	Swimming pool owner (Hotel)
Brain F. Carr, Senior Project Engineer	Middlesex Water Company	bcarr@middlesexwater.com	Water Treatment Company
Jayantha, Chief Engineer	Crown Plaza (Edison)		Water Treatment Company
Clifton Pressley, Chief Engineer	Hilton Woodcliff Lake	clifton.pressley@columbiasussex.com	Swimming pool owner (Hotel)
Phil Lamberti, Chief Engineer	Westminster Hotel (Livingston)	plamberti@westminsterhotel.net	Swimming pool owner

Table A.1 Continued

Scott Woodruff, Director of Facilities	Hilton Pearl River	scott.woodruff@hilton.com	Swimming pool owner (Hotel)
Robert Smith, Chief Engineer	Hilton Garden Inn (Wayne)	RSmith@BuffaloLodging.com	Swimming pool owner (Hotel)
Hermes, Chief Engineer	Sheraton Mahwah Hotel	(201)529-1660	Swimming pool owner (Hotel)
Ron Hellwig, Chief Engineer	Courtyard Marriott (Wast Orange)	Ronald.Hellwig@marriott.com	Swimming pool owner (Hotel)
Luis Balderas, General Manager	The Club@HQ Plaza(Morristown)	(973)644-9590	Swimming pool owner (Fitness)
Ekatrina, pool supervisor and operator	Hilton Inn, New Brunswick		Swimming pool owner (Hotel)
Edda Arata, General Manager	Holiday Inn Express & Suites, New Brunswick		Swimming pool owner (Hotel)
Brian Kosa, General Manager	Glenpointe Spa & Fitness	bkosa@GlenpointeSpaandFitness.com	Swimming pool owner (Fitness)
Don Cosman, Chief Engineer	Hilton Garden Inn Ridgefield Park	Dcosman@hgiridgefieldpark.com	Swimming pool owner (Hotel)
Rachel Walker, Guest Services Manager	Hampton Inn by Hilton (Ridgefield Park)	RFPNJ.Hampton@gmail.com	Swimming pool owner (Hotel)
Carlos Alvarez, Chief Engineer	Crowne Plaza (englewood)	(201)871-2020	Swimming pool owner (Hotel)
George Hondros, Club Manager	24 hour fitness (Hasbrouck Heights)	cmclub654@24hourfit.com	Swimming pool owner (Fitness)
Brain Stevens, certified pool operator	YMCA of Greater Bergen County		Swimming pool owner (Fitness)
Gordon, Engineer (state certified)	Holiday Inn/Rahway-NJ	(732)541-9500	Swimming pool owner (Hotel)
Dewey M., shift engineer	Hilton Meadowlands	(201) 896-0500	Swimming pool owner (Hotel)
Karen P.	LA fitness (Kearny)		Swimming pool owner (Fitness)

Table A.1 Continued

Ryan Scott, Front office manager	Home2suites by Hilton/Rahway-NJ	(732)388-5500	Swimming pool owner (Hotel)
Ronnie, Pool supervisor	RJW Rahway fitness & wellness center at Carteret/Rahway-NJ	(732)541-2333	Swimming pool owner (Fitness)
Representative	In the Swim	(800)288-7946	Swimming pool supplier
Representative	Eco-lab	(800)352-5326	Swimming pool supplier
Helen Flores, Executive Director	YMCA / Livingston	hflores@metroymcas.org	Swimming pool owner (Fitness)
Bob Hansen, Asst. HVAC manager	New Jersey Institute of Technology	robert.l.hansen@njit.edu	Swimming pool owner (School/College)
Roberto Cardona, Chief Engineer	Homewood Suites by Hilton / East Rutherford	(201)460-9030	Swimming pool owner (Hotel)
Jimmy Cruz, Chief Engineer	Hampton Inn & Suites / Newark-Harrison Riverwalk	tony.cartagena@hilton.com	Swimming pool owner (Hotel)
Dwayne Cronce, General Manager	Wyndham Garden Hotel, Newark	(973) 824-4000	Swimming pool owner (Hotel)
Tom Lee, Aquatics Coordinator	Rutgers University	tomlee@newark.rutgers.edu	Swimming pool owner (School/College)
Bin Wang, Owner, designer	Private pool	woobin811@126.com	Swimming pool Owner and designer
Bob, Maintenance technician	Stay bridge suites/Princeton-NJ	(732)940-2250	Swimming pool owner (Hotel)
Kevin, Chief engineer	Courtyard Marriott/Princeton-NJ	(800)207-5499	Swimming pool owner (Hotel)
Wilson, Pool supervisor	Home suites by Hilton/Princeton-NJ	(609)720-0550	Swimming pool owner (Hotel)
Jose, chief engineer	Double tree by Hilton/Princeton-NJ	(855)275-4790	Swimming pool owner (Hotel)
Frank, engineer	Hilton garden inn/Trenton-NJ	(855)618-4697	Swimming pool owner (Hotel)

Table A.1 Continued

Megan White, administrator	Ruthorford High School		Swimming pool owner (School/College)
Thomas Dobrowolski, Owner	Action Pools & supplies	(732) 855-0044	Swimming pool supplier
Jimmy, Salesman	Leslie's pool supplies/Springfield	(973)258-9696	Swimming pool supplier
Jeff, Owner	Woodbridge Pools	(732)636-0061	Swimming pool supplier
Carol, Manager	Leslie's/Edison NJ	(732)632-2080	Swimming pool supplier
Janet, Pool manager	Five Star Swim School	(732)902-2267	Swimming pool owner (School/College)
Jack, Maintenance Engineer	Sheraton Brooklyn New York Hotel		Swimming pool owner (Hotel)
Madhur Patel, Aquatic Director	YMCA Mcburney NYC	(212)912-2300	Swimming pool owner (Fitness)
Richard Kosty, General Manager	The Heldrich	(732)729-4670	Swimming pool owner (Fitness)
Rana kamel	Robert wood Johnson fitness and wellness centre	(732)873-1222	Swimming pool owner (Fitness)
Jeff Zeszotarski, Aquatics Coordinator	Werblin Recreational Centre	(848)445-1336	Swimming pool owner (Fitness)
James Crist, Store Manager	Leslie Pool Supplies/East Brunswick	(732)257-5704	Swimming pool supplier
Andrew Smith, Recruiting Director	American Pool	(732)-423-3870	Swimming pool supplier
Brian Bergeski, President	American Pool		Swimming pool supplier
Winnie Shih, Application Engineering Manager	Nanostone water	(310)869-6977	Water Treatment Company (Supplier)
Ryan, Pool supervisor	Hampton inn by Hilton/Trenton-NJ	(855)213-0582	Swimming pool owner (Hotel)

Travis Nilmeyer, specialty markets	Myron L Company	(760)438-2021	Water Treatment Company (Supplier)
Jantje Johnson, Business development director	Desalitech	jantje@desalitech	Water Treatment Company (Supplier)
Daniel Stenberg, Design Engineer	Forsta Filters	(310)837-7177	Water Treatment Company (Supplier)
Stefan Strasser, Product Manager	Lenzing Technik	s.strasser@lenzing.com	Water Treatment Company (Supplier)
Takafumi Takeda, CFM & WPS sales section	Meidensha Corporation	takeda-ta@mb.meidensha.co.jp	Water Treatment Company (Supplier)
Min Gyoo Kim, Business Development Manager	Doosan Hudro Technology	mkim@doosanhydro	Water Treatment Company (Supplier)
Jeff Kaminski, Regional Sales Manager	Amiad water system	jeff.kaminski@amiad.com	Water Treatment Company (Supplier)
Allan Pascual, Sales Engineer	Pure Aqua Inc	allan@pureaqua.com	Water Treatment Company (Supplier)
Paul Jung, Executive Director	Econity	paul.jung@econity.com	Water Treatment Company (Supplier)
Richard Chmielewski	Protec-arisawa	RDC@protec-arisawa.com	Water Treatment Company (Supplier)
Stephen Katz, MBR Product Applications Leader	GE Power & Water	stephen.katz@ge.com	Water Treatment Company (Supplier)
Rabee Mazahreh, Sales Manager	Pentair	rabee.mazahreh@pentair.com	Water Treatment Company (Supplier)

Table A.1 Continued

Chris Hanson,	MRI meurerresearch	chanson@meurerresearch.com	Water Treatment Company (Supplier)
Dr. Jens Lipnizki, head of technical marketing membrane	LANXESS	jens.lipnizki@lanxess.com	Water Treatment Company (Supplier)
Alejandro C, Customer Service Associate	Leslies pool	(800)537-5437	Swimming pool supplier
anonymous	Leslie Pool Supplies/Clifton, NJ		Swimming pool supplier
Megan Bado, Assistant Manager	Leslie's Pool Supplies/Pompton Lakes		Swimming pool supplier
Janet Bush, General Manager	Quality Inn Choice Suites	(570)420-1000	Swimming pool owner (Hotel)
Kevin Baade, Maintenance Supervisor	Staybridge Suites Poconos	(570)420-2828	Swimming pool owner (Hotel)
Michele Kuna, Aquatics Director	he YMCA-Stroudsburg , PA	(570)421-2525	Swimming pool owner (Fitness)
Ryan Hurtack, Assistant General Manager	Fairfield Inn Marriot	(814)238-3871	Swimming pool owner (Hotel)
Scott Mangene, General Manager	Hampton Inn And Suites Williamsburg Square	(814)231-1899	Swimming pool owner (Hotel)
Rhea, SPA Supervisor	Bally's Hotel - Atlantic city	(609) 340-2000	Swimming pool owner (Hotel)
David Hoylman, General Manager	University Park Inn & Suites	(814)234-8393	Swimming pool owner (Hotel)
William Rojas, chief Engineer	Courtyard Marriot Hotel -State College , PA	(814)238-1881	Swimming pool owner (Hotel)
Corey, Maintenance Engineer	Days Inn Hotel -State College, PA	ettubs@centrehotel.com	Swimming pool owner (Hotel)

Table A.1 Continued

Steven Barnes, Sales Associate	Pocono Pools and Spa Retailer	(570)476-0888	Swimming pool supplier
Lisa, assistant Engineer	The Penn stater Conference Center Hotel	(814)863-5000	Swimming pool supplier
Kelly, Maintenance Supervisor	BERKEY FILTERS		Swimming pool supplier
S. Baker	HAYWARD POOL PRODUCTS	sbaker@hayward.com	Swimming pool supplier

REFERENCES

1. Cho, Y. H.; Lee, H. D.; Park, H. B., Integrated membrane processes for separation and purification of organic acid from a biomass fermentation process. *Ind. Eng. Chem. Res.* **2012,** *51* (30), 10207-10219.

2. Gryta, M.; Markowska-Szczupak, A.; Bastrzyk, J.; Tomczak, W., The study of membrane distillation used for separation of fermenting glycerol solutions. *J. Membr. Sci.* **2013,** *431*, 1-8.

3. Uduman, N.; Qi, Y.; Danquah, M. K.; Forde, G. M.; Hoadley, A., Dewatering of microalgal cultures: A major bottleneck to algae-based fuels. *J. Renew. Sust. Energ. Rev.* **2010,** *2* (1), 012701.

4. Vandamme, D.; Foubert, I.; Muylaert, K., Flocculation as a low-cost method for harvesting microalgae for bulk biomass production. *Trends Biotechnol.* **2013,** *31* (4), 233-239.

5 Molina Grima, E.; Belarbi, E.-H.; Acién Fernández, F.; Robles Medina, A.; Chisti, Y., Recovery of microalgal biomass and metabolites: Process options and economics. *Biotechnol. Adv.* **2003,** *20* (7), 491-515.

6 Shen, Y.; Yuan, W.; Pei, Z. J.; Wu, Q.; Mao, E., Microalgae mass production methods. *Trans. ASABE* **2009,** *52* (4), 1275-1287.

7 Van Den Hende, S.; Vervaeren, H.; Desmet, S.; Boon, N., Bioflocculation of microalgae and bacteria combined with flue gas to improve sewage treatment. *New Biotech.* **2011,** *29* (1), 23-31.

8 Mohn, F., *Harvesting of micro-algal biomass.* Cambridge, MA: Cambridge University Press, 1988.

9 Bhave, R.; Kuritz, T.; Powell, L.; Adcock, D., Membrane-based energy efficient dewatering of microalgae in biofuels production and recovery of value added co-products. *Environ. Sci. Technol.* **2012,** *46* (10), 5599-5606.

10 Babel, S.; Takizawa, S., A study on membrane fouling due to algal deposition. *Water Sci. Technol.* **2000,** *41* (10-11), 327-335.

11 Zhang, Y.; Tang, C. Y.; Li, G., The role of hydrodynamic conditions and pH on algal-rich water fouling of ultrafiltration. *Water Res.* **2012,** *46* (15), 4783-4789.

12 Qu, F.; Liang, H.; Wang, Z.; Wang, H.; Yu, H.; Li, G., Ultrafiltration membrane fouling by extracellular organic matters (EOM) of *Microcystis aeruginosa* in stationary phase: Influences of interfacial characteristics of foulants and fouling mechanisms. *Water Res.* **2012,** *46* (5), 1490-1500.

13 Qu, F.; Liang, H.; He, J.; Ma, J.; Wang, Z.; Yu, H.; Li, G., Characterization of dissolved extracellular organic matter (dEOM) and bound extracellular organic matter (bEOM) of *Microcystis aeruginosa* and their impacts on UF membrane fouling. *Water Res.* **2012**, *46* (9), 2881-2890.

14 Scholz, M. J.; Weiss, T. L.; Jinkerson, R. E.; Jing, J.; Roth, R.; Goodenough, U.; Posewitz, M. C.; Gerken, H. G., Ultrastructure and composition of the nannochloropsis gaditana cell wall. *Eukaryot. Cell* **2014,** *13* (11), 1450-1464.

15 Lee, J. Y., Yoo, C., Jun, S. Y., Ahn, C. Y., & Oh, H. M. , Comparison of several methods for effective lipid extraction from microalgae. *Bioresour. Technol.* **2010,** *101* (1), S75-S77.

16 C.H. Cheng, T. B. D., H.C. Pi, S.M. Jang, Y.H. Lin, H.T. Lee, Comparative study of lipid extraction from microalgae by organic solvent and supercritical CO_2. *Bioresour. Technol.* **2011,** *102*, 10151–10153.

17 Günerken, E.; D'Hondt, E.; Eppink, M. H. M.; Garcia-Gonzalez, L.; Elst, K.; Wijffels, R. H., Cell disruption for microalgae biorefineries. *Biotechnol. Adv.* **2015,** *33* (2), 243-260.

18 Park, J.-Y.; Park, M. S.; Lee, Y.-C.; Yang, J.-W., Advances in direct transesterification of algal oils from wet biomass. *Bioresour. Technol.* **2015,** *184*, 267-275.

19 Greenly, J. M.; Tester, J. W., Ultrasonic cavitation for disruption of microalgae. *Bioresour. Technol.* **2015,** *184*, 276-279.

20 Cravotto, G., Boffa, L., Mantegna, S., Perego, P., Avogadro, M., Cintas, P., Improved extraction of vegetable oils under high-intensity ultrasound and/or microwaves. *Ultrason. Sonochem.* **2008,** *15*, 898–902.

21 Virot, M., Tomao, V., Ginies, C., Visinoni, F., Chemat, F., Microwave-integrated Extraction of Total Fats and Oils. *J. Chromatogr.* **2008,** *A1196*, 57–64.

22 Demuez, M.; Mahdy, A.; Tomás-Pejó, E.; González-Fernández, C.; Ballesteros, M., Enzymatic cell disruption of microalgae biomass in biorefinery processes. *Biotechnol. bioeng.* **2015**.

23 Harun, R.; Jason, W.; Cherrington, T.; Danquah, M. K., Exploring alkaline pre-treatment of microalgal biomass for bioethanol production. *Appl. Energy* **2011,** *88* (10), 3464-3467.

24 Brentner, L. B.; Eckelman, M. J.; Zimmerman, J. B., Combinatorial life cycle assessment to inform process design of industrial production of algal biodiesel. *Environ. Sci. Technol.* **2011,** *45* (16), 7060-7067.

25 Chen, G.; Betterton, E. A.; Arnold, R. G., Electrolytic oxidation of trichloroethylene using a ceramic anode. *J. Appl. Electrochem.* **1999,** *29* (8), 961-970.

26 Bejan, D.; Malcolm, J. D.; Morrison, L.; Bunce, N. J., Mechanistic investigation of the conductive ceramic Ebonex® as an anode material. *Electrochim. Acta* **2009,** *54* (23), 5548-5556.

27 Scialdone, O.; Galia, A.; Filardo, G., Electrochemical incineration of 1,2-dichloroethane: Effect of the electrode material. *Electrochim. Acta* **2008,** *53* (24), 7220-7225.

28 Huang, C.; Chen, X.; Liu, T.; Yang, Z.; Xiao, Y.; Zeng, G.; Sun, X., Harvesting of *Chlorella* sp. using hollow fiber ultrafiltration. *Environ. Sci. Pollut. Res. Int.* **2012,** *19* (5), 1416-1421.

29 Huang, W.; Chu, H.; Dong, B., Characteristics of algogenic organic matter generated under different nutrient conditions and subsequent impact on microfiltration membrane fouling. *Desalination* **2012,** *293*, 104-111.

30 Henderson, R. K.; Baker, A.; Parsons, S. A.; Jefferson, B., Characterisation of algogenic organic matter extracted from cyanobacteria, green algae and diatoms. *Water Res.* **2008,** *42* (13), 3435-3445.

31 Tang, T.; Fadaei, H.; Hu, Z., Rapid evaluation of algal and cyanobacterial activities through specific oxygen production rate measurement. *Ecol. Eng.* **2014,** *73*, 439-445.

32 Mulbry, W.; Westhead, E. K.; Pizarro, C.; Sikora, L., Recycling of manure nutrients: use of algal biomass from dairy manure treatment as a slow release fertilizer. *Bioresour. Technol.* **2005,** *96* (4), 451-458.

33 Su, Y.; Mennerich, A.; Urban, B., Municipal wastewater treatment and biomass accumulation with a wastewater-born and settleable algal-bacterial culture. *Water Res.* **2011,** *45* (11), 3351-3358.

34 Valigore, J. M.; Gostomski, P. A.; Wareham, D. G.; O'Sullivan, A. D., Effects of hydraulic and solids retention times on productivity and settleability of microbial (microalgal-bacterial) biomass grown on primary treated wastewater as a biofuel feedstock. *Water Res.* **2012,** *46* (9), 2957-2964.

35 Zhu, L.; Wang, Z.; Shu, Q.; Takala, J.; Hiltunen, E.; Feng, P.; Yuan, Z., Nutrient removal and biodiesel production by integration of freshwater algae cultivation with piggery wastewater treatment. *Water Res.* **2013,** *47* (13), 4294-4302.

36 Li, P.; Zhang, L.; Wang, W.; Su, J.; Feng, L., Rapid catalytic microwave method to damage Microcystis aeruginosa with FeCl3-loaded active carbon. *Environ. Sci. Technol.* **2011,** *45* (10), 4521-4526.

37 Pivokonsky, M.; Safarikova, J.; Baresova, M.; Pivokonska, L.; Kopecka, I., A comparison of the character of algal extracellular versus cellular organic matter produced by cyanobacterium, diatom and green alga. *Water Res.* **2014,** *51*, 37-46.

38 Lavoie, M.; Campbell, P. G.; Fortin, C., Predicting cadmium accumulation and toxicity in a green alga in the presence of varying essential element concentrations using a biotic ligand model. *Environ. Sci. Technol.* **2014,** *48* (2), 1222-1229.

39 Linkous, C. A.; Carter, G. J.; Locuson, D. B.; Ouellette, A. J.; Slattery, D. K.; Smitha, L. A., Photocatalytic inhibition of algae growth using TiO_2, WO_3, and cocatalyst modifications. *Environ. Sci. Technol.* **2000,** *34* (22), 4754-4758.

40 Robertson, B.; Button, D.; Koch, A., Determination of the biomasses of small bacteria at low concentrations in a mixture of species with forward light scatter measurements by flow cytometry. *Appl. Environ. Microbiol.* **1998,** *64* (10), 3900-3909.

41.   Hancke, K.; Hancke, T. B.; Olsen, L. M.; Johnsen, G.; Glud, R. N., temperature effects on microalgal photosynthesis-light responses measured by o2 production, pulse-amplitude-modulated fluorescence, and ^{14}C assimilation 1. *J. Phycol.* **2008,** *44* (2), 501-514.

42 Lin, J.-H.; Kao, W.-C.; Tsai, K.-P.; Chen, C.-Y., A novel algal toxicity testing technique for assessing the toxicity of both metallic and organic toxicants. *Water Res.* **2005,** *39* (9), 1869-1877.

43 Buffle, J.; Horvai, G., In situ monitoring of aquatic systems. *Chemical analysis and speciation* **2000**.

44 Yasukawa, T.; Uchida, I.; Matsue, T., Microamperometric measurements of photosynthetic activity in a single algal protoplast. *Biophys. J.***1999,** *76* (2), 1129-1135.

45 Matsue, T.; Koike, S.; Uchida, I., Microamperometric estimation of photosynthesis inhibition in a single algal protoplast. *Biochem. Biophys. Res. Commun.***1993,** *197* (3), 1283-1287.

46 Beutler, M.; Wiltshire, K. H.; Meyer, B.; Moldaenke, C.; Lüring, C.; Meyerhöfer, M.; Hansen, U.-P.; Dau, H., A fluorometric method for the differentiation of algal populations in vivo and in situ. *Photosynth. Res.* **2002,** *72* (1), 39-53.

47 Dewez, D.; Geoffroy, L.; Vernet, G.; Popovic, R., Determination of photosynthetic and enzymatic biomarkers sensitivity used to evaluate toxic effects of copper and fludioxonil in alga Scenedesmus obliquus. *Aquat. Toxicol.***2005,** *74* (2), 150-159.

48 Goldman, E. A.; Smith, E. M.; Richardson, T. L., Estimation of chromophoric dissolved organic matter (CDOM) and photosynthetic activity of estuarine phytoplankton using a multiple-fixed-wavelength spectral fluorometer. *Water Res.* **2013,** *47* (4), 1616-1630.

49 Halsey, K. H.; Milligan, A. J.; Behrenfeld, M. J., Physiological optimization underlies growth rate-independent chlorophyll-specific gross and net primary production. *Photosynth. Res.* **2010,** *103* (2), 125-137.

50 Ellis, T. G.; Barbeau, D. S.; Smets, B. F.; Grady, C., Respirometric technique for determination of extant kinetic parameters describing biodegradation. *Water. Environ. Res.* **1996,** *68* (5), 917-926.

51 Ellis, T. G.; Smets, B. F.; Grady, C., Effect of simultaneous biodegradation of multiple substrates on the extant biodegradation kinetics of individual substrates. *Water. Environ. Res.* **1998,** *70* (1), 27-38.

52 Chandran, K.; Hu, Z.; Smets, B. F., A critical comparison of extant batch respirometric and substrate depletion assays for estimation of nitrification biokinetics. *Biotechnol. Bioeng.* **2008,** *101* (1), 62-72.

53 Chen, C. Y.; Chen, S. L.; Christensen, E. R., Individual and combined toxicity of nitriles and aldehydes to Raphidocelis subcapitata. *Environ. Toxicol. Chem.* **2005,** *24* (5), 1067-1073.

54 Tang, T.; Fadaei, H.; Hu, Z., Rapid evaluation of algal and cyanobacterial activities through specific oxygen production rate measurement. *Ecol. Eng.* **2014,** *73*, 439-445.

55 Günerken, E.; d'Hondt, E.; Eppink, M.; Garcia-Gonzalez, L.; Elst, K.; Wijffels, R., Cell disruption for microalgae biorefineries. *Biotechnol. Adv.* **2015,** *33* (2), 243-260.

56 Phull, S.; Newman, A.; Lorimer, J.; Pollet, B.; Mason, T., The development and evaluation of ultrasound in the biocidal treatment of water. *Ultrason. Sonochem.* **1997,** *4* (2), 157-164.

57 Zhang, G.; Zhang, P.; Wang, B.; Liu, H., Ultrasonic frequency effects on the removal of Microcystis aeruginosa. *Ultrason. Sonochem.* **2006,** *13* (5), 446-450.

58 Lee, T.-J.; Nakano, K.; Matsumura, M., A novel strategy for cyanobacterial bloom control by ultrasonic irradiation. *Wat. Sci. Tech.* **2002,** *46* (6-7), 207-215.

59 Nakano, K.; Lee, T. J.; Matsumura, M., In situ algal bloom control by the integration of ultrasonic radiation and jet circulation to flushing. *Environ. Sci. Technol.* **2001,** *35* (24), 4941-4946.

60 Ahn, C.-Y.; Park, M.-H.; Joung, S.-H.; Kim, H.-S.; Jang, K.-Y.; Oh, H.-M., Growth inhibition of cyanobacteria by ultrasonic radiation: laboratory and enclosure studies. *Environ. Sci. Technol.* **2003,** *37* (13), 3031-3037.

61 Heng, L.; Jun, N.; Wen-jie, H.; Guibai, L., Algae removal by ultrasonic irradiation–coagulation. *Desalination* **2009,** *239* (1-3), 191-197.

62 Merino, N.; Qu, Y.; Deeb, R. A.; Hawley, E. L.; Hoffmann, M. R.; Mahendra, S., Degradation and Removal Methods for Perfluoroalkyl and Polyfluoroalkyl Substances in Water. *Environ. Eng. Sci.* **2016,** *33* (9), 615-649.

63 Lindstrom, A. B.; Strynar, M. J.; Libelo, E. L., Polyfluorinated compounds: past, present, and future. *Environ. Sci. Technol.* **2011,** *45* (19), 7954-7961.

64 Post, G. B.; Cohn, P. D.; Cooper, K. R., Perfluorooctanoic acid (PFOA), an emerging drinking water contaminant: a critical review of recent literature. *Environmental research* **2012,** *116*, 93-117.

65 Kunacheva, C.; Fujii, S.; Tanaka, S.; Seneviratne, S.; Lien, N. P. H.; Nozoe, M.; Kimura, K.; Shivakoti, B. R.; Harada, H., Worldwide surveys of perfluorooctane sulfonate (PFOS) and perfluorooctanoic acid (PFOA) in water environment in recent years. *Wat. Sci. Tech.* **2012,** *66* (12), 2764-2771.

66 Yang, S.; Xu, F.; Wu, F.; Wang, S.; Zheng, B., Development of PFOS and PFOA criteria for the protection of freshwater aquatic life in China. *Science of the Total Environment* **2014,** *470*, 677-683.

67 DiGangi, J.; Blum, A.; Bergman, Å.; de Wit, C. A.; Lucas, D.; Mortimer, D.; Schecter, A.; Scheringer, M.; Shaw, S. D.; Webster, T. F., San Antonio statement on brominated and chlorinated flame retardants. *Environ. Health Perspect.* **2010,** *118* (12), A516-A518.

68 Blum, A.; Balan, S. A.; Scheringer, M.; Trier, X.; Goldenman, G.; Cousins, I. T.; Diamond, M.; Fletcher, T.; Higgins, C.; Lindeman, A. E., The Madrid statement on poly-and perfluoroalkyl substances (PFASs). *Environ. Health Perspect.* **2015,** *123* (5), A107-A111.

69 Fact sheet PFOA & PFOS drinking water health advisories. *U.S. Environmental Protection Agency (USEPA)* **2016**.

70 Hu, X. C.; Andrews, D. Q.; Lindstrom, A. B.; Bruton, T. A.; Schaider, L. A.; Grandjean, P.; Lohmann, R.; Carignan, C. C.; Blum, A.; Balan, S. A., Detection of poly-and perfluoroalkyl substances (PFASs) in US drinking water linked to

industrial sites, military fire training areas, and wastewater treatment plants. *Environ. Sci. Technol. letters* **2016,** *3* (10), 344.

71   Schaefer, C. E.; Andaya, C.; Burant, A.; Condee, C. W.; Urtiaga, A.; Strathmann, T. J.; Higgins, C. P., Electrochemical treatment of perfluorooctanoic acid and perfluorooctane sulfonate: Insights into mechanisms and application to groundwater treatment. *Chem. Eng. J.* **2017,** *317*, 424-432.

72   Choi, G.-H.; Lee, D.-Y.; Jeong, D.-K.; Kuppusamy, S.; Lee, Y. B.; Park, B.-J.; Kim, J.-H., Perfluorooctanoic acid (PFOA) and perfluorooctanesulfonic acid (PFOS) concentrations in the South Korean agricultural environment: a national survey. **2017**.

73   Ge, S.; Agbakpe, M.; Wu, Z.; Kuang, L.; Zhang, W.; Wang, X., Influences of Surface Coating, UV Irradiation and Magnetic Field on the Algae Removal Using Magnetite Nanoparticles. *Environ. Sci. Technol.* **2014,** *49* (2), 1190-1196.

74.   Ge, S.; Agbakpe, M.; Zhang, W.; Kuang, L., Heteroaggregation between PEI-coated magnetic nanoparticles and algae: effect of particle size on algal harvesting efficiency. *ACS Appl. Mater. Interfaces* **2015,** *7* (11), 6102-6108.

75   Agbakpe, M.; Ge, S.; Zhang, W.; Zhang, X.; Kobylarz, P., Algae harvesting for biofuel production: Influences of UV irradiation and polyethylenimine (PEI) coating on bacterial biocoagulation. *Bioresour. Technol.* **2014,** *166* ( ), 266–272.

76   Babel, S.; Takizawa, S., A Study on Membrane Fouling due to Algal Deposition. *Water Sci. Technol.* **2000,** *41* (10-11), 327-335.

77   Zhang, Y.; Tang, C. Y.; Li, G., The Role of hydrodynamic conditions and ph on algal-rich water fouling of ultrafiltration. *Water Res.* **2012,** *46* (15), 4783-4789.

78   Zaky, A. M.; Chaplin, B. P., Porous substoichiometric TiO$_2$ anodes as reactive electrochemical membranes for water treatment. *Environ. Sci. Technol.* **2013,** *47* (12), 6554-6563.

79   Chaplin, B. P.; Duran, M.; Zaky, A. M.; Ding, K. In Substoichiometric Titanium Dioxide Reactive Electrochemical Membranes for Water Treatment, *Abstr. Pap. Am. Chem. S.*, Amer Chemical Soc 1155 16th St, Nw, Washington, DC 20036 USA: 2013.

80   Liu, H.; Vecitis, C. D., Reactive transport mechanism for organic oxidation during electrochemical filtration: mass-transfer, physical adsorption, and electron-transfer. *J. Phys. Chem. C* **2011,** *116* (1), 374-383.

81   Zhao, G.; Zhang, Y.; Lei, Y.; Lv, B.; Gao, J.; Zhang, Y.; Li, D., Fabrication and electrochemical treatment application of a novel lead dioxide anode with superhydrophobic surfaces, high oxygen evolution potential, and oxidation capability. *Environ. Sci. Technol.* **2010,** *44* (5), 1754-1759.

82   Chaplin, B. P., Critical review of electrochemical advanced oxidation processes for water treatment applications. *Environ. Sci. Process. Impacts.* **2014,** *16* (6), 1182-1203.

83   Zaky, A. M.; Chaplin, B. P., Mechanism of p-substituted phenol oxidation at a Ti_4O_7 reactive electrochemical membrane. *Environ. Sci. Technol.* **2014,** *48* (10), 5857-5867.

84   Chen, G.; Bare, S. R.; Mallouk, T. E., Development of supported bifunctional electrocatalysts for unitized regenerative fuel cells. *J. Electrochem. Soc.* **2002,** *149* (8), A1092-A1099.

85   Hayfield, P., Development of a New Material: Monolithic Ti_4O_7 Ebonex Ceramic. Royal Society of Chemistry: Thomas Graham House, Science Park, Milton Road, Cambridge CB4 0WF, UK, 2002.

86   Gerken, H. G.; Donohoe, B.; Knoshaug, E. P., Enzymatic cell wall degradation of chlorella vulgaris and other microalgae for biofuels production. *Planta* **2013,** *237* (1), 239-253.

87   Engler, C. R., Disruption of microbial cells in comprehensive biotechnology. M. Moo-Young, C. L. C., Ed. Pergamon: UK, 1985; Vol. 2, pp 305–324.

88   Hetherington, P. J., Follows, M., Dunnill, P. and Lilly, M. D, *Trans. Inst. Chem. Eng* **1971,** *49*, 142.

89   Doulah, M. S., Mechanism of disintegration of biological cells in ultrasonic cavitation. *Biotechnol. Bioeng.* **1977,** *19* (5), 649-660.

90   Middelberg, A. P. J., Process-scale disruption of microorganisms. *Biotechnol. Adv.* **1995,** *13* (3), 491–551.

91   Mercer, P., and Roberto E. Armenta, Developments in oil extraction from microalgae. *Eur. J. Lipid Sci. Technol.* **2011,** *113* (5), 539-547.

92   Lardon, L.; Hélias, A.; Sialve, B.; Steyer, J.-P.; Bernard, O., Life-cycle assessment of biodiesel production from microalgae. *Environ. Sci. Technol.* **2009,** *43* (17), 6475-6481.

93   Bejan, D.; Malcolm, J. D.; Morrison, L.; Bunce, N. J., Mechanistic investigation of the conductive ceramic Ebonex® as an anode material. *Electrochim. Acta* **2009,** *54* (23), 5548-5556.

94   Scialdone, O.; Galia, A.; Filardo, G., Electrochemical incineration of 1,2-dichloroethane: effect of the electrode material. *Electrochim. Acta* **2008,** *53* (24), 7220-7225.

95   Fulton, L. M. Nutrient removal by algae grown in CO_2-enriched wastewater over a range of nitrogen-to-phosphorus ratios. California Polytechnic State University November, 2009.

96.   Su, Y.; Mennerich, A.; Urban, B., Coupled nutrient removal and biomass production with mixed algal culture: impact of biotic and abiotic factors. *Bioresour. Technol.* **2012,** *118* (0), 469-476.

97   Wei, L.; Thakkar, M.; Chen, Y.; Ntim, S. A.; Mitra, S.; Zhang, X., Cytotoxicity effects of water dispersible oxidized multiwalled carbon nanotubes on marine alga, Dunaliella Tertiolecta. *Aquat. Toxicol.* **2010,** *100* (2), 194-201.

98   Arndt-Jovin, D. J.; Jovin, T. M., Fluorescence labeling and microscopy of DNA. *Methods in cell biology* **1989,** *30*, 417-448.

99.   Pragya, N.; Pandey, K. K.; Sahoo, P., A Review on Harvesting, Oil Extraction and Biofuels Production Technologies from Microalgae. *Renewable Sustainable Energy Rev.* **2013,** *24*, 159-171.

100.   Hossain, A. S.; Salleh, A.; Boyce, A. N.; Chowdhury, P.; Naqiuddin, M., Biodiesel Fuel Production from Algae as Renewable Energy. *Am. J. Biochem. Biotechnol.* **2008,** *4* (3), 250-254.

101.   Wang, D.; Li, Y.; Hu, X.; Su, W.; Zhong, M., Combined Enzymatic and Mechanical Cell Disruption and Lipid Extraction of Green Alga Neochloris oleoabundans. *International journal of molecular sciences* **2015,** *16* (4), 7707-7722.

102.   Xu, N.; Zhang, X.; Fan, X.; Han, L.; Zeng, C., Effects of nitrogen source and concentration on growth rate and fatty acid composition of Ellipsoidion sp.(Eustigmatophyta). *J. Appl. Phycol.* **2001,** *13* (6), 463-469.

103.   Wang, B.; Xin, H.; Li, X.; Cheng, J.; Yang, G.; Nie, F., Mesoporous CNT@ TiO_2-C nanocable with extremely durable high rate capability for lithium-ion battery anodes. *Scientific reports* **2014,** *4*, 3729.

104.   Hung, M.; Liu, J., Microfiltration for separation of green algae from water. *Colloids Surf., B* **2006,** *51* (2), 157-164.

105.   Her, N.; Amy, G.; Park, H.-R.; Song, M., Characterizing algogenic organic matter (aom) and evaluating associated nf membrane fouling. *Water Res.* **2004,** *38* (6), 1427-1438.

106.   Qu, F.; Liang, H.; Tian, J.; Yu, H.; Chen, Z.; Li, G., Ultrafiltration (UF) membrane fouling caused by cyanobateria: fouling effects of cells and extracellular organics matter (EOM). *Desalination* **2012,** *293*, 30-37.

107.   Chiou, Y.-T.; Hsieh, M.-L.; Yeh, H.-H., Effect of algal extracellular polymer substances on UF membrane fouling. *Desalination* **2010,** *250* (2), 648-652.

108.   Plottu, A.; Her, N.; Houssais, B.; Amy, G.; Gatel, D.; Cavard, J., Effect of Ozonated Water on Membrane Fouling. *Water Supp.* **2003,** *3* (5), 191-197.

109.   Hoyer, O.; Lusse, B.; Bernhardt, H., Isolation and characterization of extracellular organic matter (EOM) from algae. *Z Wasser Abwass For* **1985,** *18* (2), 76-90.

110.   Her, N.; Amy, G.; Jarusutthirak, C., seasonal variations of nanofiltration (nf) foulants: identification and control. *Desalination* **2000,** *132* (1), 143-160.

111.   Tabatabai, S. A. A.; Schippers, J. C.; Kennedy, M. D., Effect of coagulation on fouling potential and removal of algal organic matter in ultrafiltration pretreatment to seawater reverse osmosis. *Water Res.* **2014,** *59*, 283-294.

112.   Henderson, R. K.; Baker, A.; Parsons, S. A.; Jefferson, B., Characterisation of algogenic organic matter extracted from cyanobacteria, green algae and diatoms. *Water Res.* **2008,** *42* (13), 3435-3445.

113.   Edzwald, J., Coagulation in Drinking Water Treatment: Particles, Organics and Coagulants. *Water Sci. Technol.* **1993,** *27* (11), 21-35.

114.   Linh, N. T. Effect of Pre-treatment on Algal Cell Properties and its separation via dispersed air flotation. Master's Thesis, 2011.

115.   Uyguner, C. S.; Bekbolet, M., Evaluation of Humic Acid Photocatalytic Degradation by UV–vis and Fluorescence Spectroscopy. *Catal. Today* **2005,** *101* (3), 267-274.

116.   Helms, J. R.; Stubbins, A.; Ritchie, J. D.; Minor, E. C.; Kieber, D. J.; Mopper, K., Absorption spectral slopes and slope ratios as indicators of molecular weight, source, and photobleaching of chromophoric dissolved organic matter. *Limnol. Oceanogr.* **2008,** *53* (3), 955-969.

117.   Fichot, C. G.; Benner, R., The spectral slope coefficient of chromophoric dissolved organic matter (S275-295) as a tracer of terrigenous dissolved organic carbon in river-influenced ocean margins. *Limnol. Oceanogr.* **2012,** *57* (5), 1453-1466.

118.   Shen, Y.; Fichot, C. G.; Benner, R., Floodplain influence on dissolved organic matter composition and export from the Mississippi-Atchafalaya River system to the Gulf of Mexico. *Limnol. Oceanogr.* **2012,** *57* (4), 1149-1160.

119.   Mollah, M. Y. A.; Morkovsky, P.; Gomes, J. A. G.; Kesmez, M.; Parga, J.; Cocke, D. L., Fundamentals, present and future perspectives of electrocoagulation. *J. Hazard. Mater.***2004,** *114* (1–3), 199-210.

120. Dalrymple, O. K.; Halfhide, T.; Udom, I.; Gilles, B.; Wolan, J.; Zhang, Q.; Ergas, S., Wastewater use in algae production for generation of renewable resources: a review and preliminary results. *Aquat. Biosyst.* **2013,** *9*, 2-2.

121. Nguyen, T. L.; Lee, D.; Chang, J.; Liu, J., Effects of ozone and peroxone on algal separation via dispersed air flotation. *Colloids Surf., B* **2013,** *105*, 246-250.

122. Huang, Y.; Hong, A.; Zhang, D.; Li, L., Comparison of cell rupturing by ozonation and ultrasonication for algal lipid extraction from chlorella vulgaris. *Environ. Technol.* **2014,** *35* (8), 931-937.

123. Steriti, A.; Rossi, R.; Concas, A.; Cao, G., A Novel Cell Disruption Technique to Enhance Lipid Extraction from Microalgae. *Bioresource Technol* **2014,** *164*, 70-77.

124. Eing, C.; Goettel, M.; Straessner, R.; Gusbeth, C.; Frey, W., Pulsed electric field treatment of microalgae—benefits for microalgae biomass processing. *IEEE Trans. Plasma Sci* **2013,** *41* (10), 2901-2907.

125. Sheng, J.; Vannela, R.; Rittmann, B., Disruption of synechocystis PCC 6803 for lipid extraction. *Water Sci. Technol.* **2012,** *65* (3), 567-573.

126. Zbinden, M. D. A.; Sturm, B. S.; Nord, R. D.; Carey, W. J.; Moore, D.; Shinogle, H.; Stagg-Williams, S. M., Pulsed electric field (PEF) as an intensification pretreatment for greener solvent lipid extraction from microalgae. *Biotechnol. Bioeng.* **2013,** *110* (6), 1605-1615.

127. Doucha, J.; Lívanský, K., Influence of processing parameters on disintegration of chlorella cells in various types of homogenizers. *Appl. Microbiol. Biotechnol.* **2008,** *81* (3), 431-440.

128. Lee, A. K.; Lewis, D. M.; Ashman, P. J., Force and energy requirement for microalgal cell disruption: an atomic force microscope evaluation. *Bioresour. Technol.* **2013,** *128*, 199-206.

129. Lee, A. K.; Lewis, D. M.; Ashman, P. J., Disruption of microalgal cells for the extraction of lipids for biofuels: processes and specific energy requirements. *Biomass Bioenergy* **2012,** *46*, 89-101.

130. Halim, R.; Harun, R.; Danquah, M. K.; Webley, P. A., Microalgal cell disruption for biofuel development. *Appl. Energy* **2012,** *91* (1), 116-121.

131. Sheng, J.; Vannela, R.; Rittmann, B. E., Evaluation of cell-disruption effects of pulsed-electric-field treatment of synechocystis PCC 6803. *Environ. Sci. Technol.* **2011,** *45* (8), 3795-3802.

132. Coustets, M.; Al-Karablieh, N.; Thomsen, C.; Teissié, J., Flow Process for electroextraction of total proteins from microalgae. *J. Membr. Biol.* **2013,** *246* (10), 751-760.

133. Schütte, H.; Kroner, K.; Hustedt, H.; Kula, M.-R., Experiences with a 20 litre industrial bead mill for the disruption of microorganisms. *Enzyme Microb. Technol.* **1983,** *5* (2), 143-148.

134. Kula, M. R.; Schütte, H., Purification of Proteins and the Disruption of Microbial Cells. *Biotechnol. Progr.* **1987,** *3* (1), 31-42.

135. Shirgaonkar, I. Z.; Lothe, R. R.; Pandit, A. B., Comments on the mechanism of microbial cell disruption in high-pressure and high-speed devices. *Biotechnol. Progr.* **1998,** *14* (4), 657-660.

136. Kumar, P. S.; Pandit, A., Modeling Hydrodynamic Cavitation. *Chem. Eng. Technol.* **1999,** *22* (12), 1017-1027.

137. Chandler, D. P.; Brown, J.; Bruckner-Lea, C. J.; Olson, L.; Posakony, G. J.; Stults, J. R.; Valentine, N. B.; Bond, L. J., Continuous spore disruption using radially focused, high-frequency ultrasound. *Anal. Chem.* **2001,** *73* (15), 3784-3789.

138. Taylor, M. T.; Belgrader, P.; Furman, B. J.; Pourahmadi, F.; Kovacs, G. T.; Northrup, M. A., Lysing bacterial spores by sonication through a flexible interface in a microfluidic system. *Anal. Chem.* **2001,** *73* (3), 492-496.

139. Onyeche, T.; Schläfer, O.; Bormann, H.; Schröder, C.; Sievers, M., Ultrasonic cell disruption of stabilised sludge with subsequent anaerobic digestion. *Ultrasonics* **2002,** *40* (1), 31-35.

140. Fykse, E. M.; Olsen, J. S.; Skogan, G., Application of sonication to release DNA from bacillus cereus for quantitative detection by real-time PCR. *J. Microbiol. Methods* **2003,** *55* (1), 1-10.

141. Borthwick, K.; Coakley, W.; McDonnell, M.; Nowotny, H.; Benes, E.; Gröschl, M., Development of A Novel Compact Sonicator for Cell Disruption. *J. Microbiol. Methods* **2005,** *60* (2), 207-216.

142. Gogate, P. R.; Pandit, A. B., Application of cavitational reactors for cell disruption for recovery of intracellular enzymes. *J. Chem. Technol. Biotechnol.* **2008,** *83* (8), 1083-1093.

143. Pan, X.; Niu, G.; Liu, H., Comparison of microwave-assisted extraction and conventional extraction techniques for the extraction of tanshinones from salvia miltiorrhiza bunge. *Biochem. Eng. J.* **2002,** *12* (1), 71-77.

144. Terigar, B.; Balasubramanian, S.; Boldor, D.; Xu, Z.; Lima, M.; Sabliov, C., Continuous microwave-assisted isoflavone extraction system: design and performance evaluation. *Bioresour. Technol.* **2010,** *101* (7), 2466-2471.

145. Balasubramanian, S.; Allen, J. D.; Kanitkar, A.; Boldor, D., Oil extraction from scenedesmus obliquus using a continuous microwave system–design, optimization, and quality characterization. *Bioresour. Technol.* **2011,** *102* (3), 3396-3403.

146. Andrews, B.; Asenjo, J., Enzymatic lysis and disruption of microbial cells. *Trends Biotechnol.* **1987,** *5* (10), 273-277.

147. Harrison, S. T., Bacterial Cell Disruption: A key unit operation in the recovery of intracellular products. *Biotechnol. Adv.* **1991,** *9* (2), 217-240.

148. Mendes-Pinto, M.; Raposo, M.; Bowen, J.; Young, A.; Morais, R., Evaluation of Different Cell Disruption Processes on Encysted Cells of Haematococcus Pluvialis: Effects on Astaxanthin Recovery and Implications for Bio-availability. *J. Appl. Phycol.* **2001,** *13* (1), 19-24.

149. Harun, R.; Danquah, M. K., Influence of acid pre-treatment on microalgal biomass for bioethanol production. *Process Biochem.* **2011,** *46* (1), 304-309.

150. Miranda, J.; Passarinho, P. C.; Gouveia, L., Pre-treatment optimization of scenedesmus obliquus microalga for bioethanol production. *Bioresour. Technol.* **2012,** *104*, 342-348.

151. Brown, R.; Bartoletti, D.; Harrison, G.; Gamble, T.; Bliss, J.; Powell, K.; Weaver, J., Multiple-pulse electroporation: uptake of a macromolecule by individual cells of saccharomyces cerevisiae. *J. Electroanal. Chem.* **1992,** *343* (1), 235-245.

152. Muraji, M.; Tatebe, W.; Konishi, T.; Fujii, T.; Berg, H., Effect of Electrical Energy on the Electropermeabilization of Yeast Cells. *Bioelectrochem. Bioenerg.* **1993,** *31* (1), 77-84.

153. Ganeva, V.; Galutzov, B.; Teissié, J., Electric field mediated loading of macromolecules in intact yeast cells is critically controlled at the wall level. *BBA-Biomembranes* **1995,** *1240* (2), 229-236.

154. Qin, B.-L.; Pothakamury, U. R.; Vega, H.; Martin, O.; Barbosa-Canovas, G. V.; Swanson, G.; Mermelstein, N., Food pasteurization using high-intensity pulsed electric fields. *Food Technol-Chicago* **1995,** *49* (12), 55-60.

155. Ho, S.; Mittal, G., Electroporation of cell membranes: a review. *Crit. Rev. Biotechnol.* **1996,** *16* (4), 349-362.

156.   Muraji, M.; Tatebe, W.; Berg, H., The influence of extracellular alkali and alkaline-earth ions on electropermeation of saccharomyces cerevisiae. *Bioelectrochem. Bioenerg.* **1998,** *46* (2), 293-295.

157.   Muraji, M.; Taniguchi, H.; Tatebe, W.; Berg, H., Examination of the Relationship Between Parameters to Determine Electropermeability of Saccharomyces Cerevisiae. *Bioelectrochem. Bioenerg.*   **1999,** *48* (2), 485-488.

158.   Ade-Omowaye, B.; Taiwo, K.; Eshtiaghi, N.; Angersbach, A.; Knorr, D., Comparative evaluation of the effects of pulsed electric field and freezing on cell membrane permeabilisation and mass transfer during dehydration of red bell peppers. *Innovative Food Sci. Emerg. Technol.* **2003,** *4* (2), 177-188.

159.   Smith, G. J.; Daniels, V., Algal blooms of the 18th and 19th centuries. *Toxicon* **2018,** *142*, 42-44.

160.   Sheehan, J.; Dunahay, T.; Benemann, J.; Roessler, P., A look back at the US Department of Energy's aquatic species program: biodiesel from algae. *National Renewable Energy Laboratory* **1998,** *328*.

161.   Chisti, Y., Biodiesel from microalgae. *Biotechnol Adv* **2007,** *25* (3), 294-306.

162.   Zhou, W.; Cheng, Y.; Li, Y.; Wan, Y.; Liu, Y.; Lin, X.; Ruan, R., Novel fungal pelletization-assisted technology for algae harvesting and wastewater treatment. *Applied Biochemistry and Biotechnology* **2012,** *167* (2), 214-228.

163.   Gerardo, M. L.; Oatley-Radcliffe, D. L.; Lovitt, R. W., Integration of membrane technology in microalgae biorefineries. *J. Membr. Sci.***2014,** *464*, 86-99.

164.   Bilad, M. R.; Discart, V.; Vandamme, D.; Foubert, I.; Muylaert, K.; Vankelecom, I. F., Harvesting microalgal biomass using a magnetically induced membrane vibration (MMV) system: filtration performance and energy consumption. *Bioresour. Technol.* **2013,** *138*, 329-338.

165.   Barros, A. I.; Gonçalves, A. L.; Simões, M.; Pires, J. C., Harvesting techniques applied to microalgae: a review. *Renewable and Sustainable Energy Reviews* **2015,** *41*, 1489-1500.

166.   Gerardo, M. L.; Van Den Hende, S.; Vervaeren, H.; Coward, T.; Skill, S. C., Harvesting of microalgae within a biorefinery approach: A review of the developments and case studies from pilot-plants. *Algal Research* **2015,** *11*, 248-262.

167.   Meng, F.; Yang, F.; Shi, B.; Zhang, H., A comprehensive study on membrane fouling in submerged membrane bioreactors operated under different aeration intensities. *Sep. Purif. Technol.* **2008,** *59* (1), 91-100.

168. Bilad, M. R.; Vandamme, D.; Foubert, I.; Muylaert, K.; Vankelecom, I. F., Harvesting microalgal biomass using submerged microfiltration membranes. *Bioresour. Technol.* **2012,** *111*, 343-352.

169. Li, W.; Zhou, Q.; Hua, T., Removal of organic matter from landfill leachate by advanced oxidation processes: a review. *Int. J. Chem. Eng.* **2010,** *2010*.

170. Chen, G., Electrochemical technologies in wastewater treatment. *Sep. Purif. Technol.* **2004,** *38* (1), 11-41.

171. Del Moro, G.; Prieto-Rodríguez, L.; De Sanctis, M.; Di Iaconi, C.; Malato, S.; Mascolo, G., Landfill leachate treatment: Comparison of standalone electrochemical degradation and combined with a novel biofilter. *Chem. Eng. J.* **2016,** *288*, 87-98.

172. Müller, G. T.; Giacobbo, A.; dos Santos Chiaramonte, E. A.; Rodrigues, M. A. S.; Meneguzzi, A.; Bernardes, A. M., The effect of sanitary landfill leachate aging on the biological treatment and assessment of photoelectrooxidation as a pre-treatment process. *Waste Manage.* **2015,** *36*, 177-183.

173. Bashir, M. J.; Aziz, H. A.; Aziz, S. Q.; Abu Amr, S. S., An overview of electro-oxidation processes performance in stabilized landfill leachate treatment. *Desalin. Water Treat.* **2013,** *51* (10-12), 2170-2184.

174. Kinani, S.; Richard, B.; Souissi, Y.; Bouchonnet, S., Analysis of inorganic chloramines in water. *TrAC Trends in Anal. Chem.* **2012,** *33*, 55-67.

175. Zhang, H.; Ran, X.; Wu, X.; Zhang, D., Evaluation of electro-oxidation of biologically treated landfill leachate using response surface methodology. *J. Hazard. Mater.* **2011,** *188* (1), 261-268.

176. Hua, L.; Guo, L.; Thakkar, M.; Wei, D.; Agbakpe, M.; Kuang, L.; Magpile, M.; Chaplin, B. P.; Tao, Y.; Shuai, D., Effects of anodic oxidation of a substoichiometric titanium dioxide reactive electrochemical membrane on algal cell destabilization and lipid extraction. *Bioresour. Technol.* **2016,** *203*, 112-117.

177. Zaky, A. M.; Chaplin, B. P., Mechanism of p-Substituted Phenol Oxidation at a Ti_4O_7 Reactive Electrochemical Membrane. *Environ. Sci. Technol.* **2014,** *48* (10), 5857-5867.

178. Nah, Y. C.; Paramasivam, I.; Schmuki, P., Doped TiO_2 and TiO_2 nanotubes: synthesis and applications. *ChemPhysChem* **2010,** *11* (13), 2698-2713.

179. Nowotny, J.; Alim, M. A.; Bak, T.; Idris, M. A.; Ionescu, M.; Prince, K.; Sahdan, M. Z.; Sopian, K.; Teridi, M. A. M.; Sigmund, W., Defect chemistry and defect engineering of TiO_2-based semiconductors for solar energy conversion. *Chem. Soc. Rev.* **2015,** *44* (23), 8424-8442.

180. Yang, Y.; Hoffmann, M. R., Synthesis and stabilization of blue-black TiO_2 nanotube arrays for electrochemical oxidant generation and wastewater treatment. *Environ. Sci. Technol.* **2016,** *50* (21), 11888-11894.

181. Neamen, D. A., Semiconductor physics and devices: basic principles. New York, NY: McGraw-Hill: 2012.

182. Kohtani, S.; Kawashima, A.; Miyabe, H., Reactivity of trapped and accumulated electrons in titanium dioxide photocatalysis. *Catalysts* **2017,** *7* (10), 303.

183. Di Valentin, C.; Pacchioni, G.; Selloni, A., Reduced and n-type doped TiO_2: nature of Ti^{3+} species. *The J. Phys. Chem. C* **2009,** *113* (48), 20543-20552.

184. Panayotov, D. A.; Yates Jr, J. T., n-Type doping of TiO_2 with atomic hydrogen-observation of the production of conduction band electrons by infrared spectroscopy. *Chem. Phys. Lett.* **2007,** *436* (1-3), 204-208.

185. Alves, C. S.; Melo, M. N.; Franquelim, H. G.; Ferre, R.; Planas, M.; Feliu, L.; Bardají, E.; Kowalczyk, W.; Andreu, D.; Santos, N. C., Escherichia coli cell surface perturbation and disruption induced by antimicrobial peptides BP100 and pepR. *J. Biol. Chem.* **2010,** *285* (36), 27536-27544.

186. Zhang, W.; Kalive, M.; Capco, D. G.; Chen, Y., Adsorption of hematite nanoparticles onto Caco-2 cells and the cellular impairments: effect of particle size. *Nanotechnology* **2010,** *21* (35), 355103.

187. Corbett, J. C.; McNeil-Watson, F.; Jack, R. O.; Howarth, M., Measuring surface zeta potential using phase analysis light scattering in a simple dip cell arrangement. *Colloids Surf. A* **2012,** *396*, 169-176.

188. Swan, J. W.; Furst, E. M., A simpler expression for Henry's function describing the electrophoretic mobility of spherical colloids. *J. Colloid Interface Sci.* **2012,** *388* (1), 92-94.

189. Zaky, A. M.; Chaplin, B. P., Porous substoichiometric TiO_2 anodes as reactive electrochemical membranes for water treatment. *Environ. Sci. Technol.* **2013,** *47* (12), 6554-6563.

190. Jing, Y.; Guo, L.; Chaplin, B. P., Electrochemical impedance spectroscopy study of membrane fouling and electrochemical regeneration at a sub-stoichiometric TiO_2 reactive electrochemical membrane. *J. Membr. Sci.* **2016,** *510*, 510-523.

191. Yu, S.; Zuo, X.; Bao, R.; Xu, X.; Wang, J.; Xu, J., Effect of SiO_2 nanoparticle addition on the characteristics of a new organic–inorganic hybrid membrane. *Polymer* **2009,** *50* (2), 553-559.

192. Vatanpour, V.; Madaeni, S. S.; Rajabi, L.; Zinadini, S.; Derakhshan, A. A., Boehmite nanoparticles as a new nanofiller for preparation of antifouling mixed matrix membranes. *J. Membr. Sci.***2012,** *401–402*, 132-143.

193. Zinadini, S.; Zinatizadeh, A. A.; Rahimi, M.; Vatanpour, V.; Zangeneh, H., Preparation of a novel antifouling mixed matrix PES membrane by embedding graphene oxide nanoplates. *J. Membr. Sci.***2014,** *453*, 292-301.

194. Elgrishi, N.; Rountree, K. J.; McCarthy, B. D.; Rountree, E. S.; Eisenhart, T. T.; Dempsey, J. L., A practical beginner's guide to cyclic voltammetry. *J. Chem. Educ.* **2017,** *95* (2), 197-206.

195. Gabrielli, C.; Huet, F.; Keddam, M.; Rousseau, P.; Vivier, V., Scanning electrochemical microscopy for investigating gas bubble/liquid interfaces. *Electrochem. Solid-State Lett.***2003,** *6* (10), E23-E26.

196. Hung, M.; Liu, J., Microfiltration for separation of green algae from water. *Colloids Surf B Biointerfaces.* **2006,** *51* (2), 157-164.

197. Ge, S.; Agbakpe, M.; Zhang, W.; Kuang, L.; Wu, Z.; Wang, X., recovering magnetic Fe_3O_4-ZnO nanocomposites from algal biomass based on hydrophobicity shift under UV irradiation. *ACS Appl. Mater. Inter.* **2015,** *7* (21), 11677-11682.

198. Ge, S.; Agbakpe, M.; Zhang, W.; Kuang, L., Heteroaggregation between PEI-Coated Magnetic Nanoparticles and Algae: Effect of Particle Size on Algal Harvesting Efficiency. *ACS Appl. Mater. Inter.* **2015,** *7* (11), 6102-6108.

199. Song, L., Flux decline in crossflow microfiltration and ultrafiltration: mechanisms and modeling of membrane fouling. *J. Membr. Sci.***1998,** *139* (2), 183-200.

200. Chu, H.; Zhao, F.; Tan, X.; Yang, L.; Zhou, X.; Zhao, J.; Zhang, Y., The impact of temperature on membrane fouling in algae harvesting. *Algal Research* **2016,** *16*, 458-464.

201. Bacchin, P.; Aimar, P.; Field, R. W., Critical and sustainable fluxes: theory, experiments and applications. *J. Membr. Sci.***2006,** *281* (1-2), 42-69.

202. van der Marel, P.; Zwijnenburg, A.; Kemperman, A.; Wessling, M.; Temmink, H.; van der Meer, W., An improved flux-step method to determine the critical flux and the critical flux for irreversibility in a membrane bioreactor. *J. Membr. Sci.***2009,** *332* (1), 24-29.

203. Zhao, F.; Chu, H.; Su, Y.; Tan, X.; Zhang, Y.; Yang, L.; Zhou, X., Microalgae harvesting by an axial vibration membrane: the mechanism of mitigating membrane fouling. *J. Membr. Sci.***2016,** *508*, 127-135.

204. Zhang, X.; Hu, Q.; Sommerfeld, M.; Puruhito, E.; Chen, Y., Harvesting algal biomass for biofuels using ultrafiltration membranes. *Bioresour. Technol.* **2010,** *101* (14), 5297-5304.

205. Zhang, X.; Chen, Y.; Konsowa, A.; Zhu, X.; Crittenden, J. C., Evaluation of an innovative polyvinyl chloride (PVC) ultrafiltration membrane for wastewater treatment. *Sep. Purif. Technol.* **2009,** *70* (1), 71-78.

206. Wu, X.; Zhou, C.; Li, K.; Zhang, W.; Tao, Y., Probing the fouling process and mechanisms of submerged ceramic membrane ultrafiltration during algal harvesting under sub-and super-critical fluxes. *Sep. Purif. Technol.* **2018,** *195*, 199-207.

207. Aimar, P.; Howell, J.; Turner, M., Effects of concentration boundary layer development on the flux limitations in ultrafiltration. *Chemical engineering research & design* **1989,** *67* (3), 255-261.

208. Field, R.; Wu, D.; Howell, J.; Gupta, B., Critical flux concept for microfiltration fouling. *J. Membr. Sci.***1995,** *100* (3), 259-272.

209. Rushton, A.; Ward, A.; Holdich, R., Filtration fundamentals. *Solid-Liquid Filtration and Separation Technology* **1996**, 33-83.

210. Bai, R.; Leow, H., Microfiltration of activated sludge wastewater—the effect of system operation parameters. *Sep. Purif. Technol.* **2002,** *29* (2), 189-198.

211. Lee, J.-D.; Lee, S.-H.; Jo, M.-H.; Park, P.-K.; Lee, C.-H.; Kwak, J.-W., Effect of coagulation conditions on membrane filtration characteristics in coagulation-microfiltration process for water treatment. *Environ. Sci. Technol.* **2000,** *34* (17), 3780-3788.

212. Papaioannou, T. G.; Stefanadis, C., Vascular wall shear stress: basic principles and methods. *Hellenic J Cardiol* **2005,** *46* (1), 9-15.

213. Lousada-Ferreira, M., *Filterability and sludge concentration in Membrane Bioreactors*. TU Delft, Delft University of Technology: 2011.

214. Rosenberger, S.; Kubin, K.; Kraume, M., Rheology of activated sludge in membrane bioreactors. *Engineering in life sciences* **2002,** *2* (9), 269-275.

215. Meng, F.; Shi, B.; Yang, F.; Zhang, H., New insights into membrane fouling in submerged membrane bioreactor based on rheology and hydrodynamics concepts. *J. Membr. Sci.***2007,** *302* (1-2), 87-94.

216. Laera, G.; Giordano, C.; Pollice, A.; Saturno, D.; Mininni, G., Membrane bioreactor sludge rheology at different solid retention times. *Water Res.* **2007,** *41* (18), 4197-4203.

217   Yang, F.; Bick, A.; Shandalov, S.; Brenner, A.; Oron, G., Yield stress and rheological characteristics of activated sludge in an airlift membrane bioreactor. *J. Membr. Sci.* **2009,** *334* (1-2), 83-90.

218.   Le-Clech, P.; Chen, V.; Fane, T. A., Fouling in membrane bioreactors used in wastewater treatment. *J. Membr. Sci.* **2006,** *284* (1-2), 17-53.

219.   Toh, P. Y.; Ng, B. W.; Ahmad, A. L.; Chieh, D. C. J.; Lim, J., The role of particle-to-cell interactions in dictating nanoparticle aided magnetophoretic separation of microalgal cells. *Nanoscale* **2014**.

220.   Ge, S.; Agbakpe, M.; Wu, Z.; Kuang, L.; Zhang, W.; Wang, X., Influences of Surface Coating, UV Irradiation and Magnetic Field on the Algae Removal Using Magnetite Nanoparticles. *Environ Sci Technol* **2014,** *49* (2), 1190-1196.

221.   Zhang, W.; Zhang, X., Adsorption of MS2 on oxide nanoparticles affects chlorine disinfection and solar inactivation. *Water Res.* **2015,** *69*, 59-67.

222.   Grasso, D.; Subramaniam, K.; Butkus, M.; Strevett, K.; Bergendahl, J., A review of non-DLVO interactions in environmental colloidal systems. *Rev. Environ. Sci. Biotechnol.* **2002,** *1* (1), 17-38.

223   Yoon, R.-H.; Flinn, D. H.; Rabinovich, Y. I., Hydrophobic interactions between dissimilar surfaces. *J. Colloid Interface Sci.* **1997,** *185* (2), 363-370.

224.   Park, B.-J.; Abu-Lail, N. I., The role of the pH conditions of growth on the bioadhesion of individual and lawns of pathogenic< i> Listeria monocytogenes</i> cells. *J. Colloid Interface Sci.* **2011,** *358* (2), 611-620.

225.   Van Oss, C.; Good, R.; Chaudhury, M., The role of van der Waals forces and hydrogen bonds in "hydrophobic interactions" between biopolymers and low energy surfaces. *J. Colloid Interface Sci.* **1986,** *111* (2), 378-390.

226.   Oss, C. v.; Good, R.; Busscher, R., Estimation of the polar surface tension parameters of glycerol and formamide, for use in contact angle measurements on polar solids. *J. Dispers. Sci. Technol.* **1990,** *11* (1), 75-81.

227.   Ahadpour Shal, A.; Jafari, A., Study of structural and magnetic properties of superparamagnetic fe_3o_4–zno core–shell nanoparticles. *J Supercond Nov Magn* **2014,** *27* (6), 1531-1538.

228.   Agbakpe, M.; Ge, S.; Zhang, W.; Zhang, X.; Kobylarz, P., Algae harvesting for biofuel production: Influences of UV irradiation and polyethylenimine (PEI) coating on bacterial biocoagulation. *Bioresour. Technol.* **2014,** *166*, 266–272.

229.   Oss, C. J. v., *Interfacial Forces in Aquaeous Media*. Second Edition ed.; Taylor & Francis Group: Boca Raton, Florida, 2006; p 81-83.

230. Abu-Lail, N. I.; Camesano, T. A., Role of ionic strength on the relationship of biopolymer conformation, DLVO contributions, and steric interactions to bioadhesion of Pseudomonas putida KT2442. *Biomacromolecules* **2003,** *4* (4), 1000-12.

231. Runkana, V.; Somasundaran, P.; Kapur, P. C., A population balance model for flocculation of colloidal suspensions by polymer bridging. *Chem Eng Sci* **2006,** *61* (1), 182-191.

232. Zhang, Q. Synthesis and Characterization of Novel Magnetite Nanoparticle Block Copolymer Complexes. Virginia Polytechnic Institute and State University, 2007.

233. Acha, C.; Monteverde, M.; Nunez-Regueiro, M.; Kuhn, A.; Franco, M. A., Electrical resistivity of the Ti $\mathsf{_4}$ O $\mathsf{_7}$ Magneli phase under high pressure. *The European Physical Journal B-Condensed Matter and Complex Systems* **2003,** *34* (4), 421-428.

234. Conze, S.; Veremchuk, I.; Reibold, M.; Matthey, B.; Michaelis, A.; Grin, Y.; Kinski, I., Magnéli phases Ti4O7 and Ti8O15 and their carbon nanocomposites via the thermal decomposition-precursor route. *Journal of Solid State Chemistry* **2015,** *229*, 235-242.

235. Park, H.; Choi, W., Effects of TiO2 surface fluorination on photocatalytic reactions and photoelectrochemical behaviors. *The J. Phys. Chem. B* **2004,** *108* (13), 4086-4093.

236. Walsh, F.; Wills, R., The continuing development of Magnéli phase titanium sub-oxides and Ebonex® electrodes. *Electrochimica Acta* **2010,** *55* (22), 6342-6351.

237. Nayak, S.; Chaplin, B. P., Fabrication and characterization of porous, conductive, monolithic Ti4O7 electrodes. *Electrochimica Acta* **2018,** *263*, 299-310.

238. Zhang, Q.; Xu, R.; Xu, P.; Chen, R.; He, Q.; Zhong, J.; Gu, X., Performance study of ZrO2 ceramic micro-filtration membranes used in pretreatment of DMF wastewater. *Desalination* **2014,** *346*, 1-8.

239. Chung, C. M.; Tobino, T.; Cho, K.; Yamamoto, K., Alleviation of membrane fouling in a submerged membrane bioreactor with electrochemical oxidation mediated by in-situ free chlorine generation. *Water Res.* **2016,** *96*, 52-61.

240. Trellu, C.; Coetsier, C.; Rouch, J.-C.; Esmilaire, R.; Rivallin, M.; Cretin, M.; Causserand, C., Mineralization of organic pollutants by anodic oxidation using reactive electrochemical membrane synthesized from carbothermal reduction of TiO2. *Water Res.* **2018,** *131*, 310-319.

241.   Elcik, H.; Cakmakci, M., Harvesting microalgal biomass using crossflow membrane filtration: critical flux, filtration performance, and fouling characterization. *Environmental technology* **2017,** *38* (12), 1585-1596.

242.   Wicaksana, F.; Fane, A. G.; Pongpairoj, P.; Field, R., Microfiltration of algae (Chlorella sorokiniana): Critical flux, fouling and transmission. *J. Membr. Sci.* **2012,** *387*, 83-92.

243.   Zhao, F.; Su, Y.; Tan, X.; Chu, H.; Zhang, Y.; Yang, L.; Zhou, X., Effect of temperature on extracellular organic matter (EOM) of Chlorella pyrenoidosa and effect of EOM on irreversible membrane fouling. *Colloids Surf B Biointerfaces.* **2015,** *136*, 431-439.

244.   Tan, X.; Chu, H.; Zhang, Y.; Yang, L.; Zhao, F.; Zhou, X., Chlorella pyrenoidosa cultivation using anaerobic digested starch processing wastewater in an airlift circulation photobioreactor. *Bioresour. Technol.* **2014,** *170*, 538-548.

245.   Zhang, Y.; Zhao, Y.; Chu, H.; Zhou, X.; Dong, B., Dewatering of Chlorella pyrenoidosa using diatomite dynamic membrane: filtration performance, membrane fouling and cake behavior. *Colloids Surf B Biointerfaces.* **2014,** *113*, 458-466.

246.   Kanchanatip, E.; Su, B.-R.; Tulaphol, S.; Den, W.; Grisdanurak, N.; Kuo, C.-C., Fouling characterization and control for harvesting microalgae Arthrospira (Spirulina) maxima using a submerged, disc-type ultrafiltration membrane. *Bioresour. Technol.* **2016,** *209*, 23-30.

247.   Rossi, N.; Jaouen, P.; Legentilhomme, P.; Petit, I., Harvesting of cyanobacterium Arthrospira platensis using organic filtration membranes. *Food and bioproducts processing* **2004,** *82* (3), 244-250.

248.   Iritani, E.; Katagiri, N.; Takenaka, T.; Yamashita, Y., Membrane pore blocking during cake formation in constant pressure and constant flux dead-end microfiltration of very dilute colloids. *Chemical Engineering Science* **2015,** *122*, 465-473.

249.   He, P. J.; Zheng, Z.; Zhang, H.; Shao, L. M.; Tang, Q. Y., PAEs and BPA removal in landfill leachate with Fenton process and its relationship with leachate DOM composition. *Sci. Total Environ.* **2009,** *407* (17), 4928-33.

250.   Lindim, C.; van Gils, J.; Cousins, I. T., Europe-wide estuarine export and surface water concentrations of PFOS and PFOA. *Water Res.* **2016,** *103*, 124-32.

251.   Rossignol, N.; Vandanjon, L.; Jaouen, P.; Quemeneur, F., Membrane technology for the continuous separation microalgae/culture medium: Compared performances of cross-flow microfiltration and ultrafiltration. *Aquacult. Eng.* **1999,** *20* (3), 191-208.

252.   7th Annual Report on Carcinogens. *US Department of Health and Human Services* **1994,**   (PB95-109781).

253.   Sharma, V. K.; Johnson, N.; Cizmas, L.; McDonald, T. J.; Kim, H., A review of the influence of treatment strategies on antibiotic resistant bacteria and antibiotic resistance genes. *Chemosphere* **2016,** *150*, 702-714.

254   Devi, L.; Kumar, S.; Reddy, K., Photo fenton like process $Fe^{3+}/(NH_4)_2S_2O_8/UV$ for the degradation of Di azo dye congo red using low iron concentration. *Open Chemistry* **2009,** *7* (3), 468-477.

255.   Dickenson, E. R.; Higgins, C., Treatment Mitigation Strategies for Poly-and Perfluoroalkyl Substances [Project# 4322]. **2016**.

256.   Choi, J. Y.; Lee, Y.-J.; Shin, J.; Yang, J.-W., Anodic oxidation of 1, 4-dioxane on boron-doped diamond electrodes for wastewater treatment. *J. Hazard. Mater.***2010,** *179* (1-3), 762-768.

257.   Jiang, C. R.; Xu, Z. C.; Guo, Q. W.; Zhuo, Q. F., Degradation of bisphenol A in water by the heterogeneous photo-Fenton. *Environmental Technology* **2014,** *35* (8), 966-972.

258.   Staples, C. A.; Dorn, P. B.; Klecka, G. M.; O'Block, S. T.; Harris, L. R., A review of the environmental fate, effects, and exposures of bisphenol A. *Chemosphere* **1998,** *36* (10), 2149-2173.

259.   Fassi, S.; Djebbar, K.; Bousnoubra, I.; Chenini, H.; Sehili, T., Oxidation of bromocresol green by different advanced oxidation processes: Fenton, Fenton-like, photo-Fenton, photo-Fenton-like and solar light. Comparative study. *Desalin. Water Treat.* **2014,** *52* (25-27), 4982-4989.

260.   Song, J. M.; Wang, H.; Hu, G.; Zhao, S. J.; Hu, H. Q.; Jin, B. K., $ZnWO_4$–Cu system with enhanced photocatalytic activity by photo-Fenton-like synergistic reaction. *Materials Research Bulletin* **2012,** *47* (11), 3296-3300.

261.   Zakersalehi, A.; Choi, H.; Andersen, J.; Dionysiou, D. D., Photocatalytic ceramic membranes. *Encyclopedia of Membrane Science and Technology* **2013**.

262.   Sabate, J.; Anderson, M.; Kikkawa, H.; Xu, Q.; Cervera-March, S.; Hill, C., Nature and properties of pure and nb-doped Ti02 ceramic membranes affecting the photocatalytic degradation of 3-chlorosalicylic acid as a model of halogenated organic compounds. *J. Catal.* **1992,** *134* (1), 36-46.

263.   Song, L.; Zhu, B.; Gray, S.; Duke, M.; Muthukumaran, S., Performance of Hybrid Photocatalytic-Ceramic Membrane System for the Treatment of Secondary Effluent. *Membranes* **2017,** *7* (2), 20.

264.   Lim, T.-T.; Goei, R., Combined photocatalysis–separation processes for water treatment using hybrid photocatalytic membrane reactors. In *Photocatalysis*, 2016; pp 130-156.

265.   Athanasekou, C. P.; Moustakas, N. G.; Morales-Torres, S.; Pastrana-Martínez, L. M.; Figueiredo, J. L.; Faria, J. L.; Silva, A. M.; Dona-Rodriguez, J. M.; Romanos, G. E.; Falaras, P., Ceramic photocatalytic membranes for water filtration under UV and visible light. *Appl. Catal. B.* **2015,** *178*, 12-19.

266.   Bejan, D.; Guinea, E.; Bunce, N. J., On the nature of the hydroxyl radicals produced at boron-doped diamond and Ebonex® anodes. *Electrochim. Acta* **2012,** *69*, 275-281.

267.   Neta, P.; Dorfman Leon, M., Pulse radiolysis studies. XIII. Rate constants for the reaction of hydroxyl radicals with aromatic compounds in aqueous solutions. In *Radiation Chemistry*, American Chemical Society: 1968; Vol. 81, pp 222-230.

268.   Haag, W.; Yao, C., Rate constants for reaction of hydroxyl radicals with several drinking water contaminants *Environ. Sci. Technol.* **1992,** *26*, 1005-1013.

269.   Tsitonaki, A.; Petri, B.; Crimi, M.; Mosbaek, H.; Siegrist, R. L.; Bjerg, P. L., In situ chemical oxidation of contaminated soil and groundwater using persulfate: A review. *Crit. Rev. Environ. Sci. Technol.* **2010,** *40* (1), 55-91.

270.   Martínez-Huitle, C. A.; Brillas, E., Electrochemical alternatives for drinking water disinfection. *Angew. Chem. Int. Ed.* **2008,** *47* (11), 1998-2005.

271.   Vecitis, C. D.; Schnoor, M. H.; Rahaman, M. S.; Schiffman, J. D.; Elimelech, M., Electrochemical multiwalled carbon nanotube filter for viral and bacterial removal and inactivation. *Environ. Sci. Technol.* **2011,** *45* (8), 3672-3679.

272.   Rajeshwar, K.; Ibanez, J.; Swain, G., Electrochemistry and the environment. *J. Appl. Electrochem.* **1994,** *24* (11), 1077-1091.

273.   Panizza, M.; Bocca, C.; Cerisola, G., Electrochemical treatment of wastewater containing polyaromatic organic pollutants. *Water Res.* **2000,** *34* (9), 2601-2605.

274.   Schaefer, C. E.; Andaya, C.; Urtiaga, A.; McKenzie, E. R.; Higgins, C. P., Electrochemical treatment of perfluorooctanoic acid (PFOA) and perfluorooctane sulfonic acid (PFOS) in groundwater impacted by aqueous film forming foams (AFFFs). *J. Hazard. Mater.* **2015,** *295*, 170-175.

275.   Jasmann, J. R.; Borch, T.; Sale, T. C.; Blotevogel, J., Advanced electrochemical oxidation of 1,4-dioxane via dark catalysis by novel titanium dioxide (TiO_2) pellets. *Environ. Sci. Technol.* **2016,** *50* (16), 8817-8826.

276. Jasmann, J. R.; Borch, T.; Sale, T. C.; Blotevogel, J., Advanced electrochemical oxiddation of 1,4-dioxane via dark catalysis by novel titanium dioxide (TiO$_2$) pellets. *Environ. Sci. Technol.* **2016**.

277. Fang, C.; Megharaj, M.; Naidu, R., Electrochemical Advanced Oxidation Processes (EAOP) to degrade per-and polyfluoroalkyl substances (PFASs). *Journal of Advanced Oxidation Technologies* **2017,** *20* (2).

278. Trautmann, A.; Schell, H.; Schmidt, K.; Mangold, K.-M.; Tiehm, A., Electrochemical degradation of perfluoroalkyl and polyfluoroalkyl substances (PFASs) in groundwater. *Wat. Sci. Tech.* **2015,** *71* (10), 1569-1575.

279. Panizza, M.; Cerisola, G., Direct and mediated anodic oxidation of organic pollutants. *Chem. Rev.* **2009,** *109* (12), 6541-6569.

280. Mohr, T. K.; Stickney, J. A.; DiGuiseppi, W. H., Environmental investigation and remediation: 1, 4-dioxane and other solvent stabilizers. CRC Press: 2016.

281. Toxicological Profile for 1,4-Dioxane. *Agency for Toxic Substances and Disease Registry (ATSDR).* **2012**.

282. Agency, U. S. E. P., Emerging Contaminant Fact Sheet--1,4-Dioxane;. *Office of Solid Waste and Emergency Response* **2009,** *EPA-505-F-09−006*.

283. Agency, U. S. E. P., The third unregulated contaminant monitoring rule (ucmr 3) data summary. **2016,** *EPA-815-S16−002*.

284. Barndõk, H.; Hermosilla, D.; Han, C.; Dionysiou, D. D.; Negro, C.; Blanco, Á., Degradation of 1, 4-dioxane from industrial wastewater by solar photocatalysis using immobilized NF-TiO2 composite with monodisperse TiO$_2$ nanoparticles. *Appl. Catal. B.* **2016,** *180*, 44-52.

285. Stepien, D. K.; Diehl, P.; Helm, J.; Thoms, A.; Püttmann, W., Fate of 1, 4-dioxane in the aquatic environment: From sewage to drinking water. *Water Res.* **2014,** *48*, 406-419.

286. Mohr, T. K., Solvent Stabilizers. **2001**.

287. De Clercq, J.; Van de Steene, E.; Verbeken, K.; Verhaege, M., Electrochemical oxidation of 1, 4-dioxane at boron-doped diamond electrode. *J. Chem. Technol. Biot.* **2010,** *85* (8), 1162-1167.

288. Aksu, Z.; Tatlı, A. İ.; Tunç, Ö., A comparative adsorption/biosorption study of Acid Blue 161: Effect of temperature on equilibrium and kinetic parameters. *Chem. Eng. J.* **2008,** *142* (1), 23-39.

289. Kadirvelu, K.; Kavipriya, M.; Karthika, C.; Radhika, M.; Vennilamani, N.; Pattabhi, S., Utilization of various agricultural wastes for activated carbon

preparation and application for the removal of dyes and metal ions from aqueous solutions. *Bioresour. Technol.* **2003,** *87* (1), 129-132.

290.   May-Lozano, M.; Mendoza-Escamilla, V.; Rojas-García, E.; López-Medina, R.; Rivadeneyra-Romero, G.; Martinez-Delgadillo, S. A., Sonophotocatalytic degradation of Orange II dye using low cost photocatalyst. *Journal of cleaner production* **2017,** *148*, 836-844.

291.   Jain, R.; Mathur, M.; Sikarwar, S.; Mittal, A., Removal of the hazardous dye rhodamine B through photocatalytic and adsorption treatments. *J. Environ. Manage.***2007,** *85* (4), 956-964.

292.   Kousha, M.; Daneshvar, E.; Sohrabi, M. S.; Jokar, M.; Bhatnagar, A., Adsorption of acid orange II dye by raw and chemically modified brown macroalga Stoechospermum marginatum. *Chem. Eng. J.* **2012,** *192*, 67-76.

293.   Gupta, V.; Suhas; Ali, I.; Saini, V., Removal of rhodamine B, fast green, and methylene blue from wastewater using red mud, an aluminum industry waste. *Ind. Eng. Chem. Res.***2004,** *43* (7), 1740-1747.

294.   Mollah, M. Y. A.; Gomes, J. A.; Das, K. K.; Cocke, D. L., Electrochemical treatment of Orange II dye solution—Use of aluminum sacrificial electrodes and floc characterization. *J. Hazard. Mater.***2010,** *174* (1-3), 851-858.

295.   Valica, M.; Hostin, S., Electrochemical treatment of water contaminated with methylorange. *Nova Biotechnologica et Chimica* **2016,** *15* (1), 55-64.

296   National Oceanic and Atmospheric Administration, Distribution of HABs in the U.S. *http://www.whoi.edu/redtide/regions/us-distribution (accessed 21 July 2016)* **(last updated February 25, 2016). (2016)**

297.   Carmichael, W. W.; Boyer, G. L., Health impacts from cyanobacteria harmful algae blooms: Implications for the North American Great Lakes. *Harmful Algae* **2016,** *54*, 194-212.

298.   Dehghani, M. H., Removal of cyanobacterial and algal cells from water by ultrasonic waves — A review. *J. Mol. Liq.***2016,** *222*, 1109-1114.

299.   Anderson, D. M., Turning back the harmful red tide. *Nature* **1997,** *388* (6642), 513.

300.   Brooks, B. W.; Lazorchak, J. M.; Howard, M. D. A.; Johnson, M.-V. V.; Morton, S. L.; Perkins, D. A. K.; Reavie, E. D.; Scott, G. I.; Smith, S. A.; Steevens, J. A., Are harmful algal blooms becoming the greatest inland water quality threat to public health and aquatic ecosystems? *Environ. Toxicol. Chem.* **2016,** *35* (1), 6-13.

301.   Berdalet, E.; Fleming, L. E.; Gowen, R.; Davidson, K.; Hess, P.; Backer, L. C.; Moore, S. K.; Hoagland, P.; Enevoldsen, H., Marine harmful algal blooms, human health and wellbeing: challenges and opportunities in the 21st century. *Journal of the Marine Biological Association of the United Kingdom* **2016,** *96* (1), 61-91.

302.   Jones, J. R.; Bachmann, R. W., Prediction of phosphorus and chlorophyll levels in lakes. *J. Water. Pollut. Control. Fed.***1976**, 2176-2182.

303.   Backer, L. C.; Manassaram-Baptiste, D.; LePrell, R.; Bolton, B., Cyanobacteria and algae blooms: review of health and environmental data from the harmful algal bloom-related illness surveillance system (HABISS) 2007–2011. *Toxins* **2015,** *7* (4), 1048-1064.

304.   National Science and Technology Council, Harmful algal blooms and hypoxia comprehensive research plan and action strategy: an interagency report. **2016**.

305.   Ho, J. C.; Michalak, A. M., Challenges in tracking harmful algal blooms: a synthesis of evidence from Lake Erie. *J. Great. Lakes. Res.***2015,** *41* (2), 317-325.

306.   U.S. EPA, E. P. A., Algal Toxin Risk Assessment and Management Strategic Plan for Drinking Water, Strategy Submitted to Congress to Meet the Requirements of P.L. 114-45. EPA Doc. 810R04003. **2015**.

307.   Wen, G.; Zhu, H.; Wei, Y.; Huang, T.; Ma, J., Formation of assimilable organic carbon during the oxidation of water containing Microcystis aeruginosa by ozone and an advanced oxidation process using ozone/hydrogen peroxide. *Chem. Eng. J.* **2017,** *307*, 364-371.

308.   Zamyadi, A.; MacLeod, S. L.; Fan, Y.; McQuaid, N.; Dorner, S.; Sauvé, S.; Prévost, M., Toxic cyanobacterial breakthrough and accumulation in a drinking water plant: a monitoring and treatment challenge. *Water Res.* **2012,** *46* (5), 1511-1523.

309.   Liu, Y.; Ren, J.; Wang, X.; Fan, Z., Mechanism and Reaction Pathways for Microcystin-LR Degradation through UV/H2O2 Treatment. *PloS one* **2016,** *11* (6), e0156236.

310.   Park, J.-A.; Yang, B.; Park, C.; Choi, J.-W.; van Genuchten, C. M.; Lee, S.-H., Oxidation of microcystin-LR by the Fenton process: Kinetics, degradation intermediates, water quality and toxicity assessment. *Chem. Eng. J.* **2017,** *309* (Supplement C), 339-348.

311.   Moon, B.-R.; Kim, T.-K.; Kim, M.-K.; Choi, J.; Zoh, K.-D., Degradation mechanisms of Microcystin-LR during UV-B photolysis and UV/H2O2

processes: Byproducts and pathways. *Chemosphere* **2017,** *185* (Supplement C), 1039-1047.

312. Bosma, R.; Miazek, K.; Willemsen, S. M.; Vermuë, M. H.; Wijffels, R. H., Growth inhibition of *Monodus subterraneus* by free fatty acids. *Biotechnol. Bioeng.* **2008,** *101* (5), 1108-1114.

313. Azov, Y.; Goldman, J. C., Free ammonia inhibition of algal photosynthesis in intensive cultures. *Appl. Environ. Microbiol.* **1982,** *43* (4), 735-739.

314. Kearney, D.; Bejan, D.; Bunce, N. J., The use of Ebonex electrodes for the electrochemical removal of nitrate ion from water. *Can. J. Chem.* **2012,** *90* (8), 666-674.

315. El-Sherif, S.; Bejan, D.; Bunce, N. J., Electrochemical oxidation of sulfide ion in synthetic sour brines using periodic polarity reversal at Ebonex® electrodes. *Can. J. Chem.* **2010,** *88* (9), 928-936.

316. Li, L.; Liu, Y., Ammonia removal in electrochemical oxidation: Mechanism and pseudo-kinetics. *J. Hazard. Mater.* **2009,** *161* (2-3), 1010-1016.

317. Stylianou, S. K.; Katsoyiannis, I. A.; Ernst, M.; Zouboulis, A. I., Impact of O3 or O_3/H_2O_2 treatment via a membrane contacting system on the composition and characteristics of the natural organic matter of surface waters. *Environ. Sci. Pollut. Res. Int.* **2017**, 1-10.

318. Hua, G.; Reckhow, D. A., Characterization of disinfection byproduct precursors based on hydrophobicity and molecular size. *Environ. Sci. Technol.* **2007,** *41* (9), 3309-3315.

319. Radjenovic, J.; Sedlak, D. L., Challenges and opportunities for electrochemical processes as next-generation technologies for the treatment of contaminated water. *Environ. Sci. Technol.* **2015,** *49* (19), 11292-11302.

320. Särkkä, H.; Vepsäläinen, M.; Sillanpää, M., Natural organic matter (NOM) removal by electrochemical methods—A review. *J. Electroanal. Chem.* **2015,** *755*, 100-108.

321. Organization, W. H., Assessing Microbial Safety of Drinking Water Improving Approaches and Methods: Improving Approaches and Methods. OECD Publishing: 2003.

322. Lavonen, E. E.; Gonsior, M.; Tranvik, L. J.; Schmitt-Kopplin, P.; Köhler, S. J., Selective chlorination of natural organic matter: identification of previously unknown disinfection byproducts. *Environ. Sci. Technol.* **2013,** *47* (5), 2264-2271.

323. Daiber, E. J.; DeMarini, D. M.; Ravuri, S. A.; Liberatore, H. K.; Cuthbertson, A. A.; Thompson-Klemish, A.; Byer, J. D.; Schmid, J. E.; Afifi, M. Z.; Blatchley, E. R.; Richardson, S. D., Progressive increase in disinfection byproducts and mutagenicity from source to tap to swimming pool and spa water: impact of human inputs. *Environ. Sci. Technol.* **2016,** *50* (13), 6652-6662.

324. Jeong, C. H.; Postigo, C.; Richardson, S. D.; Simmons, J. E.; Kimura, S. Y.; Mariñas, B. J.; Barcelo, D.; Liang, P.; Wagner, E. D.; Plewa, M. J., Occurrence and comparative toxicity of haloacetaldehyde disinfection byproducts in drinking water. *Environ. Sci. Technol.* **2015,** *49* (23), 13749-13759.

325. Zhai, H.; Zhang, X.; Zhu, X.; Liu, J.; Ji, M., Formation of Brominated disinfection byproducts during chloramination of drinking water: new polar species and overall kinetics. *Environ. Sci. Technol.* **2014,** *48* (5), 2579-2588.

326. Shi, P.; Jia, S.; Zhang, X.-X.; Zhang, T.; Cheng, S.; Li, A., Metagenomic insights into chlorination effects on microbial antibiotic resistance in drinking water. *Water Res.* **2013,** *47* (1), 111-120.

327. Loo, S.-L.; Fane, A. G.; Lim, T.-T.; Krantz, W. B.; Liang, Y.-N.; Liu, X.; Hu, X., Superabsorbent cryogels decorated with silver nanoparticles as a novel water technology for point-of-use disinfection. *Environ. Sci. Technol.* **2013,** *47* (16), 9363-9371.

328. Chiao, T.-H.; Clancy, T. M.; Pinto, A.; Xi, C.; Raskin, L., Differential resistance of drinking water bacterial populations to monochloramine disinfection. *Environ. Sci. Technol.* **2014,** *48* (7), 4038-4047.

329. Krasner, S. W.; Weinberg, H. S.; Richardson, S. D.; Pastor, S. J.; Chinn, R.; Sclimenti, M. J.; Onstad, G. D.; Thruston, A. D., Occurrence of a New generation of disinfection byproducts. *Environ Sci Technol* **2006,** *40* (23), 7175-7185.

330. Mahmoudi, M.; Serpooshan, V., Silver-Coated engineered magnetic nanoparticles are promising for the success in the fight against antibacterial resistance threat. *ACS NANO* **2012,** *6* (3), 2656-2664.

331. Wu, M.-C.; Deokar, A. R.; Liao, J.-H.; Shih, P.-Y.; Ling, Y.-C., Graphene-based photothermal agent for rapid and effective killing of bacteria. *ACS NANO* **2013,** *7* (2), 1281-1290.

332 Scialdone, O.; Galia, A.; Filardo, G., Electrochemical incineration of 1, 2-dichloroethane: effect of the electrode material. *Electrochimica Acta* **2008,** *53* (24), 7220-7225.

333 Wang, J.; Zhi, D.; Zhou, H.; He, X.; Zhang, D., Evaluating tetracycline degradation pathway and intermediate toxicity during the electrochemical oxidation over a Ti/Ti$_4$O$_7$ anode. *Water Res.* **2018,** *137*, 324-334.

334.   Almassi, S.; Li, Z.; Xu, W.; Pu, C.; Zeng, T.; Chaplin, B. P., Simultaneous adsorption and electrochemical reduction of n-nitrosodimethylamine using carbon-ti$_4$o$_7$ composite reactive electrochemical membranes. *Environ. Sci. Technol.* **2018,** *53* (2), 928-937.

335.   Jasmann, J. R.; Gedalanga, P. B.; Borch, T.; Mahendra, S.; Blotevogel, J., Synergistic treatment of mixed 1,4-dioxane and chlorinated solvent contaminations by coupling electrochemical oxidation with aerobic biodegradation. *Environ. Sci. Technol.* **2017,** *51* (21), 12619-12629.

336.   Barndok, H.; Hermosilla, D.; Cortijo, L.; Torres, E.; Blanco, Á., Electrooxidation of industrial wastewater containing 1, 4-dioxane in the presence of different salts. *Environ. Sci. Pollut. Res. Int.* **2014,** *21* (8), 5701-5712.

337.   Nakagawa, H.; Takagi, S.; Maekawa, J., Fered-Fenton process for the degradation of 1, 4-dioxane with an activated carbon electrode: A kinetic model including active radicals. *Chem. Eng. J.* **2016,** *296*, 398-405.

338.   Lin, H.; Niu, J.; Ding, S.; Zhang, L., Electrochemical degradation of perfluorooctanoic acid (PFOA) by Ti/SnO$_2$–Sb, Ti/SnO$_2$–Sb/PbO$_2$ and Ti/SnO2–Sb/MnO2 anodes. *Water Res.* **2012,** *46* (7), 2281-2289.

339.   Gomez-Ruiz, B.; Gómez-Lavín, S.; Diban, N.; Boiteux, V.; Colin, A.; Dauchy, X.; Urtiaga, A., Efficient electrochemical degradation of poly- and perfluoroalkyl substances (PFASs) from the effluents of an industrial wastewater treatment plant. *Chem. Eng. J.* **2017,** *322*, 196-204.

340.   Urtiaga, A.; Fernández-González, C.; Gómez-Lavín, S.; Ortiz, I., Kinetics of the electrochemical mineralization of perfluorooctanoic acid on ultrananocrystalline boron doped conductive diamond electrodes. *Chemosphere* **2015,** *129*, 20-26.

341.   Cañizares, P.; Gadri, A.; Lobato, J.; Nasr, B.; Paz, R.; Rodrigo, M.; Saez, C., Electrochemical oxidation of azoic dyes with conductive-diamond anodes. *Ind. Eng. Chem. Res.***2006,** *45* (10), 3468-3473.

342.   Serra, A. C.; Docal, C.; Gonsalves, A. d. A. R., Efficient azo dye degradation by hydrogen peroxide oxidation with metalloporphyrins as catalysts. *J. Mol. Catal. A-Chem.***2005,** *238* (1), 192-198.

343   Zainal, Z.; Lee, C. Y.; Kassim, A.; Hussein, M. Z.; Yusof, N. A., Photoelectrochemical Degradation of Methyl Orange Using TiO$_2$/Ti Films Prepared via Sol-Gel Technique. *Acta Chimica Slovenica* **2007,** *54* (1).

344.   Szpyrkowicz, L.; Juzzolino, C.; Kaul, S. N., A comparative study on oxidation of disperse dyes by electrochemical process, ozone, hypochlorite and Fenton reagent. *Water Res.* **2001,** *35* (9), 2129-2136.

345.   Abu Ghalwa, N. M.; Zaggout, F. R., Electrodegradation of methylene blue dye in water and wastewater using lead oxide/titanium modified electrode. *J. Environ. Sci. Health A* **2006,** *41* (10), 2271-2282.

346.   Ong, S.-T.; Keng, P.-S.; Lee, W.-N.; Ha, S.-T.; Hung, Y.-T., Dye waste treatment. *Water* **2011,** *3* (1), 157-176.

347.   Lei, L.; Dai, Q., High performance on the degradation of cationic red X-GRL by wet electrocatalytic oxidation process. *Ind. Eng. Chem. Res.***2007,** *46* (26), 8951-8958.

348.   Lee, Y.-J.; Han, H.; Kim, S.-H.; Yang, J.-W., Combination of electrokinetic separation and electrochemical oxidation for acid dye removal from soil. *Sep. Sci. Technol.* **2009,** *44* (10), 2455-2469.

349.   Drees, K. P.; Abbaszadegan, M.; Maier, R. M., Comparative electrochemical inactivation of bacteria and bacteriophage. *Water Res.* **2003,** *37* (10), 2291-2300.

350   Liang, W.; Qu, J.; Chen, L.; Liu, H.; Lei, P., Inactivation of Microcystis aeruginosa by continuous electrochemical cycling process in tube using Ti/RuO2 electrodes. *Environ. Sci. Technol.* **2005,** *39* (12), 4633-4639.

351   Polcaro, A.; Vacca, A.; Mascia, M.; Palmas, S.; Pompei, R.; Laconi, S., Characterization of a stirred tank electrochemical cell for water disinfection processes. *Electrochimica Acta* **2007,** *52* (7), 2595-2602.

352   Fang, Q.; Shang, C.; Chen, G., MS2 inactivation by chloride-assisted electrochemical disinfection. *J. Environ. Eng.* **2006,** *132* (1), 13-22.

353   Song, Q.; Li, M.; Wang, L.; Ma, X.; Liu, F.; Liu, X., Mechanism and optimization of electrochemical system for simultaneous removal of nitrate and ammonia. *J. Hazard. Mater.***2019,** *363*, 119-126.

354   Johnston, S.; Suryanto, B. H. R.; MacFarlane, D. R., Electro-oxidation of ammonia on electrochemically roughened platinum electrodes. *Electrochimica Acta* **2019,** *297*, 778-783.

355.   Wang, Y.; Guo, X.; Li, J.; Yang, Y.; Lei, Z.; Zhang, Z., Efficient Electrochemical Removal of Ammonia with Various Cathodes and Ti/RuO$_2$-Pt Anode. *Open J. Appl. Sci.* **2012,** *02* (04), 241-247.

356   Hu, W.-w.; Gong, B.; Feng, C.-p., Electrochemical oxidation of ammonia-containing wastewater using Ti/RuO$_2$-Pt electrode. *Water Sci. Technol.* **2009,** *2* (4), 103-109.

357   Xu, W.; Lan, R.; Du, D.; Humphreys, J.; Walker, M.; Wu, Z.; Wang, H.; Tao, S., Directly growing hierarchical nickel-copper hydroxide nanowires on carbon

fibre cloth for efficient electrooxidation of ammonia. *Appl. Catal. B.* **2017,** *218*, 470-479.

358.   Ntagia, E.; Fiset, E.; da Silva Lima, L.; Pikaar, I.; Zhang, X.; Jeremiasse, A. W.; Prévoteau, A.; Rabaey, K., Anode materials for sulfide oxidation in alkaline wastewater: An activity and stability performance comparison. *Water Res.* **2019,** *149*, 111-119.

359.   Waterston, K.; Bejan, D.; Bunce, N. J., Electrochemical oxidation of sulfide ion at a boron-doped diamond anode. *J. Appl. Electrochem.* **2007,** *37* (3), 367-373.

360   Ateya, B. G.; Al-Kharafi, F. M.; Abdallah, R. M.; Al-Azab, A. S., Electrochemical removal of hydrogen sulfide from polluted brines using porous flow through electrodes. *J. Appl. Electrochem.* **2005,** *35* (3), 297-303.

361   McCann, J.; Pezy, J., The Measurement of the Flatband Potentials of n-Type and p-Type Semiconductors by Rectified Alternating Photocurrent Voltammetry. *J. Electrochem. Soc.* **1981,** *128* (8), 1735-1740.

362   Hubler, D.; Baygents, J.; Chaplin, B.; Farrell, J., Understanding chlorite and chlorate formation associated with hypochlorite generation at boron doped diamond film anodes. *J. Electrochem. Soc.* **2014,** *161* (12), E182-E189.

363   Jeong, J.; Kim, C.; Yoon, J., The effect of electrode material on the generation of oxidants and microbial inactivation in the electrochemical disinfection processes. *Water Res.* **2009,** *43* (4), 895-901.

364   Jeong, J.; Kim, J. Y.; Yoon, J., The role of reactive oxygen species in the electrochemical inactivation of microorganisms. *Environ. Sci. Technol.* **2006,** *40* (19), 6117-6122.

365   Bader, H., Determination of ozone in water by the indigo method: a submitted standard method. **1982**.

366.   Brunet, L. n.; Lyon, D. Y.; Hotze, E. M.; Alvarez, P. J.; Wiesner, M. R., Comparative photoactivity and antibacterial properties of C_{60} fullerenes and titanium dioxide nanoparticles. *Environ. Sci. Technol.* **2009,** *43* (12), 4355-4360.

367.   Lee, J.; Fortner, J. D.; Hughes, J. B.; Kim, J.-H., Photochemical production of reactive oxygen species by C_{60} in the aqueous phase during UV irradiation. *Environ. Sci. Technol.* **2007,** *41* (7), 2529-2535.

368.   Shrivastava, A.; Gupta, V. B., Methods for the determination of limit of detection and limit of quantitation of the analytical methods. *Chron. Young Sci.* **2011,** *2* (1), 21.

369. Yang, X.; Zhang, Y.; Wang, F.; Wang, L. J.; Richardson, D.; Shameem, M.; Ambrogelly, A., Analysis and purification of IgG$_4$ bispecific antibodies by a mixed-mode chromatography. *Analytical biochemistry* **2015,** *484*, 173-179.

370. Li, Y.; Zhang, W.; Niu, J.; Chen, Y., Mechanism of photogenerated reactive oxygen species and correlation with the antibacterial properties of engineered metal-oxide nanoparticles. *ACS nano* **2012,** *6* (6), 5164-5173.

371. Neppolian, B.; Park, J.-S.; Choi, H., Effect of Fenton-like oxidation on enhanced oxidative degradation of para-chlorobenzoic acid by ultrasonic irradiation. *Ultrason. Sonochem.* **2004,** *11* (5), 273-279.

372. Ishibashi, K.-i.; Fujishima, A.; Watanabe, T.; Hashimoto, K., Detection of active oxidative species in TiO$_2$ photocatalysis using the fluorescence technique. *Electrochem. Commun.* **2000,** *2* (3), 207-210.

373. Xiao, Q.; Si, Z.; Zhang, J.; Xiao, C.; Tan, X., Photoinduced hydroxyl radical and photocatalytic activity of samarium-doped TiO2 nanocrystalline. *J. Hazard. Mater.* **2008,** *150* (1), 62-67.

374. Yu, J.; Wang, W.; Cheng, B.; Su, B.-L., Enhancement of photocatalytic activity of mesoporous TiO2 powders by hydrothermal surface fluorination treatment. *The J. Phys. Chem.   C* **2009,** *113* (16), 6743-6750.

375. Furuta, T.; Tanaka, H.; Nishiki, Y.; Pupunat, L.; Haenni, W.; Rychen, P., Legionella inactivation with diamond electrodes. *Diam Relat Mater.* **2004,** *13* (11), 2016-2019.

376. Park, Y.-M.; Pyo, H.; Park, S.-J.; Park, S.-K., Development of the analytical method for 1, 4-dioxane in water by liquid–liquid extraction. *Analytica Chimica Acta* **2005,** *548* (1-2), 109-115.

377. Jirka, A. M.; Carter, M. J., Micro semiautomated analysis of surface and waste waters for chemical oxygen demand. *Anal. Chem.* **1975,** *47* (8), 1397-1402.

378. Gassie, L. W.; Englehardt, J. D.; Wang, J.; Brinkman, N.; Garland, J.; Gardinali, P.; Guo, T., Mineralizing urban net-zero water treatment: Phase II field results and design recommendations. *Water Res.* **2016,** *105*, 496-506.

379. da Silva Lacerda, V.; López-Sotelo, J. B.; Correa-Guimarães, A.; Hernández-Navarro, S.; Sánchez-Báscones, M.; Navas-Gracia, L. M.; Martín-Ramos, P.; Martín-Gil, J., Rhodamine B removal with activated carbons obtained from lignocellulosic waste. *J. Environ. Manage.***2015,** *155*, 67-76.

380. Lachheb, H.; Puzenat, E.; Houas, A.; Ksibi, M.; Elaloui, E.; Guillard, C.; Herrmann, J.-M., Photocatalytic degradation of various types of dyes (Alizarin S, Crocein Orange G, Methyl Red, Congo Red, Methylene Blue) in water by UV-irradiated titania. *Appl. Catal. B.* **2002,** *39* (1), 75-90.

381.   Hambly, A.; Arvin, E.; Pedersen, L.-F.; Pedersen, P. B.; Seredyńska-Sobecka, B.; Stedmon, C., Characterising organic matter in recirculating aquaculture systems with fluorescence EEM spectroscopy. *Water Res.* **2015,** *83*, 112-120.

382.   Liu, S.; Tang, L.; Wu, M.; Fu, H.; Xu, J.; Chen, W.; Ma, F., Parameters influencing elimination of geosmin and 2-methylisoborneol by K_2FeO_4. *Sep. Purif. Technol.* **2017,** *182*, 128-133.

383.   Lu, J.; Wills, P. S.; Wilson, P. C., Trace analysis of off-flavor/odor compounds in water using liquid-liquid microextraction coupled with gas chromatography—positive chemical ionization-tandem mass spectrometry. *Frontiers of Environmental Science & Engineering* **2016,** *10* (3), 477-481.

384.   Matilainen, A.; Gjessing, E. T.; Lahtinen, T.; Hed, L.; Bhatnagar, A.; Sillanpää, M., An overview of the methods used in the characterisation of natural organic matter (NOM) in relation to drinking water treatment. *Chemosphere* **2011,** *83* (11), 1431-1442.

385.   Fellman, J. B.; Hood, E.; Spencer, R. G., Fluorescence spectroscopy opens new windows into dissolved organic matter dynamics in freshwater ecosystems: A review. *Limnol. Oceanogr.* **2010,** *55* (6), 2452-2462.

386.   Stedmon, C. A.; Bro, R., Characterizing dissolved organic matter fluorescence with parallel factor analysis: a tutorial. *Limnol. Oceanogr.: Methods* **2008,** *6* (11), 572-579.

387.   Huber, S. A.; Balz, A.; Abert, M.; Pronk, W., Characterisation of aquatic humic and non-humic matter with size-exclusion chromatography–organic carbon detection–organic nitrogen detection (LC-OCD-OND). *Water Res.* **2011,** *45* (2), 879-885.

388.   Li, Q.; Page, M. A.; Mariñas, B. J.; Shang, J. K., Treatment of coliphage MS2 with palladium-modified nitrogen-doped titanium oxide photocatalyst illuminated by visible light. *Environ. Sci. Technol.* **2008,** *42* (16), 6148-6153.

389.   Yu, F.; Zhou, M.; Yu, X., Cost-effective electro-Fenton using modified graphite felt that dramatically enhanced on H_2O_2 electro-generation without external aeration. *Electrochimica Acta* **2015,** *163*, 182-189.

390.   Oliveira, F. H.; Osugi, M. E.; Paschoal, F. M.; Profeti, D.; Olivi, P.; Zanoni, M. V. B., Electrochemical oxidation of an acid dye by active chlorine generated using $Ti/Sn_{(1-x)}IrxO_2$ electrodes. *J. Appl. Electrochem.* **2007,** *37* (5), 583-592.

391.   Rajab, M.; Heim, C.; Letzel, T.; Drewes, J. E.; Helmreich, B., Electrochemical disinfection using boron-doped diamond electrode–The synergetic effects of in situ ozone and free chlorine generation. *Chemosphere* **2015,** *121*, 47-53.

392.   Son, H.-S.; Choi, S.-B.; Khan, E.; Zoh, K.-D., Removal of 1,4-dioxane from water using sonication: Effect of adding oxidants on the degradation kinetics. *Water Res.* **2006,** *40* (4), 692-698.

393.   Barndõk, H.; Blanco, L.; Hermosilla, D.; Blanco, Á., Heterogeneous photo-Fenton processes using zero valent iron microspheres for the treatment of wastewaters contaminated with 1,4-dioxane. *Chem. Eng. J.* **2016,** *284*, 112-121.

394.   Lan, Y.; Coetsier, C.; Causserand, C.; Serrano, K. G., An experimental and modelling study of the electrochemical oxidation of pharmaceuticals using a boron-doped diamond anode. *Chem. Eng. J.* **2018,** *333*, 486-494.

395.   Stefan, M. I.; Bolton, J. R., Mechanism of the degradation of 1,4-dioxane in dilute aqueous solution using the UV/hydrogen peroxide process. *Environ. Sci. Technol.* **1998,** *32* (11), 1588-1595.

396.   Beckett, M. A.; Hua, I., Elucidation of the 1,4-dioxane decomposition pathway at discrete ultrasonic frequencies. *Environ. Sci. Technol.* **2000,** *34* (18), 3944-3953.

397.   Yanagida, S.; Nakajima, A.; Kameshima, Y.; Okada, K., Effect of applying voltage on photocatalytic destruction of 1,4-dioxane in aqueous system. *Catalysis Communications* **2006,** *7* (12), 1042-1046.

398.   Schuchmann, M. N.; Bothe, E.; von Sonntag, J.; von Sonntag, C., Reaction of OH radicals with benzoquinone in aqueous solutions. A pulse radiolysis study. *J. Chem. Soc., Perkin Trans 2* **1998,**   (4), 791-796.

399.   Jasmann, J. R.; Borch, T.; Sale, T. C.; Blotevogel, J., Advanced electrochemical oxidation of 1,4-dioxane via dark catalysis by novel titanium dioxide (tio2) pellets. *Environ Sci Technol* **2016,** *50* (16), 8817-26.

400.   Song, W.; O'Shea, K. E., Ultrasonically induced degradation of 2-methylisoborneol and geosmin. *Water Res.* **2007,** *41* (12), 2672-2678.

401.   Xue, Q.; Li, M.; Shimizu, K.; Utsumi, M.; Zhang, Z.; Feng, C.; Gao, Y.; Sugiura, N., Electrochemical degradation of geosmin using electrode of Ti/IrO_2–Pt. *Desalination* **2011,** *265* (1-3), 135-139.

402.   Hua, L.; Guo, L.; Thakkar, M.; Wei, D.; Agbakpe, M.; Kuang, L.; Magpile, M.; Chaplin, B. P.; Tao, Y.; Shuai, D.; Zhang, X.; Mitra, S.; Zhang, W., Effects of anodic oxidation of a substoichiometric titanium dioxide reactive electrochemical membrane on algal cell destabilization and lipid extraction. *Bioresour. Technol.* **2015,** *203*, 112-117.

403.   Osterwalder, A.; Pigneur, Y., Business model generation: a handbook for visionaries, game changers, and challengers. *John Wiley & Sons*: 2010.

301